Polylogarithmic, elliptic, and Calabi–Yau Feynman integrals from a hybrid bootstrap

Matthew D. Schwartz
Department of Physics, Harvard University

October 1, 2026

Abstract

Multi-loop Feynman integrals are a bottleneck of precision collider physics. At low orders many evaluate to polylogarithms, but those with internal masses and more scales can involve elliptic curves and Calabi–Yau manifolds. Each such integral has traditionally been a research project of its own. We present thirty Feynman integrals from the three classes, all computed with a hybrid bootstrap by a large language model operating the BootLoops toolkit. For each we give a closed form or a differential equation with boundary data, and a standalone evaluation code. Fifteen are known results, recomputed as a test of the method, and fifteen are to our knowledge new. The new results include the nonplanar branch of two-loop W-pair production with exact top-quark mass that the planar computations left open, on one unphysical kinematic line, and the simplest two-mass nonplanar hexa-box for diboson-plus-jet production, along two kinematic paths. They also include two elliptic masters of $gg \to Z\gamma$ at exact top mass and three-loop light-by-light integrals with a massive fermion loop, among them a crossed box in which K3 periods appear. Finally, we determine the threshold coefficients of the three- and four-loop banana periods when one mass equals the sum of the others.

Contents

1 Introduction **3**

2 Conventions and function classes **5**
2.1 Integral families and notation 5
2.2 Function classes and the form of the results 6
2.3 The computation in brief 7
2.4 Acceptance criterion and available data 8

3 Overview of the thirty integrals **9**
3.1 Classification and summary table 9
3.2 Organization of the entries 11

4 Polylogarithmic integrals **13**
4.1 The two-loop Sudakov form factor 13
4.2 The massless planar double box 15
4.3 The three-loop C_5 ladder 17
4.4 The one-loop massless pentagon 19
4.5 The outer-mass double box 21

4.6 The central-mass double box . . . 23
4.7 The four-mass kite with a massless rung . . . 25
4.8 The nonplanar hexa-box with two equal-mass legs . . . 27

5 Elliptic integrals **31**
5.1 The sunrise family . . . 31
5.2 The equal-mass kite . . . 34
5.3 Elliptic functions in $gg \to H$ . . . 36
5.4 The unequal-mass kite . . . 37
5.5 Ice-cream cone integrals . . . 40
5.6 Elliptic masters in $gg \to Z\gamma$ . . . 45
5.7 The light-by-light box with a sunrise insertion . . . 49
5.8 Light-by-light boxes with self-energy insertions . . . 51
5.9 Nonplanar two-loop W-pair production . . . 55

6 K3 and Calabi–Yau integrals **59**
6.1 The three-loop equal-mass banana . . . 60
6.2 The four-loop equal-mass banana . . . 62
6.3 Banana threshold coefficients . . . 64
6.4 The three-loop crossed light-by-light box . . . 67

7 Scope of the results **72**
7.1 Kinematic domains and function classes reached . . . 72
7.2 Integrals not computed here . . . 73

8 Conclusions **73**

A Reference values **74**

B Word lists of the central-mass double box **82**

C Data for the elliptic entries **84**
C.1 The cone alphabet for generic masses . . . 84
C.2 Resonant boundary constants of the generic-mass cone . . . 85
C.3 Ice-cream cones away from the slice . . . 85
C.4 The $gg \to Z\gamma$ masters at fixed s . . . 86

D Nonplanar W-pair data on the line **86**
D.1 Block content and alphabets . . . 86
D.2 Local data of sector 481 . . . 87
D.3 Boundary constants . . . 88
D.4 The second line and the data files . . . 89

E Five-point alphabet and symbol-space bound **90**
E.1 The sub-alphabet of the generic-mass families . . . 90
E.2 Symbol-space dimensions . . . 90
E.3 Layered forms and boundary constants of the hexa-box . . . 91

F Crossed light-by-light box data **92**
F.1 The connection in two variables 92
F.2 Depth of the system in the raw frame 93
F.3 Kernels of the word form 93
F.4 Boundary constants of the kernel components 94

G Evaluation codes and data files **94**

1 Introduction

Predictions for hadron-collider observables at the percent level require scattering amplitudes at two and three loops. The Feynman integrals in those amplitudes are usually the hardest part of the calculation whenever massive particles propagate in the loops. At one loop every integral reduces to a small set of scalar integrals [98] with classical expressions in logarithms and dilogarithms. Beyond one loop, integrals with massless propagators and few external scales still evaluate to multiple polylogarithms (MPLs). However, when internal masses and more external scales are present, the maximal cut of an integral may instead define an elliptic curve, a K3 surface or a Calabi–Yau threefold. The integral is then an iterated integral whose kernels involve the periods of that variety. Integrals of this kind occur in two-loop electroweak corrections with the exact top-quark mass, in Higgs-plus-jet and diboson production, in light-by-light scattering through massive fermion loops, and in equal-mass self-energy graphs at three and four loops. Each such integral has typically required a dedicated analysis with its own function basis and boundary conditions.

The methods for computing multi-loop integrals are by now well developed. In dimensional regularization [112] the integrals of a given graph reduce through integration-by-parts (IBP) identities to a finite basis of master integrals [89, 110, 81], which satisfy first-order differential equations in the kinematic invariants [77]. If a basis exists in which the dependence on the dimensional regulator ε factorizes and the connection is a sum of logarithmic one-forms [76], the solution at each order in ε is a combination of MPLs. Their symbol letters are the arguments of those logarithms [71], and only boundary constants remain to be fixed. The simplest integral outside this class is the two-loop sunrise graph with three massive lines. Its maximal cut is an elliptic curve, and the finite part evaluates to an elliptic dilogarithm [25, 8, 102]. Developments since then include iterated integrals of modular forms and elliptic multiple polylogarithms (eMPLs) [10, 5, 33, 26], and ε-factorized differential equations whose kernels are periods and quasi-periods in place of logarithms [11, 65, 118]. At three loops and beyond, the equal-mass banana graphs involve periods of K3 surfaces and Calabi–Yau threefolds [24, 101, 100, 28], and ε-factorized bases for these geometries are being constructed case by case [59]. In every class, series solutions of the differential equations give accurate numerical values of the integrals at any kinematic point [78], and purely numerical methods, auxiliary-mass flow in particular [95], supply independent values for comparison.

Several integrals relevant to precision collider predictions are not yet available in the literature. The two-loop master integrals for W-pair production in quark–antiquark annihilation with the exact top-quark mass are known for the planar topologies [75] but not for the nonplanar topology. The two-loop amplitudes for diphoton production through a heavy-quark loop are known analytically, including the elliptic sectors [22], as are the $gg \to Z\gamma$ amplitudes with massless quarks [68]. To our knowledge, the elliptic master integrals of $gg \to Z\gamma$ with the exact dependence on both the Z mass and the top-quark mass have not been computed analytically. For W^+W^- and WZ production in association with a jet, the planar families of two-loop five-point integrals with two massive legs are available [3]. The nonplanar hexa-boxes are known with one massive leg [4, 80], and as far

as we know the two-mass nonplanar families are open. In light-by-light scattering the three-loop amplitudes are known with massless internal lines [17] and the two-loop amplitudes with a massive fermion loop [1]. The full set of three-loop integrals with a massive loop, which contains elliptic and K3 subsectors, does not appear to be available. Finally, the analytic structure of the equal-mass banana integrals is understood at every loop order [28, 101, 100]. When one internal mass equals the sum of the others, the monodromy of the period at threshold is no longer unipotent and the local expansion contains a branch with a fractional exponent. We are not aware of earlier closed forms for the constants that multiply this branch.

In this paper we present thirty Feynman integrals from the three function classes (polylogarithmic, elliptic, and K3 or Calabi–Yau), computed by one method, which we call a hybrid bootstrap. When the integral lies in a finite-dimensional space of known functions, we construct that space from the singularities of the integrand, using Landau analysis and the geometry of the maximal cut [74, 63, 73]. We then fix the coefficients by analytic constraints and by integer-relation fits to high-precision numerical values at a few kinematic points [18]. When no finite basis appears to be adequate, we solve the differential equations directly, in ε-factorized form where one is available and otherwise by transporting boundary data along a path. A result here consists of an analytic expression, or a Picard–Fuchs operator with its boundary vector, together with a standalone numerical code that evaluates it. We regard an integral as computed only when that code reproduces independent numerical values to at least thirty digits at kinematic points that entered neither a fit nor the boundary data, which is the criterion of eq. (7). The computations were run by a large language model operating the BootLoops toolkit. The method and the role of the model are described in a companion paper [105], the constructions for elliptic and Calabi–Yau geometries in a second one [107], and the evaluation codes are collected in [106]. Fifteen of the thirty integrals are known results, with references in Table 1. We recompute them by the same procedure as the new integrals, as a test of the method, and reproduce the published results. Where we take an intermediate result from the literature, such as a differential equation, a boundary limit or a function space, we say so in the entry.

The other fifteen integrals are new, in the sense that we have found no earlier computation of them, at the kinematics stated in their entries, that was checked against independent values. In particular, for the nonplanar topology of two-loop W-pair production with the exact top-quark mass, the topology not treated in [75], we obtain the master integrals analytically along one kinematic line, which lies in an unphysical region. For the simplest two-mass nonplanar hexa-box, in which the two massive legs are non-adjacent and of equal mass, we give the master integrals along two kinematic paths. We compute two elliptic master integrals of $gg \to Z\gamma$ with the exact top-quark mass at one fixed ratio of the Z and top masses. The new entries also include three-loop light-by-light integrals with a massive fermion loop, namely boxes with a sunrise or another two-loop self-energy inserted into one massive line, and a top-sector master integral of the crossed box. We evaluate the latter by transporting boundary values with its differential equation and show that it contains an iterated integral of a K3 period, which excludes a polylogarithmic form over the letters of its maximal cut. We also determine the threshold coefficients of the three-loop and four-loop banana periods with one internal mass equal to the sum of the others, the constants multiplying the fractional-exponent branch. These coefficients are properties of the K3 and Calabi–Yau periods themselves, and their closed forms are derived in [107]. Here we define them, give the closed form of the three-loop coefficient, and recover them from the maximal-cut differential operators of the two families. Among the remaining new entries are an unequal-mass kite at fixed rational masses, whose function space is known in general [35, 69], and a four-mass kite with a massless rung, also at fixed masses. The others are the ice-cream-cone integrals [56] on a symmetric kinematic slice, with equal internal masses at orders ε^0 and ε^1 and with generic masses at order ε^0. Several of the

new results therefore hold on a restricted kinematic domain, a slice, a line or path, or a fixed mass point, and Table 1 gives the domain of each.

In section 2 we fix conventions, recall the three function classes, outline the computation and state the acceptance criterion, and section 3 collects the thirty integrals in Table 1 and Figure 1. Sections 4–6 present the polylogarithmic, elliptic, and K3 and Calabi–Yau integrals, section 7 summarizes the kinematic domains reached and the integrals we did not compute, and the appendices collect reference values, longer expressions and the evaluation codes.

2 Conventions and function classes

In this section we fix notation and recall the function classes in which the thirty results are written. It contains no new results, and a reader familiar with the material may read only the acceptance criterion, eq. (7), and pass to Table 1.

2.1 Integral families and notation

All external momenta p_i are incoming, with $\sum_i p_i = 0$, and the Lorentz invariants are $s_{ij} = (p_i+p_j)^2$. For four-point integrals we write $s = (p_1 + p_2)^2$, $t = (p_2 + p_3)^2$ and $u = (p_1 + p_3)^2$, related by $s+t+u = \sum_i p_i^2$, unless an entry states another labeling. Internal masses m_i are real and positive. We regulate divergences dimensionally [112], in $d = 4 - 2\varepsilon$ unless an entry states otherwise. An integral family with L loops and n propagators is the set

$$I_{\nu_1\cdots\nu_n}(d;\{s_{ij}\},\{m_i^2\}) = \int \prod_{l=1}^{L} \frac{d^d k_l}{i\pi^{d/2}} \prod_{j=1}^{n} \frac{1}{D_j^{\nu_j}}, \qquad D_j = q_j^2 - m_j^2 + i0, \tag{1}$$

where each q_j is a linear combination of the loop momenta k_l and the external momenta, and the indices ν_j are integers. We use the Minkowski prescription $+i0$ and include no factor of $e^{\gamma_E \varepsilon}$ or $(4\pi)^{\varepsilon}$ in eq. (1).

Indices $\nu_j \leq 0$ denote irreducible scalar products (ISPs) in the numerator, and a sector is the set of integrals sharing the same positive indices. Each entry lists its propagators and kinematics. For some families we multiply the integral by $e^{L\gamma_E\varepsilon}$, by a power of an invariant, or by the leading singularity of the top sector to make the Laurent coefficients pure, and the entry then states this normalization. Several elliptic and Calabi–Yau families, among them the sunrise family, the ice-cream cones and the bananas, are instead defined in $d = 2 - 2\varepsilon$.

Integration-by-parts (IBP) identities reduce every member of a family to a finite set of master integrals [89, 110]. We perform the reductions with `Kira` [81]. We expand each master integral in the dimensional regulator,

$$I(\vec{x};\varepsilon) = \sum_{k\geq k_{\min}} \varepsilon^k \, I^{(k)}(\vec{x}), \tag{2}$$

where $\vec{x}$ collects the dimensionless kinematic variables of the family, $k_{\min} \leq 0$ is the order of the leading pole, and $I^{(k)}$ is the coefficient at order ε^k. For a suitably normalized integral the coefficient $I^{(k)}$ has uniform transcendental weight $k - k_{\min}$, with log and π of weight one and ζ_n of weight n [76]. Such integrals are called pure, or of uniform transcendental weight.

By the Euclidean region we mean the region where every invariant the integral depends on is negative and every mass is positive; there the integral is real and free of thresholds. Unless stated otherwise, results and reference values are quoted in this region, and where a result is also continued to physical kinematics we use the Feynman prescription $s \to s + i0$. Dimensionless variables are

chosen family by family, for example $u = 4m^2/(-s)$ and $v = 4m^2/(-t)$ for the outer-mass double box, where this u is not the Mandelstam invariant $(p_1 + p_3)^2$.

In the figures, thin black lines are massless and thick colored lines massive, one color per distinct mass, with violet reserved for a heavy mass such as the top quark. External legs carry arrows and are drawn thick, wavy or dashed when off shell or massive, and each caption names the masses and invariants of its graph.

2.2 Function classes and the form of the results

The master integrals $\vec{f}$ of a family satisfy linear differential equations in the kinematic variables, obtained by differentiation followed by IBP reduction [77, 117]. In many cases a basis exists in which the dependence on ε factorizes and the connection is a sum of logarithmic one-forms,

$$d\vec{f}(\vec{x};\varepsilon) = \varepsilon \Big(\sum_i A_i \, \mathrm{d}\log \alpha_i(\vec{x}) \Big) \, \vec{f}(\vec{x};\varepsilon). \tag{3}$$

Here the A_i are constant rational matrices. The system is then said to be in canonical form [76]. We call the algebraic functions α_i letters and their set the alphabet. Order by order in ε the solution of eq. (3) is a combination of iterated integrals of the forms $\mathrm{d}\log\alpha_i$, whose symbol [71, 54] is read off from the matrices A_i. When the letters are rational functions of the variables (possibly after a change of variables rationalizing square roots), these iterated integrals are multiple polylogarithms (MPLs) [70],

$$G(a_1,\dots,a_w;x) = \int_0^x \frac{dt}{t-a_1}\, G(a_2,\dots,a_w;t), \qquad G(;x) = 1, \qquad G(\underbrace{0,\dots,0}_{w};x) = \frac{\log^w x}{w!}, \tag{4}$$

of weight w. For one variable with $a_i \in \{0, \pm 1\}$ these are harmonic polylogarithms (HPLs), and we write GPL (Goncharov polylogarithm) when the indices a_i are algebraic.

With internal masses the maximal cut need not be an algebraic function. For example, for the two-loop sunrise with three massive lines in two dimensions it is the integral of dx/y over an elliptic curve $y^2 = Q(x)$. Here Q has degree three or four in the Baikov variable x, with coefficients that depend on the kinematics [25, 8]. The homogeneous solutions are then the periods ψ_1, ψ_2 of the curve, which are complete elliptic integrals of the kinematics, and the $\mathrm{d}\log$ forms of eq. (3) are replaced by one-forms built from ψ_1, its derivative and the letters [11, 34, 65, 118]. In the variable $\tau = \psi_2/\psi_1$, with q the associated nome (normalized as stated in each entry), the solution becomes a combination of iterated integrals of modular forms whenever the monodromy group of the family is a congruence subgroup [10, 33].

The monodromy group is $\Gamma_1(6)$ for the equal-mass sunrise, kite [5, 102] and ice-cream cone, and for the light-by-light integrals with sunrise or self-energy insertions, which inherit the sunrise cut. For the $gg \to Z\gamma$ masters it is $\Gamma_0(4)$. However, when the masses are unequal or a further scale enters, the monodromy group is in general no longer a congruence subgroup, and we call the curve non-modular. In that case we write the results as elliptic multiple polylogarithms (eMPLs) [38, 35, 26] or, by variation of parameters, as iterated integrals of the period pair. At a boundary point where the curve has complex multiplication (CM), the periods reduce to Γ functions at rational arguments [108], and we call the resulting constants CM Γ-periods.

At three loops and beyond, the maximal cut of the L-loop banana with massive lines is a period of a Calabi–Yau variety of dimension $L-1$ [24, 28]. At three loops this is a K3 surface and at four loops a Calabi–Yau threefold, written CY_3 [100]. In the equal-mass case the K3 surface is

the symmetric square of the sunrise curve: its periods are products of the sunrise periods, and the modular forms that enter are again those of $\Gamma_1(6)$ [101, 37].

For the Calabi–Yau varieties of the banana graphs the homogeneous differential equation is $\mathcal{L}\varpi = 0$ with a Picard–Fuchs operator $\mathcal{L}$ of order L, which has a point of maximal unipotent monodromy (MUM point) where all local exponents coincide. The Frobenius basis there consists of one holomorphic solution ϖ_0 and solutions with up to $L-1$ powers of the logarithm [83]. Moreover, canonical ε-factorized forms of these systems are known [99, 57, 59]. For such entries we give the operator, the Frobenius data, the inhomogeneous subsector terms and a boundary vector. The degenerations of these geometries at threshold, which determine the coefficients listed as Nos. 31 and 32 of Table 1, are analyzed in the companion paper [107], and the coefficients are defined and checked in section 6.3.

In every class we write the result for a Laurent coefficient as

$$I^{(k)}(\vec{x}) = \sum_j c_j\, \phi_j(\vec{x}), \qquad c_j \in \mathbb{Q} \text{ or a stated ring of constants,} \tag{5}$$

where the ϕ_j span the stated function space. For polylogarithmic integrals they are MPL or HPL words in the letters, and in the elliptic class eMPLs, iterated integrals of modular forms, or iterated integrals of the period pair multiplied by powers of ψ_1. In the K3 and Calabi–Yau class they are Frobenius solutions of $\mathcal{L}$ and their iterated primitives. The constants that enter, through the c_j or through boundary values, are in most cases rational numbers, ζ values, logarithms of algebraic numbers, Clausen and L-function values or CM Γ-periods. Otherwise we define the constant by a convergent integral written out in the entry, or by transporting analytic boundary values along a specified path with the differential equation. Where no finite basis $\{\phi_j\}$ is available on the whole kinematic space, the result is the connection with its boundary data and its solution along a stated path or curve (Table 1, domain column).

2.3 The computation in brief

For most of the integrals we determine the c_j of eq. (5) without integrating the differential equation. The Landau singularities, obtained from principal Landau determinants and from the geometry of the maximal cut [74, 97, 64, 45], fix the alphabet, or the curve or operator, and with it a finite candidate set $\{\phi_j\}$. Most candidates are typically removed by linear conditions: the first-entry condition, integrability of the symbol, regularity at pseudo-thresholds, and the known behavior at cusps and in soft or large-momentum limits.

We fix the coefficients that survive the linear conditions by integer-relation fits [18] to high-precision values, computed at Euclidean points $\vec{x}_a$ with the auxiliary-mass-flow method (`AMFlow`) [95] or by numerical solution of the differential equation. The PSLQ integer-relation algorithm returns integers m_0, m_j of bounded size with

$$\left| m_0\, I^{(k)}(\vec{x}_a) - \sum_j m_j\, \phi_j(\vec{x}_a) \right| < 10^{-P} \tag{6}$$

at working precision P, whence $c_j = m_j/m_0$; such fits have long been used in multi-loop calculations [16]. If the candidate set lacks a letter or a function, no relation with small integers reproduces values known to hundreds of digits, and PSLQ then returns none below its size bound. The accepted fit is tested at further points (section 2.4).

Where no finite candidate set is available, as for non-modular kernels, Calabi–Yau periods and large coupled systems, we integrate the differential equation itself. We bring the system to

ε-factorized form where we can [93], or else solve the coupled blocks by variation of parameters around their period solutions. In either case the solution is then continued along a path by matched local series expansions, the method of `DiffExp` and `SeaSyde` [78, 15]. We fix boundary values by regularity at pseudo-thresholds, by the behavior at a cusp or MUM point, by vacuum integrals, or by a large-momentum limit. For a few integrals a boundary value is instead taken from `AMFlow` at one point, which the entry names, and the comparison of section 2.4 then uses different points.

The computations reported here were carried out by a large language model operating the BootLoops toolkit. The model selected and ran the steps described above, and every number was produced by a deterministic program. The method, its decision rules and the toolkit are described in [105], the code in [106], and the elliptic and Calabi–Yau constructions in [107].

2.4 Acceptance criterion and available data

Given the form eq. (5), or an operator with its boundary data, we regard an integral as computed when two further conditions hold. A standalone numerical implementation of that form at arbitrary working precision must exist, and for every order k given in the entry it must satisfy

$$\left| I^{(k)}_{\text{form}}(\vec{x}_b) - I^{(k)}_{\text{num}}(\vec{x}_b) \right| < 10^{-30} \left| I^{(k)}_{\text{num}}(\vec{x}_b) \right| \tag{7}$$

at kinematic points $\vec{x}_b$ that entered no fit and no boundary determination. Here $I^{(k)}_{\text{form}}$ is the implementation of the printed result and $I^{(k)}_{\text{num}}$ an independent numerical value, from `AMFlow` [95] unless the entry names another source. We repeat the comparison of eq. (7) at two working precisions and require the same outcome, which excludes accidental agreement of truncated numbers. We refer to the points $\vec{x}_b$ as held out from the derivation, and to this criterion as the BootLoops standard.

For the $gg \to H$ functions, $I^{(k)}_{\text{num}}$ is obtained by rotating `AMFlow` values into the canonical basis of the source paper, and for the four-loop banana also from a Bessel-moment representation. Finally, for the banana threshold coefficients, to which auxiliary-mass flow does not apply, the comparison uses ball arithmetic with an independent transport and the family's maximal-cut operator.

Elliptic and Calabi–Yau Feynman integrals are usually presented in two forms. The first is an ε-factorized differential equation over a stated alphabet, with boundary values at a cusp or a MUM point [65, 100]. The second is a set of eMPLs or of iterated integrals of modular forms or Calabi–Yau periods [10, 5, 33, 56], which may be evaluated with general-purpose codes [116] and compared with independent numerical evaluations. Both are complete answers, and our results take the same forms. We add, for all thirty entries, a self-contained numerical implementation of each printed form and the comparison of eq. (7) at points outside the construction, taking many-digit agreement as evidence for a closed form as in [91, 90].

For each of the thirty integrals a standalone evaluation code is available on that integral's page of the BootLoops site [106]. Appendix G lists them with their inputs.[1] The codes use no reduction or auxiliary-mass software at run time. Those for Nos. 24 and 35 start from stored boundary values, and the precision of their output is therefore limited by that of the stored values, as stated in sections 4.8 and 5.9. Two entries carry part of their boundary data as digit strings that are not reduced to named constants or written integrals: the constant K_{12} of the $gg \to Z\gamma$ masters (No. 20, section 5.6), given to 137 digits, and the 447 boundary constants of the hexa-box (No. 24, section 4.8), given to 78–83 significant digits.

[1] The codes are written in Python with `mpmath`; some also import `sympy` or `python-flint` for exact rational arithmetic and the bookkeeping of the ε expansion.

3 Overview of the thirty integrals

The thirty integrals range from the one-loop massless pentagon to the four-loop equal-mass banana, and most carry internal masses. Table 1 indexes them and Figure 1 shows their graphs in the order used in sections 4–6. We group them by the geometry of the maximal cuts in each family, and this geometry determines which class of functions we expect in the ε expansion.

3.1 Classification and summary table

In the polylogarithmic class every maximal cut in the family has genus zero, with leading singularities that are algebraic functions of the invariants, and we expect the ε expansion to evaluate to multiple polylogarithms over a finite alphabet. In the elliptic class at least one sector has its maximal cut on a curve of genus one. The results are elliptic multiple polylogarithms, iterated integrals of modular forms for $\Gamma_1(6)$ or $\Gamma_0(4)$ when that curve is modular, or iterated integrals over its periods otherwise. In the third class the maximal cut is a period of a family of K3 surfaces or Calabi–Yau threefolds. We write the result in the Frobenius basis of the Picard–Fuchs operator with a boundary vector of coefficients. In the crossed light-by-light box (No. 21) K3 periods appear together with polylogarithms.

Table 1: The thirty integrals, fifteen known and fifteen new, grouped by the geometry of the maximal cut, with the known integrals first in each class. Each agrees, in the sense of eq. (7), with an independent evaluation at points used neither in a fit nor to fix a boundary value, to the number of digits given in the last column. *No.* is the label of the integral in this paper, in the companion papers [105, 107] and in the evaluation codes [106]; Nos. 3, 22, 25, 26 and 30 are not used. The next columns give the integral with its figure; its loops, external legs, and massive internal lines by count and mass or by squared masses; and the kinematic domain of the result, with any continuation above threshold. The remaining columns give the function class, the form of the result, whether the integral is known (with the reference) or new, and the check, namely the independent evaluation used, the number of points and the digits of agreement. In the last column `AMFlow` denotes a value computed with the auxiliary-mass-flow program [95]. MPL, HPL, GPL and eMPL stand for multiple, harmonic, Goncharov and elliptic multiple polylogarithms, and $\Gamma_1(6)$, $\Gamma_0(4)$ for the congruence subgroups under which the periods of the maximal cut are modular.

No.	Integral	Loops; legs; masses	Domain	Class, geometry	Form of the result	Known or new	Check
Polylogarithmic integrals (section 4)							
6	Two-loop Sudakov form factor; Fig. 2	2; 3; none	single scale $q^2 = s$; exact in d	Γ functions; ζ values	product of Γ functions	known [72, 87, 66]	`AMFlow`, $s = -1, -2, \geq 78$
2	Massless planar double box; Fig. 3	2; 4; none	Euclidean, all $x = t/s$	MPL; HPLs on $\{x, 1+x\}$	HPL tower, rational coefficients	known [109]	`AMFlow`, two points, ≥ 89; [109], ≥ 142
4	Three-loop C_5 ladder, block f_3; Fig. 4	3; 3; none	$x = p_1^2/(p_3^2 - p_1^2) > 0$	MPL; polylogarithms on $\{x, 1+x\}$	four-term tower $\ln^k x \, \mathrm{Li}_{6-k}(-x)$	known [114, 49]	[114], ≥ 461; `AMFlow`, one point, 72
5	One-loop massless pentagon; Fig. 5	1; 5; none	Euclidean $v_i < 0$; to order ε^0	MPL; 15 letters and $\sqrt{\Delta_5}$	sum over the five one-mass boxes	known [23, 12]	`AMFlow`, one point, 68
1	Outer-mass double box; Fig. 6	2; 4; six of mass m	Euclidean $u, v > 0$	MPL, weight 4; 12 letters, three roots	one weight-4 symbol	known [40]	`AMFlow`, four points, ≥ 86
7	Central-mass double box; Fig. 7	2; 4; one of mass m	Euclidean (s, t); to weight 4	MPL; seven rational letters	two-variable GPLs	known [104], master J_{17}^C	`AMFlow`, twenty points, 109–112
23	Four-mass kite, massless rung; Fig. 8	2; 2; $(1, 4, 9, 2)$, rung 0	$t = p^2 < 0$, at these masses	genus 0; seven letters, four square roots	iterated integrals from $p^2 = 0$	new at these masses; MPL status open	`AMFlow`, seven points, 81–110

continued

Table 1: The thirty integrals (continued).

No.	Integral	Loops; legs; masses	Domain	Class, geometry	Form of the result	Known or new	Check
24	Hexa-box, legs $p_1^2 = p_3^2 = m^2$; Fig. 9	2; 5; none	path segments in six-scale space	MPL; radical $\sqrt{Q_4}$ on the path	layered iterated integrals; 447 stored constants	new; adjacent-mass case open	`AMFlow`, one point, ≥ 66
Elliptic integrals (section 5)							
8	Equal-mass sunrise, order ε^0; Fig. 10	2; 2; three of mass m	Euclidean $t = p^2/m^2 < 0$	elliptic, $\Gamma_1(6)$	period times $L(\chi_{-3}, 2)$ plus iterated integral of the cusp form f_3	known [10]	`AMFlow`, $t = -3$, 140; $t = -9$, 159
9	Sunrise $(1,1,2)$, order ε^0; Fig. 10	2; 2; $(1,1,2)$	$t < 0$; continued to $t = 16, 20$	unequal-mass curve	depth-two Kronecker eMPLs	known space [26]; rederived	`AMFlow`, $t = -3, -7$, 159; $t = 16, 20$, ≥ 71
10	Sunrise $(1,2,3)$, order ε^0; Fig. 10	2; 2; $(1,2,3)$	$t < 0$	unequal-mass curve	Kronecker eMPLs, per puncture	known space [26]; rederived	`AMFlow`, $t = -3, -9$, 159
11	Sunrise $(1,1,4)$, order ε^0; Fig. 10	2; 2; $(1,1,4)$	$t < 0$	unequal-mass curve	Kronecker eMPLs, per puncture	known space [26]; rederived	`AMFlow`, $t = -3$, 289; two more, 159
12	Sunrise, order ε^1, three mass sets; Fig. 10	2; 2; as Nos. 9–11	$t < 0$	Kronecker eMPLs of depth ≤ 3	two terms with a 101-word eMPL polynomial	known space [26]; rederived	`AMFlow`, nine points, 288–308
13	Equal-mass kite; Fig. 11	2; 2; three of mass m	Euclidean $t < 1$; continued to $t = 4, 16$	elliptic, $\Gamma_1(6)$	five-term eMPL word list	known [5]	`AMFlow`, $t = -3, -10$, 160, 130
18	$gg \to H$ functions G_1, G_2; Fig. 12	2; 3; five of m_t, one of M	Euclidean (s, M^2)	elliptic, non-modular; one period	single integrals over the period	known [96]; evaluated here	`AMFlow` via the rotation of [96], 57, 48
14	Unequal-mass kite $(1,1,2)$; Fig. 13	2; 2; $(1,1,2)$	$s = p^2 < 0$; continued to $s = 16$	elliptic, non-modular curve	single integral over the period pair	new at these masses; family form in [35]	`AMFlow`, three points, ≥ 125
15	Equal-mass ice-cream cone, order ε^0; Fig. 14	2; 3; four of mass m	slice $p_{12}^2 = p_{34}^2 = x < -1/4$, $p_{56}^2 = -1$; also $x = 12$	elliptic, $\Gamma_1(6)$; $d = 2 - 2\varepsilon$	length-two eMPL; one constant $T(-1)$	new on this slice; $d = 2$ structure [88, 51, 47]	`AMFlow`, $x = -2$, 134; $x = 12$, 57
16	Ice-cream cone $(1,2,3,5)$; Fig. 14	2; 3; $(1,2,3,5)$	the same slice	elliptic, non-modular, non-CM	as No. 15	new, as No. 15	`AMFlow`, $x = -2$, 118; $(1,3,2,7)$, ≥ 86
17	Ice-cream cones, order ε^1; Fig. 14	2; 3; as Nos. 15, 16	the same slice	length-three iterated integrals	weight-4 word list	new, as No. 15	`AMFlow`, $x = -2$, 134
20	$gg \to Z\gamma$ six-propagator elliptic pair, exact m_t; Fig. 15	2; 4; top loop m_t	$m_Z^2/m_t^2 = 7/25$, $t = -1/3$, s from 0 to $-1/4$	elliptic, $\Gamma_0(4)$	Eichler integral plus terms from polylogarithmic subsectors; K_{12} to 137 digits	new; $m_Z = 0$ case in [22]	`AMFlow`, 22 masters, 109–112
27	LBL3E, box with sunrise insertion; Fig. 16	3; 4; six of mass m	Euclidean $s, t < 0$, $m^2 = 1$	elliptic, $\Gamma_1(6)$ from the sunrise	dispersion over the sunrise cut	new; massless case in [17]	`AMFlow`, three points, ≥ 45
28	LBL3SE, box with kite insertion, stub power $\nu = 0$; Fig. 17	3; 4; one mass m	two Euclidean points	elliptic, $\Gamma_1(6)$ from the kite cut	dispersion over a closed-form density	new; $\nu = 0$ pinch, not a QED graph	`AMFlow`, two points, 59
29	LBL3KP, QED parents, $\nu = 2, 1$; Fig. 17	3; 4; one mass m	the same two points	elliptic, $\Gamma_1(6)$ from the kite cut	same density, stub kernels	new; kite in [79]	`AMFlow`, first point, 68; second, 50
33	LBL3VP, vacuum polarization, N_f^2; Fig. 17	3; 4; one mass m	exact in d; five points	elliptic, $\Gamma_1(6)$ from the three-body cut	density with a sunrise-period integral	new	`AMFlow`, 8 values of ε, 56–59; four points, ≥ 37

continued

Table 1: The thirty integrals (continued).

No.	Integral	Loops; legs; masses	Domain	Class, geometry	Form of the result	Known or new	Check
35	Nonplanar W-pair branch $\mathcal{T}_4$, exact m_t; Fig. 18	2; 4; two of m_t	line $(x, z) = (17/2, 5/3)$, unphysical	dlog, radical blocks; one elliptic cut	GPL words, layered iterated integrals	new; planar branches in [75]	`AMFlow`, two points, 79 functions, ≥ 37
K3 and Calabi–Yau integrals (section 6)							
19	Three-loop equal-mass banana; Fig. 19	3; 2; four of mass m	$\lvert t\rvert < 4$, $d = 2 - 2\varepsilon$; also $t > 16$	K3, $\Gamma_1(6)$	$7\zeta_3\varpi_0 - \mathrm{Part}_{\mathrm{reg}}$	known [101]	`AMFlow`, 18 points, ≥ 110
34	Four-loop equal-mass banana; Fig. 20	4; 2; five of mass m	$p^2 < 0$ about the MUM point; $d = 2 - 2\varepsilon$	CY_3, AESZ 34	log-Frobenius series	known [100, 28, 27]	Bessel moments, 116; `AMFlow`, 67
31	Banana threshold coefficient $c_{3/2}$; Fig. 21	3; 2; $(1, 1, 1, 9)$	period-level, heavy threshold	K3, non-unipotent, order 2	$c_{3/2} = -\sqrt{3}/(36\pi)$	new; period-level [107]	ball arithmetic, 195; IBP operator, 47
32	Banana threshold coefficients $c_{5/4}$, $c_{7/4}$; Fig. 21	4; 2; $(1, 1, 1, 1, 16)$	period-level, heavy threshold	CY_3, non-unipotent, order 4	closed forms in $\Gamma(\frac{1}{4})$ and π, printed in [107]	new; period-level [107]	ball arithmetic, 197; IBP operator, 45
21	LBL3X, crossed light-by-light box; Fig. 22	3; 4; four of mass m	curve $1/s+1/t = -3/8$ and listed points	MPL cut, K3, rank-nine system	words in 13 integration kernels on the curve	new; no GPL form over cut letters	`AMFlow`, six points, 33–46; two more, 72

The domain column of Table 1 states the kinematic region, slice, line, path segments, mass point or sector on which each result holds, and marks Nos. 9, 13, 14, 15 and 19 as also continued above threshold. The thirty entries are twenty-eight distinct computations, because Nos. 12 and 17 are the order-ε^1 terms of the sunrise and ice-cream-cone integrals whose order-ε^0 terms are Nos. 9–11 and 15–16. In addition, Nos. 9–11 are three mass assignments of one graph, and Nos. 31 and 32 are coefficients in the threshold expansion of banana-graph periods, given at the level of the period.

3.2 Organization of the entries

Every entry opens with what the integral is, where it arises and whether it was known, and then has the same five parts. *Definition* displays the propagators, masses, kinematics, dimension and normalization, and states the domain of the result. *Function space* displays the alphabet, the curve with its periods and level, or the Picard–Fuchs operator and its indicial data. *Result* displays the closed form, with long expressions continued in the appendices. *Boundary data* says how we fix the integration constants and names any value taken from `AMFlow` [95], and *Checks* says what we compared the result with, at which points and to how many digits, in the sense of eq. (7). Entries that share a family give the first two parts once, and in the sunrise family (section 5.1) the last three form one block per integral. Appendix A collects reference values and comparisons for all thirty integrals at fixed kinematic points.

Fifteen of the thirty integrals are known. In the polylogarithmic class these are the outer-mass and massless double boxes, the C_5 ladder, the pentagon, the planar Sudakov ladder and the central-mass double box [40, 109, 114, 23, 66, 104]. In the elliptic class they are the sunrise entries, the equal-mass kite and the $gg \to H$ functions [10, 26, 5, 96]. In the K3 and Calabi–Yau class they are the two equal-mass banana graphs [101, 100, 28]. Each such entry cites the original computation and states what we take from it, such as a function space or an inhomogeneous term.

We call an integral new when we have found no earlier computation of it, at the kinematics stated in its entry, that was checked against independent values. Among the new entries, Nos. 14 and 23 are kites evaluated at fixed masses. For the family of No. 14 an elliptic-polylogarithm form [35] and an ε-factorized differential equation [69] are known, whereas for No. 23, whose rung

Polylogarithmic

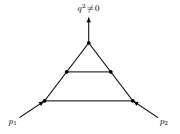

6 planar Sudakov ladder

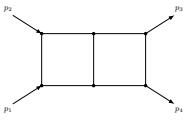

2 massless double box

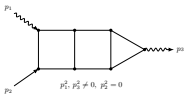

4 C_5 ladder

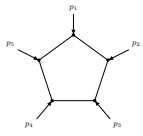

5 massless pentagon

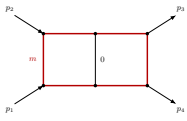

1 outer-mass double box

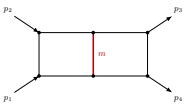

7 central-mass double box

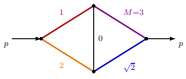

23† four-mass kite, massless rung

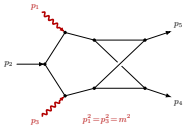

24† two-mass hexa-box

Elliptic

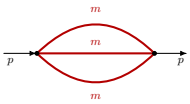

8 equal-mass sunrise

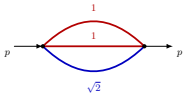

9 sunrise $(1,1,2)$

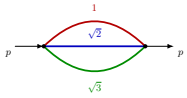

10 sunrise $(1,2,3)$

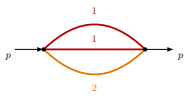

11 sunrise $(1,1,4)$

12 sunrise, order ε^1

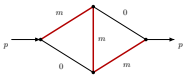

13 equal-mass kite

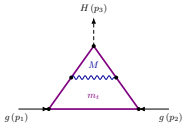

18 $gg \to H$ functions

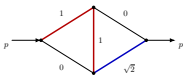

14† unequal-mass kite

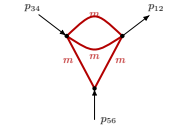

15† equal-mass ice-cream cone

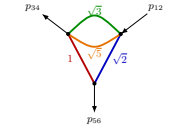

16† generic-mass ice-cream cone

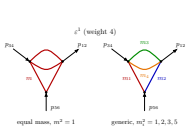

17† ice-cream cone, order ε^1

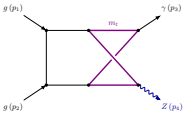

20† $gg \to Z\gamma$ masters

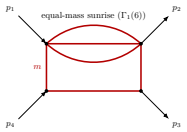

27† LBL3E, sunrise insertion

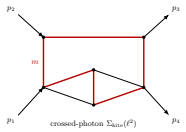

28† LBL3SE, kite insertion

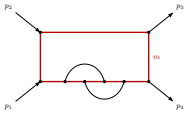

29† LBL3KP, kite parent

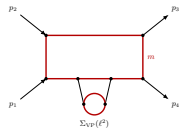

33† LBL3VP, N_f^2

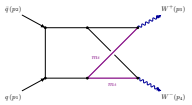

35† nonplanar W-pair $\mathcal{T}_4$

K3 and Calabi–Yau

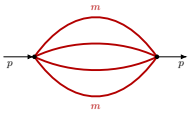

19 three-loop banana

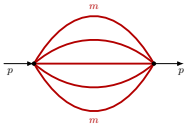

34 four-loop banana

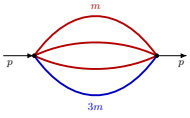

31† banana $(1,1,1,9)$, $c_{3/2}$

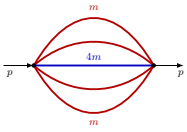

32† banana $(1,1,1,1,16)$, $c_{5/4}, c_{7/4}$

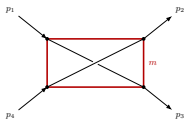

21† LBL3X crossed box

Figure 1: The thirty integrals of Table 1, grouped by function class in the order of the table. Bold numbers are the entry numbers of Table 1, and a dagger marks the fifteen new integrals. Thin black internal lines are massless and thick colored lines massive, one color per mass value; external legs carry arrows, and those drawn thick, wavy or dashed are off shell. In graphs 31 and 32 the blue line is the single heavy line, of mass $3m$ and $4m$ respectively. Each graph is drawn at full size, with momenta labeled, at the head of its entry.

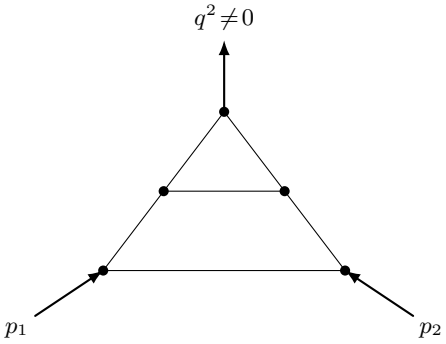

Figure 2: The two-loop Sudakov ladder $I[1,0,1,1,1,1,1]$ of the family (8) (No. 6 of Table 1). A triangle on D_1, D_3, D_7 has the off-shell leg $q = p_1 + p_2$ at its apex and shares the rung D_7 with a box on D_4, D_5, D_6, D_7, whose far corners carry the on-shell legs p_1 and p_2. All internal lines are massless and $q^2 = s$ is the only scale.

is massless, we leave open whether the result evaluates to multiple polylogarithms. Nos. 31 and 32 are period-level coefficients derived in closed form in the companion paper [107]. Finally, Nos. 15–17 are given on a kinematic slice, Nos. 28, 29 and 33 at the Euclidean points specified in their entries, and Nos. 20, 21, 24 and 35 on the restricted domains listed in Table 1.

4 Polylogarithmic integrals

The eight integrals of this section have maximal cuts of genus zero, and no elliptic curve or higher-dimensional period enters their differential equations. The alphabets of Nos. 6, 2, 4 and 7 of Table 1 are rational in the kinematics, and those of Nos. 5, 1, 23 and 24 also involve square roots of kinematic polynomials. Nos. 23 and 24 are, to our knowledge, new, and we give them on the restricted kinematics stated in their entries. The other six were computed before, and we reproduce them here as Γ functions, harmonic polylogarithms or Goncharov polylogarithms. We present the integrals with one- or two-letter alphabets first, then the known integrals with larger alphabets, and Nos. 23 and 24 last.

4.1 The two-loop Sudakov form factor

The scalar ladder of Figure 2 (No. 6 of Table 1) enters the two-loop massless Sudakov form factor. It is the planar two-loop vertex with two massless on-shell legs, $p_1^2 = p_2^2 = 0$, and one off-shell leg with $s = q^2 = (p_1 + p_2)^2$; it depends on this single scale and evaluates to a sum of products of Γ functions, exact in d. Planar two-loop vertex integrals of this kind were obtained in closed form long ago [72, 87], and the three master integrals of the family are given as Γ functions in Ref. [66]. We list the integral for completeness. The result given here is a recomputation from the family's own reduction onto its three Γ-function master integrals. An earlier version of this entry had evaluated a different member of the family (8), the seven-propagator integral with the irreducible scalar product in the denominator, which is not a graph and whose samples passed every internal consistency check of that computation: consistency checks are not controls.

Definition. With loop momenta k_1, k_2 we take the seven propagators

$$D_1 = k_1^2, \quad D_2 = (k_1+p_1)^2, \quad D_3 = (k_1+p_1+p_2)^2, \quad D_7 = (k_1-k_2)^2,$$
$$D_4 = k_2^2, \quad D_5 = (k_2+p_1)^2, \quad D_6 = (k_2+p_1+p_2)^2, \tag{8}$$

$$I[a_1,\ldots,a_7](s) = \int \prod_{l=1}^{2} \frac{d^d k_l}{i\pi^{d/2}} \prod_{j=1}^{7} \frac{1}{D_j^{a_j}}, \qquad d = 4-2\varepsilon, \tag{9}$$

in the conventions of eq. (1), with no factor $e^{\varepsilon\gamma_E}$ or $(4\pi)^\varepsilon$. Two loops and two independent external momenta give seven scalar products. For any six-line graph of the family one of the seven D_j is therefore an irreducible scalar product, and the integral with all seven indices positive is not a graph. The ladder of Figure 2 is $I[1,0,1,1,1,1,1]$. The integral $I[1,1,0,1,1,1,1]$, with an on-shell leg at the apex of the triangle, is a different graph, with leading pole $3/(4\varepsilon^3)$ in place of the ladder's $1/(4\varepsilon^4)$. We give the closed form for all s through the factor $(-s)^{-2-2\varepsilon}$ and quote numerical values at $s=-1$.

Function space. With one scale the alphabet is the single letter s, and each order in ε at $s=-1$ is a rational combination of products of zeta values, of uniform weight. An integration-by-parts reduction [81] leaves three master integrals, all products of one-loop Γ functions [110]: the sunrise $I[0,0,1,1,0,0,1]$, the bubble-inserted triangle $I[0,1,0,1,0,1,1]$ and the product of two q-channel bubbles $I[1,0,1,1,0,1,0]$. These are the masters A_3, A_4 and A_2^2 of Ref. [66]. There is no six-line master integral, and for the ladder the reduction reads

$$\begin{aligned} I[1,0,1,1,1,1,1] = &-\frac{6}{d-4}\, I[1,0,1,0,1,0,2] + \frac{4(d-3)^2}{(d-4)^2}\, I[1,0,1,1,0,1,0] \\ &+ \frac{6(3d-10)}{(d-4)^2}\, I[0,0,1,1,0,0,2], \end{aligned} \tag{10}$$

where $I[1,0,1,0,1,0,2]$ is the dotted bubble-inserted triangle with k_1 and k_2 interchanged. The dotted integrals are rational multiples of the undotted ones, $-(1-2\varepsilon)(2-3\varepsilon)/\varepsilon$ times the sunrise for $I[0,0,1,1,0,0,2]$ and $(1-2\varepsilon)(1-3\varepsilon)/(2\varepsilon)$ times the bubble-inserted triangle for $I[0,1,0,1,0,1,2]$.

Result. Inserting the Γ-function values of the masters into eq. (10), we obtain the closed form

$$\begin{aligned} I[1,0,1,1,1,1,1](s) = (-s)^{-2-2\varepsilon}\Big[&-\frac{3}{\varepsilon}\, G(1,2)\, T(1,1{+}\varepsilon,1) + \frac{(1-2\varepsilon)^2}{\varepsilon^2}\, G(1,1)^2 \\ &+ \frac{3(1-3\varepsilon)}{\varepsilon^2}\, G(1,2)\, G(1{+}\varepsilon,1)\Big], \end{aligned} \tag{11}$$

with the one-loop bubble and the one-loop triangle with two on-shell legs

$$\begin{aligned} G(a,b) &= \frac{\Gamma(a+b-\frac{d}{2})\,\Gamma(\frac{d}{2}-a)\,\Gamma(\frac{d}{2}-b)}{\Gamma(a)\,\Gamma(b)\,\Gamma(d-a-b)}, \\ T(a,b,c) &= \frac{\Gamma(a+b+c-\frac{d}{2})\,\Gamma(\frac{d}{2}-a-b)\,\Gamma(\frac{d}{2}-b-c)}{\Gamma(a)\,\Gamma(c)\,\Gamma(d-a-b-c)}. \end{aligned} \tag{12}$$

At $s=-1$, eq. (11) multiplied by $e^{2\varepsilon\gamma_E}$ expands into products of zeta values,

$$\begin{aligned} e^{2\varepsilon\gamma_E}\, I[1,0,1,1,1,1,1](-1) = &\frac{1}{4\varepsilon^4} + \frac{5\pi^2}{24\varepsilon^2} + \frac{29\zeta_3}{6\varepsilon} + \frac{3\pi^4}{32} + \varepsilon\Big[\frac{329\zeta_5}{10} - \frac{107\pi^2\zeta_3}{36}\Big] \\ &+ \varepsilon^2\Big[\frac{1723\pi^6}{60480} - \frac{833\zeta_3^2}{18}\Big] + \varepsilon^3\Big[\frac{3149\zeta_7}{14} - \frac{211\pi^2\zeta_5}{12} - \frac{73\pi^4\zeta_3}{48}\Big] + O(\varepsilon^4), \end{aligned} \tag{13}$$

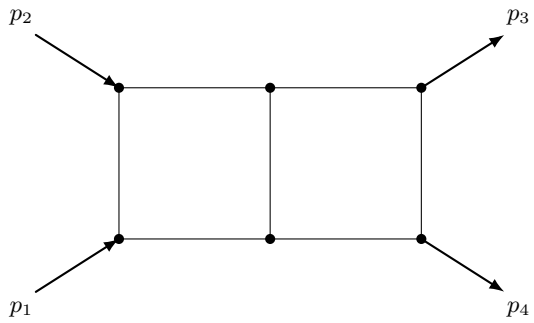

Figure 3: The massless planar double box (No. 2 of Table 1): two boxes sharing the central rung D_7, with all seven propagators of eq. (15) massless and four massless on-shell legs $p_1, \dots, p_4$. The invariants are $s = (p_1 + p_2)^2$ and $t = (p_2 + p_3)^2$, and $x = t/s$.

with no ε^{-3} term. The coefficient of ε^j has uniform weight $j + 4$, and the higher orders follow from eq. (11) in the same way. For example, the coefficient of ε^6 is

$$-\tfrac{64793}{21}\zeta_3\zeta_7 - \tfrac{63209}{50}\zeta_5^2 + \tfrac{46603\,\pi^{10}}{22\,809\,600} + \tfrac{6961}{720}\pi^4\zeta_3^2 + \tfrac{16907}{90}\pi^2\zeta_3\zeta_5 = -1235.936250\ldots . \tag{14}$$

Boundary data. No boundary data are required, since eq. (11) is exact in d and its only inputs are the reduction (10) and the three Γ-function masters. To compare with Ref. [66], whose measure is $d^dk/(2\pi)^d$ with $S_\Gamma = (4\pi)^\varepsilon/(16\pi^2\,\Gamma(1-\varepsilon))$, we set $I = -A/(S_\Gamma^2\,\Gamma(1-\varepsilon)^2)$ in the normalization of eq. (9) at $s = -1$, where every power of $(-q^2)$ is unity.

Checks. We compared eq. (11) and the three masters with `AMFlow` [95] values at $s = -1$ and, from an independent reduction, at $s = -2$, where every integral scales by the exact factor $2^{\,4-\sum_j a_j}\,2^{-2\varepsilon}$. We find agreement to at least 78 digits at every order from ε^{-4} through ε^6, limited by the precision of the numerical values.

4.2 The massless planar double box

The planar double box with seven massless propagators and four massless on-shell legs (Figure 3, No. 2 of Table 1) is the simplest two-loop four-point integral with two scales. Smirnov computed it in closed form in terms of harmonic polylogarithms of $x = t/s$ [109], and the nonplanar double box followed [113]. The integral is also a standard example for the method of differential equations in canonical form [76]. In this entry we rederive the ε expansion of Ref. [109] through the finite order.

Definition. With loop momenta k_1, k_2, incoming massless momenta $p_1, \dots, p_4$ and $d = 4 - 2\varepsilon$, we define

$$\begin{gathered} D_1 = k_1^2, \quad D_2 = (k_1 + p_1)^2, \quad D_3 = (k_1 + p_1 + p_2)^2, \quad D_4 = k_2^2, \\ D_5 = (k_2 + p_1 + p_2)^2, \quad D_6 = (k_2 + p_1 + p_2 + p_3)^2, \quad D_7 = (k_1 - k_2)^2, \\ J(s,t) = \int \prod_{l=1}^{2} \frac{d^dk_l}{i\pi^{d/2}} \prod_{j=1}^{7} \frac{1}{D_j}, \qquad x = \frac{t}{s}, \end{gathered} \tag{15}$$

in the conventions of eq. (1), with $s = (p_1 + p_2)^2$ and $t = (p_2 + p_3)^2$. We write the result for the Euclidean region $s, t < 0$, where $x > 0$ and J is real.

Function space. The maximal cut is rational and, once the leading singularity is factored out, the pure function has the two-letter alphabet

$$\mathcal{A} = \{\, x,\ 1+x \,\}, \qquad x = \frac{t}{s}. \tag{16}$$

Every order is then a combination of the polylogarithms $G(a_1, \ldots, a_w; x)$ of eq. (4) with $a_i \in \{0, -1\}$, which are harmonic polylogarithms. The only branch points are the zeros of the two letters,

$$x = 0 \ \ (s \to \infty \text{ at fixed } t, \text{ equivalently } t = 0), \qquad x = -1 \ \ (s + t = 0, \text{ i.e. } u = 0), \tag{17}$$

consistent with a planar box that has cuts in the s and t channels and none in u. The coefficient of ε^j has uniform weight $4+j$. We impose three conditions [54, 74] on the words before any coefficient is fitted. The first entry of the symbol must be one of the two letters, whose vanishing is a Landau singularity; the symbol must be integrable; and discontinuities may occur only in s and t. The words that satisfy these conditions, together with their products with zeta values of complementary weight, span an ansatz of dimension

$$(\, n_0, n_1, n_2, n_3, n_4 \,) = (1,\ 2,\ 5,\ 11,\ 23) \qquad \text{at weight } w = (0, 1, 2, 3, 4). \tag{18}$$

Result. From the maximal cut we compute the leading singularity of the seven-propagator integral,

$$\mathrm{LS} = \frac{1}{-2\, s^2\, t}. \tag{19}$$

We factor out this rational function and the dimension-carrying power $(-s)^{-2\varepsilon}$ by writing

$$\begin{gathered} J(s,t) = \frac{e^{-2\gamma_E \varepsilon}}{(-s)^{2+2\varepsilon}\,(-t)}\, K(x,\varepsilon), \qquad K(x,\varepsilon) = \sum_{j \geq -4} \varepsilon^j K^{(j)}(x), \\ K^{(j)}(x) = \sum_{|\vec{a}| \leq 4+j} c^{(j)}_{\vec{a}}\, G(a_1, \ldots, a_{|\vec{a}|}; x), \end{gathered} \tag{20}$$

where the $c^{(j)}_{\vec{a}}$ are rational multiples of 1, ζ_2, ζ_3 or ζ_4 such that each term has weight $4+j$, and K coincides with the function $K(x,\varepsilon)$ of Ref. [109]. Through the finite order we find

$$\begin{aligned} K^{(-4)} &= -4, \qquad K^{(-3)} = 5\, G(0;x), \qquad K^{(-2)} = -4\, G(0,0;x) + 15\, \zeta_2, \\ K^{(-1)} &= -4\, G(0,0,0;x) + 4\, G(-1,0,0;x) - 33\, \zeta_2\, G(0;x) + 12\, \zeta_2\, G(-1;x) + \tfrac{65}{3}\, \zeta_3, \\ K^{(0)} &= 32\, G(0,0,0,0;x) - 16\, G(-1,0,0,0;x) - 20\, G(0,-1,0,0;x) + 4\, G(-1,-1,0,0;x) \\ &\quad + 72\, \zeta_2\, G(0,0;x) - 20\, \zeta_2\, G(-1,0;x) - 60\, \zeta_2\, G(0,-1;x) + 12\, \zeta_2\, G(-1,-1;x) \\ &\quad - \tfrac{88}{3}\, \zeta_3\, G(0;x) + 4\, \zeta_3\, G(-1;x) + 87\, \zeta_4. \end{aligned} \tag{21}$$

All coefficients are rational with denominators at most 3. The only singularities of eq. (21) are the two branch points of eq. (17).

Boundary data. No boundary condition is imposed. At each weight we determine the coefficients of eq. (21) as exact rational numbers by an integer-relation fit of the ansatz (18) to numerical values of J.

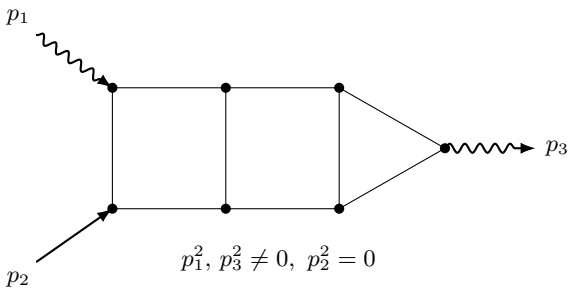

Figure 4: The three-loop triangle ladder $C^{(3)}$ of eq. (23) (No. 4 of Table 1): nine massless lines, two rails of three segments meeting at the p_3 vertex and three rungs. The legs p_1 and p_3 are off shell (wavy). The drawing shows the configuration $p_2^2 \to 0$ of the off-shell ladder function $\Phi^{(3)}(X, Y)$, whose one-variable block $f_3(x)$ of eq. (27) is the function reproduced here.

Checks. The fit used `AMFlow` [95] values at ten Euclidean points, and at the two further points $x = 2/5$ and $x = 3/4$, neither of them used in the fit, eq. (21) agrees with `AMFlow` to at least 89 digits at every order. It also agrees with the closed form of Ref. [109], evaluated with an independent implementation of the polylogarithms, to at least 142 digits through order ε^0. For reference, with $J = \sum_j \varepsilon^j J^{(j)}$ at $s = -1$, we find

$$J^{(0)}\big|_{t=-2/5} = 144.4685602\ldots, \qquad J^{(0)}\big|_{t=-3/4} = -7.244798182\ldots, \tag{22}$$

and the pole coefficients at the same points are listed in Appendix A.

4.3 The three-loop C_5 ladder

The triangle ladder with nine massless lines and three off-shell legs (Figure 4, No. 4 of Table 1) is the $L = 3$ member of the ladder series $C^{(L)}$, which Usyukina and Davydychev evaluated for all L in terms of classical polylogarithms [114]. An operator derivation is given in Ref. [49], an integral representation valid for all L in Ref. [32], and the conformal properties of the series are discussed in Ref. [52]. We include it as a test of the fitting step on a function space where the answer is known, and recover the rational coefficients of the $L = 3$ closed form by an integer-relation fit.

Definition. With loop momenta k_1, k_2, k_3, incoming momenta p_1, p_2 and $p_3 = p_1 + p_2$ outgoing, the nine massless propagators and the ladder function are

$$\begin{gathered} D_1 = (k_1{+}k_2{+}k_3{-}p_1)^2, \quad D_2 = (k_1{+}k_2{+}k_3{+}p_2)^2, \quad D_3 = (k_2{+}k_3{-}p_1)^2, \quad D_4 = (k_3{-}p_1)^2, \\ D_5 = (k_2{+}k_3{+}p_2)^2, \quad D_6 = (k_3{+}p_2)^2, \quad D_7 = k_1^2, \quad D_8 = k_2^2, \quad D_9 = k_3^2, \\ C^{(3)}(p_1^2, p_2^2, p_3^2) = \frac{1}{(p_3^2)^3}\,\Phi^{(3)}(X, Y), \qquad X = \frac{p_1^2}{p_3^2}, \quad Y = \frac{p_2^2}{p_3^2}, \end{gathered} \tag{23}$$

where $C^{(3)}$ is the scalar integral with unit powers of $D_1, \ldots, D_9$ in the measure of eq. (1), and $\Phi^{(3)}$ is dimensionless and finite in four dimensions. We reproduce the one-variable block $f_3(x)$ of eq. (27), related to $\Phi^{(3)}$ at $X = x/(1+x)$, on the half-line $x > 0$, that is $0 < p_1^2 < p_3^2$. We also evaluate the two-variable function $\Phi^{(3)}(X, Y)$ in the region $4XY > (X + Y - 1)^2$.

Function space. For all L the ladder function $\Phi^{(L)}$ has uniform transcendental weight $2L$. In the variables $z, \bar{z}$ with $X = z\bar{z}$ and $Y = (1-z)(1-\bar{z})$, for which $4XY - (X+Y-1)^2 = 4(\mathrm{Im}\, z)^2$, the ladder function is the combination of classical polylogarithms [114, 49]

$$\Phi^{(L)}(z,\bar{z}) = \frac{1}{z-\bar{z}} \sum_{k=0}^{L} c_k^{(L)}\, \ln^k(z\bar{z})\, \big[\mathrm{Li}_{2L-k}(z) - \mathrm{Li}_{2L-k}(\bar{z})\big], \qquad c_k^{(L)} = (-1)^k\, \frac{(2L-k)!}{k!\,(L-k)!}, \tag{24}$$

which is eq. (d4) of Ref. [49]. The one-variable block is a harmonic polylogarithm of weight $2L = 6$ over the two-letter alphabet

$$\mathcal{A}_{C_5} = \{\, x,\ 1+x \,\} \qquad \Longleftrightarrow \qquad \Big\{ \tfrac{dx}{x},\ \tfrac{dx}{1+x} \Big\}, \tag{25}$$

with Goncharov indices $a_i \in \{0, -1\}$ in the notation of eq. (4) [70]. In the variable $x = p_1^2/(p_3^2 - p_1^2)$ the letters x and $1+x$ vanish at $p_1^2 \to 0$ and $p_3^2 \to 0$ respectively, and $p_1^2 = p_3^2$ lies at $x \to \infty$. This alphabet has 2^w words of weight w, that is 64 at $w = 6$.

Result. The holomorphic building block of eq. (24) at $z = -x$, the function of one variable from which the two-variable function is assembled, is the sum of classical polylogarithms

$$f_L(x) = \sum_{k=0}^{L} c_k^{(L)}\, (\ln x)^k\, \mathrm{Li}_{2L-k}(-x), \qquad c_k^{(L)} = (-1)^k\, \frac{(2L-k)!}{k!\,(L-k)!}, \tag{26}$$

and at $L = 3$ the coefficients are $c^{(3)} = \{120, -60, 12, -1\}$,

$$f_3(x) = 120\, \mathrm{Li}_6(-x) - 60\, \ln x\, \mathrm{Li}_5(-x) + 12\, \ln^2 x\, \mathrm{Li}_4(-x) - \ln^3 x\, \mathrm{Li}_3(-x). \tag{27}$$

As Goncharov words, $f_3 = -6\, G(0,0,0,-1,0,0;x) + 6\, G(0,0,-1,0,0,0;x)$. Each word carries a single index -1, and the shuffle-regularized combination collapses to eq. (27), whose singular locus is $x \in \{0, -1, \infty\}$. Equation (26) also gives the one-loop box function at $L = 1$ and the massless double-box function at $L = 2$, with $c^{(2)} = \{12, -6, 1\}$. The relation between f_3 and $\Phi^{(3)}(X,Y)$ at $X = x/(1+x)$ is an algebraic identity and involves no limit, because $\Phi^{(3)}$ diverges as $\ln^3 Y$ when $Y \to 0$. In the small-Y expansion of $(1-X)\,\Phi^{(3)}$ organized in powers of $\Lambda = \ln((1-X)/Y)$, $f_3(x)$ is 3! times the Λ-independent part, with the two constants left by the polylogarithm inversion subtracted.

Boundary data. The prefactor of eq. (23) fixes the normalization of the ladder function, and no boundary point is used. We obtain the coefficients by an integer-relation fit over the full basis of 64 weight-six words $G(a_1, \ldots, a_6; x)$, $a_i \in \{0, -1\}$, to high-precision values of the one-variable block f_3 at points $x \in [0.01, 0.71]$. The fit returns the coefficients -6 and $+6$ of the two words in f_3 and zero for every other word, which is eq. (27) exactly.

Checks. An `AMFlow` [95] evaluation of the nine-line family at $(X,Y) = (\frac{2}{3}, \frac{3}{4})$, a point not used elsewhere, reproduces $\Phi^{(3)}(X,Y)$ of eq. (24) to 72 digits, with every pole coefficient zero. We also evaluated $\Phi^{(3)}$ at $(X,Y) = (\frac{421}{1225}, \frac{596}{1225})$ and $(\frac{424}{225}, \frac{109}{225})$ from eq. (24) and from a one-fold integral representation, which agree to at least 60 digits, and the fitted coefficients reproduce the closed form of Ref. [114] at three further points $x \in \{1/3,\ 2/9,\ 7/9\}$, none of them a fit point, to at least 461 digits at working precision 462. For reference,

$$f_3(11/20) = -87.265091\ldots, \tag{28}$$

and further values of f_3 are listed in Appendix A.

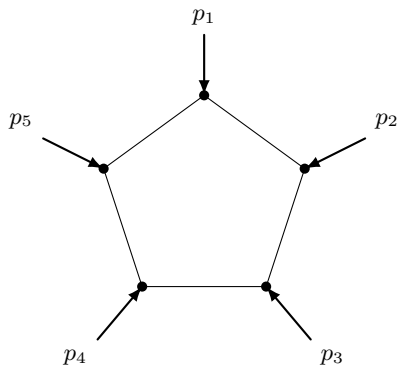

Figure 5: The one-loop scalar pentagon, No. 5 of Table 1: five massless propagators and five massless external legs $p_1, \dots, p_5$, all incoming, with $p_i^2 = 0$ and $\sum_i p_i = 0$. The kinematic variables are the five cyclic invariants $v_i = s_{i,i+1} = (p_i + p_{i+1})^2$, i mod 5.

4.4 The one-loop massless pentagon

The scalar pentagon with massless propagators and massless external legs, Figure 5, is the five-point integral of one-loop massless amplitudes. It is known through order ε^0 [23, 12] in the form given by Bern, Dixon and Kosower, a sum over the five one-mass boxes obtained by contracting one propagator [23]. We restate that result in the cyclic invariants and give the parity-odd symbol that first appears at order ε.

Definition. With all momenta incoming and $q_1 = l$, $q_k = l + p_1 + \cdots + p_{k-1}$, the integral is

$$I_5(v_1, \dots, v_5) = \int \frac{d^{4-2\varepsilon} l}{i\pi^{2-\varepsilon}} \prod_{k=1}^{5} \frac{1}{q_k^2}\,, \qquad v_i = s_{i,i+1} = (p_i + p_{i+1})^2, \quad p_i^2 = 0, \tag{29}$$

with indices taken mod 5 and no factor of $e^{\gamma_E \varepsilon}$ in the measure. We give the result in the Euclidean region $v_i < 0$, where it is real.

Function space. Fifteen rational letters, all linear in the cyclic invariants, form three cyclic orbits of five,

$$\underbrace{v_i}_{\text{self}}, \qquad \underbrace{u_i = v_{i+3} - v_i - v_{i+1} = s_{i,i+2}}_{\text{next-to-adjacent}}, \qquad \underbrace{d_i = v_{i+2} - v_i}_{\mathrm{Li}_2\text{-numerator}}, \qquad i = 1, \dots, 5. \tag{30}$$

One parity-odd letter is built on the Gram determinant,

$$\sqrt{\Delta_5}, \qquad \Delta_5 = \det\!\left(2\, p_i \cdot p_j\right)_{i,j=1}^{4} = \mathrm{tr}_5^2. \tag{31}$$

Through order ε^0 only the rational letters occur. The function is a sum of logarithms and of dilogarithms whose arguments $1 - v_i/v_{i+2}$ involve the difference letters d_i, and it is singular at $v_i = 0$ and at $v_i = v_{i+2}$. The parity-odd branch point $\Delta_5 = 0$ first appears at order ε, where the alphabet of the one-loop family has 21 letters, namely the fifteen rational ones, Δ_5, and five parity-odd ratios $W_i = (a_i - \sqrt{\Delta_5})/(a_i + \sqrt{\Delta_5})$ with a_i quadratic in the v_j. At two loops the planar pentagon functions require the larger 26-letter alphabet of [67, 43]. Over the 21 letters we find that the integrable parity-odd weight-three symbol [71, 54] with physical first entries is

unique once cyclic symmetry is imposed. Of the 9261 weight-three words, 2205 pass the first-entry condition, and the integrable combinations of these span a 601-dimensional space whose parity-odd part has dimension 100. Within this part the symbols invariant under cyclic permutations form a one-dimensional space, and up to normalization the invariant symbol is

$$\begin{aligned}\mathcal{S}_3^{\rm odd} = \sum_{k=0}^{4} \sigma^k \Big[& v_1\otimes d_1\otimes W_2 - v_1\otimes d_1\otimes W_4 + v_1\otimes d_4\otimes W_2 - v_1\otimes d_4\otimes W_5 \\ & + v_1\otimes v_2\otimes W_5 - v_1\otimes v_3\otimes W_2 - v_1\otimes v_4\otimes W_2 + v_1\otimes v_5\otimes W_4 \Big], \\ W_i = \frac{a_i - \sqrt{\Delta_5}}{a_i + \sqrt{\Delta_5}}, \qquad & a_1 = v_1v_2 - v_1v_5 - v_2v_3 + v_3v_4 - v_4v_5, \qquad a_{i+1} = \sigma\, a_i,\end{aligned} \tag{32}$$

where σ is the cyclic shift $v_j \to v_{j+1}$ acting on every index. All 40 terms have coefficients ± 1 and carry a parity-odd letter in the last entry.

Result. In $d = 4-2\varepsilon$ the pentagon reduces to its five one-mass boxes $I_4^{(i)}$, the box with propagator i contracted, plus a remainder proportional to $d-4$,

$$I_5 = -\tfrac{1}{2}\sum_{i=1}^{5} c_i\, I_4^{(i)} + (d-4)\,(\cdots), \qquad c_i = \sum_j (S^{-1})_{ij}, \quad S_{ij} = -\tfrac{1}{2}\,(q_i - q_j)^2. \tag{33}$$

Inserting the one-mass box in d dimensions, we obtain through order ε^0 [23]

$$\begin{aligned} I_5 = r_\Gamma \sum_{j=1}^{5} \frac{1}{v_{j-2}\,v_{j-1}\,v_j} & \left[\frac{(-v_{j-2})(-v_{j-1})(-v_j)}{(-v_{j+1})(-v_{j+2})}\right]^{-\varepsilon} \\ & \times \left[\frac{1}{\varepsilon^2} + 2\,\mathrm{Li}_2\Big(1 - \frac{v_{j+3}}{v_{j+1}}\Big) + 2\,\mathrm{Li}_2\Big(1 - \frac{v_j}{v_{j+2}}\Big) - \frac{\pi^2}{6}\right] + O(\varepsilon), \end{aligned} \tag{34}$$

with $r_\Gamma = \Gamma(1+\varepsilon)\Gamma^2(1-\varepsilon)/\Gamma(1-2\varepsilon)$. The double pole is $\sum_j 1/(v_{j-2}v_{j-1}v_j)$, negative for all $v_i < 0$. Because the five prefactors $1/(v_{j-2}v_{j-1}v_j)$ are distinct rational functions, the order-ε^0 coefficient of I_5 is not $\sqrt{\Delta_5}$ times a single pure function. In particular, the unit-coefficient sum $\sum_i B_i$ of the box functions $B_i = \mathrm{Li}_2(1 - v_i/v_{i+2}) + \mathrm{Li}_2(1 - v_i/v_{i+3}) + \frac{1}{2}\log^2(v_{i+2}/v_{i+3})$ differs from the finite part of the pentagon in every normalization. At order ε the $(d-4)$ remainder contributes through the six-dimensional pentagon $I_5^{D=6}$, which is finite and known in closed form as a one-dimensional integral [86, 48, 84]. The symbol of $\sqrt{\Delta_5}\, I_5^{D=6}$ is the cyclic-invariant parity-odd word $\mathcal{S}_3^{\rm odd}$, up to normalization.

Boundary data. The rational prefactors follow from the reduction and the transcendental functions from the one-mass box of [23], and therefore no constant is fitted in this entry.

Checks. At the Euclidean point $(v_1,\dots,v_5) = (-1,-2,-3,-4,-5)$, where $\Delta_5 = 289 > 0$, the coefficients of ε^{-2}, ε^{-1} and ε^0 in eq. (34) are

$$I_5\big|_{(-1,-2,-3,-4,-5)}: \qquad -\tfrac{3}{8}, \qquad 0.1798058444\ldots, \qquad 0.2872248726\ldots\,. \tag{35}$$

These three coefficients agree with `AMFlow` [95] to 68 digits, the precision to which two `AMFlow` runs of the massless family at this point confirm each other, and to 107 with the more precise run; at

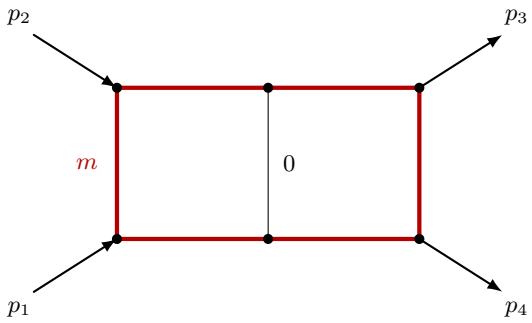

Figure 6: The outer-mass planar double box, No. 1 of Table 1. The six perimeter propagators carry a common mass m (thick red), while the central rung and the four external legs are massless (thin black), $p_i^2 = 0$. The invariants are $s = (p_1+p_2)^2$ and $t = (p_2+p_3)^2$, and the results are written in $u = 4m^2/(-s)$ and $v = 4m^2/(-t)$.

twelve further Euclidean points we find agreement to 67. As a test of the fitting step, we also fitted five integer coefficients of the functions B_i to their analytic sum sampled at 25 Euclidean points. The fit returns unit coefficients and reproduces that sum to 60 digits at three points not used in it, which compares the fit with the analytic box functions of [23] and does not determine the prefactors of eq. (34). Finally, at order ε we checked that `AMFlow` values of the pentagon, of its five boxes and of the six-dimensional pentagon at thirteen Euclidean points satisfy the dimension-shift relation to one part in 10^{58}.

4.5 The outer-mass double box

The planar double box with six massive perimeter propagators and a massless central rung, Figure 6, is finite in four dimensions and, once its leading singularity is divided out, evaluates to a weight-four polylogarithm. It was computed by Caron-Huot and Henn [40], its alphabet, maximal cuts and symbol were derived from the Landau equations in [74], and it was evaluated by regression from numerical samples in [18]. We reproduce the known symbol as a single element of a constrained weight-four basis, without using the symbol of [40] as input.

Definition. With all momenta incoming, $p_4 = -p_1 - p_2 - p_3$, the seven propagators and the kinematic variables are

$$\begin{gathered} D_1 = k_1^2 - m^2, \quad D_2 = (k_1+p_1)^2 - m^2, \quad D_3 = (k_1+p_1+p_2)^2 - m^2, \quad D_4 = k_2^2 - m^2, \\ D_5 = (k_2+p_1+p_2)^2 - m^2, \quad D_6 = (k_2+p_1+p_2+p_3)^2 - m^2, \quad D_7 = (k_1-k_2)^2, \\ p_i^2 = 0, \qquad s = (p_1+p_2)^2, \quad t = (p_2+p_3)^2, \qquad u = \frac{4m^2}{-s}, \quad v = \frac{4m^2}{-t}\,. \end{gathered} \tag{36}$$

We denote by I_{db} the scalar member of this family with unit powers of $D_1, \ldots, D_7$, taken in $d = 4$, where it is finite, and normalized as in [40]. We set $m = 1$ and work at Euclidean $s, t < 0$, that is $u, v > 0$, where eq. (41) holds as a function of both variables.

Function space. Three square roots in the kinematic variables enter the alphabet as algebraic letters,

$$\beta_u = \sqrt{1+u}, \qquad \beta_v = \sqrt{1+v}, \qquad \beta_{uv} = \sqrt{1+u+v}. \tag{37}$$

We rationalize them simultaneously by $u=(1-w^2)(1-z^2)/(w-z)^2$, $v=4wz/(w-z)^2$, so that $\beta_u=(1-wz)/(w-z)$, $\beta_v=(w+z)/(w-z)$ and $\beta_{uv}=(1+wz)/(w-z)$. The region $u,v>0$ maps to $0<z<w<1$, and the function is an ordinary multiple polylogarithm in w and z. Its symbol alphabet consists of the twelve letters $L_1,\dots,L_{12}$ of [74, Tab. II], each a monomial in the twelve factors

$$\{\,w,\ z,\ 1{-}w,\ 1{+}w,\ 1{-}z,\ 1{+}z,\ w{-}z,\ w{+}z,\ 1{-}wz,\ 1{+}wz,\ 1{-}w{+}z{+}wz,\ 1{+}w{-}z{+}wz\,\},$$

namely

$$\begin{aligned}
&L_1=u, && L_2=v, && L_3=1{+}u, && L_4=1{+}v,\\
&L_5=u{+}v, && L_6=\frac{\beta_u-1}{\beta_u+1}, && L_7=\frac{\beta_v-1}{\beta_v+1}, && L_8=\frac{\beta_{uv}-1}{\beta_{uv}+1},\\
&L_9=\frac{\beta_{uv}-\beta_u}{\beta_{uv}+\beta_u}, && L_{10}=\frac{\beta_{uv}-\beta_v}{\beta_{uv}+\beta_v}, && L_{11}=1{+}u{+}v, && L_{12}=\frac{\beta_{uv}-\beta_u\beta_v}{\beta_{uv}+\beta_u\beta_v}.
\end{aligned} \tag{38}$$

Here β_v enters only through L_7, L_{10} and L_{12}, and each letter is defined only up to a constant factor, which drops out of the symbol. The function is singular only on the Landau loci of the graph: on the physical sheet the normal thresholds $s=4m^2$ and $t=4m^2$ ($1{+}u=0$, $1{+}v=0$) and $s,t\to\infty$ ($u,v\to0$); on other sheets also $s=0$, $t=0$ ($u,v\to\infty$), $s+t=0$ ($u{+}v=0$) and the pseudo-threshold $st=4m^2(s+t)$ ($1{+}u{+}v=0$). On the physical sheet it vanishes as $u,v\to\infty$, and this limit is the boundary condition used below.

On the weight-four words over the twelve letters we impose three conditions, none of which uses the maximal cuts of [74]. The first is integrability of the symbol [71, 54]. The second restricts the first entry to the seven branch-cut combinations

$$\{\,L_1/L_3,\ \ L_2/L_4,\ \ L_3L_8/(L_5L_{10}),\ \ L_4L_8/(L_5L_9),\ \ L_6,\ \ L_7,\ \ L_{12}\,\}, \tag{39}$$

which lets only the thresholds in s and t and the pseudo-thresholds open a cut. The third is the square-root parity $(\sigma_u,\sigma_v,\sigma_{uv})=(1,0,1)$ of the function multiplying $1/(\beta_u\beta_{uv})$, odd under $\beta_u\to-\beta_u$ and $\beta_{uv}\to-\beta_{uv}$ and even under $\beta_v\to-\beta_v$. These three conditions reduce the weight-four space to a 161-dimensional subspace with basis $\{G_a\}$.

Result. We write $g_{10}=\mathrm{LS}\cdot\sum_{a=1}^{161}c_a\,G_a$, with the normalized function g_{10} and the leading singularity LS as defined in eq. (41), and determine the c_a by an integer-relation fit [16] to `AMFlow` values [95] on a Euclidean grid. We find a single nonzero coefficient, with height and denominator both equal to one,

$$c_a=\delta_{a,52},\qquad c_{52}=1. \tag{40}$$

The normalized weight-four function is then the leading singularity times one basis element,

$$g_{10}\ =\ -\tfrac{1}{8}\,s^2\,t\,\beta_u\,\beta_{uv}\,I_{\mathrm{db}}\ =\ \mathrm{LS}\cdot G_{52},\qquad \mathrm{LS}=\tfrac{1}{8}\sqrt{s\,(s-4m^2)}\,\sqrt{s\,t\,(s\,t-4m^2(s+t))}\,, \tag{41}$$

and its symbol, written in the letters $L_1,\dots,L_{12}$, is the eighteen-term word

$$\begin{aligned}
\mathcal{S}(G_{52})=\ &-L_6{\otimes}L_1{\otimes}L_6{\otimes}L_9+L_6{\otimes}L_3{\otimes}L_6{\otimes}L_9-L_6{\otimes}L_1{\otimes}L_9{\otimes}L_6+L_6{\otimes}L_3{\otimes}L_9{\otimes}L_6\\
&+L_6{\otimes}L_6{\otimes}L_1{\otimes}L_9+L_6{\otimes}L_6{\otimes}L_2{\otimes}L_9-L_6{\otimes}L_6{\otimes}L_3{\otimes}L_9-L_6{\otimes}L_6{\otimes}L_5{\otimes}L_9\\
&+L_6{\otimes}L_9{\otimes}L_2{\otimes}L_6-L_6{\otimes}L_9{\otimes}L_5{\otimes}L_6+L_6{\otimes}L_6{\otimes}L_8{\otimes}L_6+L_6{\otimes}L_9{\otimes}L_8{\otimes}L_9\\
&+L_7{\otimes}L_{10}{\otimes}L_2{\otimes}L_6-L_7{\otimes}L_{10}{\otimes}L_5{\otimes}L_6+L_7{\otimes}L_{10}{\otimes}L_8{\otimes}L_9\\
&+L_7{\otimes}L_7{\otimes}L_1{\otimes}L_9-L_7{\otimes}L_7{\otimes}L_5{\otimes}L_9+L_7{\otimes}L_7{\otimes}L_8{\otimes}L_6.
\end{aligned} \tag{42}$$

The word (42) coincides term by term with the symbol of [40, 74].

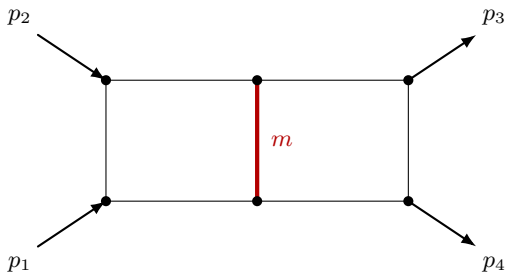

Figure 7: The central-mass double box, No. 7 of Table 1: a planar two-loop four-point graph with massless external legs, $p_i^2 = 0$, six massless propagators (thin black) and a single propagator of mass m on the central rung (thick red). The invariants are $s = (p_1{+}p_2)^2$ and $t = (p_2{+}p_3)^2$, and the results are quoted at $m^2 = 1$.

Boundary data. We obtain the function G_{52} from eq. (42) by iterated integration in w and z from the line $w = z$, which is the limit $u, v \to \infty$ where g_{10} vanishes. Because every first-entry letter equals one on that line, the integration converges and introduces no constant beyond the symbol.

Checks. Two reference values of g_{10}, for comparison with an independent integration of eq. (42) or with the ancillary file of [40], are

$$g_{10}\Big(u{=}\tfrac{16}{3},\, v{=}\tfrac{10}{3}\Big) = 0.043932114\ldots, \qquad g_{10}(u{=}v{=}4) = 0.053038629\ldots, \tag{43}$$

the second being the value at $u = v = 4$ quoted in [40]. Equation (41) agrees with `AMFlow` [95] to at least 86 digits at the four Euclidean points $(u, v) \in \{(16/3, 10/3), (10/3, 16/3), (23/4, 9/4), (5/2, 4)\}$, none of which was used in the fit.

4.6 The central-mass double box

The planar double box with massless external legs and one massive propagator on the central rung, Figure 7, is the γ-Z-γ ladder of electroweak Møller and Bhabha scattering at next-to-next-to-leading order. Likewise, it is the g-V-g ladder of mixed QCD-electroweak four-fermion scattering. It has seven propagators and three scales $\{s, t, m^2\}$, and it reaches transcendental weight four. The family is topology C of Schwanemann and Weinzierl [104], who give all nineteen of its master integrals in multiple polylogarithms through weight four. The scalar top-sector integral computed here, one of three masters in the top sector, equals their canonical master J^C_{17} up to the factor $(s/m^2)^{2\varepsilon}$ and the normalization of eq. (44). Its alphabet is seven rational letters with no square root, and our result agrees with theirs exactly at weights one and two and numerically through weight four. We derive the result from the family's own reduction and from integer-relation fits, without using the expressions of [104] as input.

Definition. With all momenta incoming, the propagators and the normalized function are

$$\begin{gathered} D_1 = k_1^2, \quad D_2 = (k_1+p_1)^2, \quad D_3 = (k_1+p_1+p_2)^2, \quad D_4 = k_2^2, \\ D_5 = (k_2+p_1+p_2)^2, \quad D_6 = (k_2+p_1+p_2+p_3)^2, \quad D_7 = (k_1-k_2)^2 - m^2, \\ p_i^2 = 0, \qquad s = (p_1+p_2)^2, \quad t = (p_2+p_3)^2, \\ g(\varepsilon) = \sum_{w\geq 0} g^{(w)}\varepsilon^w = R\,\varepsilon^4 e^{2\varepsilon\gamma_E} J, \qquad R = s^2\,(t-m^2), \end{gathered} \tag{44}$$

where J is the scalar integral with unit powers of $D_1, \ldots, D_7$ in $d = 4 - 2\varepsilon$ and the measure is normalized so that $g^{(0)} = 1$ exactly. We set $m^2 = 1$ and give $g^{(1)}, \ldots, g^{(4)}$ as functions of both s and t on the Euclidean sheet $s, t < 0$.

Function space. The family has no algebraic letter, since its canonical differential equation is rational [104, 76]. The alphabet of the top-sector integral through weight four is the seven letters

$$\mathcal{A} = \Big\{ s,\ \ t,\ \ s+t,\ \ s+1,\ \ 1-s,\ \ 1-t,\ \ s+t-st \Big\} \qquad (m^2 = 1), \tag{45}$$

the last letter being $m^2(s+t) - st$ for general mass. All seven are faces of the principal A-determinant of the Lee–Pomeransky polynomial [94]. They coincide with the ε-form alphabet of the nineteen-master family, whose eight letters $e_1, \ldots, e_8$ in [104] reduce to the seven d log forms of eq. (45) at fixed m^2 and μ^2. The first-entry set is $\{s,\ 1-s,\ 1-t\}$, and the function is singular where one of the letters of eq. (45) vanishes. At weight two only the six letters $\{s, t, s+1, 1-s, 1-t,\ s+t-st\}$ occur, and $s+t$ first enters at weight three.

We reduce the family with `Kira` [81] to nineteen master integrals. We then constrain a weight-graded ansatz for the $g^{(w)}$ by three exact conditions: every word is built from the seven letters of $\mathcal{A}$, the symbol is integrable, and its first entries lie in $\{s, 1-s, 1-t\}$ [71, 54]. The remaining rational coefficients are fixed by integer-relation fits [16] to `AMFlow` values [95]. At weight three these conditions, together with matching to the symbol on the slice $s = -1$ (determined separately over the slice alphabet $\{t,\ t-1,\ 2t-1\}$), reduce a 281-column ansatz to 42 free coefficients. A weighted least-squares fit to 204 high-precision values then determines all 42 as rationals.

Result. Through weight two the pure function is

$$g^{(0)} = 1 \qquad \text{(exact integer)}, \tag{46}$$

$$g^{(1)} = -2\log(-s) \ - \ 4\log(1-t), \tag{47}$$

$$\begin{aligned} g^{(2)} = {} & 2\log^2(-s) \ - \ 2\log(-s)\log(s+1) \ + \ 8\log(-s)\log(1-t) \ + \ 8\log^2(1-t) \\ & - \ 2\,\mathrm{Li}_2(-s) \ + \ 10\,\mathrm{Li}_2(t) \ + \ 2\,\mathrm{Li}_2(s+t-st) \ - \ \tfrac{1}{6}\pi^2, \end{aligned} \tag{48}$$

where all coefficients are rational and $g^{(2)}$ has eight terms. At weights three and four we use a fibration basis. Its elements are Goncharov polylogarithms $G(\vec{a}; x)$ in $x = -t$ with letters drawn from $\{0,\ -1,\ s,\ s/(1-s)\}$, the d log images of t, $1-t$, $s+t$ and $s+t-st$, times $G(\vec{b}; y)$ in $y = -s$ with letters from $\{0, 1, -1\}$, the images of s, $s+1$ and $1-s$. Powers of logarithms and $\zeta_2, \zeta_3, \zeta_4$ multiply these products. In this basis we obtain $g^{(3)}$ as a list of 39 nonzero terms with coefficients in the ring $\mathbb{Q}[\zeta_2, \zeta_3]$ whose rational parts have height at most 65. For $g^{(4)}$ we obtain a t-dependent part of 123 terms with denominators in $\{1, 3\}$ plus a t-independent remainder of 29 terms with denominators in $\{1, 3, 4\}$. Both lists are printed in Appendix B and supplied with exact rational coefficients as a data file [106] (Appendix G).

Boundary data. Every constant is classical, namely $-\frac{1}{6}\pi^2$ at weight two, ζ_2 and ζ_3 at weight three, and $\zeta_2, \zeta_3, \zeta_4$ at weight four; the integer-relation fits that produce $g^{(2)}, \ldots, g^{(4)}$ also determine the rational coefficient multiplying each constant. The data for all fits are `AMFlow` values [95], and the fit of the t-independent weight-four remainder uses values at 44 additional points.

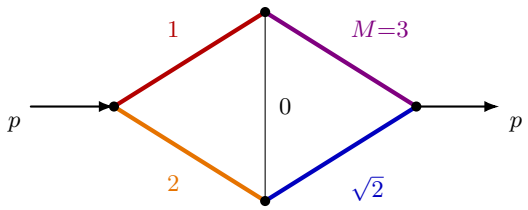

Figure 8: The four-mass kite with a massless rung (No. 23 of Table 1). The external momentum p enters at the left vertex and leaves at the right one. The left rim carries the masses m_1=1 (red) and m_2=2 (orange), the right rim M=3 (violet) and m_3=$\sqrt{2}$ (blue), and the thin line joining the two internal vertices is massless, so the squared masses are $(1, 4, 9, 2, 0)$.

Checks. The weight ≤ 2 forms agree with `AMFlow` [95] to 108 digits on the eight slices $s = -\frac{7}{2}$, -3, $-\frac{5}{2}$, $-\frac{3}{2}$, $-\frac{4}{5}$, $-\frac{2}{3}$, $-\frac{1}{2}$, $-\frac{1}{3}$, four of which, $s = -\frac{7}{2}$, -3, $-\frac{5}{2}$ and $-\frac{3}{2}$, were excluded from every fit. On those four slices the weight-three and weight-four forms agree with `AMFlow` at all twenty points to at least 109. Moreover, at the further point $(s, t) = (-4, -2)$, off every slice, the five Laurent coefficients $\varepsilon^{-4}, \ldots, \varepsilon^{0}$ of the top-sector integral obtained from the closed forms agree with `AMFlow` to at least 129. On the $s + i0$ sheet, $(s/m^2)^{2\varepsilon} g(\varepsilon)$ reproduces the published J^C_{17} of [104] identically at weights one and two and to the working precision through weight four at two Euclidean points. In the limit $s, t \to 0$ at fixed m the massive rung shrinks to a point and the graph factorizes into two one-loop triangles,

$$g(\varepsilon) \;\longrightarrow\; \left[e^{\gamma_E \varepsilon}\,\Gamma(1+\varepsilon)\Gamma(1-\varepsilon)^2/\Gamma(1-2\varepsilon)\right]^2 (-s)^{-2\varepsilon}. \tag{49}$$

At $s = t = -\lambda$, $\lambda \to 0^+$, we find that the difference between the closed forms and this limit vanishes with λ at every weight through four. We also integrate an ε-form differential equation in t at fixed $s = -1$ whose connection is built from the same reduction with no numerical input. Transported along a Euclidean path from a numerical boundary value at $t_0 = -1/3$, its solution reproduces the closed forms at weights two through four to at least 37 digits.

4.7 The four-mass kite with a massless rung

The kite of Figure 8 is a two-loop self-energy with five propagators, namely four rim lines of distinct mass and a massless line joining the two internal vertices. Kites with massive lines are standard examples of two-point integrals that evaluate to elliptic functions [20, 102, 5, 35, 69]. We place this kite among the polylogarithmic entries because every one of its subtopologies has a genus-zero maximal cut. At the mass assignment of eq. (50) the entry, No. 23, is to our knowledge new.

Definition. In the notation of eq. (1), with $d = 4 - 2\varepsilon$ and $t = p^2$, the propagators and the top integral are

$$\begin{gathered} D_1 = k_1^2 - 1, \quad D_2 = (k_1 - p)^2 - 4, \quad D_3 = k_2^2 - 9, \quad D_4 = (k_2 - p)^2 - 2, \quad D_5 = (k_1 - k_2)^2, \\ \mathrm{TOP}(t) \equiv I_{1,1,1,1,1}(4 - 2\varepsilon;\, t;\, 1, 4, 9, 2, 0), \end{gathered} \tag{50}$$

where D_1, D_2 form the left bubble of Figure 8, D_3, D_4 the right bubble, and D_5 is the rung. The two three-line cuts through D_5 are $\{D_1, D_4, D_5\}$, with squared masses $(1, 2, 0)$, and $\{D_2, D_3, D_5\}$, with $(4, 9, 0)$. We reduce the family with `Kira` [81] to 22 master integrals, of which the top sector contributes the single integral TOP. We give the result at the squared masses $(1, 4, 9, 2, 0)$ of eq. (50) for spacelike momentum, $t < 0$, as a function of t on that half-line. The comparisons below use seven points on it and a second mass assignment, $(1, 4, 9, 3, 0)$.

Function space. Both three-line cuts contain the massless line D_5. A sunrise with one massless line has a genus-zero maximal cut, because the Källén function of the pair containing the massless line is a perfect square and only a quadratic remains under the root. Without D_5 the two loops decouple, and the massive triple $(1,4,9)$, for example, is the product of the left bubble and the tadpole of mass 3. No subtopology therefore defines an elliptic curve. The differential equation in t that we derive from the reduction has a connection singular at

$$t \in \Big\{ 0,\ 1,\ 9,\ 25,\ \tfrac{85}{4},\ 3 \pm 2\sqrt{2},\ 11 \pm 6\sqrt{2} \Big\}, \tag{51}$$

with no pole on the negative axis. Its rational letters are

$$\{\, t,\ t-1,\ t-9,\ t-25,\ 85-4t,\ t^2-6t+1,\ t^2-22t+49 \,\}, \tag{52}$$

seven polynomials irreducible over $\mathbb{Q}$, and no other denominator occurs in the connection. The two quadratics split over $\mathbb{Q}(\sqrt{2})$, and their zeros are the threshold and pseudo-threshold $3 \pm 2\sqrt{2}$ of the $(1,0,\sqrt{2})$ cut and $11 \pm 6\sqrt{2}$ of the $(3,\sqrt{2})$ bubble. Among the zeros of the linear letters, $t = 9$ and $t = 25$ are the thresholds of the $(1,2)$ bubble and of the $(2,0,3)$ cut, $t = 1$ is their common pseudo-threshold, and $t = 85/4$ is a Landau point of the kite itself. The algebraic letters are the four square roots

$$\sqrt{(t-1)(t-9)}, \qquad \sqrt{(t-1)(t-25)}, \qquad \sqrt{t^2-6t+1}, \qquad \sqrt{t^2-22t+49} \tag{53}$$

of the two bubbles and the two cuts, and no coupled block of the connection is larger than 3×3. Whether the top master is a multiple polylogarithm over these roots is not decided here. We give it as an iterated integral with kernels rational in the letters (52) and boundary data built from Γ functions.

Result. In the top sector the diagonal entry of the connection is $(\varepsilon-1)/t - 4\varepsilon/(4t-85)$, which integrates to $H(t) = t^{\varepsilon-1}(1-4t/85)^{-\varepsilon}$. Since $H(t)$ is unbounded at $t = 0$ and TOP is bounded at this vacuum point, the homogeneous term is absent and we obtain the convergent integral

$$\mathrm{TOP}(t) \;=\; H(t) \int_0^t H(u)^{-1}\, R(u)\, du, \qquad R \;=\; \textstyle\sum_{j \neq 21} A_{21,j}(\varepsilon, u)\, M_j(u). \tag{54}$$

Here $A(\varepsilon, u)$ is the connection matrix of the 22 masters, in a basis with TOP as master 21, and the sum runs over the subsector masters M_j. Each subsector master M_j satisfies an equation of the same form, with its own subsector masters in the inhomogeneous term and kernels rational in the letters (52). Its homogeneous constant is again set to zero by boundedness at $u = 0$, and the innermost constants are built from the tadpole T_1 and the vacuum sunset $T(a,b,0)$ of eq. (57) below. Iterating eq. (54) gives $4t\,\mathrm{TOP}_{\varepsilon^0}(t)$ as a sum of iterated integrals with these kernels; the individual terms are listed with the evaluation code (Appendix G). Alternatively, the top integral at $t = 0$ can be written as a single integral over Bessel functions,

$$\mathrm{TOP}(0) = -\tfrac{8}{21} \int_0^\infty \frac{dx}{x} \left[K_1(x) - 2K_1(2x)\right] \left[\sqrt{2}\, K_1(\sqrt{2}\, x) - 3K_1(3x)\right] = -0.2910157568\ldots, \tag{55}$$

the second mass difference of the coordinate-space vacuum sunset with one massless line, in agreement with the value assembled from eq. (57).

Boundary data. We fix the solution analytically at the vacuum point $t = 0$, without numerical input. The residue matrix $A_{-1} = \mathrm{Res}_{t=0} A$ of the connection has the eigenvalues

$$\{\, 0 \ (\times 8), \quad -1 + \varepsilon \ (\times 13), \quad -2 + 2\varepsilon \ (\times 1) \,\}, \tag{56}$$

none of them a positive integer. Every non-analytic local solution is therefore unbounded at $t = 0$, and the physical solution is the unique analytic one. The Frobenius recursion $(n\,\mathbf{1} - A_{-1})\, a_n = \sum_{m<n} A_{n-1-m}\, a_m$ then determines it from its value at $t = 0$. To obtain that value we apply partial fractions to the propagator pairs that are degenerate at $t = 0$ and reduce all 22 masters to two-loop vacuum integrals [30], namely products of tadpoles $T_1(m^2) = -\Gamma(-1+\varepsilon)(m^2)^{1-\varepsilon}$ and the vacuum sunset with one massless line. For the latter we derive from a Mellin–Barnes representation, collapsed with $\Gamma(1-\varepsilon-n)\Gamma(n+\varepsilon) = (-1)^n \Gamma(\varepsilon)\Gamma(1-\varepsilon)$, the closed form

$$T(a,b,0) \;=\; -\,\frac{\Gamma(\varepsilon)\Gamma(1-\varepsilon)}{1-\varepsilon}\, a^{1-2\varepsilon}\Big[\,\Gamma(2\varepsilon-1)\,(1-r)^{1-2\varepsilon} \;-\; r^{1-\varepsilon}\,\frac{\Gamma(\varepsilon)}{\Gamma(2-\varepsilon)}\,{}_2F_1(\varepsilon,1;2-\varepsilon;r)\,\Big], \tag{57}$$

with $r = b/a$ for internal squared masses a and b. Its ε expansion contains only logarithms and dilogarithms.

Checks. We compared $\mathrm{TOP}_{\varepsilon^0}$ with `AMFlow` [95] at the seven points $t = -1, -2, -3, -4, -5, -6, -8$, none of which enters the construction. The agreement ranges from 81 to 110 digits and is limited by the precision of the `AMFlow` values. Two of the values are

$$\mathrm{TOP}_{\varepsilon^0}(-1) = -0.27540984\ldots, \qquad \mathrm{TOP}_{\varepsilon^0}(-8) = -0.20336554\ldots, \tag{58}$$

and Appendix A lists the rest. The construction does not depend on the value of m_3: at the squared masses $(1, 4, 9, 3, 0)$ the reduction again has 22 masters, the singular points that move are $85/4 \to 297/8$, $3 \pm 2\sqrt{2} \to (1 \pm \sqrt{3})^2$ and $11 \pm 6\sqrt{2} \to (3 \pm \sqrt{3})^2$, and the boundary argument is unchanged. There the same construction reproduces `AMFlow` at the two points $t = -2$ and $t = -7/3$ to 98 digits.

4.8 The nonplanar hexa-box with two equal-mass legs

Two-loop five-point integrals with two massive external legs are master integrals for diboson-plus-jet production at NNLO, W^+W^-+jet and WZ+jet. The planar two-mass families are known [3], as are the massless pentagon functions [43, 2] and the one-mass nonplanar hexa-boxes [80]. To our knowledge no two-mass nonplanar family has been computed. The hexa-box graph admits inequivalent placements of the two massive legs. We solve the simplest of them, with equal masses on the non-adjacent legs p_1 and p_3 (Figure 9, top); it is No. 24 of Table 1 and is new. The placement with adjacent massive legs, which carries the two-mass threshold of the diboson amplitudes, is not solved, and we summarize what is known about it and about the generic-mass families at the end of this section.

Definition. In the notation of eq. (1), with $d = 4 - 2\varepsilon$, the eight denominators of the top sector are massless,

$$\begin{gathered} D_1 = k_1^2, \quad D_2 = k_2^2, \quad D_3 = (k_1 - k_2 + p_4)^2, \quad D_4 = (k_2 - p_4)^2, \quad D_5 = (k_1 - p_5)^2, \\ D_6 = (k_1 - k_2 - p_5)^2, \quad D_7 = (k_1 - k_2 + p_2 + p_3 + p_4)^2, \quad D_8 = (k_1 - k_2 + p_3 + p_4)^2, \\ p_1^2 = p_3^2 = m^2, \qquad p_2^2 = p_4^2 = p_5^2 = 0, \end{gathered} \tag{59}$$

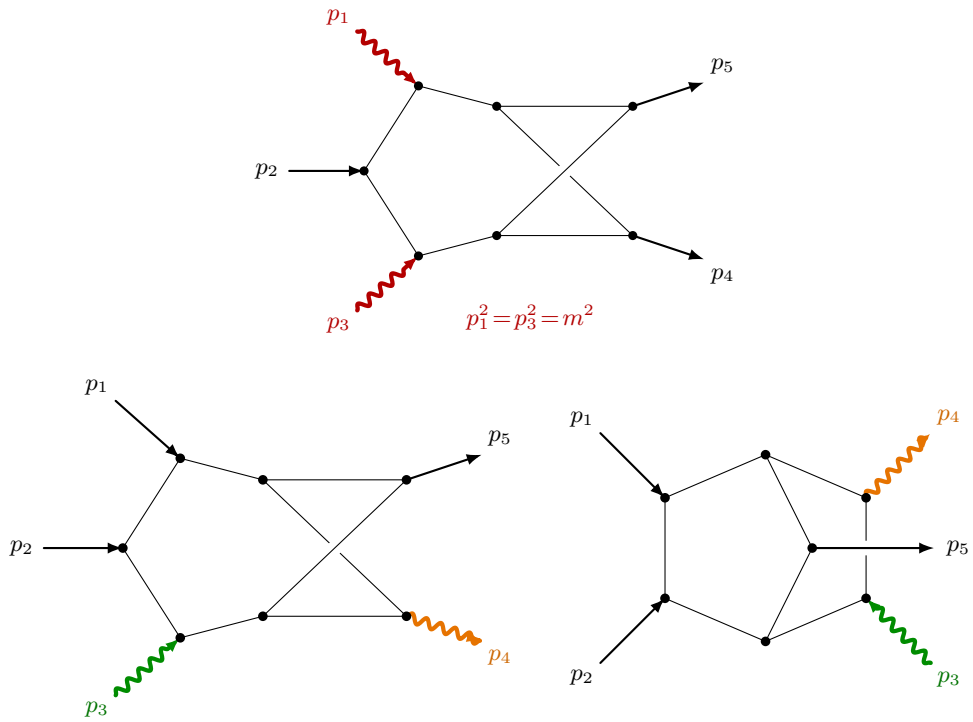

(a) non-planar pentagon-box (hexa-box) (b) non-planar double-pentagon

Figure 9: Two-loop five-point nonplanar graphs with two off-shell legs. All internal lines are massless, and the crossed line is drawn without a vertex at the crossing. Top: the hexa-box of No. 24, with equal-mass legs $p_1^2 = p_3^2 = m^2$ (red, wavy) at non-adjacent positions and p_2, p_4, p_5 massless. Bottom: (a) the hexa-box and (b) the double-pentagon with adjacent off-shell legs $p_3^2 = M_3$ (green) and $p_4^2 = M_4$ (orange), which are not computed here.

and the family is completed by irreducible scalar products in the numerator. It depends on the six scales $\{s_{12}, s_{23}, s_{34}, s_{45}, s_{15}, m^2\}$. We reduce it with `Kira` [81] to 98 master integrals in 62 sectors. Of these, 76 belong to one-mass five-point and two-mass four-point subtopologies that are known, and they enter only as boundary data. The 22 new masters reduce under the reflection σ that exchanges p_1 and p_3 to six sector orbits with 13 representatives, three of them in the top sector. Our results hold along straight segments in the six-scale space and give the masters as functions of the segment parameter; they are not yet functions of all six invariants. The three segments are

$$\begin{aligned}
&\text{I:} \quad (s_{12}, s_{23}, s_{34}) = (-3, -5, -7), \quad s_{45} = -2 - 9t, \quad s_{15} = -11 - 6t, \quad m^2 = 1 + t, \quad 0 \le t \le 1, \\
&\text{II:} \quad \text{all six scales varied (subsector orbits only)}, \\
&\text{III:} \quad (s_{45}, s_{15}, m^2) = (-2, -11, 1) \text{ fixed}, \quad P_0 \;\to\; P_3 = (-5, -7, -9, -2, -11, 1),
\end{aligned} \tag{60}$$

where segments I and III start at the Euclidean point $P_0 = (s_{12}, s_{23}, s_{34}, s_{45}, s_{15}, m^2) = (-3, -5, -7, -2, -11, 1)$, the point $t = 0$ of segment I, and segment II includes detours into the complex t plane around poles of the connection. We give the three top-sector masters on segment I as Laurent series in ε and on segment III at fixed d, and the five subsector orbits on all three segments.

Function space. From a Landau analysis of the two-mass hexa-box families by the principal A-determinant [97, 63, 74] we obtain exactly two square-root letters,

$$R_1 = \Delta_5 = \sqrt{\det \mathrm{Gram}_5} \text{ (the parity-odd } \mathrm{tr}_5), \qquad R_2 = r_{34} = \sqrt{\lambda(s_{34}, M_3, M_4)}, \tag{61}$$

with λ the Källén function, M_3, M_4 the squared masses of adjacent legs p_3, p_4, and Δ_5 the root itself, written $\sqrt{\Delta_5}$ in section 4.4. The root R_2 arises in the channel that contains both massive legs and is present only when they are adjacent. Both roots rationalize, R_2 under $s_{34} = M_3 + M_4 - \sqrt{M_3 M_4}\,(z + 1/z)$ and R_1 in the five-point momentum-twistor parametrization [2], and therefore the maximal cuts are genus zero and the families are polylogarithmic [71, 54]. For the non-adjacent placement (59) the root R_2 is absent, since $\lambda(s_{34}, m^2, 0)$ is a perfect square, while the Gram root R_1 is present and does not rationalize on segment I. There $\mathrm{Gram}_5 = \det(2\, p_i \cdot p_j)_{i,j\le 4}$ restricts to the irreducible quartic

$$Q_4(t) = 3721t^4 + 6724t^3 + 11824t^2 + 16400t + 7040, \qquad Q_4(0) = 7040, \quad Q_4(1) = 45709, \tag{62}$$

whose zero set on the segment is the second-type (Gram) Landau locus of the eight-propagator sector. The homogeneous solution of the top block carries $\sqrt{Q_4}$ with indicial exponents $(\frac{1}{2}, \frac{1}{2}, 0)$.

A canonical ε-form [76] of the 98-master system on segment I is obstructed by half-integer exponents like those of the top block. In 8 of its 31 diagonal blocks the ε^0 eigenvalues at irreducible quadratic letters are half-integers, and an ε-factorized basis would then itself carry the square roots of those letters as prefactors. Constant rational balances [93] bring at most 17 of the 31 blocks to ε-factorized form, and only 2 of the 16 blocks linear in ε are in $\mathrm{d}\log$ form. We therefore keep the radicals, write the connection as $A = \sum_m \varepsilon^m A^{(m)}$ and the masters as $y_i = \sum_k \varepsilon^k y_{i,k}$, and solve the graded system

$$y'_{i,k}(t) = \sum_{j,m} A^{(m)}_{ij}(t)\, y_{j,k-m}(t) \tag{63}$$

layer by layer in k by variation of parameters. We express the solutions in the form

$$F(t) = \sum C \cdot \sqrt{\mathrm{rad}} \cdot R(t) \cdot G_{\mathrm{word}}(t), \tag{64}$$

a sum of products of a boundary constant C, a radical monomial $\sqrt{\mathrm{rad}}$ continued along a fixed contour above the real axis, a rational function $R(t)$, and an iterated integral G_{word} over $\mathrm{d}\log$, rational and algebraic kernels. This class is closed under sums, products, d/dt and $\int_0^t$, the only operations that the recursion uses, and every kernel $A^{(m)}_{ij}(t)$ that enters is an exact rational function of t.

Result. On segment I the ε^{-4} coefficients of the three top-sector masters are rational in the kinematics. With $s_{35} = m^2 + s_{12} - s_{34} - s_{45} = 7 + 10t$, $s_{14} = m^2 + s_{23} - s_{15} - s_{45} = 9 + 16t$ and

$$D(t) = m^2\,(-s_{15})\, s_{45}^2\, s_{35}\, s_{14} = (t+1)(6t+11)(9t+2)^2(10t+7)(16t+9), \tag{65}$$

they are

$$\begin{aligned}
&-\frac{12840\,t^3 + 40093\,t^2 + 34960\,t + 9177}{105\,D(t)},\\
&\frac{183840\,t^4 + 915198\,t^3 + 1564973\,t^2 + 1055732\,t + 240492}{420\,D(t)},\\
&-\frac{1227360\,t^5 + 8249742\,t^4 + 21107169\,t^3 + 25290010\,t^2 + 13922056\,t + 2808708}{420\,D(t)},
\end{aligned} \tag{66}$$

where $105 = -s_{12}s_{23}s_{34}$. These functions satisfy the top-sector rows of eq. (63) identically and take the values $-571/1079925$, $46591/8639400$ and $-854177/8639400$ at $t = 1$. We obtain the ε^{-3} coefficients as fully expanded symbolic expressions of the form (64), and the ε^{-2}, ε^{-1} and ε^{0} coefficients as layered iterated integrals of the same form, with the exact rational $A_{ij}^{(m)}(t)$ as kernels and $\sqrt{Q_4}$ as the algebraic prefactor. We find that the $\sqrt{Q_4}$-odd part of the finite coefficients is of order one at $t = 1$, so the radical cannot be absorbed into a normalization. Moreover, along this straight line $\sqrt{\mathrm{Gram}_5}$ is the square root of an irreducible quartic, and we find no representation by Goncharov polylogarithms in t. This obstruction is a property of the straight-line parametrization, and a polylogarithmic representation in the six invariants, where R_1 rationalizes, may still exist. The layered expressions are too long to print; Appendix E describes their kernels and layer structure, and the expressions themselves are supplied as a data file with the evaluation code (Appendix G) [106].

Boundary data. We reconstruct the entries of the connection on each segment as exact rational functions of the segment parameter from their values at numerical sample points. The boundary vector on each segment is an `AMFlow` evaluation [95] of all 98 masters at a single point. The layered top-sector solution carries 447 boundary constants C of eq. (64). We define each constant as a transport integral along a path in an auxiliary mass η, with initial values given by vacuum integrals known in closed form in terms of Γ functions. The values computed from this definition are supplied alongside the layered expressions as decimal strings with 78 to 83 significant figures. Six boundary constants have closed forms, the three rational ε^{-4} values and three imaginary parts at order ε^{-3} that are rational multiples of π. For the rest we find no integer relations [16] with the expected transcendental constants, and ten of the 447 are fixed independently by regularity conditions (Appendix E). The evaluation code (Appendix G) re-derives the layer recursion at run time but starts from stored boundary values of the masters with 50 and 70 significant figures, a set distinct from the 447 constants C, and this limits its precision above order ε^{-4} to that level.

Checks. All fifteen Laurent coefficients of the three top-sector masters on segment I, ε^{-4} through ε^{0}, agree with an independent `AMFlow` evaluation at a second point of the segment, not used in the construction, to at least 66 digits, the precision of that evaluation. At the same point the five subsector orbits agree with `AMFlow` to at least 31 digits through order ε^2. The ε^1 and ε^2 layers of the top sector require four further kernels $A^{(5,6)}_{97,\{0,2\}}$ coupling the top sector; with these they reproduce the `AMFlow` values to 40 and 35 digits. On segment III we integrated the reconstructed connection at the fixed values $d = 13/3$, $9/2$ and $11/2$ from P_0 to P_3, since the masters have poles at integer d from 5 to 7. The result reproduces an independent `AMFlow` evaluation at P_3 to at least 61 digits on all 98 masters.

Two further two-mass configurations of Figure 9 are not solved here. The first is the hexa-box with the equal-mass legs adjacent, $p_3^2 = p_4^2 = m^2$. Its reduction has 154 masters and its alphabet carries the two-mass threshold root r_{34} of eq. (61); for its three top-sector masters we have `AMFlow` values at two Euclidean points and no function of the kinematics. The others are the generic-mass hexa-box and double-pentagon of Figure 9(a,b), with $p_3^2 = M_3$, $p_4^2 = M_4$ and 219 and 190 masters, for which we have a statement at the level of the symbol only.

For the two generic-mass families we obtain from the principal A-determinant, in the seven physical invariants $\{s_{12}, s_{23}, s_{34}, s_{45}, s_{15}, M_3, M_4\}$, a sub-alphabet of 20 letters, nineteen even ones and the parity-odd Δ_5. That computation does not extend to the faces of the Newton polytope of the graph polynomial that are associated with the top sector, and the full alphabet is therefore larger. On words in this sub-alphabet we impose physical first entries, the Steinmann relations

for overlapping channels [111, 39], cluster adjacency [53] and integrability, as in the pentagon-function bootstrap [43, 50]. This leaves $K = [9, 28, 62, 120]$ integrable symbols at weights one to four, with ζ_2, ζ_3 and ζ_4 the only constants beyond the symbol. Because the sub-alphabet omits letters, these dimensions bound the symbol spaces of the two families from below and do not determine them, and no coefficient of an individual master has been fixed. Appendix E lists the sub-alphabet, its reflection symmetry, the counts K split by leading channel, and the form of the resulting ansatz. We have evaluated one top-sector integral of the 190-master double-pentagon, the scalar integral with all eight propagators, by sector decomposition at one Euclidean point. Its value is accurate to 7 digits at the weakest order in double precision, a first numerical value that is far from the accuracy of eq. (7). Finally, the finite-field Euler-characteristic method of Ref. [42], which handles nonplanar six-point two-loop families, may extend to the polytope faces not covered by our principal A-determinant computation and yield the letters that they contribute to the generic-mass alphabet.

5 Elliptic integrals

The seventeen entries Nos. 8–18, 20, 27–29, 33 and 35 of Table 1 have a maximal cut, or a subgraph, whose geometry is an elliptic curve. For the equal-mass sunrise, kite and ice-cream cone the curve is modular for $\Gamma_1(6)$, the light-by-light boxes inherit that curve through a cut of three equal-mass lines, and the curve of the $gg \to Z\gamma$ masters is modular for $\Gamma_0(4)$. In these cases the results involve iterated integrals of modular forms, eMPLs at torsion points, or dispersive integrals over such functions. The unequal-mass sunrise and kite, the generic-mass cone and the $gg \to H$ functions at generic boson mass are not of this type, and their results are Kronecker-form eMPLs at the marked points of the propagators or one-fold integrals over the periods. In the nonplanar W-pair family a single sector has an elliptic maximal cut whose curve is non-modular, and that sector enters the sectors that contain it only through their source terms. The results for the sunrise family, the equal-mass kite and the $gg \to H$ functions are known, and those for the six families that follow them are new.

5.1 The sunrise family

The two-loop sunrise with three massive lines (Figure 10) is the simplest Feynman integral whose maximal cut is an elliptic curve [30, 20, 92, 25, 6, 7]. Adams and Weinzierl wrote the equal-mass integral as an iterated integral of modular forms for $\Gamma_1(6)$ [10], and Bogner, Müller-Stach and Weinzierl gave the arbitrary-mass integral to all orders in ε as iterated integrals on the moduli space $\overline{\mathcal{M}}_{1,3}$ [26]. Both results are eMPLs in the sense of [36, 34] and together cover the five entries of this subsection, which are therefore known. We recompute the equal-mass integral at order ε^0 (No. 8), the three unequal-mass assignments $(m_1^2, m_2^2, m_3^2) = (1, 1, 2)$, $(1, 2, 3)$ and $(1, 1, 4)$ at order ε^0 (Nos. 9–11), and the order-ε^1 term of these three assignments (No. 12). In each case we take the function space from [10, 26] and determine every coefficient independently of the published expressions, from the integrability and branch-cut conditions of the differential equation and from numerical values.

Definition. With $t = p^2$ and masses m_1, m_2, m_3 on the three lines,

$$J[\nu_1, \nu_2, \nu_3](t) = \int \frac{d^d k_1}{i\pi^{d/2}} \frac{d^d k_2}{i\pi^{d/2}} \frac{1}{D_1^{\nu_1} D_2^{\nu_2} D_3^{\nu_3}}, \qquad D_i = q_i^2 - m_i^2 + i0, \qquad d = 2 - 2\varepsilon, \tag{67}$$

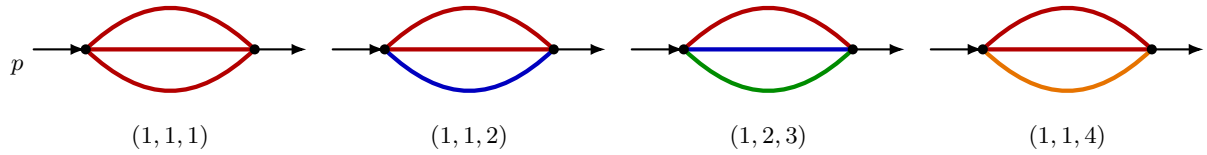

Figure 10: The two-loop sunrise family. The external momentum p, with $t = p^2$, flows through two vertices joined by three massive lines. From left to right: the equal-mass assignment $(m_1^2, m_2^2, m_3^2) = (1, 1, 1)$ and the three unequal assignments $(1, 1, 2)$, $(1, 2, 3)$, $(1, 1, 4)$. Line color encodes the internal mass: $m = 1$ red, $m = \sqrt{2}$ blue, $m = \sqrt{3}$ green, $m = 2$ orange.

where $q_1 = k_1$, $q_2 = k_2$, $q_3 = p - k_1 - k_2$ and no factor $e^{2\gamma_E \varepsilon}$ is included. We expand $J[1, 1, 1] = \sum_{k \geq 0} \varepsilon^k J[1, 1, 1]^{(k)}$ and quote reference values for $E^{(k)}(t) = J[1, 1, 1]^{(k)}(t)/\hat{\psi}_1(t)$, where $\hat{\psi}_1 = \psi_1/\pi$ is the holomorphic period of the maximal-cut curve in the normalization of [10]. At order ε^0 we also use the equivalent two-dimensional coordinate-space representation [16]

$$J[1, 1, 1]^{(0)}(t) = -4 \int_0^\infty r \, J_0(\sqrt{-t}\, r) \, K_0(m_1 r) \, K_0(m_2 r) \, K_0(m_3 r) \, dr \,, \qquad t < 0, \tag{68}$$

as a check that is independent of the differential equation. All results of this subsection hold for real $t < 0$. We give the continuation of No. 9 above its threshold together with that entry. The other assignments should continue in the same way but are not evaluated above threshold here.

Function space. For equal masses the maximal cut of $J[1, 1, 1]$ is the elliptic curve

$$y^2 = \widetilde{D}(t) = (t - 1)^3 (t - 9) \,, \tag{69}$$

with singular points $t \in \{0, 1, 9\}$, the zeros of the polylogarithmic letters $\{t, t - 1, t - 9\}$. The family (69) is modular for $\Gamma_1(6)$ [25, 10]. We use the period ratio τ_F in the convention of [10] and the nome $q_C = -e^{i\pi\tau_F}$, in which the period $\hat{\psi}_1$ and the unique cusp form $f_3 \in S_3(\Gamma_1(6))$ are q_C-series. Moreover, the third Kronecker–Eisenstein form [36, 34] at the torsion point $z = \frac{1}{6}$ of the cut torus of modulus τ_C is proportional to this cusp form, $g^{(3)}(\frac{1}{6}, \tau_C) = -\frac{(2\pi)^3}{6} f_3(\tau_C)$. The transcendental content of No. 8 is then the depth-two iterated integral $I(1, f_3)$ of f_3 along $\mathrm{d} \log q_C$ and the cusp constant $L(\chi_{-3}, 2)$.

For unequal masses the curve depends on the assignment. At $(1, 1, 2)$ the singular fibers sit at $t = 0,\ 2,\ 6 \pm 4\sqrt{2}$ and ∞, of Kodaira types I_1, I_4, I_2 and I_3. With these five singular fibers the family is a semistable rational elliptic surface of Mordell–Weil rank one, and it is not the $\Gamma_1(6)$ surface [26]. The polylogarithmic letters become $\{t, t - 2, t^2 - 12t + 4\}$, the points $6 \pm 4\sqrt{2}$ being the roots of one quadratic letter irreducible over $\mathbb{Q}$. The elliptic arguments are the Abel–Jacobi images z_1, z_2, z_3 of the three propagators on the torus, with $z_1 + z_2 + z_3 = 0$. They are distinct for $(1, 2, 3)$, and $z_1 = z_2$ for $(1, 1, 2)$ and $(1, 1, 4)$. We write the results in the Kronecker-form eMPLs

$$W(z, N) = I(1, g^{(3)}(z, N\tau_C); q_C) = \sum_{n \geq 1} b_n(z, N) \, \frac{q_C^n}{n^2} \,, \qquad N \in \{1, 2\}, \tag{70}$$

at the marked points, together with the elliptic dilogarithm $C_{4,2}(t) = \sum_j \frac{1}{2i} [\mathrm{Li}_2(\bar{w}_j) - \mathrm{Li}_2(1/\bar{w}_j)]$, $\bar{w}_j = e^{2\pi i z_j}$, of [25, 7].

We restrict the words that can appear at each weight by two conditions [105], integrability of the connection and the first-entry condition that only the soft point and the physical thresholds

open a branch cut. The only admissible constants are then those associated with the cusps of the curve, $L(\chi_{-3},2)$ at order ε^0 and ζ_3 at order ε^1. We fix the remaining rational coefficients by PSLQ fits to `AMFlow` values [95] of the master integrals of an integration-by-parts reduction [81] at Euclidean points.

No. 8, equal masses, order ε^0. The result is

$$J[1,1,1]^{(0)}(t) = -\hat{\psi}_1(t)\Big(\underbrace{\tfrac{3}{2}\sqrt{3}\,L(\chi_{-3},2)}_{B_0} + I(1,f_3;q_C)\Big), \qquad q_C = -e^{i\pi\tau_F}, \tag{71}$$

the form given in [10]. Here $B_0 = \frac{3}{2}\sqrt{3}\,L(\chi_{-3},2) = 2.0298832\ldots$ is the only boundary constant, and $I(1,f_3;q_C) = \sum_{n\geq 1} a_n q_C^n/n^2$ is the depth-two iterated integral along $\mathrm{d}\log q_C$ of $f_3 = 36\sqrt{3}\,(e_1^3 - e_1^2e_2 - 4e_1e_2^2 + 4e_2^3) \in M_3(\Gamma_0(12),\chi)$, the level-six cusp form written in a basis e_1, e_2 of Eisenstein series of weight one and level twelve, in which $\hat{\psi}_1 = 2\sqrt{3}\,(e_1+e_2)$ [10]. We fitted the coefficients of the weight-graded ansatz to `AMFlow` values at five Euclidean points, and the resulting value of B_0 reproduces its closed form to 70 digits. With the point $t=-3$ left out of the fit, eq. (71) agrees with `AMFlow` there to 140 digits, and at a sixth point, $t=-9$, to 159 digits, the precision of that reference value.

No. 9, masses $(1,1,2)$, order ε^0. The result is

$$\frac{J[1,1,1]^{(0)}(t)}{\hat{\psi}_1(t)} = -C_{4,2}(t) - \frac{6}{(2\pi)^3}\,\frac{\big(2W(z_1,1)+W(z_3,1)\big) - 8\big(2W(z_1,2)+W(z_3,2)\big)}{3}, \tag{72}$$

with singular points $t \in \{0, 2, 6\pm 4\sqrt{2}\}$. We fitted the three rational coefficients multiplying $C_{4,2}$, the τ_C-words and the $2\tau_C$-words, with the common normalization factor $6/(2\pi)^3$, to `AMFlow` values at $t = -\frac{1}{2}, -1, -2, -5$, and PSLQ recognizes them as $c = [-1, -\frac{1}{3}, +\frac{8}{3}]$. At two further points, $t=-3$ and $t=-7$, eq. (72) agrees with `AMFlow` to 159 digits. Moreover, when continued along a path in the upper half t-plane ($t \to t + i0$), with the depth-two words resummed as dilogarithms, the same expression reproduces the `AMFlow` values above the threshold $t = (2+\sqrt{2})^2$, at $t=16$ and $t=20$, to at least 71 digits in real and imaginary parts.

Nos. 10 and 11, masses $(1,2,3)$ and $(1,1,4)$, order ε^0. With three distinct marked points the result has one term per puncture, with the same rational coefficients as for $(1,1,2)$,

$$\frac{J[1,1,1]^{(0)}(t)}{\hat{\psi}_1(t)} = -C_{4,2}(t) - \frac{6}{(2\pi)^3}\,\frac{1}{3}\sum_{j=1}^{3}\big(W(z_j,1) - 8\,W(z_j,2)\big), \tag{73}$$

and eq. (72) is the $z_1 = z_2$ case of this formula. For $(1,2,3)$ we fitted at $t = -7, -5, -2, -1, -\frac{1}{2}, -\frac{1}{3}$ and for $(1,1,4)$ at $t = -5, -2, -1, -\frac{1}{2}$, and both fits return $[-1, -\frac{1}{3}, \frac{8}{3}]$ under PSLQ. At points not used in the fit, the $(1,2,3)$ result agrees with `AMFlow` to 159 digits at $t=-3$ and $t=-9$, and the $(1,1,4)$ result to 289 at $t=-3$ and to 159 at $t=-9$ and $t=-11$, each figure being the precision of the reference value. Evaluated at a fifth assignment, $(1,1,3)$, which entered no fit, eq. (73) agrees with `AMFlow` to 160 and 159 digits at $t=-3$ and $t=-6$.

No. 12, order ε^1 for the three unequal assignments. The result is

$$E^{(1)}(t) \equiv \frac{J[1,1,1]^{(1)}(t)}{\hat{\psi}_1(t)} = -J_4^{(3)}(t) + \big(2\gamma_E + 2\log m_3^2\big)\,J_4^{(2)}(t), \qquad a=-1,\;\; b = 2\gamma_E + 2\log m_3^2, \tag{74}$$

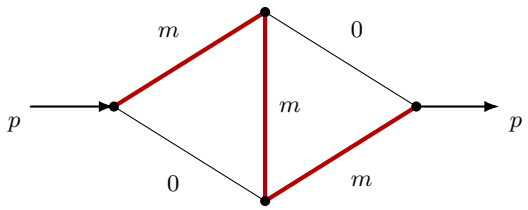

Figure 11: The equal-mass kite. The off-shell momentum p, with $t = p^2/m^2$ and $m^2 = 1$, enters at the left vertex and exits at the right. Thin black lines are massless and red lines carry mass m: the two massless lines sit on opposite rims, and the three massive lines are the remaining two rim lines and the central rung. Contracting both massless lines gives the equal-mass sunrise.

where $J_4^{(2)} = -E^{(0)}$ is the order-ε^0 function of eqs. (72) and (73) in the normalization of [26], and $J_4^{(3)}$ is the Kronecker-form polynomial of depth at most three of that reference. It has 101 words over a 14-letter alphabet of Kronecker forms, and ζ_3 enters through its boundary term $C_{4,3}$, a Nielsen polylogarithm $S_{1,2}$ evaluated on the unit circle. The coefficient $a = -1$ and the mixing constant $b = 2\gamma_E + 2\log m_3^2$ are exact ($b = 2.5407256\ldots$ for $(1,1,2)$). The constant b accounts for the difference between the normalization of eq. (67) and that in which $J_4^{(2)}, J_4^{(3)}$ are defined, and eq. (74) therefore has no fitted parameter.

As a test of the polynomial $J_4^{(3)}$ we left all 101 coefficients and the two normalization terms $\gamma_E J_4^{(2)}$ and $\log m_3^2\, J_4^{(2)}$ free. An integer-lattice fit to `AMFlow` values at 15 Euclidean points then returns exactly the coefficients of [26] and the value of b, and reproduces the values at four further points to at least 104 digits. The coefficient of the one word that vanishes identically in the tangential-base-point prescription, $C_{4,2}\, I(\omega_0)$, cannot be fitted and is fixed instead by regularity at the soft point. We take the 14-letter alphabet itself from [26]. The soft-point condition alone leaves 2926 of its 3151 words free, and we expect the remaining reduction to follow from the integrability analysis on $\overline{\mathcal{M}}_{1,3}$ of that reference, which we have not repeated. At nine Euclidean points, three per mass assignment, eq. (74) agrees with `AMFlow` to 288–308 digits.

For comparison at single points,

$$\begin{aligned}
(1,1,2): \quad & E^{(0)}(-1) = -2.3471191\ldots, \qquad E^{(0)}(-5) = -3.2711938\ldots, \\
& E^{(1)}(-5) = 12.166814\ldots, \\
(1,1,4): \quad & E^{(0)}(-7) = -3.3260720\ldots, \\
(1,1,3): \quad & E^{(0)}(-3) = -2.7788109\ldots .
\end{aligned} \tag{75}$$

The coordinate-space representation (68), evaluated in ball arithmetic, reproduces each order-ε^0 value quoted here and encloses it to 103 digits.

5.2 The equal-mass kite

The kite (Figure 11) is the two-loop two-point graph that reduces to the equal-mass sunrise when its two massless lines are contracted. It enters the two-loop electron self-energy [103, 79], and Adams, Bogner, Schweitzer and Weinzierl computed it to all orders in ε in terms of elliptic polylogarithms [5] (see also [102, 9]). Here we recompute its order-ε^0 term from the function space and `AMFlow` values alone.

Definition. With the momenta of Figure 11, $m^2 = 1$ and $t = p^2/m^2$,

$$I_{\text{kite}}(t) = \Big[\int \frac{d^dk_1}{i\pi^{d/2}} \frac{d^dk_2}{i\pi^{d/2}} \frac{1}{D_1 D_2 D_3 D_4 D_5} \Big]_{\varepsilon^0}, \qquad d = 4 - 2\varepsilon, \tag{76}$$

where $[\,\cdot\,]_{\varepsilon^0}$ denotes the coefficient of ε^0. The propagators are $D_1 = k_1^2 - m^2$, $D_2 = k_2^2$, $D_3 = (k_1 - k_2)^2 - m^2$, $D_4 = (k_1 - p)^2$ and $D_5 = (k_2 - p)^2 - m^2$, all with $+i0$. No factor $e^{2\gamma_E \varepsilon}$ is included, and the integral is finite at $\varepsilon = 0$. The result holds for real $t < 1$, $t \neq 0$, and we continue it to the physical region $t > 1$ at the end of this subsection.

Function space. The subsector $D_1 D_3 D_5$ in $d = 4 - 2\varepsilon$ is related by a dimension shift to the equal-mass sunrise of section 5.1 in $d = 2 - 2\varepsilon$, and the kite inherits the curve

$$\widetilde{D} \;=\; (t-1)^3\,(t-9) \tag{77}$$

of eq. (69), with singular fibers at the thresholds $t = 1$ and $t = 9$, that is, $t = m^2$ and $t = 9m^2$, and cusps at $t \to 0, \infty$. The kite therefore has the modular group $\Gamma_1(6)$ of the sunrise, with a Hauptmodul of level six, the periods ψ_1, ψ_2 and the nome $q = e^{i\pi\tau}$, $\tau = \psi_2/\psi_1$ [25, 10]. Its massless lines add only the polylogarithmic letters $\{0, 1\}$ in t, and there is no algebraic letter.

Because the curve is modular, the kernel ψ_1^3/W, with $W = \psi_1\psi_2' - \psi_2\psi_1'$ the Wronskian, is itself a q-series at the 3-torsion point $\varrho = e^{2\pi i/3}$, equal to $-6\,\overline{E}_{0;-2}(\varrho; -1; -q)$ in the notation of [5, 8]. Once the algebraic prefactor $1/(4t)$ is divided out, the order-ε^0 term is therefore a combination of eMPL words with constant coefficients [105]. That term is finite and of weight at most three, which leaves five words: three harmonic polylogarithms with letters $\{0, 1\}$ and two $\Gamma_1(6)$ elliptic polylogarithms $\overline{E}$ at ϱ in the nome $-q$.

Result.

$$\begin{aligned} I_{\text{kite}}(t) \;=\; \frac{1}{4t}\Big[&-\tfrac{2\pi^2}{3}\,G(1;t) \;-\; 8\,G(0,1,1;t) \;+\; 4\,G(1,0,1;t) \\ &-\; 108\,\mathrm{Cl}_2\!\left(\tfrac{2\pi}{3}\right)\overline{E}_{1;-1}(\varrho;1;-q) \;-\; 108\,\overline{E}_{0,2;-2,0;2}(\varrho,\varrho;1,-1;-q)\Big], \end{aligned} \tag{78}$$

with singular points $t \in \{0, 1, 9\}$.

Boundary data. The only constant beyond rational numbers and π^2 is the Clausen value $\mathrm{Cl}_2(2\pi/3)$, the cusp constant of $\Gamma_1(6)$. We fitted the five coefficients to `AMFlow` values [95] at Euclidean points, among them $t = -1$ and $t = \frac{1}{2}$, and PSLQ recognizes them as $\{-2\pi^2/3,\, -8,\, +4\}$ and $\{-108\,\mathrm{Cl}_2(2\pi/3),\, -108\}$.

Checks. We compared eq. (78) with `AMFlow` at two points not used in the fit, $t = -3$ and $t = -10$, where it agrees to 160 and 130 digits, each limited by the precision of the reference value. It also reproduces numerically the order-ε^0 term of [5]. For comparison, in the normalization of eq. (76),

$$I_{\text{kite}}(-1) \;=\; -1.3317114\ldots, \tag{79}$$

and $I_{\text{kite}}(-3) = -0.88550175\ldots$. Finally, for $t > 1$ we continue the nome along $t \to t + i0$ through the upper half t-plane and take the $t + i0$ boundary values of the harmonic polylogarithms. The continued expression reproduces the `AMFlow` values at $t = 4$ and $t = 16$, and at $t = 12$, 50 and 100 its imaginary part matches the kite spectral density used in section 5.8, in each case to at least 67 digits.

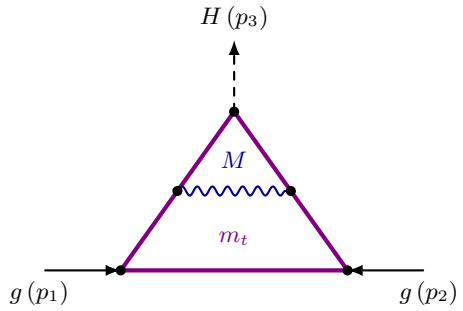

Figure 12: The two-loop mixed QCD–electroweak $gg \to H$ topology, drawn as sector 63 (the six lines D_1–D_6) of family 2 of [96]. A closed top-quark loop (violet, mass m_t) carries an internal electroweak-boson line of mass M (blue wavy). Two on-shell gluons enter and the Higgs (dashed) exits with $p_3 = p_1 + p_2$. The elliptic sectors of families 2 and 5 share the (m_t, m_t, M) sunrise sub-curve.

5.3 Elliptic functions in $gg \to H$

The two-loop mixed QCD–electroweak corrections to $gg \to H$ contain elliptic sectors in families 2 and 5 of Marzucca, McLeod and Nega [96], whose maximal cuts define the two-mass sunrise curve with masses (m_t, m_t, M) [6], M an electroweak-boson mass. The canonical basis of [96] is built from functions defined in its eqs. (3.15), (3.17) and (3.18), namely the holomorphic period ϖ_0 of that curve and two one-fold integrals G_1, G_2 over ϖ_0. All ingredients of this entry are known: the curve, the differential equation, the kernels and the boundary point are those of [96]. We add an evaluation of G_1, G_2 with a definite choice of branch for the period, reference values, and a comparison with `AMFlow` in the canonical basis of that reference. The eMPL form of the canonical master integrals themselves, which [96] leaves to future work, is not attempted here.

Definition. The integral family is family 2 of [96], with the six propagators D_1–D_6 of its eq. (3.3) drawn in Figure 12. In the dimensionless variables s and M^2 of that reference, with $m_t = 1$,

$$\begin{aligned} G_i(s) &= \int_0^s K_i(s')\,\varpi_0(s')\,\mathrm{d}s', \qquad G_i(0) = 0 \text{ (exact, cusp boundary)}, \\ K_1 &= \frac{2\,(M^2-1)\,(M^2-s-4)}{(M^2+3s-4)^2}, \\ K_2 &= \frac{2\,r_1 r_2 r_3 r_4\,\left(M^4+3M^2s^2-13M^2s-4M^2-3s^3+16s\right)}{(s-4)^2\,s\,(M^2+3s-4)^2}, \end{aligned} \tag{80}$$

with $r_1 = \sqrt{-s}$, $r_2 = \sqrt{4-s}$, $r_3 = \sqrt{M^2}$ and $r_4 = \sqrt{4-M^2}$. For the period $\varpi_0(s)$ we use eq. (3.15) of [96] and take the square root in the argument of the complete elliptic integral K as the principal root of $(s-(M+2)^2)(s-(M-2)^2)$, positive for $s<0$, so that $\varpi_0(0) = 1/\pi$. The results hold in the Euclidean region $s<0$, $0<M^2<4$.

Function space. All elliptic master integrals of families 2 and 5 involve only the (m_t, m_t, M) sunrise curve, whose Picard–Fuchs operator has order two. For generic M this curve is non-modular, and G_1, G_2 are given as iterated integrals over the period. In the language of [36, 34] the letters are the Kronecker–Eisenstein forms on the cut torus,

$$\omega_0 = \mathrm{d}\tau_C\,(g^{(0)}=1), \qquad \omega_n^{(j)} = g^{(n)}(z_j,\, N\tau_C)\,\mathrm{d}\tau_C \quad (n \geq 1), \tag{81}$$

with τ_C the period ratio, torsion punctures $z_1 = z_2$ for the two top-quark lines and z_3 for the boson line, and $N \in \{1, 2\}$. The functions G_1, G_2 need one further puncture $z_p(s)$, which moves with s and is not a torsion point. Family 5 needs the 5-letter alphabet $\{\mathrm{d}\tau,\ g^{(3)}(z_j, N\tau_C)\}$. Family 2 adds G_2 and with it the forms $g^{(1)}, g^{(2)}$, which mix with the $\mathrm{d}\log$ letters at $s = 0, 4$, giving a 13-letter alphabet in all.

In eq. (80) the kernels K_1, K_2 multiplying ϖ_0 are rational functions of s and M^2 up to the factor $r_1 r_2 r_3 r_4$ in K_2, and the whole transcendental content is carried by the single Kronecker form of the first kind at $z_p(s)$, which pulls back to $\varpi_0(s)$. We found that a fit of numerical values to constant-coefficient words in these letters does not converge, because the ratio ϖ_0/ψ_1 of the period of [96] to the Feynman-curve period varies with s [105]; that ratio does not appear in the defining integrals (80). The only singular points of eq. (80) are the puncture $s_p = (4 - M^2)/3$, a double pole of both kernels, and the thresholds $s = 0$ and $s = 4$.

Result. Besides eq. (80), G_1 and G_2 can be written in terms of complete elliptic integrals. On the Baikov quartic of the sunrise sub-curve, $y^2 = (x^2 - 2(m+1)x + (m-1)^2)(x^2 - 2(s+1)x + (s-1)^2)$ with $m = M^2$, we write $\langle f \rangle = \nu \oint_{\gamma_0} f(x)\,\mathrm{d}x/y$, with ν fixed by $\langle 1 \rangle = \varpi_0$ and γ_0 the segment joining the branch points $x = s + 1 \pm 2i\sqrt{-s}$. Then

$$\begin{aligned} G_1 &= \frac{3ms + m + s^2 - s - 4}{m + 3s - 4}\,\varpi_0 - \langle x \rangle, \\ G_2 &= r_1 r_2 r_3 r_4 \Big[\frac{5s - m - 4}{(s-4)(m+3s-4)}\,\varpi_0 - \Big\langle \frac{1}{x-1} \Big\rangle \Big] - \frac{\sqrt{m(4-m)}}{\pi}, \end{aligned} \tag{82}$$

in which G_1 carries the period of the third kind with poles over $x = \infty$ and G_2 the one with poles over $x = 1$. The representation (82) holds in the region $(s - m)^2 < 4m$, in which γ_0 is the cycle of ϖ_0, and agrees there with eq. (80) to 59 digits at four Euclidean points.

Boundary data. Both G_1 and G_2 vanish at $s = 0$, where the elliptic sectors are regular and reduce to tadpoles, and eq. (80) contains no further constant.

Checks. We check eq. (80) against `AMFlow` [95] at one point not used elsewhere, $(s, M^2) = (-\frac{7}{4}, \frac{3}{5})$: the `AMFlow` values of the family's thirty master integrals, rotated into the canonical basis of [96] with its ancillary files, determine G_1 and G_2 there to 57 and 48 digits respectively, and eq. (80) reproduces both values. The rotation supplied with the ancillary files of [96] contains G_2 with a factor one quarter relative to its eq. (3.18), and we include that factor in the comparison. For reference, at a second point, $M^2 = 9/10$ and $s = -\frac{1}{2}$,

$$G_1 = -0.006031453047\ldots, \qquad G_2 = -0.04436252545\ldots, \tag{83}$$

both real. The physical region $s > 0$ should be reachable by continuing eq. (80) along a path in the upper half s'-plane, $s \to s + i0$, with ϖ_0 continued on the same path; we have evaluated only the Euclidean region.

5.4 The unequal-mass kite

The kite is the two-loop two-point graph of Figure 13, with two massless lines and a sunrise subgraph of three massive lines. Kite integrals of this kind appear in two-loop self-energies, for example the electron self-energy in QED [5, 79]. The kite of this entry differs from the equal-mass kite of No. 13

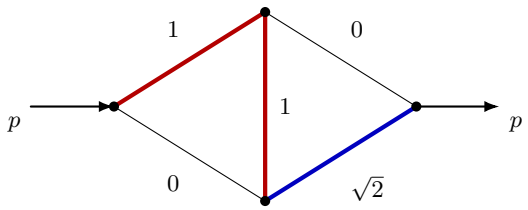

Figure 13: The unequal-mass kite, No. 14 of Table 1. Thick red lines carry mass 1, the thick blue line mass $\sqrt{2}$, and thin lines are massless. The external momentum p is off shell, $s = p^2$. Contracting the two massless lines leaves the sunrise graph with masses squared $(m_1^2, m_3^2, m_5^2) = (1, 1, 2)$.

in one of the three sunrise masses, $(m_1^2, m_3^2, m_5^2) = (1, 1, 2)$, and the elliptic curve of the sunrise subgraph is then no longer the $\Gamma_1(6)$ curve.

Broedel, Duhr, Dulat, Penante and Tancredi expressed the kite with three distinct masses as a pure combination of elliptic multiple polylogarithms of weight three [35]. Their eq. (5.6) is written, in the mass labeling of that reference, for $m_1 \neq m_2$ in the region $0 < p^2 < \min m_i^2$ and contains our mass point as its $m_1 = m_2$ limit. An ε-factorized differential equation for the five-mass kite family is also known [69]. We evaluate the finite part at our mass point for $s < 0$ with analytic boundary data, in which the only transcendental constants are γ_E, ζ_2, $\ln 2$ and Catalan's constant. We are not aware of a previous evaluation at these masses.

Definition. With loop momenta k_1, k_2, external momentum p and $s = p^2$, the propagators are

$$D_1 = k_1^2 - 1, \qquad D_2 = k_2^2, \qquad D_3 = (k_1 - k_2)^2 - 1, \qquad D_4 = (k_1 - p)^2, \qquad D_5 = (k_2 - p)^2 - 2, \tag{84}$$

and $J[\nu_1, \ldots, \nu_5](s)$ denotes the two-loop integral of $\prod_j D_j^{-\nu_j}$ in $d = 4 - 2\varepsilon$ dimensions with the measure of eq. (1), for which the one-loop tadpole of mass squared M is $T(M) = \Gamma(1 + \varepsilon)\, M^{1-\varepsilon}/(\varepsilon(1 - \varepsilon))$. We reduce the family with `Kira` [81] to 14 master integrals. The integral of this entry is the finite part of the top master, $I^{(0)}_{\text{kite}}(s) = J[1, 1, 1, 1, 1]\big|_{\varepsilon^0}$, whose ε^{-2} and ε^{-1} parts vanish. The result below holds at the mass point $(m_1^2, m_3^2, m_5^2) = (1, 1, 2)$ for real $s < 0$, and the region above the thresholds is reached by continuing the same differential equation with $s \to s + i0$.

Function space. From a Landau analysis of the family with symbolic masses [45, 74] we obtain the candidate singular locus

$$\Big\{ s,\ s-1,\ s-2,\ s-4,\ 2s-9,\quad \underbrace{s^2 - 12s + 4}_{\text{sunrise threshold}},\ \underbrace{s^2 - 6s + 1}_{\text{kite anomalous}} \Big\}. \tag{85}$$

The quadratic polynomials factor over $\mathbb{Q}(\sqrt{2})$ as $s^2 - 12s + 4 = (s - (6 + 4\sqrt{2}))(s - (6 - 4\sqrt{2}))$ and $s^2 - 6s + 1 = (s - (3 + 2\sqrt{2}))(s - (3 - 2\sqrt{2}))$, and $s = 1, 2$ are pseudo-thresholds of the sunrise subgraph.

The maximal cut of the sunrise subgraph is the elliptic curve of the unequal-mass sunrise [26] with periods ψ_1, ψ_2 and $\tau = \psi_2/\psi_1$. This family of curves is not modular, and its j-invariant differs from that of the $\Gamma_1(6)$ curve, for example $j(-2) = 10976$ against 15664.667 at equal mass. At $s = -2$, where we give the boundary value of the top integral, the fiber is the curve of conductor 128 with Cremona label 128a2,

$$y^2 = x^3 - 756\, x + 7344, \qquad j = 10976, \quad L(E, 1) = 0, \quad L'(E, 1) = 0.872544\ldots, \tag{86}$$

whose real and imaginary periods $\Omega_{1,2}$ are related to the Feynman periods by $\psi_i = 3\,\Omega_i$, with $\tau = 0.68063417\ldots$. On the minimal model $y^2 = x^3 + x^2 - 9x + 7$ the factor 3 is absorbed.

In the equal-mass kite the kernel multiplying the sunrise in the differential equation of the top integral is a modular form of $\Gamma_1(6)$, and the result is a combination of elliptic multiple polylogarithms with constant coefficients [5, 10]. For unequal masses this kernel is not modular, and words with constant coefficients on the three punctures of the sunrise do not span it. One must then either let the punctures move with s, as in Ref. [35], or adjoin the second period ψ_2. We take the second option, which is the construction Ref. [107] uses for the ice-cream cone.

Result. With $W = \psi_1\psi_2' - \psi_1'\psi_2$ the Wronskian of the periods, the top integral has the variation-of-parameters representation

$$4s\, I^{(0)}_{\text{kite}}(s) = c_1\,\psi_1(s) + c_2\,\psi_2(s) - \psi_1(s)\int_{s_\star}^{s}\frac{\psi_2\,R}{W}\,ds' + \psi_2(s)\int_{s_\star}^{s}\frac{\psi_1\,R}{W}\,ds', \tag{87}$$

with constants c_1, c_2 and the base point $s_\star = -4$ used below. The source $R(s)$ is a rational function, the image of $4s\,I^{(0)}_{\text{kite}}$ under the Picard–Fuchs operator of the periods after reduction with the differential equation of the family. We obtain the differential equation of the family, $dJ/ds = A(d,s)\,J$ for the 14 masters, by differentiation and `Kira` reduction. The matrix A is rational in d and s, and three of the entries in the equation for the top integral are

$$A_{13,1} = \frac{d-2}{2s^2-6s+4}, \quad A_{13,3} = \frac{3-d}{s^2-3s+2}, \quad A_{13,5} = \frac{-ds^2+7ds+2d+2s^2-18s-4}{2s^4-8s^3+10s^2-4s}. \tag{88}$$

Every denominator of A factors over $\{s,\ s-1,\ s-2,\ s^2-12s+4\}$, and the singular points of the differential equation, $s \in \{0, 1, 2,\ 6\pm 4\sqrt{2}\}$, therefore lie off the negative real axis. We supply the full matrix $A(d,s)$, from which R follows, with the evaluation code of this entry [106] (Appendix G). In practice we expand the 14 masters to order ε^0, which gives a system of 42 functions. We sum the Frobenius series of this system at $s = 0$ (radius of convergence 1) and continue the solution with Taylor steps along the negative axis.

Boundary data. At $s = 0$ partial fractions such as $1/[k_1^2(k_1^2-1)] = 1/(k_1^2-1) - 1/k_1^2$ reduce every master to two-loop vacuum integrals, namely products of tadpoles $T(M)$ and vacuum sunsets $V(M_1,M_2,M_3)$ with $M_i \in \{0,1,2\}$. For the top integral we find

$$J[1,1,1,1,1]\big|_{s=0} = \tfrac{1}{2}\big[V(1,1,2) - V(1,1,0) - V(0,1,2) + V(0,1,0)\big], \tag{89}$$

in which the ε^{-2} and ε^{-1} parts cancel. The vacuum sunsets are known in closed form. With $c = \sum_i M_i$ and $L_1 = \sum_i M_i \ln M_i$ their poles are $V[\varepsilon^{-2}] = c/2$ and $V[\varepsilon^{-1}] = (3/2 - \gamma_E)c - L_1$, and the only transcendental constants in the finite part are γ_E, ζ_2, $\ln 2$ and values of the Clausen function Cl_2. For $\lambda = \sum_i M_i^2 - 2\sum_{i<j} M_iM_j < 0$ the Clausen part is $\xi = -2\sqrt{-\lambda}\,\sum_i \mathrm{Cl}_2(2\alpha_i)$, with α_i the angles of the triangle of sides $\sqrt{M_i}$, and for the right isosceles triangle $(1,1,\sqrt{2})$ we find

$$\xi(1,1,2) \;=\; -8\,G \qquad (G = \text{Catalan's constant}). \tag{90}$$

The vacuum values determine the solution uniquely. The point $s = 0$ is a regular singular point, and the residue matrix $A_0 = sA|_{s=0}$ of the 42-function system has spectrum $\{0^{15}, (-1)^{24}, (-2)^3\}$, a semisimple zero eigenspace and $\ker A_0 \cap \operatorname{im} A_0 = 0$. Hence no positive integer exponent occurs and the vacuum values fix every Taylor coefficient of the bounded branch, while the last condition excludes a $\log s$ term in that branch. Since $s = 0$ is not a Landau singularity of the physical

masters, they are bounded there, and the kite masters are the unique bounded solution with these vacuum values. Because eq. (89) is a second difference of the vacuum sunset in two of its masses, the $s = 0$ value of the finite part is also a single Bessel integral in coordinate space,

$$J(0) = -4 \int_0^\infty K_1(r) \left[K_1(r) - \frac{1}{r}\right] \left[\sqrt{2}\, K_1(\sqrt{2}\, r) - \frac{1}{r}\right] dr = -1.420697671\ldots . \tag{91}$$

Integrating the system from $s = 0$ to $s_0 = -2$, we obtain the boundary value

$$N_0 \;=\; 4 s_0\, I^{(0)}_{\text{kite}}(s_0 = -2) \;=\; 7.1099373\ldots , \tag{92}$$

a weight-two period of the curve (86). In the representation (87) the same number reads

$$N_0 = c_1\, \psi_1(s_0) + c_2\, \psi_2(s_0) + \psi_2(s_0) \int_{s_\star}^{s_0} \frac{\psi_1\, R}{W}\, ds' - \psi_1(s_0) \int_{s_\star}^{s_0} \frac{\psi_2\, R}{W}\, ds', \qquad s_0 = -2, \quad s_\star = -4, \tag{93}$$

where the periods at s_0 are complete elliptic integrals of modulus $k^2(-2) = (2+\sqrt{2})/4$ and $W(-2) = \pi/8$ exactly. The constants c_1, c_2 are determined by the bounded solution at $s = 0$. We searched for an integer relation [16] between N_0 and classical weight-two constants times periods, Dirichlet L-values at the bad prime 2 and the period scale $\Gamma(1/4)^2$. We found none, as expected for a period of a curve without complex multiplication in a non-modular family.

Checks. The finite part agrees with `AMFlow` [95] at the three points $s \in \{-5/2, -3, -15\}$ to at least 125 digits. We repeated the construction at a second mass point, $(m_1^2, m_3^2, m_5^2) = (1, 1, 3)$, where the singular points are $s \in \{0, 1, 3,\ 7 \pm 4\sqrt{3}\}$, the residue spectrum at $s = 0$ is unchanged and the Clausen part has $\lambda = -3$ with angles $(\pi/6, \pi/6, 2\pi/3)$. There it reproduces `AMFlow` at the two points $s = -5/3$ and $s = -10/3$ to 128 digits. For Minkowski kinematics we continue the solution from $s = -2$ along a path in the upper half s-plane past the five real singular points to $s = 16$, above every threshold, where it agrees with an `AMFlow` evaluation to 64 digits, imaginary parts included. For comparison with other implementations, a reference value away from these points is

$$I^{(0)}_{\text{kite}}(s = -4) = J[1, 1, 1, 1, 1]\big|_{\varepsilon^0} = -0.66865601\ldots . \tag{94}$$

5.5 Ice-cream cone integrals

The two-loop ice-cream cone of Figure 14 is a triangle with a bubble inserted on one edge, with four massive propagators and three off-shell legs. It is the two-loop member of the ice cone family of Ref. [56] and the example studied in the analysis of sequential discontinuities of Ref. [73]. In $d = 2$ the maximal cut of its top sector satisfies a second-order equation with algebraic solutions, and the elliptic curves of the sunrise subsectors enter only through the inhomogeneous terms. This structure was established by Lairez and Vanhove [88], by Doran et al. [51] and by de la Cruz and Vanhove [47].

We give the top integral as an explicit function on a one-parameter kinematic slice in $d = 2 - 2\varepsilon$ dimensions, for equal masses at order ε^0 (No. 15) and at order ε^1, weight four (No. 17), and for four distinct masses at order ε^0 (No. 16). We are not aware of a previous evaluation of these functions. The bubble produces the letter L_{bub} of the alphabet given under Function space, a singularity of the top sector that no subgraph or quotient graph of the cone possesses [105].

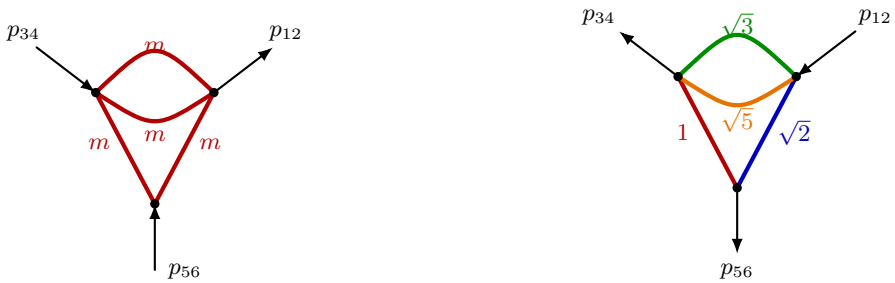

Figure 14: The two-loop ice-cream cone: a one-loop triangle (the cone) whose top edge carries a bubble (the scoop), with three off-shell external momenta, $p_{12} = p_{34} + p_{56}$. (a) Equal internal masses m, Nos. 15 and 17 of Table 1. (b) Masses $1, \sqrt{2}, \sqrt{3}, \sqrt{5}$ on the lines $D_1, \ldots, D_4$ of eq. (95), No. 16. The scoop lines carry $\sqrt{3}$ and $\sqrt{5}$.

Definition. With loop momentum l_1 in the scoop and l_2 in the cone, the propagators are

$$D_1 = l_2^2 - m_1^2, \qquad D_2 = (p_{56} - l_2)^2 - m_2^2, \qquad D_3 = l_1^2 - m_3^2, \qquad D_4 = (p_{12} - p_{56} + l_2 - l_1)^2 - m_4^2, \tag{95}$$

and $[\nu_1, \nu_2, \nu_3, \nu_4]$ denotes the two-loop integral of $\prod_j D_j^{-\nu_j}$ in $d = 2 - 2\varepsilon$ dimensions with the measure of eq. (1). Three further indices, when written, are powers of irreducible numerators. Pinching D_2 leaves the scoop sunrise $[1, 0, 1, 1]$ with masses (m_1, m_3, m_4), and pinching D_1 the sunrise $[0, 1, 1, 1]$ with masses (m_2, m_3, m_4).

All three results hold on the symmetric slice

$$p_{12}^2 = p_{34}^2 = x, \qquad p_{56}^2 = -1, \qquad d = 2 - 2\varepsilon, \tag{96}$$

with $m_i^2 = 1$ for Nos. 15 and 17 and $(m_1^2, m_2^2, m_3^2, m_4^2) = (1, 2, 3, 5)$ for No. 16, and for real $x < -\frac{1}{4}$. The elliptic curve of the generic-mass cone (No. 16) is that of its scoop sunrise $[1, 0, 1, 1]$, which depends only on the masses squared $(1, 3, 5)$, and we label the curve by that triple.

We write $T(x)$ for the order-ε^0 coefficient of the top integral $[1, 1, 1, 1]$ on the slice and $f_{4,1}(x)$ for its order-ε^1 coefficient. The top integral has the Feynman-parameter representation, valid at every order in ε,

$$T(\varepsilon; x) = \Gamma(2+2\varepsilon) \int_0^1 \mathrm{d}a \int_\Delta \mathrm{d}^2\alpha \, \big[a(1-a)\big]^{-1-\varepsilon} \, \alpha_3^{\varepsilon} \, F(\alpha; s(a); x)^{-2-2\varepsilon}, \qquad s(a) = \frac{m_3^2}{a} + \frac{m_4^2}{1-a}, \tag{97}$$

with $F = \alpha_1 m_1^2 + \alpha_2 m_2^2 + \alpha_3\, s - w\, \alpha_1\alpha_2 - x\, \alpha_3(\alpha_1 + \alpha_2)$ and $w = p_{56}^2 = -1$. The bubble acts as a single propagator of mass squared $s(a)$ and the remaining loop is a triangle with Symanzik polynomial F. For $x < -\frac{1}{4}$ the integrand is positive and the integral converges absolutely. With `Kira` [81] we find seven master integrals on the equal-mass slice and nineteen at the generic mass point.

Function space. The top integral at order ε^0 is a weight-three function on the curve of the scoop sunrise. For equal masses that curve is the modular curve $X_1(6)$ with cusps $x \in \{0, 1, 9\}$, the same $\Gamma_1(6)$ curve as for the equal-mass sunrise [10]. The d log alphabet at order ε^0 has six rational letters,

$$\{\, x,\ x-1,\ x-9,\ 2x+1,\ 4x+1,\ L_{\text{bub}} \,\}, \qquad L_{\text{bub}} = x^2 - 10x + 5 = (x - r_+)(x - r_-), \quad r_\pm = 5 \pm 2\sqrt{5}. \tag{98}$$

Here $\{x, x-1, x-9\}$ are the cusp letters, whose kernels involve the period ψ_1 of the scoop curve, and $\{2x+1, 4x+1\}$ are apparent and normalization letters of the d-dimensional system. The letter $L_{\rm bub}$, which occurs in the top sector only, is the leading Landau singularity of the cone itself, eq. (6.48) of Ref. [73] restricted to the slice. It is the locus on which the invariant mass flowing through the scoop reaches its two-particle threshold, or equivalently the Landau locus of the one-loop triangle with the same external momenta and internal masses $(m, m, 2m)$. At the boundary point $x = -1$ the cross-ratio $(x - r_+)/(x - r_-)$ equals φ^4, with φ the golden ratio.

For the masses $(1, 2, 3, 5)$ the scoop curve is the sunrise curve with masses squared $(1, 3, 5)$ [8], with threshold letter

$$Q_{\rm scoop}(x) = x^4 - 36x^3 + 302x^2 - 564x + 121 = \prod_{\pm\pm} (x - (\pm 1 \pm \sqrt{3} \pm \sqrt{5})^2), \tag{99}$$

while the sub-sunrise $(2, 3, 5)$ contributes the analogous quartic Q_{14} and the bubble letter becomes $L^{\rm gen}_{\rm bub} = x^4 - 40x^3 + 348x^2 - 880x + 196$. This family of curves is not modular. Its fiber at $x = -1$ has rational Weierstrass roots $(e_1, e_2, e_3) = (\frac{11}{3}, \frac{2}{3}, -\frac{13}{3})$, $\lambda = \frac{5}{8}$ and $j = 470596/225 = (686/15)^2$, and since j is not an algebraic integer the fiber has no complex multiplication. We give the complete nine-letter alphabet of the family with symbolic masses in Appendix C.

At order ε^0 the top sector reduces to the pair (T, F_5) with $F_5 = [1, 1, 1, 1, 0, -1, 0]$, and by eliminating F_5 we obtain a second-order equation for T alone. At equal mass it reads

$$L_T[T] = \alpha(x)\, S(x) + \beta(x)\, S'(x) + g_1(x) - g_t(x)\, {\rm Tri}_0, \tag{100}$$

where $S = [1, 0, 1, 1]_{\varepsilon^0}$ is the scoop sunrise, ${\rm Tri}_0 = 4 \ln \varphi/\sqrt{5}$ is the $d = 2$ bubble at $p^2_{56} = -1$, and

$$\begin{aligned} L_T &= \partial_x^2 + \tilde{p}_1\, \partial_x + \tilde{p}_0, \qquad \tilde{p}_1 = \frac{14x^5 - 155x^4 + 520x^3 - 316x^2 + 22x - 5}{(x-1)(4x+1)(x^2-10x+5)(x^2-4x+1)}, \\ \tilde{p}_0 &= \frac{6\,(x^4 - 8x^3 + 24x^2 - 4x + 3)}{(x-1)(4x+1)(x^2-10x+5)(x^2-4x+1)}, \end{aligned} \tag{101}$$

$$\begin{aligned} \alpha &= \frac{-8\,(2x^4 - 9x^3 - 15x^2 - 25x - 15)}{3(x-9)(x-1)(4x+1)(x^2-10x+5)(x^2-4x+1)}, \\ \beta &= \frac{-2\,(11x^5 - 63x^4 + 48x^3 - 340x^2 + 165x - 45)}{3(x-9)(x-1)(4x+1)(x^2-10x+5)(x^2-4x+1)}, \\ g_1 &= \frac{8}{(x-9)(x-1)(x^2-10x+5)}, \qquad g_t = \frac{2\,(2x^3 - 27x^2 + 18x - 1)}{(x-1)(4x+1)(x^2-10x+5)(x^2-4x+1)}. \end{aligned} \tag{102}$$

The two homogeneous solutions of L_T are algebraic,

$$\begin{aligned} y_\pm(x) &= q_\pm(x)^{-1/2}, \qquad q_\pm = \tfrac{1}{2}\Big(2x^2 + 8x - 5 \pm \sqrt{5}\,(2x-1)\sqrt{4x+1}\Big), \\ q_+ q_- &= (x-1)^2\,(x^2 - 10x + 5), \end{aligned} \tag{103}$$

and the elliptic curve therefore enters T only through the sunrise S in the source.

The singular points of T are the cusps $x \in \{0, 1, 9\}$, which enter through the source, and $x = r_\pm$, where L_T has local exponents $\{-\frac{1}{2}, 0\}$. The remaining factors $4x + 1$ and $x^2 - 4x + 1$ of L_T carry exponents $\{0, \frac{1}{2}\}$ and $\{0, 2\}$. On the generic slice the source has a third term, proportional to the $(2, 3, 5)$ sunrise S_{14} with Q_{14} in the denominator of its kernel, and the operator for T that our elimination produces is of third order. The singular set is then $\{x = 0\} \cup \{Q_{\rm scoop} = 0\} \cup \{Q_{14} = 0\} \cup \{3x^2 - 18x + 11 = 0\} \cup \{L^{\rm gen}_{\rm bub} = 0\}$.

Because the homogeneous solutions $y_\pm$ are algebraic, the function T is obtained from the sunrise S by one further integration and is a length-two elliptic polylogarithm on the scoop curve. Its third-kind punctures are at the Landau points $s_\pm(x)$ of the cone (eq. (105)), away from the cusps, and its boundary value is therefore not expected to lie in the ring of cusp values of the sunrise.

Result. No. 15 (equal masses, order ε^0). With $W = y_+y'_- - y'_+y_-$, variation of parameters over the algebraic pair gives

$$T(x) = c_+\, y_+(x) + c_-\, y_-(x) + \int_{-1}^{x} \frac{y_-(x)\, y_+(x') - y_+(x)\, y_-(x')}{W(x')} \left(\alpha S + \beta S' + g_1 - g_t \mathrm{Tri}_0\right)(x')\, \mathrm{d}x', \quad (104)$$

with $c_\pm$ fixed by $T(-1)$ and $T'(-1)$. For $x < -\frac{1}{4}$ the two kernels are complex conjugates, $c_+ = \bar{c}_-$, and T is real.

In $d = 2$ the triangle in eq. (97) reduces to its three bubbles, and the double integral collapses to a single integral over the scoop mass,

$$\begin{aligned} T(x) &= 2\int_4^\infty \frac{\mathrm{d}s}{\sqrt{s(s-4)}}\, \frac{2(c-2s)\, B(s;x) + (2c-5)\, \mathrm{Tri}_0}{2c^2 - 10s}, \qquad c = s + 1 - x, \\ B(s;x) &= \int_0^1 \frac{\mathrm{d}a}{a + s(1-a) - x\, a(1-a)}, \end{aligned} \quad (105)$$

where B is the $d = 2$ bubble. The zeros $s_\pm(x) = \frac{1}{2}(3 + 2x \pm \sqrt{5}\sqrt{4x+1})$ of $2c^2 - 10s$ are the Landau points of the effective triangle, and $L_{\mathrm{bub}}(x) = 0$ is the condition that one of them reaches the endpoint $s = 4$. We integrate the Tri_0 term in closed form through its residues at $s_\pm$, which gives $T_{\mathrm{elem}} = 4\,\mathrm{Tri}_0 \sum_\pm A_\pm \arctan\sqrt{s_\pm/(4-s_\pm)}/\sqrt{s_\pm(4-s_\pm)}$ with $A_\pm = (2(s_\pm + 1 - x) - 5)/(2(s_\pm - s_\mp))$. The remainder is the integral of the logarithm in B against $\mathrm{d}s/Y$ on the scoop curve $Y^2 = s(s-4)\,\lambda(s,1,x)$ with simple poles at $s_\pm$.

No. 16 (masses $(1,2,3,5)$, order ε^0). The variation-of-parameters representation of T has the form of eq. (104) with the third-order operator and the additional source S_{14}, and eq. (97) holds as written with $(m_1^2, m_2^2, m_3^2, m_4^2) = (1,2,3,5)$. The periods of the scoop curve that enter the source at the boundary point are the convergent integrals

$$\psi_1(-1) = 2\int_{e_1}^{\infty} \frac{\mathrm{d}t}{\sqrt{4(t-e_1)(t-e_2)(t-e_3)}}, \quad \psi_2(-1) = 2i\int_{e_2}^{e_1} \frac{\mathrm{d}t}{\sqrt{4(t-e_1)(t-e_2)(t-e_3)}}, \quad (106)$$

with $(e_1, e_2, e_3) = (\frac{11}{3}, \frac{2}{3}, -\frac{13}{3})$, giving $\psi_1(-1) = 1.3983285\ldots$ and $\psi_2(-1)/i = 1.2449101\ldots$.

No. 17 (order ε^1, weight four). Writing $f_{j,k}$ for the order-ε^k coefficient of the j-th master, so that $(T, F_5) = (f_{4,0}, f_{5,0})$, the order-$\varepsilon^1$ pair $(f_{4,1}, f_{5,1})$ satisfies the same homogeneous equations as (T, F_5). Eliminating $f_{5,1}$ therefore gives $L_T[f_{4,1}]$ equal to a source assembled from $\sum_j [A^{(0)}_{4j} f_{j,1} + A^{(1)}_{4j} f_{j,0}]$ and the analogous sum with index 5, where $A^{(0)}$ and $A^{(1)}$ are the first two orders of the connection matrix in ε. Hence $f_{4,1}$ follows from one more integration against the kernels $y_\pm$ and is a length-three iterated integral, whose sources include the order-ε^1 coefficients of the scoop masters and the order-ε^0 top pair.

Written out, $f_{4,1}$ is an iterated integral on the seven-letter alphabet $\{x,\ x-1,\ x-9,\ 2x+1,\ 4x+1,\ x-r_+,\ x-r_-\}$ with the sunrise periods ψ_1, ψ_2 in the sources. It consists of 88 words, each labeled by its last letter, source master and kernel, with residues in $\mathbb{Q}(\sqrt{5})$ that we obtain by exact partial fractions of the entries A_{4j}. For example, at $x = r_\pm$ the diagonal residue is $\mathrm{res}_{r_\pm} A^{(0)}_{4,4} = -\frac{4}{11} \mp \frac{6\sqrt{5}}{55}$ and the residue of the entry that couples the scoop sunrise to the top

integral is $\mathrm{res}_{r_\pm} A^{(0)}_{4,2} = \frac{188}{1353} \pm \frac{118\sqrt{5}}{1353}$, Galois conjugates under $\sqrt{5} \to -\sqrt{5}$. The part of each word that lies in the scoop sunrise sector involves only the cusp letters $\{0, 1, 9\}$. The complete list of the 88 words with their residues is supplied as a data file [106] (Appendix G).

Boundary data. We fix the boundary values at $x = -1$ without numerical input, from the behavior of the top sector at large x. In the variable $u = 1/x$ the operator L_T has indicial exponents $\{1, \frac{3}{2}\}$ at $u = 0$. Expansion by regions allows only integer powers of u times logarithms, which removes the $u^{3/2}$ branch. Matching to the hard bubble at large momentum Q, $B(Q; 1, 1) \simeq (2 \ln Q - \ln(m_3^2 m_4^2))/Q$, then fixes the constant term τ_0 of the u^1 branch,

$$\tau_0 = 0 \quad \text{(equal masses)}, \qquad \tau_0 = \ln 15 \cdot \ln(1+\sqrt{2})/\sqrt{2} \quad \text{(masses } (1,2,3,5)\text{)}. \tag{107}$$

Resonance at the integer indicial exponent forces the coefficient of $u \ln u$ to be $t_{11} = 2\,\mathrm{Tri}_0 = 8 \ln \varphi/\sqrt{5}$, which reproduces the logarithm of the hard bubble.

Besides γ_E and ζ_2, the boundary constants of the bubble subsector involve Tri_0 and the integral

$$J = \int_0^1 \frac{\ln(1+a-a^2)}{1+a-a^2}\,\mathrm{d}a = \frac{2}{\sqrt{5}}\Big[\ln 5\, \ln\varphi + \mathrm{Li}_2\Big(\frac{5-\sqrt{5}}{10}\Big) - \mathrm{Li}_2\Big(\frac{5+\sqrt{5}}{10}\Big)\Big] = 0.1271151779\ldots, \tag{108}$$

a combination of dilogarithms at algebraic arguments. In particular, the bubble master is

$$f_1 = -\Gamma(\varepsilon)\,\Gamma(1+\varepsilon)\int_0^1 (1+a-a^2)^{-1-\varepsilon}\,\mathrm{d}a, \qquad f_1\big|_{\varepsilon^{-1}} = -\mathrm{Tri}_0, \qquad c_{1,0} = f_1\big|_{\varepsilon^0} = 2\gamma_\mathrm{E}\,\mathrm{Tri}_0 + J, \tag{109}$$

and at the next order $c_{1,1} = -\big((2\gamma_\mathrm{E}^2 + \zeta_2)\,\mathrm{Tri}_0 + 2\gamma_\mathrm{E} J + K/2\big)$ with $K = \int_0^1 \ln^2(1+a-a^2)/(1+a-a^2)\,\mathrm{d}a$.

For No. 17 the order-ε^1 boundary conditions are of the same kind as those at order ε^0. The boundary constants of the scoop masters at order ε^1, $(-\pi^2, -18\zeta_3)$, follow as Mellin residues of the exact d-dimensional Bessel representation of the scoop sunrise,

$$[1,0,1,1] = -2^d P^{-\nu}\int_0^\infty r^{1-2\nu} J_\nu(Pr)\,K_\nu(r)^3\,\mathrm{d}r, \qquad \nu = -\varepsilon, \tag{110}$$

with P the Euclidean momentum flowing through the scoop. The constant term of the u^1 branch of the top integral follows from the two-region expansion at large x, in which the double, single and zeroth powers of the logarithm carry the coefficients Tri_0, $4\gamma_\mathrm{E}\mathrm{Tri}_0 + 2J$ and $-2\zeta_2\,\mathrm{Tri}_0$. As at order ε^0, the integer-power ansatz removes the $\sqrt{4x+1}$ branch of the dotted top integral (the top integral with one propagator squared), and the one remaining constant is set to zero by the required decay at large x. For No. 16 four of the subsector masters have resonant indicial exponents at $u = 0$, and the corresponding boundary constants, listed in Appendix C, lie in $\mathbb{Q}[\gamma_\mathrm{E}, \ln 2, \ln 3, \ln 5, \zeta_2]$.

Integrating the connection from $u = 0$ to $x = -1$ with these conditions, we obtain the boundary values

$$\text{No. 15:} \quad T(-1) = 0.60984239\ldots, \tag{111}$$

$$\text{No. 16:} \quad T(-1) = 0.13489705\ldots, \tag{112}$$

$$\text{No. 17:} \quad f_{4,1}(-1) = -0.67751873\ldots. \tag{113}$$

By direct quadrature of eq. (97) we reproduce the equal-mass $T(-1)$ to 284 digits.

We searched for integer relations [16] between $T(-1)/\psi_1$ and the $\Gamma_1(6)$ ring of cusp values $\{1, L(\chi_{-3}, 2), I(1, f_3), I(f_3), I(1, 1, f_3), \pi^3, \zeta_3, \log|q_C|\}$ extended by $\mathbb{Q}(\sqrt{5})$, where the $I(\cdots)$ are

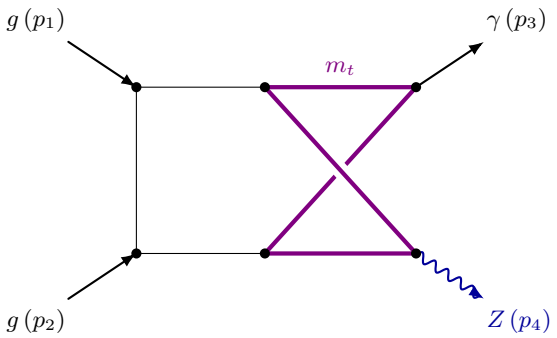

Figure 15: The nonplanar two-loop graph for $gg \to Z\gamma$ through a top-quark loop, No. 20 of Table 1. Thin lines are massless, thick violet lines carry m_t; $g(p_1)$, $g(p_2)$ and $\gamma(p_3)$ are on shell and the wavy Z leg has $p_4^2 = m_Z^2$. All seven propagators of eq. (114) are drawn (sector 127); the masters of this entry belong to sector 125, with the massless line D_2 between the gluon vertices contracted.

iterated integrals of the modular form f_3 of the equal-mass sunrise [10] at the nome q_C of $x = -1$. For No. 16 the ring is the L-value and regulator ring of $\mathbb{Q}(\sqrt{3}, \sqrt{5})$, and both searches extend to height 10^{12}. Neither search found a relation, whereas the same procedure recovers the boundary constant of the scoop sunrise. An analogous search for $f_{4,1}(-1)$ is also negative. To the heights searched, the three boundary values of Nos. 15–17 therefore lie outside the rings tested, and we regard them as new transcendental constants.

Checks. **No. 15.** At $x = -2$ the function T obtained from the differential equation agrees with an `AMFlow` [95] evaluation to 134 digits. For $x < -\frac{1}{2}$ we evaluate T by integrating the connection, and for $-\frac{1}{2} < x < -\frac{1}{4}$, beyond the letter $2x + 1 = 0$ of the connection, by quadrature of eq. (97). For Minkowski kinematics we integrate the slice connection from $x = -1$ with $x \to x + i0$ along a path past the real singular points to $x = 12$, above every threshold. All fourteen components of the continued solution vector agree there with `AMFlow` to 57 digits, imaginary parts included.

The closed forms of this subsection hold on the slice only. Off the slice the equal-mass family has nine masters, and we computed the two-variable connection (A_x, A_y) in (p_{12}^2, p_{34}^2) at $p_{56}^2 = -1$ as rational 9×9 matrices satisfying the integrability condition. Integrating it from `AMFlow` values at $(p_{12}^2, p_{34}^2) = (-3, -4)$ to the three further points $(-3, -\frac{15}{4})$, $(-\frac{5}{2}, -\frac{15}{4})$ and $(-\frac{15}{4}, -\frac{5}{2})$, we reproduce independent `AMFlow` evaluations of the nine masters through order ε^1 to 64, 64 and 48 digits (Appendix C).

No. 16. The value of T from the differential equation at $x = -2$ agrees with `AMFlow` to 118 digits. Because the connection is rational in the masses, we could repeat the boundary construction at a second mass point, $(m_1^2, m_2^2, m_3^2, m_4^2) = (1, 3, 2, 7)$, used in no fit. There $T(-2) = 0.10288957\ldots$, in agreement with `AMFlow` to at least 86 digits, the precision of the reference values at that point.

No. 17. The order-ε^1 coefficient $f_{4,1}$ from the differential equation agrees with `AMFlow` at $x = -2$ to 134 digits. For the masses $(1, 2, 3, 5)$ all nineteen order-ε^1 boundary values follow from the same conditions at $u = 0$ and agree with the `AMFlow` values to their full precision.

5.6 Elliptic masters in $gg \to Z\gamma$

The two-loop amplitudes for $gg \to Z\gamma$ with the exact dependence on the top-quark mass require the nonplanar four-point family of Ref. [13] with one massive external leg, shown in Figure 15, in which the maximal cut of the massive loop is an elliptic curve. For a massless quark loop the amplitudes

are known [68]. The heavy-quark family with all four external legs massless, which enters $gg \to \gamma\gamma$, was computed in canonical form in Refs. [22, 44], and its nonplanar three-point function at order ε^0 is that of Ref. [115]. We are not aware of an analytic treatment of the elliptic sectors at $m_Z \neq 0$. Entry No. 20 of Table 1 is the pair of elliptic master integrals of the six-propagator sector at one fixed ratio m_Z^2/m_t^2, and it is new.

Definition. With all momenta incoming, $p_1^2 = p_2^2 = p_3^2 = 0$, $p_4^2 = m_Z^2$, loop momenta k_1, k_2 and the top mass set to $m_t^2 = 1$, the propagators of Figure 15 and the kinematic variables of this entry are

$$\begin{aligned} &D_1 = k_1^2, \qquad D_2 = (k_1 - p_1)^2, \qquad D_3 = (k_1 - p_1 - p_2)^2, \qquad D_4 = k_2^2 - 1, \\ &D_5 = (k_2 - p_1 - p_2 - p_3)^2 - 1, \qquad D_6 = (k_1 - k_2)^2 - 1, \qquad D_7 = (k_1 - k_2 + p_3)^2 - 1, \\ &s = (p_1 + p_2)^2, \qquad t = (p_1 + p_3)^2, \qquad u = M - s - t, \qquad M \equiv \frac{m_Z^2}{m_t^2} = \frac{7}{25}, \end{aligned} \tag{114}$$

with the integrals $I_{\nu_1 \cdots \nu_7}$ defined by eq. (1) with $L = 2$ and $d = 4 - 2\varepsilon$. In this entry t denotes the invariant formed from the gluon momentum p_1 and the photon momentum p_3. We label sectors by the binary code of the propagators present: the graph with all seven propagators is sector 127, and contracting D_2, the massless line joining the two gluon vertices, gives sector 125. Sector 125 has two elliptic master integrals, R_a and R_b in the basis of the reduction [81], and we use the canonical combinations $g_{31} = \omega_0^{-1} e^{2\gamma_E \varepsilon} R_a$ and $g_{32} = e^{2\gamma_E \varepsilon} R_b$, with ω_0 the holomorphic period of the curve (115) at its cusp $s = 0$. The result holds at the fixed ratio $M = 7/25$. It gives the sector-125 pair on the line $t = -1/3$ for $-1/4 \leq s \leq 0$ and, through eq. (122), as a function of t at $s = -1/4$. We check the sector-127 masters only by transporting their differential equation in t along the line $s = -1/4$ from one of four `AMFlow` points to the next, where the transported and computed values agree to at least 37 digits; we give no sector-127 boundary value that does not come from `AMFlow`.

Function space. The maximal cut of the massive loop is the quartic

$$y^2 = P\,(P + s - M)\,(P^2 + (s - M)P - 4s), \tag{115}$$

in a coordinate P on the cut, an elliptic curve whose j-invariant is unchanged under $s \to M^2/s$. At $M = 0$ it is the curve of the massless-leg family, which is modular for $\Gamma_0(4)$ with Hauptmodul $x = s$ and $j = (s^2 + 16s + 16)^3/(s(s + 16))$. For nonzero Z mass, eq. (115) is obtained from that family by the quadratic base change $x = (s - M)^2/s$. The curve is therefore modular for $\Gamma_0(4)$, of index six with cusp widths $(1, 1, 4)$, and its Hauptmodul fixes the modular parameter $\tau(s)$ through

$$\Big(\frac{\eta(\tau)}{\eta(4\tau)}\Big)^8 = \frac{256\,s}{(s - M)^2}. \tag{116}$$

We refer to Ref. [107] for the identification of the modular curve from the singular fibers. The base change splits the three cusps of the $M = 0$ family into five, with fibers of Kodaira type I_4 at $s = 0$ and $s = \infty$, type I_2 at $s = M$, and type I_1 at the two roots $r_{1,2}$ of $625s^2 + 9650s + 49 = 0$, the threshold $(s - M)^2 + 16s = 0$ at $M = 7/25$. Among these points, $s = 0$ is the MUM cusp, with holomorphic period $\omega_0(s)$. Because $\Gamma_0(4)$ has no cusp forms in the weights that occur, the one elliptic letter is the Eisenstein kernel

$$\kappa(s) = \frac{s\,(625\,s^2 + 2150\,s + 49)}{625\,s^2 + 9650\,s + 49}, \tag{117}$$

which couples ω_0 to the quasi-period of the second kind and pulls back to a weight-three Eisenstein series in $M_3(\Gamma_0(4), \chi_{-4})$, the space spanned by $\eta(\tau)^4\eta(2\tau)^6\eta(4\tau)^{-4}$ and $\eta(\tau)^{-4}\eta(2\tau)^6\eta(4\tau)^4$. The other letters are logarithmic, and in (s,t) the singular locus is

$$\{\, s,\ s-4,\ s+4,\ s+16,\ t,\ s+t\,\} \ \cup\ \{(s-M)^2+16\,s\}, \tag{118}$$

while on the line $t=-1/3$ the alphabet in s is $\{s,\ s-4,\ 25s-7,\ 25s+7,\ 25s+93,\ 75s-71,\ 25s^2-7s+7,\ 625s^2+9650s+49\}$. In particular, the letters $s-4$, $25s+7$, $25s+93$, $75s-71$ and $25s^2-7s+7$ lie at interior points of the modular curve $X_0(4)$. Hence their d log forms are meromorphic modular forms [37], and the full masters are not iterated integrals of Eisenstein series alone [10].

Result. We give the pair on the line $t=-1/3$ as the solution of an exact differential equation in s with an analytic boundary vector at the cusp $s=0$, and at $s=-1/4$ as the polynomials in t of eq. (122). The homogeneous part of the solution, the maximal-cut block, has the structure of eq. (121). On the line $t=-1/3$ the reduction of sector 125 and its subsectors gives 22 master integrals, and we construct their connection $A_s(\varepsilon,s)$ exactly, as a matrix of rational functions. In the t direction the homogeneous block of the elliptic pair, in the basis (R_a,R_b), is

$$A_t^{\text{hom}} = \begin{pmatrix} 0 & 0 \\ \dfrac{-d\,s^2\,(t-u)}{(d-2)(t-u)^2-4\,t\,u} & \dfrac{4(d-1)(t-u)}{(d-2)(t-u)^2-4\,t\,u} \end{pmatrix}, \tag{119}$$

with $d=4-2\varepsilon$ and $u=M-s-t$. Because the upper entries vanish, R_a is independent of t and R_b carries all the t-dependence of the pair. In the s direction, writing A_1 for the order-ε part of the connection of this block and integrating its trace, we obtain an algebraic prefactor,

$$\text{pref}(s) \ =\ \exp\Big(\varepsilon\int \text{tr}\,A_1\,ds\Big) = s^{-2\varepsilon}\left(\tfrac{s-r_2}{s-r_1}\right)^{\frac{10\sqrt{93}}{93}\varepsilon}, \tag{120}$$

while the traceless part reduces to the single kernel κ. The general solution of the maximal-cut block is therefore

$$\begin{aligned} g_{\text{spine}}(s) \ &=\ \text{pref}(s)\,\Big[\,c_1+c_2\,\tau(s)+\text{Eich}_{\Gamma_0(4)}[B_{2,4};\ i\infty\to s](\tau(s))\,\Big], \\ B_{2,4}(\tau) &= -\tfrac{1}{24}\big(E_2(\tau)-4\,E_2(4\tau)\big), \end{aligned} \tag{121}$$

where $B_{2,4}$ is the weight-two Eisenstein series of $\Gamma_0(4)$ with constant term $a_0=1/8$, $\text{Eich}_{\Gamma_0(4)}[\,\cdot\,;i\infty\to s]$ is its Eichler integral [62] from the cusp $i\infty$, regularized there, and c_1, c_2 are constants. The full masters do not have the form of eq. (121) with constant c_1 and c_2, because nine polylogarithmic subsectors enter the equation for g_{32} at order ε^0 with t-dependent coefficients and no subtraction that depends on s alone removes them. We therefore obtain the pair by integrating the full system of 22 equations in s, from analytic boundary values at the cusp $s=0$ to $s=-1/4$.

At $s=-1/4$ the dependence of the sector-125 system on t is polynomial. We reduce it at fixed s to 14 master integrals, only three of which depend on t. No sector of this system contains a propagator carrying p_1; every corner integral is thus a two-loop vertex function of $p_{12}=p_1+p_2$ and p_3, and t enters only through the numerators $(k_1-p_1)^{2n}$. Since $p_1\cdot p_{12}=s/2$ and $p_1\cdot p_3=t/2$, each master is then a polynomial in t of degree n with t-independent coefficients. We solve the differential equation in t exactly. With $L_1\equiv 448\,\varepsilon\,t-236\,t-53$ and $D_{2q}\equiv\varepsilon\,(200t-53)^2-(60000\,t^2-31800\,t+2809)$, where $200t-53=100\,(t-u)$, we find

$$\begin{aligned} M_8 &= c_8\,(200t-53)+\tfrac{1}{2}K_5+\tfrac{1}{8}K_6+\tfrac{1}{2}K_7, & M_{11} &= c_{11}\,L_1+C_{11}(\varepsilon), \\ g_{32} &= c_{13}\,D_{2q}+B_0(\varepsilon), & g_{31} &= K_{12}, \end{aligned} \tag{122}$$

exact in ε. Here M_8, M_{11} and g_{32} are the three t-dependent masters, built from entries 8, 11 and 13 of Table 8, and $K_0, \ldots, K_{10}, K_{12}$ are the t-independent corner masters of the system, among them K_5, K_6 and K_7, entries 5–7 of that table. Both C_{11} and B_0 are $\mathbb{Q}(\varepsilon)$-linear combinations of these corner masters, and c_8, c_{11}, c_{13} are the three integration constants, fixed at one value of t. Every logarithm that the variation-of-parameters solution could generate, namely $\log(53-200t)$, $\log L_1$, $\log(-D_{2q})$ and the primitive of $1/D_{2q}$, cancels identically. Appendix C.4 lists the fourteen masters of the system at $s=-1/4$ and the structure of its connection in t.

Boundary data. We fix the boundary values at the MUM cusp, where each of the 22 masters behaves as $a(s)+b(s)\,(-s)^{-\varepsilon}+O(s,s^{1-\varepsilon})$ with a and b analytic and without logarithms. We obtain all 22 boundary values in closed form, as 11 sums of Γ functions and ${}_3F_2$ values, 6 collinear coefficients $b(0)$ given by Beta-function moments, and 5 zeros. The six corner masters $K_0, \ldots, K_5$ of eq. (122) are two-loop vertex integrals free of p_1, and we evaluate them by Mellin–Barnes representations as Γ functions and ${}_2F_1$, ${}_3F_2$ values at rational arguments. In addition, the pair satisfies 25 cusp conditions, all of which follow analytically from the Frobenius expansions at the five cusps in s and from the limit $M\to 0$ onto the massless-leg family [22, 115]. The period data of the Eichler integral in eq. (121) are those of level four, namely $a_0(B_{2,4})=1/8$, $L(\chi_{-4},1)=\pi/4$, and the constant terms $\{-3,\,3/4,\,0\}$ of the level-four E_2 at the cusps ∞, 0 and $1/2$. Under $\tau\to\tau+n$ the Eichler integral shifts by a rational multiple of $i\pi$,

$$\mathrm{Eich}_{\Gamma_0(4)}[B_{2,4}](\tau+n)-\mathrm{Eich}_{\Gamma_0(4)}[B_{2,4}](\tau)\;=\;n\cdot a_0(B_{2,4})\cdot 2\pi i\;=\;n\cdot\frac{i\pi}{4}, \tag{123}$$

and it is single valued once this cocycle is included. The weight-two constant of level four is Catalan's constant $G=L(\chi_{-4},2)=0.91596559\ldots$, and we find no integer relation between it and the boundary constants of the pair.

Integrating the system of 22 equations from $s=0$ to $s=-1/4$ at $t=-1/3$ determines the remaining constants $K_6, \ldots, K_{10}$ and K_{12} of eq. (122). Of these, K_6, K_7, K_9 and K_{10} have closed forms of the same Γ-function and ${}_3F_2$ type as those of $K_0, \ldots, K_5$. The constant K_{12}, the value of the elliptic master g_{31} at $s=-1/4$, is known numerically to 137 significant figures, and since it belongs to the elliptic sector we expect no closed form for it in classical constants. The closed forms of $K_0, \ldots, K_5$, K_6, K_7, K_9, K_{10} and the numerical value of K_{12} are supplied with the evaluation code of this entry (Appendix G) [106].

Checks. At $(s,t)=(-1/4,-1/3)$, a point that enters no boundary value, we compare the 22 masters with `AMFlow` [95] and find agreement at every order from ε^{-2} through ε^{4} to 109 digits, the precision to which the `AMFlow` values are themselves determined. Fixing the constants of eq. (122) at $t=-25$, we reproduce `AMFlow` values at $t=-1/3$ and $t=-3/2$ with the polynomial forms to a relative deviation below 10^{-126}. Finally, away from both lines we transport the 14-master system in t from the line $t=-1/3$ to 25 Euclidean points with $s\in\{-1/20,-1/10,-3/20,-1/5,-9/40\}$ and $t\in\{-1/2,-2/3,-5/6,-1,-5/4\}$. At five of them, $(s,t)=(-1/5,-1/2)$, $(-1/10,-1/2)$, $(-1/20,-5/4)$, $(-9/40,-5/4)$ and $(-3/20,-5/6)$, independent `AMFlow` evaluations agree with the result to a relative deviation below 10^{-47}. For reference, in the normalization of eq. (1) without any factor $e^{\gamma_E\varepsilon}$, at $(s,t)=(-1/4,-1/3)$ we find

$$R_a\big|_{\varepsilon^0}=0.55129454\ldots,\qquad R_a\big|_{\varepsilon^1}=0.90052626\ldots,\qquad \tau(-1/4)=-\tfrac{1}{2}+0.85824013\ldots\,i, \tag{124}$$

and Appendix A collects these values and the further comparisons.

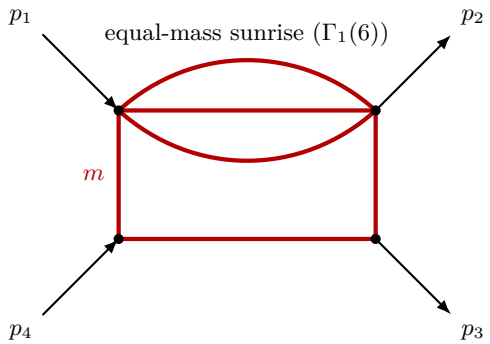

Figure 16: The three-loop light-by-light graph with a sunrise insertion, No. 27 of Table 1. Four on-shell massless photons $p_1, \ldots, p_4$ attach at the corners of a one-loop box in which one line is replaced by the two-loop equal-mass sunrise, the three lines joining two corners; all six internal lines have mass m (thick red). The invariants are $s = (p_1 + p_2)^2$ and $t = (p_2 + p_3)^2$.

5.7 The light-by-light box with a sunrise insertion

The graph of Figure 16, labeled LBL3E in Table 1, is a three-loop contribution to light-by-light scattering through a massive loop: the one-loop box with a two-loop self-energy, here the equal-mass sunrise, inserted on one internal line. Two-loop massive and three-loop massless light-by-light amplitudes are known [1, 17], and this three-loop massive graph, No. 27, is to our knowledge new. The only elliptic curve of the graph is the sunrise curve of the insertion [25, 10], and the function space is therefore that of the equal-mass sunrise, No. 8, continued to higher orders in ε.

Definition. With the photons on shell, $p_i^2 = 0$, and $s = (p_1 + p_2)^2$, $t = (p_2 + p_3)^2$, the integral of this entry is the scalar box of Figure 16 with unit powers,

$$I_{\text{box}}(s, t; m^2) = \int \prod_{j=1}^{3} \frac{d^d k_j}{i\pi^{d/2}} \prod_{i=1}^{6} \frac{1}{q_i^2 - m^2}, \qquad d = 4 - 2\varepsilon, \tag{125}$$

where q_1, q_2, q_3 are the momenta of the three sunrise lines and q_4, q_5, q_6 those of the other three box lines. Here $q_1 + q_2 + q_3 = k$ is the momentum through the box line that carries the insertion (the dressed line), and no factor $e^{\gamma_E \varepsilon}$ is included. The integral family of eq. (125) has six massive propagators and nine irreducible scalar products, with I_{box} the corner integral of its top sector, and reducing it at $(s, t, m^2) = (-7/3, -11/10, 1)$ we find 18 master integrals [81]. We also use the insertion on its own, the two-loop equal-mass sunrise $S_{111}(d; w)$ of section 5.1, as a function of the virtuality $w \equiv k^2$ of the dressed line. The box and the insertion belong to different integral families. The integration-by-parts family in which we analyzed the elliptic content assigns the sixth mass to k and contains no propagator $(k + p_1 + p_2)^2$, so it is a three-point graph whose second Symanzik polynomial does not depend on s. Its ten master integrals split into an elliptic block of seven, in sectors 15, 55*a*–*e* and 63, and a polylogarithmic block of three, in sectors 11, 51 and 59. We evaluate the four-point box of eq. (125) by a dispersion relation over the sunrise cut, eq. (127), and the result holds for $s, t < 0$ at orders ε^{-2} through ε^0.

Function space. In units $m^2 = 1$ the maximal cut of the insertion is the equal-mass sunrise curve

$$y^2 = (w - 1)^3 (w - 9), \tag{126}$$

with modular group $\Gamma_1(6)$, holomorphic period $\psi_1(w)$ and the weight-three cusp form $f_3 \in S_3(\Gamma_1(6))$. Every elliptic sector of the integration-by-parts family of the insertion has exactly the j-invariant of this curve, and the dispersion relation of eq. (127) for the box of eq. (125) requires only this elliptic content and a one-loop box kernel. The letters in w are $\{w,\, w-1,\, w-9\}$, with the three-particle threshold at $w=9$, and in (s,t) the box has the normal thresholds $s=4m^2$ and $t=16m^2$. The elliptic content common to every sector that contains the insertion is the sunrise integral $S_{111}(d;w)$. It is the period ψ_1 times an Eichler integral of f_3 on $\Gamma_1(6)$, with the higher orders in ε generated by the same kernel [9], plus a boundary series $B^{(0)}+\varepsilon B^{(1)}+\varepsilon^2 B^{(2)}+\cdots$ fixed at the cusp. There is no term linear in τ, that is, $(c_1,c_2)=(B^{(0)},0)$ in the notation of eq. (121), as in eq. (71). We compute ψ_1, or equivalently $\varpi_0=\sqrt{3}\,\psi_1/(2\pi)$, both as a Frobenius series of the sunrise Picard–Fuchs operator and as a q-series of level six [92, 10].

Result. For $s,t<0$ the box is a one-dimensional dispersion integral in the virtuality of the dressed line [102],

$$I_{\mathrm{box}}(s,t;m^2)=\int_{9m^2}^{\infty} dw\;\rho_{\mathrm{sun}}(w)\,\big[\mathcal{B}(s,t;w)\big]_{\mathrm{sub}}\;+\;U(s,t), \tag{127}$$

where $\rho_{\mathrm{sun}}(w)$ is the three-particle cut density of S_{111} and $\mathcal{B}(s,t;w)$ is the one-loop box with three lines of mass m and the dressed line of mass squared w. Here the bracket $[\,]_{\mathrm{sub}}$ denotes the box kernel $\mathcal{B}$ after two subtractions, and $U(s,t)$ is the subtraction term, in which two subtraction constants fixed at Euclidean kinematics multiply generalized one-loop triangle integrals T_n expanded to the required order in ε. The density ρ_{sun}, the subtracted kernel and the triangle integrals T_n are given in full with the evaluation code of this entry (Appendix G) [106].

Boundary data. The boundary series of the elliptic content is fixed at the cusp of the sunrise curve, and its leading coefficient is the boundary constant of the equal-mass sunrise in eq. (71),

$$B^{(0)}\;=\;2\,\mathrm{Cl}_2(\pi/3)\;=\;\tfrac{3\sqrt{3}}{2}\,L(\chi_{-3},2). \tag{128}$$

Similarly, $B^{(1)}$ and $B^{(2)}$ are the order-ε and order-ε^2 terms of the sunrise boundary series generated by ${}_2F_1(-2\varepsilon,-\varepsilon;1-\varepsilon;e^{2\pi i/3})$. In the ring of sixth-root-of-unity constants [29] extended by the log-sine integrals $\mathrm{Ls}_n^{(k)}(\theta)=-\int_0^\theta x^k\log^{n-1-k}\!\big(2\sin\tfrac{x}{2}\big)\,dx$ we find

$$\begin{aligned} B^{(1)} &= \tfrac{1}{6}\pi^3-2\,\log 3\,\mathrm{Cl}_2(\pi/3)+3\,\mathrm{Ls}_3(2\pi/3),\\ B^{(2)} &= -2\,\pi\zeta_3-\tfrac{1}{6}\pi^3\log 3+\log^2 3\,\mathrm{Cl}_2(\pi/3)+2\,\mathrm{Ls}_4(2\pi/3)-3\,\log 3\,\mathrm{Ls}_3(2\pi/3), \end{aligned} \tag{129}$$

and since $\mathrm{Ls}_3(\pi/3)=-\frac{7}{108}\pi^3$ the one new weight-three constant is $\mathrm{Ls}_3(2\pi/3)$. We identified eq. (129) by integer-relation fits of height at most 18 at a working precision of 120 decimal places, and the relations persist at 320.

Checks. We compared the elliptic content with `AMFlow` [95] evaluations of the uncut sunrise at $w=-7/3$ and $w=-4$, two points used nowhere in its construction, and it agrees with them to 71 and 69 digits at the worst order between ε^{-2} and ε^2. For the box, `AMFlow` values of I_{box} at the three Euclidean points $(s,t,m^2)=(-7/3,-11/10,1)$, $(-3/2,-9/5,1)$ and $(-5/4,-12/5,1)$ agree with eq. (127) to 46, 45 and 45 digits at order ε^0. None of the three `AMFlow` values enters the construction. At the first point the order-ε^1 term of eq. (127), which requires the cut density and

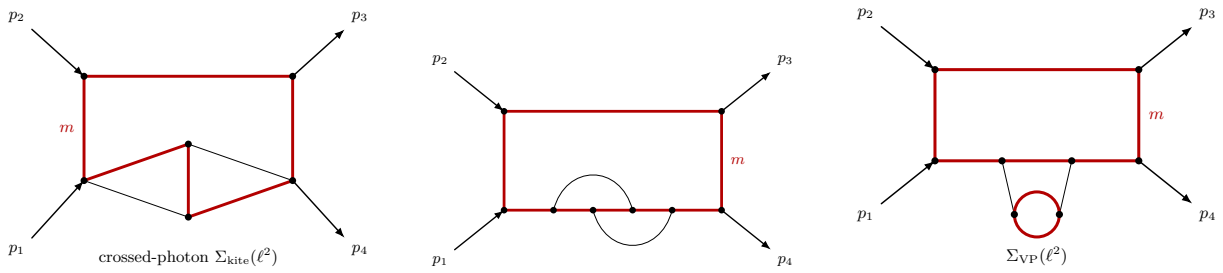

(a) (b) (c)

Figure 17: Three-loop light-by-light boxes with a self-energy insertion on one massive line; the stubs are the two segments of that line on either side of the insertion. Thick (red) lines carry mass m, thin lines are massless, and the four external photons $p_1, \ldots, p_4$ are on shell. (a) No. 28: the kite insertion with the two stub propagators removed. (b) No. 29: the QED graph, the crossed-photon self-energy with its two stubs. (c) No. 33: the self-energy whose internal photon carries a vacuum-polarization loop.

the box kernel to one higher order in ε, agrees with `AMFlow` to a relative deviation below 10^{-30}. For reference, at $(s, t, m^2) = (-7/3, -11/10, 1)$ and in the normalization of eq. (125) we find

$$I_{\text{box}}\big|_{\varepsilon^{-2}} = -0.72077283\ldots, \qquad I_{\text{box}}\big|_{\varepsilon^{-1}} = -0.79530628\ldots, \qquad I_{\text{box}}\big|_{\varepsilon^{0}} = -0.20105121\ldots, \tag{130}$$

and the values at the other two points are given in Appendix A.

5.8 Light-by-light boxes with self-energy insertions

Nos. 28, 29 and 33 of Table 1 are three-loop four-photon integrals in which one massive line of the one-loop light-by-light box carries a self-energy insertion (Figure 17). In Nos. 28 and 29 (LBL3SE and LBL3KP in Table 1) the insertion is the two-loop equal-mass kite $\Sigma_{\text{kite}}(\ell^2)$, the crossed-photon electron self-energy. In No. 33 (LBL3VP) it is the two-loop self-energy $\Sigma_{\text{VP}}(\ell^2)$ whose internal photon carries a vacuum-polarization loop, and the three-loop graph then has two closed fermion loops and hence the factor N_f^2 listed in Table 1. Such insertions are two-particle-reducible contributions to the three-loop light-by-light amplitude with a massive fermion. Each integral is therefore a dispersion integral over the mass of the dressed line, in which the one-loop box with one line of variable mass is weighted by the spectral density of the insertion [102, 20]. The massless three-loop [17] and massive two-loop [1] light-by-light amplitudes are known, and we are not aware of a previous computation of the three integrals given here. The kite's master integrals are known in terms of iterated integrals of modular forms for $\Gamma_1(6)$ [79], and the spectral functions of the two-loop electron propagator go back to Sabry [103]. We derive the spectral densities of both insertions from their differential equations and use neither the modular-form representation of the kite nor Sabry's spectral functions.

Definition. All momenta are incoming, with $p_i^2 = 0$, $s = (p_1+p_2)^2$, $t = (p_1+p_3)^2$ and $u = -s-t$. The two planar channels of the box are s and u. With loop momenta ℓ, k_1, k_2 the kite-insertion family has the propagators

$$\begin{aligned}
&D_1 = (\ell+p_1)^2 - m^2, && D_2 = (\ell+p_1+p_2)^2 - m^2, && D_3 = (\ell+p_1+p_2+p_3)^2 - m^2,\\
&D_4 = \ell^2 - m^2, && D_5 = k_1^2 - m^2, && D_6 = k_2^2 - m^2,\\
&D_7 = (\ell-k_1-k_2)^2 - m^2, && D_8 = (\ell-k_1)^2, && D_9 = (\ell-k_2)^2,
\end{aligned} \tag{131}$$

and, in the notation of eq. (1) with $L = 3$,

$$I_\nu(s,t,m^2) \;=\; I_{1,1,1,\nu,1,1,1,1,1}\,, \qquad I_{\rm KP} \equiv I_2, \qquad I_{K_1} \equiv I_1, \qquad I \equiv I_0. \tag{132}$$

Here D_1, D_2, D_3 are the undressed lines of the box, $D_5, \ldots, D_9$ form the kite, and D_4 is the electron line on either side of the insertion, whose two segments we call the stubs. Since both stubs carry the momentum ℓ, the QED graph of Figure 17(b) is $I_{\rm KP}$, with D_4 squared, while I_{K_1} has a single power of the stub. The eight-propagator member $I \equiv I_0$ (No. 28) is the $\nu = 0$ pinch of the QED graph $I_{\rm KP}$ and not itself a QED Feynman diagram, since without the stub the two box corners at the insertion are four-valent; Nos. 29 and 33 are its QED parents. We evaluate and check Nos. 28 and 29 at the reference point $(s,t,m^2) = (-1,-\frac{1}{3},1)$ and at one further point $P_1 = (-\frac{1}{2},-1,1)$, and No. 33 at the reference point at eight fixed values of ε and at four further points $P_1, \ldots, P_4$. The vacuum-polarization family of No. 33 has the propagators $D_1, \ldots, D_4$ of eq. (131) and, in place of the kite propagators,

$$\begin{aligned} &D_5 = (\ell - k_1)^2 - m^2, \qquad D_6 = k_1^2, \qquad D_7 = k_2^2 - m^2, \qquad D_8 = (k_1 - k_2)^2 - m^2, \\ &I_{\rm VP}(s,t,m^2;\varepsilon) \;=\; I_{1,1,1,2,1,2,1,1}\,. \end{aligned} \tag{133}$$

Here the photon propagator D_6 appears squared because the two photon segments on either side of the fermion loop carry the same momentum k_1. The integral I is ultraviolet finite, and we give I, $I_{\rm KP}$ and I_{K_1} at $d = 4$. Since $I_{\rm VP}$ has a double pole in ε, we give it instead at fixed ε in $d = 4 - 2\varepsilon$, together with its first Laurent coefficients. Every kinematic point of this subsection has $s < 0$ and $0 < u < 2m^2$, below the two-particle threshold $u = 4m^2$ of that channel. There every coefficient of the second Symanzik polynomial of the family is positive, and we call such points Euclidean.

Function space. These integrals are elliptic only through the self-energy subgraph, because on the maximal cut they factorize into the one-loop massive box, which is polylogarithmic, times the maximal cut of the self-energy. Above $\ell^2 = 9m^2$ the three-particle cut of either insertion is a phase-space integral on the elliptic curve of the equal-mass sunrise [25, 10]. In the phase-space variable σ of eq. (138), at fixed $v = \ell^2/m^2$, this curve is

$$y^2 = \sigma\,(\sigma - 4)\,(\sigma - x_-)(\sigma - x_+), \qquad x_\pm = (\sqrt{v} \pm 1)^2, \tag{134}$$

which for varying v is the $\Gamma_1(6)$ family of the equal-mass sunrise and kite, eq. (77). We denote by w the dispersion variable, the squared mass of the dressed line in units of m^2. Below the three-particle threshold the spectral densities are polylogarithms of weight two in w for the kite, and powers of $w - 1$ and w times Γ functions for the vacuum polarization. The results are therefore single integrals of these densities against a dilogarithmic kernel, and the elliptic curve enters only through one further integration over the three-particle phase space of the sunrise.

The pinched kite insertion I (No. 28)

Result. The dispersion relation in the mass of the dressed line is

$$I(s,t,m^2) = \frac{1}{\pi}\int_{m^2}^{\infty} \mathrm{d}w'\; \rho(w')\,\mathrm{Box}_1(s,t;M^2{=}w'), \qquad \rho(w') = -\,\mathrm{Im}\,\Sigma_{\rm kite}(w'{+}i0;m^2). \tag{135}$$

Here $\mathrm{Box}_1(s,t;M^2)$ denotes the scalar one-loop box [98] of Figure 17 with three lines of mass m and the dressed line of mass squared M^2, a closed-form combination of dilogarithms. From here on

we set $m^2 = 1$ and write $K(w) = \mathrm{Box}_1(s,t;M^2{=}w)$ for the kernel as a function of the dispersion variable w. Up to the three-particle threshold the density is polylogarithmic of weight two,

$$\rho(w) \;=\; -\frac{\pi}{w}\Big[\,2\ln(w-1)\ln w \;+\; 3\,\mathrm{Li}_2(1-w)\,\Big] \;\equiv\; \rho_{\mathrm{elem}}(w), \qquad 1 < w \le 9, \tag{136}$$

and above it the sunrise cut adds a single further integration,

$$\rho(w) \;=\; \rho_{\mathrm{elem}}(w) \;-\; \frac{1}{w}\int_9^w v\,F_{23}(v)\,\mathrm{d}v, \qquad w > 9, \tag{137}$$

with

$$\begin{aligned} F_{23}(v) &= \frac{2\,\mathrm{Im}\,S(v) - (v+3)\,\mathrm{Im}\,\dot S(v)}{v\,(v-1)^2}, \\ \mathrm{Im}\,S(v) &= -\frac{\pi}{v}\int_4^{x_-}\sqrt{(x_- -\sigma)(x_+ -\sigma)}\,\sqrt{\frac{\sigma-4}{\sigma}}\,\mathrm{d}\sigma, \qquad x_\pm = (\sqrt{v}\pm 1)^2, \\ \mathrm{Im}\,\dot S(v) &= +\frac{\pi}{v}\int_4^{x_-}\frac{(v-1+\sigma)}{\sqrt{(x_- -\sigma)(x_+ -\sigma)}}\,\sqrt{\frac{\sigma-4}{\sigma}}\,\mathrm{d}\sigma. \end{aligned} \tag{138}$$

Here $\mathrm{Im}\,S$ is the three-body cut of the $d = 4$ equal-mass sunrise and $\mathrm{Im}\,\dot S$ that of the sunrise with one line squared. We obtain $\mathrm{Im}\,\dot S$ by differentiating the cut phase-space integral with respect to an internal mass; the derivative then acts only through the polynomial factor $-2(v-1+\sigma)$, and the integrand has no cancellations at large v.

We derive ρ from the discontinuity of the differential system of the kite in w, which has nine master integrals and a connection linear in d [102, 79]. In particular, all discontinuities vanish at order ε^{-2}, and at order ε^{-1} only the one-loop bubble contributes, through the discontinuity $\pi(w{-}1)/w$ of its order-ε^0 term. The diagonal entry of the connection for the kite master is $A_0[8,8] = -1/w$, and $\phi = \mathrm{Im}\,M^{(0)}_{\mathrm{kite}} = -\rho$ therefore obeys the first-order equation $\phi' = -\phi/w + F(w)$, in which the inhomogeneity $F(w)$ collects the discontinuities of the lower masters. Regularity at the two-particle threshold, $\phi(1^+) = 0$, fixes the integration constant. The bubble terms of F give $F_{17}(v) = 2\pi\ln(v-1)/v^2$ and the sunrise with masses $(m,0,0)$ gives $F_{56}(v) = -\pi\ln v/(v(v-1))$, which integrate in closed form to eq. (136), and the equal-mass sunrise pair contributes eq. (138) for $v > 9$. The closed form has the threshold expansion and obeys the sum rule

$$\rho(w) \;\simeq\; A_1\,(w-1)\ln(w-1) + 3\pi\,(w-1), \qquad A_1 = -2\pi; \qquad\qquad \frac{1}{\pi}\int_1^\infty \rho(w)\,\mathrm{d}w \;=\; 6\zeta_3, \tag{139}$$

where the sum rule follows from the large-ℓ^2 limit of the kite, and direct quadrature of eqs. (136)–(138) reproduces it to 48 digits.

For numerical evaluation we exchange the order of integration in the elliptic term,

$$I = \frac{1}{\pi}\int_1^\infty \rho_{\mathrm{elem}}(w)\,K(w)\,\mathrm{d}w \;-\; \frac{1}{\pi}\int_9^\infty v\,F_{23}(v)\,G(v)\,\mathrm{d}v, \qquad G(v) = \int_v^\infty \frac{K(w)}{w}\,\mathrm{d}w, \tag{140}$$

which avoids the numerical cancellation between the elementary and elliptic parts of ρ at large w. The values of I at the reference point and at P_1 are

$$I(-1,-\tfrac{1}{3},1) = 0.52495777\ldots, \qquad I(-\tfrac{1}{2},-1,1) = 0.55006901\ldots. \tag{141}$$

Boundary data. The only boundary condition is threshold regularity, $\phi(1^+) = 0$, and no numerical boundary value enters eq. (140).

Checks. We compare eq. (141) with direct `AMFlow` [95] evaluations of the eight-propagator integral, which agree with it to 59 digits at the reference point and to 59 at P_1.

The QED kite insertions (No. 29)

Result. With the stubs kept, partial fractions in ℓ^2 between the dispersion denominator and the stub propagator D_4^{ν} replace K by subtracted kernels and leave the density unchanged,

$$I_{\mathrm{KP}} = \frac{1}{\pi}\int_1^\infty \rho(w)\, K_P(w)\, \mathrm{d}w, \qquad K_P = \frac{K(w)-K(1)}{(w-1)^2} - \frac{K'(1)}{w-1}, \qquad K_1 = \frac{K(w)-K(1)}{w-1}. \tag{142}$$

The same representation with K_1 in place of K_P gives I_{K_1}. Here $K(1)$ and $K'(1)$ are the kernel and its first derivative at $w=1$, the box with four lines of mass m and its derivative in the mass of one line, both taken from the closed form. The values of the two members at P_1 are

$$I_{\mathrm{KP}}(-\tfrac{1}{2},-1,1) = 0.12675212\ldots, \qquad I_{K_1}(-\tfrac{1}{2},-1,1) = -0.23637432\ldots. \tag{143}$$

Boundary data. As in No. 28, threshold regularity of the density is the only boundary condition.

Checks. We compare both members with `AMFlow` evaluations of the nine-propagator integrals at a sequence of fixed values of ε, extrapolated to $\varepsilon \to 0$. The agreement is 68 digits for I_{KP} and 68 for I_{K_1} at the reference point, which is the accuracy of that extrapolation, and 50 for each at P_1.

The vacuum-polarization insertion I_{VP} (No. 33)

Result. We evaluate the dispersion relation (135) for I_{VP} at fixed ε, with the density and the kernel both exact in d. For $1 < w < 9$ only the two-body cut contributes. The discontinuities of the self-energy's two top-sector masters then obey a differential equation in w whose inhomogeneous term is the cut of the tadpole-times-bubble master,

$$\mathrm{Im}\,(T{\cdot}B)(w;\varepsilon) \;=\; \frac{\Gamma(\varepsilon)}{1-\varepsilon}\,\pi\,\frac{\Gamma(1-\varepsilon)}{\Gamma(2-2\varepsilon)}\,(w-1)^{1-2\varepsilon}\,w^{\varepsilon-1}. \tag{144}$$

Regularity at the two-particle threshold $w=1$ again fixes the integration constants. Above $w=9$ the three-body cut opens, and we write $\rho_{\mathrm{VP}} = \rho_{\mathrm{exact}} - \mathcal{N}(\varepsilon)\,\psi_0(w;\varepsilon)\,\theta(w-9)$, where ρ_{exact} continues the expression obtained on $(1,9)$. The function ψ_0 is the Frobenius solution of the homogeneous 2×2 block of the differential system at $w=9$ with indicial exponent $d-2$, and its coefficients are rational numbers. Its normalization $\mathcal{N}(\varepsilon)$ follows from the leading coefficient of the three-particle phase space,

$$\mathcal{N}(\varepsilon) \;\propto\; \Big[\tfrac{\Gamma(1-\varepsilon)}{\Gamma(2-2\varepsilon)}\Big]^2\, 9^{-\frac{d-2}{2}}\, 48^{\frac{d-3}{2}}\, 4^{-\frac{d-2}{2}}\, B\big(\tfrac{d-1}{2},\tfrac{d-1}{2}\big)\big(\tfrac{2}{3}\big)^{d-2}, \tag{145}$$

with proportionality constant $-\pi/16$ divided by the leading Frobenius coefficient of ψ_0. The three-body discontinuities of the top-sector pair are single integrals over the three-particle cut, exact in d,

$$\mathrm{Im}_3(w;\varepsilon) \;=\; -\pi\Big[\tfrac{\Gamma(1-\varepsilon)}{\Gamma(2-2\varepsilon)}\Big]^2 w^{-\frac{d-2}{2}} \int_4^{x_-} \lambda(w,\sigma,1)^{\frac{d-3}{2}}\,\lambda(\sigma,1,1)^{\frac{d-3}{2}}\,\sigma^{-\frac{d-2}{2}}\,\sigma^{-a}\,\mathrm{d}\sigma. \tag{146}$$

Here $a=1$ and $a=2$ refer to the undotted and dotted top-sector masters, λ is the Källén function and $x_- = (\sqrt{w}-1)^2$. The integrand is the two-body phase space of the fermion pair at invariant mass σ times that of this pair and the electron at invariant mass w. We fix the overall constant of eq. (146) by matching to the elementary discontinuity of the sunrise with masses $(m,0,0)$.

For the kernel we transport the d-dimensional box in w' with its differential equation, whose coefficients are rational functions of w' and d, starting from Feynman-parameter representations of all eight master integrals of the box family at $w' = 5$. Moreover, the Taylor coefficients $\kappa_n(\varepsilon)$ of the kernel at the threshold $w' = 1$ are two-dimensional moment integrals over Feynman parameters. Let $\kappa_2(\varepsilon) = \kappa_2^{(0)} + \varepsilon\kappa_2^{(1)} + O(\varepsilon^2)$ be the second of these threshold coefficients, and let K_P be the subtracted kernel of eq. (142) at $\varepsilon = 0$. The Laurent expansion $I_{\mathrm{VP}} = \sum_{k\geq -2} c_k\,\varepsilon^k$ has $c_{-2} = -\kappa_2^{(0)}$ and

$$\begin{aligned} c_{-1} = -\kappa_2^{(1)} + 2\gamma_E\kappa_2^{(0)} + 2\int_1^2 \frac{K_P(w) - \kappa_2^{(0)}}{w-1}\,\mathrm{d}w + 2\int_2^\infty \frac{K_P(w)}{w-1}\,\mathrm{d}w \\ - \int_1^\infty \frac{K_P(w)}{w}\,\mathrm{d}w. \end{aligned} \tag{147}$$

Here the weights $2/(w-1)$ and $-1/w$ together form the order-ε^{-1} discontinuity of the insertion. The subtraction at $w = 1$ and the terms $2\gamma_E\kappa_2^{(0)}$ and $-\kappa_2^{(1)}$ come from expanding the threshold factor $(w-1)^{1-2\varepsilon}$ of eq. (144) against the double pole of the squared stub propagator. The Laurent coefficients and the fixed-ε value at the reference point are

$$\begin{aligned} c_{-2} &= -0.04540615882\ldots, \quad c_{-1} = -0.01534480\ldots, \\ c_0 &= -0.14660534\ldots, \qquad c_1 = 0.0397158224\ldots, \\ I_{\mathrm{VP}}\big|_{\varepsilon=2^{-7}} &= -746.0449580\ldots. \end{aligned} \tag{148}$$

Boundary data. Threshold regularity at $w = 1$ fixes the two-body density, $\mathcal{N}(\varepsilon)$ is given in closed form by eq. (145), and the transport of the kernel starts from exact values at $w' = 5$. The coefficient $c_{-2} = -\kappa_2^{(0)}$ is a two-dimensional Feynman-parameter integral with rational integrand, which we evaluate in ball arithmetic to within 10^{-72} at the reference point and at $P_1, \ldots, P_4$.

Checks. We compare the fixed-ε value with three-loop `AMFlow` evaluations at the eight values $\varepsilon = 2^{-6}, \ldots, 2^{-13}$, at the reference point and at $P_1 = (-\frac{1}{2}, -1, 1)$, $P_2 = (-\frac{3}{2}, -\frac{1}{4}, 1)$, $P_3 = (-\frac{3}{4}, -\frac{1}{2}, 1)$ and $P_4 = (-\frac{1}{4}, -\frac{1}{2}, 1)$. The agreement is 56–59 digits over the eight values at the reference point and, at each further point, at least 37 for every ε at the working precision used there, rising to at least 76 when both our evaluation and the `AMFlow` run are carried to higher precision. The pole coefficients c_{-2} and c_{-1} of eq. (148), which depend on (s, t) only through κ_2 and K_P, agree with the poles extracted from the same `AMFlow` values to 45 and 39 digits, the precision of that extraction. Finally, Appendix A collects the reference values and comparisons of all three entries and gives the reference-point value of I_{VP} to more figures.

5.9 Nonplanar two-loop W-pair production

Two-loop master integrals for $q\bar{q} \to W^+W^-$ with exact dependence on the top-quark mass are an ingredient of the NNLO QCD corrections to W-pair production in quark–antiquark annihilation. He, Zhang, Han, Jiang, Li and Wang [75] computed the three planar top-quark branches $\mathcal{T}_1$, $\mathcal{T}_2$ and $\mathcal{T}_3$. The nonplanar branch $\mathcal{T}_4$ of Figure 18 (No. 35 of Table 1), the top sector of their family F_C, is not treated there, and we are not aware of an earlier result for it. Its numerical values at individual kinematic points can nevertheless be obtained by auxiliary-mass flow [95]. We compute $\mathcal{T}_4$ here on one kinematic line outside the physical region, eq. (151), and obtain every master integral of the family on that line in symbolic form together with its boundary constants.

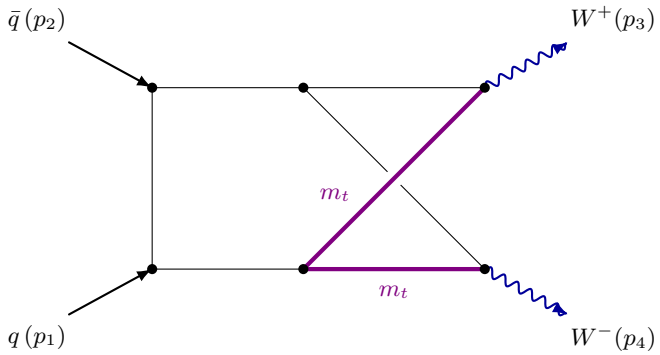

Figure 18: The nonplanar top-quark branch $\mathcal{T}_4$ of two-loop $q\bar{q} \to W^+W^-$, family F_C of Ref. [75] (their fig. 1d), top sector $[1,1,1,0,0,1,1,1,1]$, all momenta incoming. Thin lines are massless, the two thick lines carry the top-quark mass m_t (propagators D_8 and D_9 of eq. (149)), and the wavy external lines are the W bosons, $p_3^2 = p_4^2 = m_W^2$. The lines D_7 and D_9 cross without a vertex.

Definition. We use the kinematics of Ref. [75]: all momenta incoming, $p_1^2 = p_2^2 = 0$, $p_3^2 = p_4^2 = m_W^2$, $s = (p_1+p_2)^2$, $t = (p_2+p_3)^2$ and $s+t+u = 2m_W^2$, with loop momenta l_1 and l_2. The nine propagators are those of family F_C, eq. (2.14) of Ref. [75], and the integrals are normalized as in eq. (1). The seven that occur in $\mathcal{T}_4 = F_C[1,1,1,0,0,1,1,1,1]$ are

$$\begin{aligned} &D_1 = l_1^2, && D_2 = (l_1+p_1)^2, && D_3 = (l_1-p_2)^2, && D_6 = (l_2-p_2)^2, \\ &D_7 = (l_1-l_2)^2, && D_8 = (l_1-l_2-p_4)^2 - m_t^2, && D_9 = (l_2-p_2-p_3)^2 - m_t^2, \end{aligned} \tag{149}$$

in $d = 4-2\varepsilon$, and the planar propagators D_4 and D_5 of that reference enter only as numerators. This assignment of propagators to edges follows fig. 1d of Ref. [75], including the crossing of D_7 and D_9. Family F_C contains only $\mathcal{T}_4$ and its subtopology $\mathcal{T}_{4,1}$, while the elliptic sector called $\mathcal{T}_3$ in Ref. [75] belongs to their family F_B. We label a sector by the integer $\sum_{\nu_i>0} 2^{i-1}$, which gives the top sector the number 487 and the sector $[1,0,0,0,0,1,1,1,1]$ the number 481. The dimensionless variables are

$$x = -\frac{s}{m_t^2}, \qquad y = -\frac{t}{m_t^2}, \qquad z = -\frac{m_W^2}{m_t^2}. \tag{150}$$

Reducing the family with `Kira` [81], we find 76 master integrals. Of these, 53 map onto masters of the planar branches of Ref. [75], and 23, in the sectors 480–487 that contain all four of $D_6, \ldots, D_9$, are new. Adding 3 integrals of sector 487 with ISP numerators as auxiliary basis elements, we solve for a vector $\vec{f} = (f_1, \ldots, f_{79})$ with 79 components. We fix two of the three variables and work on the line

$$(x,z) = \Big(\frac{17}{2}, \frac{5}{3}\Big), \qquad 0 < y < 1, \qquad u = 2m_W^2 - s - t = \Big(\frac{31}{6} + y\Big)m_t^2 > 4m_t^2. \tag{151}$$

Every result of this subsection holds on the line of eq. (151) and nowhere else. On this line $s < 0$ and $m_W^2 < 0$, while u lies above the $t\bar{t}$ threshold, so the line belongs to a region of analytic continuation outside the physical scattering region, and 36 of the 79 basis functions are complex on it. We have reconstructed the exact differential equation in y, eq. (152) below, on a second line as well, $(x,z) = (17/2, 7/4)$, but the dependence on x and z remains open.

Function space. On the line of eq. (151) the basis satisfies

$$\frac{\partial \vec{f}(d,y)}{\partial y} = A(d,y)\,\vec{f}(d,y), \tag{152}$$

class of diagonal block	blocks	sectors
ε-factorized, rational d log letters, eq. (153)	29	all others, including the top sector 487
algebraic letters, no rational rotation to eq. (153)	6	417, 421, 449, 453, 482, 483
elliptic maximal cut, eq. (154)	1	481

Table 2: Block structure of the exact differential equation (152) for the 79 basis functions of the nonplanar W-pair family on the line (151). The matrix is block lower-triangular with 36 diagonal blocks. The 29 blocks of the first class contain 52 of the 79 functions and the remaining blocks contain 27, six of them in sector 481. Sector labels are defined below eq. (149).

where A is a 79×79 matrix of rational functions of d and y with 1240 nonzero entries. It was determined exactly by rational reconstruction in y and in d from 91 numerical reductions on the line. Because A is block lower-triangular, with 36 diagonal blocks, each block can be integrated once the blocks preceding it are known. The class of functions in which a given f_i lies is thus set by its own diagonal block and by every block that enters its inhomogeneous terms. These blocks fall into the three classes of Table 2. For 29 of them we find a rational change of basis $\vec{g}_B = T_B(\varepsilon, y)\vec{f}_B$ [93] that brings the diagonal block to the ε-factorized form of eq. (3),

$$d\vec{g}_B = \varepsilon\Big(\sum_i M_{B,i}\,\mathrm{d}\log\alpha_i(y)\Big)\vec{g}_B, \tag{153}$$

with constant rational matrices $M_{B,i}$. The letters α_i belong to a 15-letter alphabet on the line: 13 rational functions of y and a pair $r_\pm$ involving one square root. For the top sector the form of eq. (153) is reached after the basis element $F_C[1,1,1,-2,0,1,1,1,1]$ is replaced by $F_C[1,1,1,-1,-1,1,1,1,1]$, and the two letters of the block are then $18y^2+93y+50$ and $18y^2+93y+203$. The full alphabet of the family in (x,y,z), which we obtain as in Refs. [74, 97, 63], has 36 letters: 32 rational ones, among them the pseudo-threshold $x+y-z+1$, and 4 square roots. The line letters arise from these by restriction to eq. (151). For six further blocks, in sectors 417, 421, 449, 453, 482 and 483, we find no rational rotation to the form of eq. (153), and their solutions involve algebraic functions of y.

Sector 481, the single block in the last class of Table 2, has six master integrals and an elliptic maximal cut. Computing the maximal cut loop by loop in the Baikov parametrization at $d=4$, we find the integrand

$$\frac{dz_4\,dz_5}{\sqrt{g_1(z_4,z_5)\,G_2(z_4,z_5)}}\,, \qquad z_4 = l_2^2, \tag{154}$$

where g_1 and G_2 are the Baikov polynomials of the two loops and z_5 is the remaining ISP. The product g_1G_2 is cubic in z_4. At fixed z_5 the cut is therefore an elliptic curve E_{z_5}, distinct from the $\mathcal{T}_3$ curve of Ref. [75] (their eq. (3.32)). Over the z_5 line the family $\{E_{z_5}\}$ is a rational elliptic surface with singular fibers $2\,I_1+5\,I_2$, Mordell–Weil rank 3 and Euler number 12. The j-invariant varies with z_5, the Picard–Fuchs operator in z_5 has order two, and the curve is neither of complex-multiplication type nor attached to a congruence subgroup. At the same time, E_{z_5} has a rational 2-torsion point, and j therefore factors through the Hauptmodul h of $X_0(2)$,

$$j = \frac{(h+256)^3}{h^2}\,. \tag{155}$$

On the line, however, the order-ε^0 part of the rank-six block of sector 481 is reducible. Its asso-

ciated differential operator $L^{(0)}_{481}$ in y factorizes into first-order operators with rational coefficients,

$$L^{(0)}_{481} = \Big(\frac{d}{dy} - r_6(y)\Big)\Big(\frac{d}{dy} - r_5(y)\Big)\cdots\Big(\frac{d}{dy} - r_1(y)\Big), \tag{156}$$

and accordingly two of its six homogeneous solutions are rational functions of y and four are iterated integrals of algebraic functions. The local exponents of the full ε-dependent block lie in $\mathbb{Z} + \mathbb{Z}\varepsilon$ at every singular point except the zeros of the two quadratics

$$Q_1 = 225y^2 + 5370y + 19801, \qquad Q_2 = 900y^2 - 12180y - 7751, \tag{157}$$

where the exponent is $-3/2$ for every d. This block therefore has no ε-factorized form with rational letters on the line, although one over the function field extended by $\sqrt{Q_1}$ and $\sqrt{Q_2}$ may exist [65, 118].

Result. We solve eq. (152) order by order in ε, from ε^{-3} to ε^{1} (the ε^{-4} coefficients vanish identically), by variation of parameters using the exact matrix A, block by block down the triangular structure [105]. For 40 functions the diagonal block and every block entering the inhomogeneous terms belong to the first class of Table 2, and these functions are MPLs on the line. Each of their Laurent coefficients has the form of eq. (5), with rational c_j and with ϕ_j the GPLs of eq. (4) in y whose indices are zeros of the 15 line letters. The fifteen functions of sectors 417, 421, 449, 453 and 482 belong to blocks of the second class of Table 2, and their Laurent coefficients are instead iterated integrals whose kernels involve, besides the line letters, two quadratic polynomials in y with complex roots. The homogeneous solutions of sector 483 are three rational functions and two algebraic functions of y built from the letters

$$3y - 5, \qquad 6y + 41, \qquad 18y^2 + 93y + 67, \qquad 18y^2 + 93y + 305, \tag{158}$$

and those of sector 481 are the six solutions of eq. (156). Both sectors are then solved by variation of parameters with the sources from the preceding blocks. Sectors 483 and 487, which contain sector 481 as a subsector, carry no new transcendental functions of their own, and sector 481 enters them only through their source terms.

The matrix $A(d, y)$, the symbolic expressions of the 79 functions at each order and the 79 boundary constants are too long to print. They are supplied, together with $A(d, y)$ on the second line $(x, z) = (17/2, 7/4)$, as data files with the evaluation code for this entry [106] (Appendix G). Only the expressions for the six functions of sectors 421 and 453, which are much larger than the rest, are omitted from these files, and those six functions are evaluated instead by integrating eq. (152) along the line from their values at the point $y_0 = 1/3$. Appendix D gives the block content sector by sector and the local data of sector 481.

Boundary data. The residue matrix of A at $y = 0$ has spectrum

$$\{0^{\times 76},\, -1,\, -2 + \varepsilon,\, -2 - \varepsilon\}, \tag{159}$$

with no resonances, and is semisimple. Every basis function therefore has a finite limit as $y \to 0$, and these limits can serve as the 79 integration constants. We fix 39 of them directly at $y \to 0$. Of these, 23 are $y \to 0$ limits of the planar GPL expressions of Ref. [75], taken from their ancillary files and continued to our line, and 11 are closed forms in Γ functions and hypergeometric values of the family's vacuum and bubble integrals. A further 5 are defined by convergent integral representations. The remaining 40 constants, which include all those of the six sectors with

algebraic letters and of sector 481, are defined instead by the values of the corresponding functions at the reference point $y_0 = 1/3$ of the line, given by the written transport integral of eq. (161) in an auxiliary mass. We searched for integer relations between them and the Γ-function and algebraic constants of the family and found none at the heights that the available precision allows (Appendix D). That search used the values of the constants at fixed ε. For the leading Laurent coefficient, however, we find a closed form: a rational number for 22 of the 40 and a combination of logarithms for two more. These two are the constants of the sector-487 functions f_{75} and f_{78} in the basis of the data files, with leading coefficients

$$c_{75} = \frac{45\ln 2 - 27\ln 3}{2006}, \qquad c_{78} = \frac{-189\ln 2 + 432\ln 3}{10148}. \tag{160}$$

To evaluate the 40 constants defined at y_0 we give the propagators an auxiliary mass η at that point, as in the auxiliary-mass-flow method [95], and reduce the η-dependent family with `Kira`. We then integrate the resulting exact rational system from large η, where the solution is fixed by Γ-function vacuum integrals, down to $\eta \to 0$,

$$\frac{\partial \vec{f}(\varepsilon,\eta)}{\partial \eta} = B(\varepsilon,\eta)\,\vec{f}(\varepsilon,\eta), \qquad \vec{f}(\varepsilon,\eta) \to \vec{f}_{\text{vac}}(\varepsilon,\eta) \quad (\eta \to \infty), \qquad \vec{f}(\varepsilon,y_0) = \lim_{\eta\to 0} \vec{f}(\varepsilon,\eta), \tag{161}$$

with the limit taken on the branch prescribed in Ref. [95]. The 40 constants therefore depend on the auxiliary-mass method through these reductions and this integration of eq. (161), although no numerical output of the `AMFlow` program itself enters them. In particular, for sector 481 the definition by eq. (161) is forced, since the regularity conditions at $y \to 0$ place no constraint on its integration constants.

Checks. We compared all 79 functions, in real and imaginary parts and at every order from ε^{-3} to ε^{1}, with `AMFlow` [95] values at two points of the line used nowhere in the construction, $y = 1/2$ and $y = 3/5$. The weakest agreement over all functions and orders is 37 digits at a working precision of 40. In addition, the dictionary that maps the 53 shared functions onto the planar masters of Ref. [75] reproduces the values of their ancillary expressions at their benchmark point to 47–49 digits. Finally, the code of Appendix G integrates eq. (152) along the line by high-order Taylor steps as in Ref. [78], starting from stored values of the 79 functions at $y_0 = 1/3$ for 24 fixed values of ε, and returns the Laurent coefficients at a requested point of the line with 40-digit accuracy. Higher accuracy requires regenerating the stored values from eq. (161), for which the code is also supplied.

6 K3 and Calabi–Yau integrals

The banana graphs are the simplest Feynman integrals whose maximal cuts are periods of varieties of dimension greater than one. In two dimensions the maximal cut of the L-loop banana, the two-point function with $L+1$ massive lines joining two vertices, is a period of a Calabi–Yau variety of dimension $L-1$ [24, 28, 82, 27] (section 2.2). At the MUM point of its Picard–Fuchs operator the Frobenius basis, with logarithms up to $\log^{L-1}$, takes the place of the pair of elliptic periods, and ε-factorized differential equations built on it were derived for the equal-mass graphs [101, 100, 59]. Of the five entries in this section the two equal-mass bananas, Nos. 19 and 34, are known. The new entries are the threshold coefficients of two banana periods at mass configurations where the monodromy around a threshold is not unipotent, Nos. 31 and 32, and a three-loop four-point integral whose top sector couples to a K3 banana subsector, No. 21.

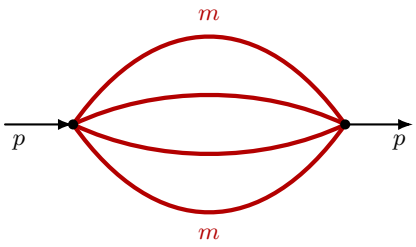

Figure 19: The three-loop equal-mass banana, No. 19 of Table 1. Four propagators of mass m (thick, red) join the two vertices, and a single momentum p flows through the graph; $t = p^2/m^2$. The maximal cut in $d = 2$ is a period of a K3 surface, the symmetric square of the sunrise elliptic curve.

6.1 The three-loop equal-mass banana

The three-loop equal-mass banana, No. 19 of Table 1 and Figure 19, is the two-point function with four propagators of equal mass in $d = 2 - 2\varepsilon$. Its maximal cut is a period of a K3 surface, the symmetric square of the equal-mass sunrise curve, and the modular variable τ and the group $\Gamma_1(6)$ are those of the sunrise [101, 28, 24]. The integral was brought to ε-factorized form with meromorphic modular forms in [101], and its value in two dimensions has been analyzed in terms of Bessel moments [24, 31, 16]. We recompute it here, taking one input from [101], the inhomogeneity of the Picard–Fuchs equation. We add a two-term closed form for the finite part of the top master, with a single boundary constant, and continue it past the threshold.

Definition. With $m^2 = 1$, $t = p^2/m^2$, and line momenta $k_1, \dots, k_4$ constrained by $\sum_i k_i = p$, the top master is

$$m_1(t;\varepsilon) = I_{1,1,1,1}(d;t) = \int \prod_{l=1}^{3} \frac{\mathrm{d}^d k_l}{i\pi^{d/2}} \prod_{i=1}^{4} \frac{1}{k_i^2 - m^2 + i0}\,, \qquad \begin{aligned} k_4 &= p - k_1 - k_2 - k_3\,, \\ d &= 2 - 2\varepsilon\,, \end{aligned} \tag{162}$$

in the convention of eq. (1), with no factor of $e^{\gamma_E \varepsilon}$ removed. On the Euclidean axis $t < 0$ the four propagators in position space give a one-dimensional representation, exact in d [24, 31],

$$m_1(t;\varepsilon) = 2^{3-3\varepsilon} \int_0^\infty r^{1+2\varepsilon}\, (ar)^{\varepsilon} J_{-\varepsilon}(ar)\, K_{\varepsilon}(r)^4 \,\mathrm{d}r\,, \qquad a = \sqrt{-t}\,. \tag{163}$$

In particular $m_1(0;0) = 8\int_0^\infty r\, K_0(r)^4\,\mathrm{d}r = 7\zeta_3$ [16, 24]. The closed form of eq. (169) holds on the disk $|t| < 4$ around the MUM point $t = 0$, both on the Euclidean side and on the segment $0 < t < 4$ below the pseudo-threshold. Written as a single Taylor series it converges up to the threshold $t = 16$, and for $t > 16$ we continue it with the differential equation.

Function space. Because the K3 surface is the symmetric square of the sunrise curve, its holomorphic period is the square of the sunrise period,

$$\varpi_0(t) = \big(\psi_1^{\text{sunrise}}(t)\big)^2 = \sum_{n\ge 0} D_n \Big(\frac{t}{64}\Big)^n, \qquad D_n = 1,\ 4,\ 28,\ 256,\ \dots, \tag{164}$$

where the D_n are the Domb numbers (OEIS A002895). The Picard–Fuchs operator, of order three, is the symmetric square of the sunrise operator and coincides with the operator of [101]; in the

form given in [24] it reads

$$\begin{aligned} \mathcal{L}_3 &= t^2(t-4)(t-16)\,\partial_t^3 + 6t\,(t^2-15t+32)\,\partial_t^2 + (7t^2-68t+64)\,\partial_t + (t-4)\,, \\ \mathcal{L}_3\,\varpi_0 &= 0\,. \end{aligned} \tag{165}$$

Its regular singular points $t \in \{0, 4, 16, \infty\}$ are the MUM point, the pseudo-threshold $(2m)^2$, the threshold $(4m)^2$ and infinity. At $t = 0$ the indicial equation is $\theta^3 = 0$, and the Frobenius basis is $\{\varpi_0,\ \varpi_0 \log t + \sigma_1,\ \frac{1}{2}\varpi_0 \log^2 t + \sigma_1 \log t + \sigma_2\}$ with σ_1, σ_2 rational power series. In the modular variable the ε-factorized connection is built from six kernels on $\Gamma_1(6)$,

$$\begin{gathered} \{\,1,\ f_{2a},\ f_{2b},\ f_{4a},\ f_{4b},\ f_6\,\}\,, \qquad \text{modular weights } (0,2,2,4,4,6)\,, \\ f_{2a}\,2\pi i\,\mathrm{d}\tau = \mathrm{d}\ln(t-4) + \mathrm{d}\ln(t-16)\,. \end{gathered} \tag{166}$$

These are the weight-doubled images of the sunrise kernels, and the weight-two kernel f_{2a} reproduces the rational $\mathrm{d}\log$ forms on the singular set [101, 37, 11].

Result. We normalize the top master by the K3 period, $g_1 = m_1/\varpi_0$ on the maximal cut. The four-master system then reduces to an ε-factorized form whose matrix does not depend on ε [93, 101],

$$m_1[\varepsilon^0](t) = \varpi_0(t)\,g_1(t)\,, \qquad \mathrm{d}g = \varepsilon\,\widetilde{A}\,g\,, \qquad \widetilde{A} = 2\pi i\,M(\tau)\,\mathrm{d}\tau\,, \tag{167}$$

$$M(\tau) = \begin{pmatrix} 0 & 0 & 0 & 0 \\ 0 & -f_{2a}-f_{2b} & 1 & 0 \\ 0 & f_{4b} & -f_{2a}+2f_{2b} & 1 \\ f_{4a} & f_6 & f_{4b} & -f_{2a}-f_{2b} \end{pmatrix}. \tag{168}$$

Since M is independent of ε, the ε^n coefficient of the canonical top integral is a finite sum of length-n iterated integrals of these kernels with integer coefficients, and the only transcendental constants are the boundary values of g.

In the canonical basis of [101] the top integral appears with a factor ε^3, as $\varepsilon^3(\pi^2/\varpi_0)\,m_1$, so that order ε^0 of m_1 is built from iterated integrals of length at most three. At this order the general solution contains four terms: the period, the two logarithmic solutions at the MUM point, and one length-three iterated integral through which the leading coefficient of the sub-banana (the graph with one line contracted) enters the top sector. However, m_1 is analytic at $p^2 = 0$, because eq. (163) at $\varepsilon = 0$ is a power series in t with Bessel moments as coefficients. The two logarithmic solutions therefore cannot appear, and the result is the two-term formula

$$m_1[\varepsilon^0](t) = 7\zeta_3\,\varpi_0(t) - \mathrm{Part}_{\mathrm{reg}}(t)\,, \qquad \mathrm{Part}_{\mathrm{reg}}(t) = \sum_{n\geq 1} b_n \Big(\frac{t}{64}\Big)^n, \quad b_1 = 24\,. \tag{169}$$

The full integral obeys $\mathcal{L}_3\,m_1 = -24$ [24], and $\mathrm{Part}_{\mathrm{reg}}$ is the solution of $\mathcal{L}_3 f = 24$ that vanishes at $t = 0$; the sequences D_n and b_n satisfy the same recurrence,

$$\begin{gathered} n^3 u_n = 2(2n-1)(5n^2-5n+2)\,u_{n-1} - 64(n-1)^3 u_{n-2}\,, \\ (D_0, D_1) = (1, 4)\,, \qquad (b_0, b_1) = (0, 24)\,. \end{gathered} \tag{170}$$

We identified the coefficient of ϖ_0 by an integer-relation fit, which also returns zero for the coefficients of the two logarithmic solutions, as analyticity requires. Taken separately, the series for ϖ_0 and $\mathrm{Part}_{\mathrm{reg}}$ converge only for $|t| < 4$, whereas the combined series $\sum_n (7\zeta_3 D_n - b_n)(t/64)^n$ converges for $|t| < 16$, since m_1 is analytic up to the threshold.

Similarly, at the next order $m_1[\varepsilon^1](t) = \alpha_1 \varpi_0(t) + \mathrm{Part}^{(1)}(t)$, with $\mathrm{Part}^{(1)}$ the regular particular solution of the same recursion at order ε^1. The one new constant is the ε^1 coefficient of eq. (163) at $t = 0$,

$$\alpha_1 = m_1[\varepsilon^1](0) = 16 \int_0^\infty r \ln r \, K_0(r)^4 \, \mathrm{d}r - 7\zeta_3 \, (2 \ln 2 + \gamma_E) \, . \tag{171}$$

The kernels f_{2a} and f_{2b} first enter at this order, f_{4b} at ε^2 and f_6 at ε^3. We have not found a closed form for α_1 in terms of zeta values, $\ln 2$, γ_E and the L-values of the weight-three modular form attached to the K3 surface.

Boundary data. The first of the three inputs that fix eq. (169) is the inhomogeneity of the top-sector equation, which comes from the sub-banana; we take its leading coefficient $m_0[\varepsilon^{-3}] = -1$ from [101]. At that order the two remaining top-sector masters, which we denote m_2 and m_3, are rational, $m_2[\varepsilon^{-3}] = -(4 + t)$ and $m_3[\varepsilon^{-3}] = -\frac{16+4t}{3}$. The second is the constant $7\zeta_3 = m_1(0; 0)$, Broadhurst's Bessel moment $8 \int_0^\infty r K_0(r)^4 \, \mathrm{d}r$ [16, 24]. It should not be confused with the cusp constant $\frac{4}{3}\zeta_3$ of the canonical integral $\varepsilon^3(\pi^2/\varpi_0) \, m_1$ of [101], which is defined with a different prefactor. The third input is the analyticity of m_1 at $t = 0$, which sets the two logarithmic coefficients to zero.

Checks. We compared eq. (169) with `AMFlow` [95] at 18 points in the disk $|t| < 4$, on both sides of $t = 0$. They agree to at least 110 digits, and to 119 at $t = -3$, where

$$m_1[\varepsilon^0](-3) = 7\zeta_3 \, \varpi_0(-3) - \mathrm{Part}_{\mathrm{reg}}(-3) = 8.0002891\ldots, \quad \varpi_0(-3) = 0.85621843\ldots \, . \tag{172}$$

Past the disk we transport the four-master system along a path in the upper half plane, $t \to t + i0$. Between the pseudo-threshold and the threshold the continued function is real, and above $t = 16$ it is complex. It agrees with `AMFlow` at $t = 5, 8, 12, 31/2$ and at $t = 18, 25, 40, 100, 200$, imaginary parts included, to at least 99 digits. For example,

$$m_1[\varepsilon^0](18) = 16.0134447\ldots + 6.20325251\ldots \, i \, . \tag{173}$$

The order-ε^1 form with α_1 from eq. (171) and no fitted parameter agrees with `AMFlow` at the same 18 points to at least 109. Finally, eq. (163) expanded in ε at $t = -8$, outside the disk, reproduces the `AMFlow` coefficients through ε^5 to 41 or more.

6.2 The four-loop equal-mass banana

The four-loop equal-mass banana, No. 34 of Table 1 and Figure 20, has five propagators of equal mass in $d = 2 - 2\varepsilon$. Its maximal cut is the holomorphic $(3, 0)$-period of the one-parameter Hulek–Verrill family of Calabi–Yau threefolds, annihilated by the fourth-order operator AESZ 34 [14, 28, 82]. The analytic structure of the integral is described in [28, 27], an ε-factorized differential equation is derived in [100], and the periods are evaluated as Bessel moments in [31]. We recompute the integral, imposing the classical large-momentum limit of [27, 100] as a boundary condition, and give all five master integrals through order ε^0 as one log-Frobenius series at the MUM point with every boundary constant in the ring of zeta values.

Definition. With $m^2 = 1$, line momenta $k_1, \ldots, k_4$ and $k_5 = p - k_1 - k_2 - k_3 - k_4$, the family is that of eq. (1) with

$$D_i = k_i^2 - m^2 + i0 \quad (i = 1, \ldots, 5) \, , \quad d = 2 - 2\varepsilon \, , \quad z = -\frac{1}{p^2} \, , \quad m_j = e^{4\gamma_E \varepsilon} \, I_j \, , \tag{174}$$

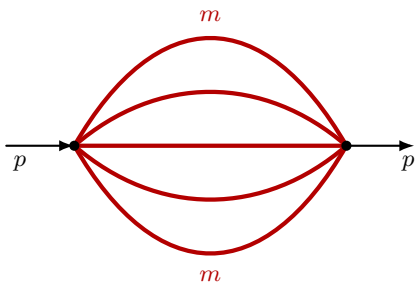

Figure 20: The four-loop equal-mass banana, No. 34 of Table 1. Five propagators of mass m (thick, red) join the two vertices and one momentum p flows through; $z = -1/p^2$ with $m^2 = 1$. The maximal cut in $d = 2$ is the holomorphic period of the Hulek–Verrill family of Calabi–Yau threefolds.

where I_j runs over the five master integrals of the reduction [81], namely the tadpole product m_0, the top integral $m_1 = e^{4\gamma_E \varepsilon} I_{1,1,1,1,1}$ and three further top-sector integrals m_2, m_3, m_4. The results hold on the Euclidean axis $p^2 < 0$, that is $z > 0$. The Frobenius series converges near the MUM point $z = 0$, and we reach any $p^2 < 0$ by Taylor transport of the differential equation along the Euclidean axis, which meets no singular point.

Function space. We assemble the ε-dependent connection of the five masters from the reduction alone. We find that its denominator factorizes as $p^2(p^2-1)(p^2-9)(p^2-25)$, the point $p^2 = 0$ and the thresholds $(m)^2$, $(3m)^2$ and $(5m)^2$, with no spurious singularity. Eliminating m_2, m_3, m_4 from its ε^0 maximal-cut block, we obtain an order-four operator that is the AESZ 34 operator exactly [14, 88]. In $\theta = z\,\mathrm{d}/\mathrm{d}z$,

$$\begin{aligned} \mathcal{L}_4 = {} & \theta^4 + z\,(35\theta^4 + 70\theta^3 + 63\theta^2 + 28\theta + 5) \\ & + z^2(\theta+1)^2(259\theta^2 + 518\theta + 285) + 225\, z^3(\theta+1)^2(\theta+2)^2\,, \end{aligned} \tag{175}$$

with the MUM point at $z = 0$, where the indicial equation is $\theta^4 = 0$, and the three thresholds at $z = -1, -\frac{1}{9}, -\frac{1}{25}$. Its holomorphic solution at $z = 0$ is the Hulek–Verrill period [28, 82],

$$\varpi_0(z) = \sum_{n\geq 0} A_n (-z)^n\,, \qquad A_n = \sum_{k_1+\cdots+k_5=n} \Big(\frac{n!}{k_1!\cdots k_5!}\Big)^2 = 1,\ 5,\ 45,\ 545,\ 7885, \ldots\,. \tag{176}$$

Result. We set $\ell = \log z$ and rescale the masters by powers of z, $\widehat{M} = (m_0,\, z^{-1}m_1,\, z\,m_2,\, z\,m_3,\, z^2 m_4)$. The rescaled system $\theta\widehat{M} = C(z,\varepsilon)\,\widehat{M}$ has polynomial numerators over the common denominator $20(1+z)(1+9z)(1+25z)$. It is regular at $z = 0$, and its residue matrix C_0, acting on the Laurent coefficients $\varepsilon^{-4}, \ldots, \varepsilon^0$ of the five masters taken together, is nilpotent of index eight. All five masters through ε^0 are therefore given by one log-Frobenius series,

$$\widehat{M}(z) = \sum_{n\geq 0} z^n \sum_{j=0}^{7} F_{n,j}\, \ell^{\,j}\,, \qquad F_0(\ell) = e^{C_0 \ell}\, v\,. \tag{177}$$

We generate the coefficients $F_{n,j}$ from $C(z,\varepsilon)$ by an exact recursion over the integers once the boundary vector v is fixed; the matrix $C(z,\varepsilon)$ itself is supplied with the evaluation code of Appendix G.

For the top master alone, eqs. (175) and (177) at ε^0 amount to an inhomogeneous fourth-order equation with a MUM boundary condition. With $s = p^2$ and $I^{(0)}$ the ε^0 coefficient of m_1,

$$\begin{aligned} \mathcal{D}\, I^{(0)} &= 5!\,, \\ \mathcal{D} &= s^2(s-1)(s-9)(s-25)\,\partial_s^4 + 2s(5s^3 - 140s^2 + 777s - 450)\,\partial_s^3 \\ &\quad + (25s^3 - 518s^2 + 1839s - 450)\,\partial_s^2 + (3s-5)(5s-57)\,\partial_s + (s-5)\,, \end{aligned} \tag{178}$$

which is $\mathcal{L}_4[(-s)I^{(0)}] = -120$ in the variable z, and at the MUM point

$$(-s)\, I^{(0)} = -5\ell^4 + 80\zeta_3\,\ell + O(z)\,. \tag{179}$$

The coefficients of $\ell^0, \ldots, \ell^4$ are thus $(0, 80\zeta_3, 0, 0, -5)$, all in $\mathbb{Q}[\zeta_3]$, with no ζ_2 or ζ_4 in this normalization.

Boundary data. The boundary vector v of eq. (177) collects, master by master, the coefficients of $\varepsilon^{-4}, \ldots, \varepsilon^0$ at $n = 0$. Its tadpole block follows from $m_0 = \Gamma(\varepsilon)^4 e^{4\gamma_E \varepsilon}$ and is $v_{m_0} = (1, 0, 2\zeta_2, -\frac{4}{3}\zeta_3, 6\zeta_4)$, while the top master is finite at $d = 2$ and has no free boundary constant, $v_{m_1} = 0$. For the remaining three masters

$$\begin{aligned} v_{m_2} &= (-1,\ -2,\ -2 - 2\zeta_2,\ -2 - 4\zeta_2 + \tfrac{4}{3}\zeta_3,\ -50 - 4\zeta_2 + \tfrac{104}{3}\zeta_3 - 6\zeta_4), \\ v_{m_3} &= (-\tfrac{3}{2},\ -1,\ -3\zeta_2,\ -2\zeta_2 + 2\zeta_3,\ -60 + \tfrac{52}{3}\zeta_3 - 9\zeta_4), \\ v_{m_4} &= (1,\ 3,\ \tfrac{9}{2} + 2\zeta_2,\ \tfrac{21}{4} + 6\zeta_2 - \tfrac{4}{3}\zeta_3,\ \tfrac{453}{8} + 9\zeta_2 - 52\zeta_3 + 6\zeta_4). \end{aligned} \tag{180}$$

We obtain eq. (180) by imposing on the general solution the exact tadpole, the vanishing of v_{m_1} in all five orders, and agreement of the $n = 0$ logarithmic tower with the large-momentum limit of [27, 100]. That limit is an alternating sum of products of Γ functions over hard and soft regions. Since the logarithms at $n = 0$ are generated by powers of C_0 acting on v, these conditions become a linear system of 50 equations for 25 unknowns, with rational coefficients and right-hand sides in the zeta ring. Its rank is 25, and eq. (180) is its unique solution in exact arithmetic.

Checks. At the two Euclidean points $p^2 = -2$ and $p^2 = -7$, neither used in the construction, the top master at ε^0 agrees to 116 digits with an independent Bessel-moment quadrature and to 67 with `AMFlow` [95], the latter limited by the precision of the `AMFlow` values. The worst of the 21 Laurent coefficients of the five masters that were compared agrees with `AMFlow` to the same 67. For the Bessel comparison we use the Euclidean position-space integral

$$I_{1,1,1,1,1}\big|_{\varepsilon^0}(p^2) = -16 \int_0^\infty x\, J_0(x\sqrt{-p^2}\,)\, K_0(x)^5\, \mathrm{d}x\,, \tag{181}$$

which is independent of the reduction and of `AMFlow` and can be evaluated at any Euclidean point.

6.3 Banana threshold coefficients

Nos. 31 and 32 of Table 1 are constants with no kinematic dependence, namely connection coefficients of the holomorphic periods of two banana families at mass configurations where the local monodromy at a threshold is no longer unipotent. When the heaviest mass of a banana graph equals the sum of the others, $\sqrt{M_N} = \sum_{i<N} \sqrt{M_i}$, the pseudo-threshold $p^2 = (\sqrt{M_N} - \sum_{i<N} \sqrt{M_i})^2$ coincides with $p^2 = 0$, and the monodromy of the period around $p^2 = 0$ acquires a part of finite order [28, 101, 107]. The order is two for the three-loop configuration $(1, 1, 1, 9)$, whose maximal

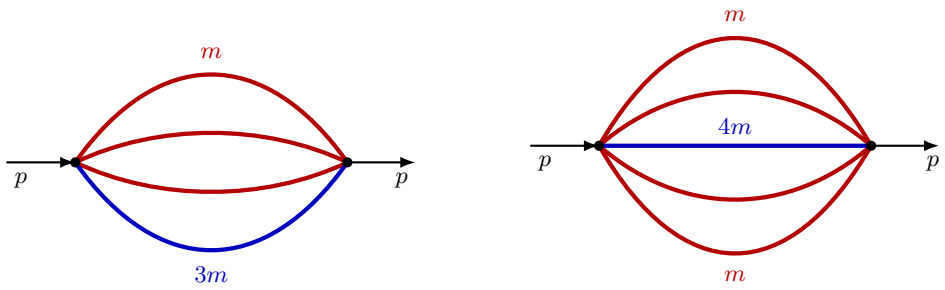

(a) (b)

Figure 21: Banana graphs at a mass coalescence, one momentum p flowing through. (a) No. 31: three lines of mass m (red) and one of mass $3m$ (blue), squared masses $(1,1,1,9)$. (b) No. 32: four lines of mass m (red) and one of mass $4m$ (blue), squared masses $(1,1,1,1,16)$. In both graphs the heavy mass equals the sum of the light masses, and the pseudo-threshold, at which the heavy line can decay into the light lines, is therefore at $p^2 = 0$.

cut is a K3 period, and four for the four-loop configuration $(1,1,1,1,16)$, a Calabi–Yau threefold period. Continued to $p^2 = 0$, the holomorphic MUM-point period is a combination of the local solutions there, some of fractional exponent. Its coefficients on the fractional-exponent solutions are derived in closed form in the companion paper [107] by applying a spectral projector onto the non-unipotent eigenspace of the local monodromy to the Bessel representation of the period. Here we define them, give the closed form for No. 31, and recover them from the maximal-cut differential operator obtained from the reduction of each family. We are not aware of a previous computation of these coefficients.

Definition. Both families are two-point functions of eq. (1) in $d = 2$ with one external momentum p (Figure 21). No. 31 has four lines of squared masses $(M_1,\dots,M_4) = (1,1,1,9)$ and No. 32 has five lines of squared masses $(M_1,\dots,M_5) = (1,1,1,1,16)$; we write J_{31} and J_{32} for the top integrals, with all indices equal to one. With $z = -1/p^2$ the MUM point is $z = 0$. The holomorphic period there, normalized to $\varpi_0(0) = 1$, is [28, 82]

$$\varpi_0(z) = \sum_{n\geq 0} (-z)^n \sum_{k_1+\cdots+k_N=n} \Big(\frac{n!}{k_1!\cdots k_N!}\Big)^2 \prod_{i=1}^{N} M_i^{k_i} = \begin{cases} 1 - 12z + O(z^2)\,, & (1,1,1,9)\,, \\ 1 - 20z + O(z^2)\,, & (1,1,1,1,16)\,. \end{cases} \tag{182}$$

We continue ϖ_0 along the Euclidean axis $z > 0$ to the neighborhood of $p^2 = 0$. There we decompose it on a local basis made of a unipotent block, with integer exponents and logarithms, and of solutions with fractional exponents,

$$\varpi_0 = \sum_k u_k\, \phi_k(p^2) + \begin{cases} c_{3/2}\, \Phi_{3/2}(p^2)\,, & (1,1,1,9)\,, \\ c_{5/4}\, \Phi_{5/4}(p^2) + c_{7/4}\, \Phi_{7/4}(p^2)\,, & (1,1,1,1,16)\,, \end{cases} \qquad \Phi_\alpha(p^2) = (p^2)^\alpha\, h_\alpha(p^2)\,. \tag{183}$$

The ϕ_k span the unipotent block, of rank three and four respectively, h_α is a power series with $h_\alpha(0) \neq 0$, and the branch of $(p^2)^\alpha$ is $\arg p^2 = -\pi$ as reached from the Euclidean axis. We normalize h_α and the ϕ_k as in [107]. The threshold coefficients are the numbers c_α of eq. (183); they depend only on the mass configuration, since the p^2 dependence is carried by the functions ϕ_k and Φ_α.

Function space. Reducing with `Kira` [81], we find at symbolic d seven master integrals (five in the top sector) for the $(1,1,1,9)$ family and nine (seven in the top sector) for the $(1,1,1,1,16)$ family. In both cases the differential operator of the maximal cut of the top integral at $d=2$ has the order of the Picard–Fuchs operator of ϖ_0, four and six respectively. We find that the two operators agree up to a unit shift of the Euler operator,

$$\mathcal{L}^{\mathrm{cut}}_{d=2}(z,\theta_z)=\mathcal{L}^{\mathrm{PF}}(z,\theta_z-1)\,,\qquad\text{so that}\qquad\mathcal{L}^{\mathrm{cut}}_{d=2}\,(z\varpi_0)=0\,. \tag{184}$$

The maximal cut is thus $\Pi_0=z\varpi_0$, and the local exponents at $p^2=0$, including the fractional ones of eq. (183), are properties of each Feynman family's own differential equation. The geometry of the two families, a one-parameter family of K3 surfaces and one of Calabi–Yau threefolds, and the degeneration at the coalescence are discussed in [107, 27, 57, 58].

The $(1,1,1,9)$ three-loop banana (No. 31)

Result. We write $\mathcal{M}_0$ for the local monodromy matrix of the rank-four system around $p^2=0$. The projector onto its eigenvalue -1 is a polynomial in $\mathcal{M}_0$,

$$P_{-1}=-\tfrac{1}{8}\,(\mathcal{M}_0-\mathbb{1})^3\,, \tag{185}$$

because $(\mathcal{M}_0-\mathbb{1})^3$ annihilates the rank-three unipotent block and acts as -8 on $\Phi_{3/2}$. Applied to the transported ϖ_0 it isolates $c_{3/2}\Phi_{3/2}$ algebraically, free of the logarithmic solutions that would otherwise dominate a numerical fit. The coefficient is an elementary number,

$$c_{3/2}=-\frac{\sqrt{3}}{36\pi}=-0.0153146915\ldots\,. \tag{186}$$

We identified it by an integer-relation fit of height 36 [16]. The sign corresponds to the branch $\arg p^2=-\pi$ and is reversed by the order-two monodromy, which makes $|c_{3/2}|$ the convention-independent quantity. We note that $36=(\sum_i\sqrt{M_i})^2$ is the normal threshold of the family and $\sqrt{3}=\sqrt{M_4}$, and that no L-value or CM Γ-period of the K3 surface enters $c_{3/2}$.

Boundary data. On the full family the top integral J_{31} is finite at $d=2$. Near the MUM point its ε^0 coefficient $J^{(0)}_{31}$ is a particular solution plus a combination of the Frobenius basis $\{\Pi_0,\ldots,\Pi_3\}$ of $\mathcal{L}^{\mathrm{cut}}_{d=2}$ at $z=0$. We take $\Pi_0=z\varpi_0$, $\Pi_1=\Pi_0\log z+\ldots$ and $\Pi_2=\frac{1}{2}\Pi_0\log^2 z+\ldots$ with correction series free of z and z^2 terms, and $\Pi_3=z^2(1+\ldots)$. The particular solution is taken free of z, $z\log z$, $z\log^2 z$ and z^2 terms. Then

$$\begin{gathered}J^{(0)}_{31}=J^{(0)}_{31,\mathrm{part}}+\sum_{i=0}^{3}a_i\,\Pi_i\,,\\ a_0=19.2329104\ldots,\quad a_1=0,\quad a_2=-13.1833474\ldots,\quad a_3=-38.5332202\ldots,\end{gathered} \tag{187}$$

with the three nonzero coefficients determined to 31 significant figures and $|a_1|<10^{-31}$. We obtained these coefficients from `AMFlow` [95] values of J_{31}, computed at two working precisions.

Checks. Auxiliary-mass flow does not apply to a connection coefficient, and the checks are of a different kind. Transport of ϖ_0 in ball arithmetic determines $c_{3/2}$ to 195 digits, and an independent transport in ordinary multiple-precision arithmetic, which differs in the integration variable and contour as well as in the series algorithm, agrees to 195. Moreover, the coefficient recomputed from

the maximal-cut operator $\mathcal{L}^{\text{cut}}_{d=2}$ of the family's own reduction, eq. (184), reproduces the first 47 digits of eq. (186). On the full family the coefficient of the $(p^2)^{3/2}$ branch in $J^{(0)}_{31}$ at $d=2$ is bounded by 10^{-32} and no logarithm appears at $p^2=0$. To this accuracy the non-unipotent monodromy is therefore confined to the maximal cut.

The $(1,1,1,1,16)$ four-loop banana (No. 32)

Result. At four loops the non-unipotent part of the monodromy around $p^2=0$ has order four. Besides a rank-four unipotent block, the local system has the two exponents $\frac{5}{4}$ and $\frac{7}{4}$ of eq. (183), with monodromy eigenvalues $e^{2\pi i\alpha}=\pm i$. The same construction with the projector onto those eigenvalues yields the conjugate pair $c_{5/4}, c_{7/4}$, the result of this entry. Both coefficients lie in the ring generated by the lemniscatic constant $\Gamma(\frac{1}{4})$ and π. Their closed forms and the derivation from the Bessel representation of the period are given in [107] and are not reprinted; below we determine the two coefficients numerically and recover them from the reduction of the family. As in the sunrise graph at the analogous mass configuration [107], the lemniscatic period thus enters a banana family as a local connection coefficient of the holomorphic period at a degenerate threshold.

Boundary data. The top integral J_{32} is again finite at $d=2$. The Frobenius basis $\{\Pi_0,\dots,\Pi_5\}$ of the order-six operator at $z=0$ has $\Pi_0=z\varpi_0$, $\Pi_{1,2,3}$ its $\log^k z/k!$ partners, $\Pi_4=z^2(1+\dots)$ and $\Pi_5=z^2\log z+\dots$, and the particular solution is taken free of $z\log^k z$ for $k\le 3$, of z^2 and of $z^2\log z$. Then

$$J^{(0)}_{32}=J^{(0)}_{32,\text{part}}+\sum_{i=0}^{5}a_i\,\Pi_i\,,\qquad \begin{aligned} &a_0=53.3249506\dots, && a_1=96.1645522\dots, && a_2=0\,,\\ &a_3=-66.5421293\dots, && a_4=-3210.34993\dots, && a_5=-1818.61697\dots, \end{aligned} \tag{188}$$

with the nonzero coefficients determined to 31 significant figures and $|a_2|<10^{-31}$. These come from an `AMFlow` [95] value of J_{32} at one point inside the disk of convergence, computed at two working precisions.

Checks. In ball arithmetic we determine $c_{5/4}$ and $c_{7/4}$ to 197 digits, and two independent transports agree to 71. The coefficients recomputed from the family's maximal-cut operator, eq. (184) at order six, reproduce the first 45 digits of each. No auxiliary-mass-flow computation exists at this mass configuration. On the maximal cut the transported period has no logarithms at $p^2=0$: its coefficients on the logarithmic partners of the unipotent block are zero to within 10^{-89} in ball arithmetic. On the full family the coefficients of the $\frac{5}{4}$ and $\frac{7}{4}$ branches of $J^{(0)}_{32}$ at $d=2$ are bounded by 10^{-23} with no logarithms, and here too the non-unipotent monodromy is confined to the maximal cut to that accuracy.

6.4 The three-loop crossed light-by-light box

Entry No. 21 of Table 1, the three-loop crossed light-by-light box (LBL3X), is the four-point integral of Figure 22. A closed loop of mass m runs around the four sides of a box, two massless lines join opposite corners and cross, and four massless on-shell momenta enter at the corners. The graph is the complete graph K_4, and the crossing of the diagonals makes it nonplanar. Three-loop light-by-light amplitudes with a massive fermion loop reduce onto this topology. The massless three-loop amplitudes are known [17], and the two-loop amplitudes with a massive loop are polylogarithmic [1]. To our knowledge, the three-loop family with the massive loop has not been computed before. The same graph is also one sector of a ten-propagator three-loop light-by-light family that we do not

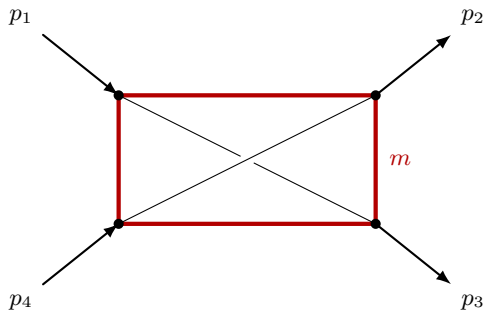

Figure 22: The three-loop crossed light-by-light box (LBL3X), No. 21 of Table 1. Thick (red) lines are the four perimeter propagators $D_1, \ldots, D_4$ of mass m; thin lines are the two massless diagonals D_5, D_6, which cross without a vertex. The external momenta $p_1, \ldots, p_4$ are massless and on shell, with $s = (p_1 + p_2)^2$, $t = (p_2 + p_3)^2$ and $u = (p_1 + p_3)^2 = -s - t$.

compute here. Its top sector has thirty masters on the maximal cut, which is an elliptic curve intrinsic to that topology.

Definition. With q_j the momentum of line j in Figure 22 (perimeter lines $j \leq 4$, diagonals $j = 5, 6$) and $m^2 = 1$, the family is

$$\begin{aligned} \mathrm{LBL3X}[\nu_1, \ldots, \nu_6](s,t) \;&=\; \int \prod_{l=1}^{3} \frac{\mathrm{d}^d k_l}{i\pi^{d/2}} \prod_{j=1}^{6} \frac{1}{D_j^{\nu_j}}\,, \qquad d = 4 - 2\varepsilon\,, \\ D_j = q_j^2 - m^2 \quad (j \leq 4)\,, &\qquad D_j = q_j^2 \quad (j = 5, 6)\,, \end{aligned} \tag{189}$$

with $+i0$ propagators. No factor of $e^{\varepsilon\gamma_E}$ is removed, and γ_E therefore appears in the expansion coefficients. The external momenta obey $p_i^2 = 0$, with $s = (p_1 + p_2)^2$, $t = (p_2 + p_3)^2$ and $u = (p_1 + p_3)^2 = -s - t$, and the crossing $s \leftrightarrow t$ acts on the family as $(D_1 \leftrightarrow D_2)(D_3 \leftrightarrow D_4)$.

Reducing by integration by parts [81, 89] at fixed rational (s, t), we find thirty-nine master integrals $m_0, \ldots, m_{38}$. Seventeen lie in subsectors, among them the three masters m_{13}, m_{14}, m_{15} of the sector with both diagonals contracted, and twenty-two in the top sector, $m_{17}, \ldots, m_{38}$. We write the differential equations in a basis of forty-one integrals, the thirty-nine masters together with two top-sector integrals that are linear combinations of the others, and refer to it as the forty-one-element basis. The integral evaluated here is the top-sector master m_{18}. Our result is the value of its ε^0 coefficient $m_{18}^{(0)}$ at $s, t < 0$, obtained by transporting the differential equation in m^2 at fixed (s, t). The evaluation code works on the curve $1/s + 1/t = -3/8$, on which we quote the value at one point and compare at a second, and we have also integrated to the six points (s, t) listed under Checks. We give no evaluation of m_{18} off this curve and these points.

Function space. The maximal cut of the top sector is rational, because the Gram polynomial of the loop momenta factors into a hyperplane and a smooth quadric. On the cut the connection is in $\mathrm{d}\log$ form [76, 77] over the eight letters

$$\mathcal{A}^{\mathrm{top}}_{\mathrm{LBL3X}} \;=\; \{\, s,\; t,\; s+t,\; s+t+4,\; s+t+16,\; s-4,\; t-4,\; 2s+t \,\}\,, \tag{190}$$

and the leading singularities of two subsectors contain the square roots $\sqrt{s(s-4)}$ and $\sqrt{t(t-4)}$, which rationalize. The letter $2s + t$, with its crossing image $s + 2t$ in the t-derivative, comes from

the numerators of the forty-one-element basis, which are not crossing symmetric. From this cut alone one would expect m_{18} to evaluate to multiple polylogarithms [70, 54].

However, the family as a whole is not polylogarithmic. Contracting both diagonals leaves the four massive perimeter lines joining two vertices, which is the three-loop equal-mass banana of No. 19 (section 6.1) at momentum squared $P^2 = u$. The maximal cut of that sector is a family of K3 surfaces with singular fibers at $u \in \{0, 4, 16\}$ [24, 101, 28]. No algebraic change of basis brings the full connection to ε-factorized $\mathrm{d}\log$ form, since at $s = 0$ its residue matrix has eigenvalues that are roots of the irreducible cubic $11\lambda^3 - 175\lambda^2 - 326\lambda + 760$.

The K3 periods enter the top sector through the coupling of m_{18} to the banana master m_{13}. Partial-fractioning the s-derivative at $d = 4$ and $t = -5$, we find for that entry of the connection

$$A_s\big[m_{18} \to m_{13}\big]\Big|_{d=4,\,t=-5} \;=\; \frac{9743}{660\,s} \;-\; \frac{8}{15\,u} \;+\; \frac{21}{u-4} \;+\; \frac{35}{2(u-4)^2} \;-\; \frac{87}{22(u-16)}\,, \tag{191}$$

with the Picard–Fuchs letters $\{u, u-4, u-16\}$ of the banana and a pole at $s = 0$. When the equation is integrated in s at fixed t, that pole generates $\int^u m_{13}(u')\,\mathrm{d}u'/(u'+t)$, and the K3 part of $m_{18}^{(0)}$ therefore depends on s and t separately. This K3 part involves the crossing-symmetric iterated integrals

$$I_{st}^{(k)}(s,t) \;=\; \int_{u_0}^{u} \frac{m_k(u') - m_k(-t)}{u'+t}\,\mathrm{d}u' \;+\; (s \leftrightarrow t)\,, \qquad k \in \{13, 14, 15\}\,, \tag{192}$$

together with single $\mathrm{d}\log(u-4)$ and $\mathrm{d}\log(u-16)$ iterations of the m_k, and the term $m_k(u)/(u-4)$ that the double pole in eq. (191) produces on integration by parts. These functions enter $m_{18}^{(0)}$ through the variation-of-parameters integral over the coupled top-sector block, in which m_{13} appears as an inhomogeneous term.

Moreover, the top-sector block carries a second local system, of rank nine, singular along a curve $P_7(s,t) = 0$ of degree seven. The polynomial P_7 is neither among the letters (190) nor a function of u alone. Transporting the differential equation in m^2 at fixed (s,t) moves the dimensionless point $(s/m^2,\, t/m^2)$ along a ray through the origin. Restricted to that ray, the monodromy of the second system, generated by loops around every component of its singular locus, acts irreducibly and preserves a nondegenerate symmetric bilinear form of signature $(5,4)$. The system may underlie a polarized variation of Hodge structure. If it does, the polarization is this bilinear form, and a K3-type structure with Hodge numbers $(1,7,1)$, whose polarization has signature $(2,7)$, is excluded. We have not determined its Hodge type.

An exact constraint on $m_{18}^{(0)}$ itself follows from the m^2 connection, in which the derivative of m_{18} at $m^2 = 1$ involves only two other masters,

$$A_{m^2}\big[m_{18} \to m_j\big]\Big|_{d=4,\,m^2=1} \;=\; 2\,\delta_{j,34} + 2\,\delta_{j,35}\,, \tag{193}$$

an entry independent of ε and of (s,t). Combined with Euler's relation for the homogeneous function m_{18} of (s,t,m^2), it gives

$$(s\partial_s + t\partial_t)\,m_{18}^{(0)}(s,t) \;=\; -2\,\Delta(s,t)\,, \qquad \Delta(s,t) \;\equiv\; m_{34}^{(0)}(s,t) + m_{35}^{(0)}(s,t) + 3\zeta_3\,. \tag{194}$$

Crossing relates the two masters on the right, $m_{35}(s,t) = m_{34}(t,s)$, and numerically $m_{34}^{(0)}(0,0) = m_{35}^{(0)}(0,0) = -\frac{3}{2}\zeta_3$. Hence Δ vanishes at the origin, and eq. (194) determines $m_{18}^{(0)}$ from Δ and the boundary value $m_{18}^{(0)}(0,0)$ given under Boundary data, with no further constant.

Result. We integrate the m^2 connection of the thirty-nine masters at fixed (s,t), order by order in ε, from the limit $m^2 \to \infty$ to $m^2 = 1$. In that limit every master reduces to the vacuum integrals of eq. (199). The path runs in the complex m^2 plane around the poles of the connection, and we continue the solution by matching Taylor expansions from one disk to the next. The pole part of m_{18} does not depend on the kinematics,

$$m_{18}(s,t) \;=\; \frac{c_{18}}{\varepsilon} + m_{18}^{(0)}(s,t) + O(\varepsilon)\,, \qquad c_{18} = 2\zeta_3\,, \tag{195}$$

where c_{18} is also the pole coefficient of the tetrahedral vacuum integral V_{4N} [29] to which m_{18} reduces as $m^2 \to \infty$.

On the curve $1/s + 1/t = -3/8$ we find at $(s,t) = (-7, -56/13)$, where $u = 147/13$,

$$m_{18}^{(0)}(-7, -\tfrac{56}{13}) \;=\; -10.41519682\ldots \tag{196}$$

in the normalization of eq. (189). The second point on the curve, used only for comparison with an independent evaluation, is $(s,t) = (-8,-4)$, where $u = 12$. Along the curve, $m_{18}^{(0)}$ is an iterated integral of finite length, which we call its word form: a linear combination, with exact coefficients, of words in thirteen integration kernels on the curve, several of them modular forms pulled back from the banana K3 [101]. The general solution of the top block branches at one further locus on the curve. We find that the coefficients of the branched words in $m_{18}^{(0)}$ vanish, and the physical combination is single valued there. The kernels and the word list are long, and we supply them as a data file accompanying the code for this entry (Appendix G) [106]. Appendix F describes the two-variable connection in the forty-one-element basis from which they are built.

We obtain the thirteen polylogarithmic subsector masters $m_0, \ldots, m_{12}$ in closed form, as multiple polylogarithms through order ε^3. In terms of the invariant x on which each block depends, the banana-type blocks among these polylogarithmic masters have the two-letter alphabet $\{x, x-4\}$ and the triangle blocks the alphabet $\{x,\, x \pm 1,\, x^2 - 3x + 1\}$, whose quadratic letter has roots in $\mathbb{Q}(\sqrt{5})$. Their boundary constants lie in the ring of zeta values with denominators 6^{w+4} at weight w. We identify most of them by integer-relation fits and carry the rest numerically. The banana master with both diagonals contracted, LBL3X$[1,1,1,1,0,0]$, has a pole part polynomial in u,

$$\begin{aligned} c_{-3} &= 2\,, \qquad c_{-2} = \tfrac{23}{3} - 6\gamma_E - \tfrac{u}{3}\,, \\ c_{-1} &= \tfrac{35}{2} - 23\gamma_E + 9\gamma_E^2 + \tfrac{\pi^2}{2} - \left(\tfrac{3}{2} - \gamma_E\right) u + \tfrac{u^2}{36}\,, \end{aligned} \tag{197}$$

where c_k denotes its coefficient of ε^k.

Besides the value of $m_{18}^{(0)}$ on the curve, we can make two statements about its functional form. The first concerns the alphabet (190): $m_{18}^{(0)}$ is not a combination of multiple polylogarithms over the letters of its maximal cut. This exclusion follows from four facts: first, the banana block of the connection is an irreducible K3 system, coupled to m_{18} at ε^0 by eq. (191). Second, the point $u = 16$ enters the equation for $m_{18}^{(0)}$ only through the Picard–Fuchs equation of the period, since the residue of the connection at $u = 16$ vanishes in the polylogarithmic part of the top block. Third, when we fit Δ in eq. (194) to weight-four polylogarithms over the admissible letters $\{s, t, u, s-4, t-4, u-4\}$, the residual is the iterated integral of the K3 period. Finally, on the curve $1/s + 1/t = -3/8$ the ε^0 solution vector, continued around $u = 16$ and then around a zero of P_7, does not return to itself, and the change lies in the top block alone. These facts show that an iterated integral of the K3 period enters $m_{18}^{(0)}$ with nonzero coefficient. They say nothing about polylogarithmic alphabets in other bases.

The second statement about the functional form of $m_{18}^{(0)}$ concerns the differential system in the forty-one-element basis before any ε-dependent change of basis, which we call the raw frame. We order the integrals by the support of the ε^0 part of the exact two-variable connection, which defines a directed dependency graph among them. Its strongly connected components form a directed acyclic graph of depth four, whose top component is a block $\vec{f}$ of twenty-four integrals (the twenty-two top-sector masters and the two additional elements of the basis) coupled irreducibly at ε^0:

$$\mathrm{d}\vec{f} \;=\; B(s,t;\varepsilon)\,\vec{f} \;+\; (\text{lower components})\,, \qquad B \text{ rational in } \varepsilon\,, \quad B\big|_{\varepsilon^0} \supset \text{irreducible } 23\times 23 \text{ block}\,. \tag{198}$$

In the raw frame the equations are thus a coupled Volterra system, whose evaluation needs the fundamental matrix of that 23×23 block, and it becomes a Chen iterated integral of finite length [41] only after an ε-factorizing rotation of the block [76, 93]. We attempted that rotation by Moser–Lee reduction [93]. All 529 entries of the block carry ε in the denominator, and the reduction stalled at pole-order excess 5 without reaching an ε-form, which is not a proof that none exists. Appendix F describes the exact connection data from which the dependency graph and its strongly connected components can be recomputed. Of the entries of the two-variable connection, 40 remain undetermined and are absent from those data.

Boundary data. The boundary values from which we integrate are known in closed form. As $m^2 \to \infty$ at fixed (s,t), equivalently $(s,t)\to(0,0)$, the thirty-nine masters reduce rationally to a six-line vacuum family with three masters. With the measure of eq. (189) and $m^2=1$ these are

$$\begin{aligned} T \;&=\; -\,\Gamma\!\left(1-\tfrac{d}{2}\right)^{3}, \qquad S \;=\; \frac{2^{2d-3}\,\Gamma\!\left(\frac{d}{2}-1\right)^{2}}{\Gamma\!\left(\frac{d}{2}\right)}\,\frac{\sqrt{\pi}\,\Gamma(3-d)\,\Gamma\!\left(2-\frac{d}{2}\right)\Gamma\!\left(4-\frac{3d}{2}\right)}{4\,\Gamma\!\left(\frac{7}{2}-d\right)}\,, \\ B \;&=\; \frac{2^{d+1}}{\Gamma\!\left(\frac{d}{2}\right)}\int_0^\infty x^{3-d}\,K_{d/2-1}(x)^4\,\mathrm{d}x\,, \end{aligned} \tag{199}$$

two products of Γ functions and one convergent Bessel moment [16]. The ε expansion of B lies in the ring of zeta values through ε^1 and is defined by the integral beyond that order. We express every boundary value in terms of $\{T,S,B\}$ by an integration-by-parts reduction exact in d.

The top master itself tends to the tetrahedral vacuum integral V_{4N} of Ref. [29], with four massive and two non-adjacent massless lines on K_4. In the normalization of that reference,

$$V_{4N}(\varepsilon) \;=\; \frac{2\,\zeta_3}{\varepsilon} \;+\; \left(\,6\,\zeta_3 - 14\,\zeta_4 - 16\,U_{3,1}\,\right) \;+\; O(\varepsilon)\,, \qquad U_{3,1} \;=\; \sum_{m>n>0} \frac{(-1)^{m+n}}{m^3\,n}\,, \tag{200}$$

with $U_{3,1} = \frac{1}{2}\zeta_4 + \frac{1}{2}\zeta_2\ln^2 2 - \frac{1}{12}\ln^4 2 - 2\,\mathrm{Li}_4(\frac{1}{2})$, and in the normalization of eq. (189)

$$\begin{aligned} c_{18} = 2\,\zeta_3 &= 2.4041138\ldots\,, \\ 6\,\zeta_3 - 14\,\zeta_4 - 16\,U_{3,1} &= -6.0541678\ldots\,, \\ m_{18}^{(0)}(0,0) &= V_{4N}^{(0)} - 6\gamma_E\zeta_3\,. \end{aligned} \tag{201}$$

Similarly, the boundary values of the banana master m_{13} at its point of maximal unipotent monodromy lie in the $\mathbb{Q}$-span of $\{1,\pi^2,\zeta_3\}$. The word form of $m_{18}^{(0)}$ on the curve contains four constants $c_7,\ldots,c_{10}$, which we first fix numerically by the integration and then identify in the ring of zeta values of weight at most three,

$$c_7 = \zeta_3 - \tfrac{673}{72}\,, \qquad c_8 = \tfrac{11203}{1152} - \tfrac{\pi^2}{32} + \tfrac{31}{32}\zeta_3\,, \qquad c_9 = \tfrac{3587}{144} - \zeta_3\,, \qquad c_{10} = -\tfrac{19103}{1152} - \tfrac{3\pi^2}{32} + \tfrac{67}{32}\zeta_3\,. \tag{202}$$

Ten of the boundary constants R_j of the individual kernel components at $(s,t)\to(0,0)$ lie in the same ring and are listed in eq. (229) of Appendix F. For those of the components coupled to the banana block we have found no closed form.

Checks. We compared our values with `AMFlow` [95] evaluations used nowhere in the construction. At the six points $(s,t) = (-25,-25)$, $(-11,-2)$, $(-14,-3)$, $(-23,-10)$, $(-25,-11)$ and $(-19,-18)$ the ε^0 coefficients of the top-sector masters m_{17}, m_{34} and m_{35} agree with `AMFlow` to between 33 and 46 digits (Appendix A). Five of these points lie above the threshold $u = 16m^2$ of the diagonal channel, where the masters are complex, and there we compare real and imaginary parts. For $m_{18}^{(0)}$ itself, the values at $(s,t) = (-8,-4)$ and at $(-7,-56/13)$ on the curve each agree with an `AMFlow` evaluation at the same point to 72 digits, limited by the precision of those reference values.

Furthermore, the thirteen polylogarithmic subsector masters agree with `AMFlow` to at least 52 digits over $\varepsilon^{-3},\dots,\varepsilon^3$ at a point not used in their fits, and the pole coefficients c_{-3}, c_{-2}, c_{-1} to at least 113 at nineteen points on the line $s = -3$. The constants of eq. (202) agree to at least 38 digits with reference values derived from an independent `AMFlow` computation of the subsector masters at $(s,t) = (-6,-\frac{24}{5})$ on the curve.

7 Scope of the results

Each result holds on the kinematic domain stated in its entry and in Table 1, and for several new entries that domain is a slice, a line, a set of path segments or one mass assignment. The function classes of the results range from multiple polylogarithms to Calabi–Yau periods. Section 7.2 lists closely related integrals that remain uncomputed.

7.1 Kinematic domains and function classes reached

The Sudakov form factor, the three double boxes, the C_5 ladder and the pentagon are functions on their whole Euclidean region. So are the sunrise family, the equal-mass kite, the $gg \to H$ functions, the two equal-mass bananas and the light-by-light box with a sunrise insertion. For the boxes with self-energy insertions we give dispersion integrals over closed-form densities and evaluate them only at the Euclidean points listed in Table 1. The $(1,1,2)$ sunrise, the equal-mass kite and the three-loop banana are also continued above threshold, as are the unequal-mass kite and the equal-mass ice-cream cone among the entries on restricted kinematics.

All entries on restricted kinematics are new. We evaluate the unequal-mass kite and the four-mass kite with a massless rung at one mass assignment each, and reproduce independent values at a second. The ice-cream cone results hold on a symmetric slice of the external virtualities, and the sector-125 pair of $gg \to Z\gamma$ is given at one value of m_Z^2/m_t^2, on the lines stated in its entry. Along straight path segments in the six-scale space, the hexa-box masters are functions of the segment parameter, and the nonplanar W-pair masters are given on one line outside the physical region. We give the crossed light-by-light box as a transported value on one (s,t) curve and at the points listed in its entry; the banana threshold coefficients are period-level constants with no kinematic dependence.

The polylogarithmic entries have rational or algebraic $\mathrm{d}\log$ alphabets. For the hexa-box the alphabet is known only along the path segments, where we give the masters as iterated integrals. Most elliptic entries involve the $\Gamma_1(6)$ curve of the equal-mass sunrise, either directly or through a sunrise subgraph, as in the equal-mass kite, the equal-mass cone and the light-by-light insertions. This curve also appears in the three-loop banana, whose K3 surface is its symmetric square. In the $gg \to Z\gamma$ family the solutions of the homogeneous block involve an Eichler integral on $\Gamma_0(4)$. On non-modular curves, the unequal-mass sunrise integrals are Kronecker elliptic polylogarithms at marked points, the $gg \to H$ functions are one-fold integrals over the holomorphic period, and the unequal-mass kite and the generic-mass cone are written with the period pair by variation

of parameters. One W-pair sector has a fiberwise elliptic maximal cut. We give the four-loop banana as a Frobenius solution at the point of maximal unipotent monodromy, and the threshold coefficients as connection data at singular points with non-unipotent monodromy. The differential equation of the crossed light-by-light box couples its top block to polylogarithmic subsectors, to the K3 banana and to a second rank-nine local system.

7.2 Integrals not computed here

Of the inequivalent placements of the two massive legs on the nonplanar hexa-box graph, we solve the simplest in section 4.8. The placement with the massive legs adjacent carries in its alphabet the two-mass threshold root r_{34} of the diboson-plus-jet amplitudes [3]. We have not solved its 154-master family, although its three top-sector masters have been evaluated with `AMFlow` [95] through ε^0 at two Euclidean points. For the generic-mass hexa-box and double-pentagon families, with 219 and 190 masters, we have the lower bound of eq. (221) on the symbol space and a double-precision value of one top-sector master at one point.

For the nonplanar W-pair masters (section 5.9) we do not yet know the dependence on the kinematics away from the unphysical line, the continuation to the physical region or closed forms for the forty boundary constants left as transport integrals. Boundary values for the masters of sector 127, the seven-propagator parent of sector 125 in the $gg \to Z\gamma$ family, are taken only from `AMFlow`. An external momentum enters sector 127 through a propagator, so its masters lack the polynomial dependence on t that we use to determine the sector-125 pair. It remains to find a boundary condition for sector 127 not taken from `AMFlow` and to obtain that pair at other values of m_Z^2/m_t^2. Giving the crossed light-by-light box as a function of (s,t) away from the curve of section 6.4 requires the undetermined entries of the two-variable connection of its top block. With an ε-form of that block, which the Moser–Lee reduction did not reach, the box would in addition become an iterated integral of finite length in both variables. A natural next step in the three-loop light-by-light family is to compute the crossed box's ten-propagator parent graph, whose maximal cut is an elliptic curve intrinsic to the topology. Among Calabi–Yau integrals we expect the unequal-mass four-loop banana as a function of p^2 to be the next case.

Several classes of known results lie outside the reach of the method [105]. For closed forms exact in d, such as those for bubble chains and one-loop N-point functions [85, 46], we obtain only the expansion in ε. Because the method proceeds order by order in the loop expansion, it does not apply to all-order results at finite coupling, such as the Basso–Dixon fishnet determinant [19, 55]. Moreover, maximal cuts of genus two or higher lead to Siegel modular forms, which do not belong to the elliptic function spaces used here [61, 21], and near an irregular singular point of a differential equation the solutions are not iterated integrals. Finally, we assume throughout that an alphabet taken from a Landau analysis is complete with respect to second-type singularities. We have tested this assumption for the hexa-box and W-pair families with the Euler-characteristic criterion of [42], and for the W-pair family we found four letters missing from the Landau analysis (Appendix D).

8 Conclusions

We have presented thirty Feynman integrals, most with internal masses and several scales. They span the three function classes encountered in precision collider calculations: multiple polylogarithms, functions on elliptic curves, and periods of K3 surfaces and Calabi–Yau threefolds. Fifteen reproduce results from the literature without using published values in any fit, and the other fifteen are new on the kinematic domains stated in Table 1. All thirty satisfy the acceptance criterion of eq. (7), the BootLoops standard. For each integral we give the definition, the function space,

and the result in closed form, as a Picard–Fuchs operator with boundary data, or as a differential equation with boundary data solved along a stated path. Reference values at rational points and a standalone evaluation code accompany each result.

The construction of the results is the same in all three classes, and apart from the function class the integrals differ mainly in the arithmetic nature of their boundary constants. For the one- and two-scale integrals the boundary data reduce to a few classical constants or a single new one. These constants range from rational multiples of zeta values, for the massless polylogarithmic integrals and the three-loop banana at ε^0, to numbers that we can define only by a convergent integral of their own, for the ice-cream cones. For the cone constants we find no shorter classical expression by integer-relation searches, as expected for periods at generic moduli [60, 107]. Between these extremes lie a Clausen value for the box with a sunrise insertion, Catalan's constant in the vacuum data of the unequal-mass kite, and values in the lemniscatic $\Gamma(\frac{1}{4})$ ring for the threshold coefficients of the four-loop banana. However, the boundary value of the unequal-mass kite on the negative s axis is again a period that we could not reduce to classical constants. For the integrals with the most scales the boundary data consist of many constants. We give each constant in closed form where we found one and otherwise define it by transporting analytic initial values with a differential equation; for two of these integrals the values so defined are available only as high-precision decimal strings. Several of the new results, including all of those with the most scales, hold on a restricted domain, stated for each of them in Table 1 and discussed in section 7.

The method is documented in the companion paper [105], including the choice, for each integral, between an ansatz fit and direct integration of the differential equation, and the part taken by the language model that ran the computations. The elliptic and Calabi–Yau constructions we rely on are derived in [107]. Several integrals closely related to those computed here remain open, and section 7.2 lists them. The first of these is the hexa-box with the two massive legs adjacent, whose alphabet contains the two-mass threshold of the diboson amplitudes and for which we have the reduction and top-sector reference values. Two others are the nonplanar W-pair masters away from the unphysical line on which we give them, in particular in the physical region, and the crossed light-by-light box away from the curve on which we transport its differential equation. These computations will be the subject of future work, and we expect the same combination of Landau singularity analysis and direct integration of the differential equations to apply to them.

Acknowledgments

Funding for this project was provided by Anthropic. This is not an official Anthropic project and results and views are not endorsed by Anthropic.

A Reference values

In this appendix we collect numerical values of the thirty integrals at fixed kinematic points, against which an independent implementation can be tested, together with the comparisons quoted in sections 4–6. Tables 3, 4 and 6 follow the order of Table 1. Each line gives the kinematic point in the variables of the entry's *Definition* display, the order in ε, the value of our result in the normalization of that display, what we compared it with, and the number of digits to which the two agree. Where the "compared with" column reads `AMFlow`, the comparison value is an auxiliary-mass-flow evaluation [95] of the same family at that point, used in no fit and in no boundary value. In most cases the agreement is then limited by the precision of that evaluation. A line with a digit count and an empty value cell refers to a comparison whose values we do not print

here. A line with a value and an empty digits cell gives our result at a fit point, marked as such, or at a point where no comparison is quantified. Trailing dots indicate that a printed value is truncated, and further digits can be obtained with the evaluation codes of Appendix G [106]. For the sunrise family, Table 5 also lists the finite part $J[1,1,1]^{(0)}(t)$ computed in ball arithmetic from the coordinate-space representation eq. (68), and this determination uses neither the differential equation nor `AMFlow`.

Table 3: Reference values and comparisons for the polylogarithmic entries of section 4, in the order of Table 1. The columns give the entry number, the kinematic point in the variables of the entry's *Definition* display, the order in ε (the weight w for Nos. 1 and 7, the loop order L for No. 4), the value of our result in the normalization of that display, what it was compared with, and the number of digits to which the two agree. `AMFlow` denotes an auxiliary-mass-flow evaluation [95] of the same family at that point, used in no fit. An empty comparison cell marks a value that entered no comparison, and an empty last cell a comparison whose agreement is not quantified here.

No.	point	order	value	compared with	digits
6	$s=-1$	ε^{-4} to ε^{6}	$e^{2\varepsilon\gamma_E} I[1,0,1,1,1,1,1](-1)$: exact ζ values, eq. (13) through ε^3; the ε^6 coefficient is $-1235.936250\ldots$	`AMFlow`	≥ 78
2	$s=-1$, $t=-\frac{2}{5}$ ($x=\frac{2}{5}$)	ε^{-4} to ε^{0}	$J^{(j)}$ of eq. (203)	`AMFlow`	≥ 89
2	$s=-1$, $t=-\frac{3}{4}$ ($x=\frac{3}{4}$)	ε^{-4} to ε^{0}	$J^{(j)}$ of eq. (203)	`AMFlow`	≥ 89
2	$x=\frac{2}{5},\ \frac{3}{4}$	ε^{-4} to ε^{0}		closed form of [109], independent polylogarithm implementation	≥ 142
4	$x=\frac{11}{20}$	$L=3$	$f_3=-87.265091\ldots$, eq. (27)	two-variable representation through $\Phi^{(3)}$	80
4	$x=\frac{1}{50}$	$L=3$	$f_3=-11.953531\ldots$	same	80
4	$x=\frac{7}{25}$	$L=3$	$f_3=-60.574737\ldots$	same	80
4	$x=\frac{1}{3},\ \frac{2}{9},\ \frac{7}{9}$	$L=1,2,3$		closed form of [114, 49]	≥ 461 (working precision 462)
4	$(X,Y)=(\frac{2}{3},\frac{3}{4})$	ε^{0}	$\Phi^{(3)}(X,Y)$; every pole coefficient zero	`AMFlow`, nine-line family	72
4	$(X,Y)=(\frac{421}{1225},\frac{596}{1225})$, $(\frac{424}{225},\frac{109}{225})$		$\Phi^{(3)}(X,Y)$	two independent representations	≥ 60
5	$(v_1,\ldots,v_5)=(-1,-2,-3,-4,-5)$	ε^{-2}	$I_5=-\frac{3}{8}$	`AMFlow`	68
5	same	ε^{-1}	$I_5=0.1798058444\ldots$	`AMFlow`	68
5	same	ε^{0}	$I_5=0.2872248726\ldots$	`AMFlow`	68
5	same	ε^{-2} to ε^{0}		the more precise of the two `AMFlow` runs	107
5	twelve further Euclidean points	ε^{-2} to ε^{0}		`AMFlow`	67
1	$(u,v)=(\frac{16}{3},\frac{10}{3})$	$w=4$	$g_{10}=0.043932114\ldots$	`AMFlow`	≥ 86
1	$(u,v)=(4,4)$	$w=4$	$g_{10}=0.053038629\ldots$	value quoted in [40]	
1	$(u,v)=(\frac{10}{3},\frac{16}{3})$, $(\frac{23}{4},\frac{9}{4})$, $(\frac{5}{2},4)$	$w=4$		`AMFlow`	≥ 86

Table 3: Reference values, polylogarithmic entries (continued).

No.	point	order	value	compared with	digits
7	eight lines of fixed s, four not used in the fit; $m^2 = 1$	$w \leq 2$	eqs. (46)–(48), exact	`AMFlow`	108
7	twenty points on $s = -\frac{7}{2}, -3, -\frac{5}{2}, -\frac{3}{2}$	$w = 3$; $w = 4$		`AMFlow`	109–112; 109–111
7	$(s,t) = (-4,-2)$, $m^2 = 1$	ε^{-4} to ε^0		`AMFlow`	≥ 129
23	$t = -1$	ε^0	$\mathrm{TOP}_{\varepsilon^0} = -0.27540984\ldots$	`AMFlow`	110
23	$t = -2$	ε^0	$\mathrm{TOP}_{\varepsilon^0} = -0.26163647\ldots$	`AMFlow`	109
23	$t = -3$	ε^0	$\mathrm{TOP}_{\varepsilon^0} = -0.24936351\ldots$	`AMFlow`	109
23	$t = -4$	ε^0	$\mathrm{TOP}_{\varepsilon^0} = -0.23833892\ldots$	`AMFlow`	97
23	$t = -5$	ε^0	$\mathrm{TOP}_{\varepsilon^0} = -0.22836711\ldots$	`AMFlow`	97
23	$t = -6$	ε^0	$\mathrm{TOP}_{\varepsilon^0} = -0.21929335\ldots$	`AMFlow`	97
23	$t = -8$	ε^0	$\mathrm{TOP}_{\varepsilon^0} = -0.20336554\ldots$	`AMFlow`	81
23	$t = 0$	ε^0	$\mathrm{TOP}(0) = -0.2910157568\ldots$, the boundary value as a one-dimensional Bessel integral	analytic vacuum value at $p^2 = 0$	49 (fifty working digits)
23	masses^2 $(1,4,9,3,0)$, $t = 0$	ε^0	$\mathrm{TOP}(0) = -0.2694310421\ldots$	analytic vacuum value at $p^2 = 0$	49 (fifty working digits)
23	masses^2 $(1,4,9,3,0)$, $t = -2, -\frac{7}{3}$	all orders, 22 masters		`AMFlow`	98
24	segment I, endpoint $t = 1$	ε^{-4}	three top-sector masters, eq. (66): $-\frac{571}{1079925}$, $\frac{46591}{8639400}$, $-\frac{854177}{8639400}$, exact		
24	segment I, second point	ε^{-4} to ε^0	fifteen top-sector coefficients	`AMFlow`	≥ 66
24	segment I, second point	through ε^2	five subsector orbits	`AMFlow`	31–40
24	segment I, second point	ε^1; ε^2	top sector	`AMFlow`	40; 35
24	segment III, endpoint P_3	$d = \frac{13}{3}$, $\frac{9}{2}$, $\frac{11}{2}$	all 98 masters at $P_3 = (-5,-7,-9,-2,-11,1)$	`AMFlow`	≥ 61

For No. 2, with $J(s,t)$ of eq. (20) expanded as $J = \sum_{j \geq -4} \varepsilon^j J^{(j)}$ at $s = -1$, the five coefficients at

the two comparison points are

$$
\begin{aligned}
t = -\tfrac{2}{5}: \qquad J^{(-4)} &= -10\,, \\
J^{(-3)} &= 0.090679149603718897336151654547910227716 92\ldots, \\
J^{(-2)} &= 64.045959605108058861749005759729470501 67\ldots, \\
J^{(-1)} &= 144.497028112859828690885814786994125858 4\ldots, \\
J^{(0)} &= 144.468560258047663935390369467089428335 0\ldots, \\
t = -\tfrac{3}{4}: \qquad J^{(-4)} &= -5.333333333333333333333333333333333333333333\ldots, \\
J^{(-3)} &= 4.239086609271144330208002254253443054426\ldots, \\
J^{(-2)} &= 31.338148866595200624424142844782477266 45\ldots, \\
J^{(-1)} &= 37.461220975964120589791867866378865672 24\ldots, \\
J^{(0)} &= -7.244798182559349287848013151756462832364\ldots\,.
\end{aligned}
\tag{203}
$$

The leading coefficients are the exact values $K^{(-4)}/x = -4/x$ of eq. (21).

Table 4: Reference values and comparisons for the elliptic entries of section 5, in the order of Table 1; columns as in Table 3. For the sunrise family, $E^{(k)}(t) = J[1,1,1]^{(k)}(t)/\hat{\psi}_1(t)$ as in section 5.1, and the finite parts $J[1,1,1]^{(0)}$ themselves are in Table 5. "Fit point" marks a value at a point used to determine coefficients. Points with $t + i0$, $s + i0$ or $x + i0$ lie above threshold and the comparison includes the imaginary parts.

No.	point	order	value	compared with	digits
8	$(1,1,1)$, $t=-3$	ε^0	Table 5	`AMFlow`	140
8	$(1,1,1)$, $t=-9$	ε^0	Table 5	`AMFlow`	159
9	$(1,1,2)$, $t=-1$	ε^0	$E^{(0)} = -2.3471191\ldots$	fit point	
9	$(1,1,2)$, $t=-5$	ε^0	$E^{(0)} = -3.2711938\ldots$	fit point	
9	$(1,1,2)$, $t=-3,\,-7$	ε^0	Table 5	`AMFlow`	159
9	$(1,1,2)$, $t=16,\,20$ $(t+i0)$	ε^0		`AMFlow`	≥ 71
10	$(1,2,3)$, $t=-3,\,-9$	ε^0	Table 5	`AMFlow`	159
11	$(1,1,4)$, $t=-3$	ε^0	Table 5	`AMFlow`	289
11	$(1,1,4)$, $t=-9,\,-11$	ε^0	Table 5	`AMFlow`	159
11	$(1,1,4)$, $t=-7$	ε^0	$E^{(0)} = -3.3260720\ldots$	`AMFlow`	160
11	$(1,1,4)$, $t=-\frac{5}{2}$	ε^0	Table 5	`AMFlow`	159
9–11	$(1,1,3)$, $t=-3$	ε^0	$E^{(0)} = -2.7788109\ldots$, the per-puncture formula eq. (73) at a fifth mass assignment	`AMFlow`	160
9–11	$(1,1,3)$, $t=-6$	ε^0	Table 5	`AMFlow`	159
12	$(1,1,2)$, $t=-5$	ε^1	$E^{(1)} = 12.166814\ldots$, eq. (74)	`AMFlow`	291
12	nine points, three per mass assignment	ε^1		`AMFlow`	288–308
13	$t=-1$	ε^0	$I_{\text{kite}} = -1.3317114\ldots$, eq. (78)	representation of [5] (fit point)	~ 180
13	$t=-3$	ε^0	$I_{\text{kite}} = -0.88550175\ldots$	`AMFlow`	160
13	$t=-10$	ε^0		`AMFlow`	130
18	$(s, M^2) = (-\frac{1}{2}, \frac{9}{10})$	ε^0	$G_1 = -0.006031453047\ldots$, $G_2 = -0.04436252545\ldots$, eq. (80)		

Table 4: Reference values, elliptic entries (continued).

No.	point	order	value	compared with	digits
18	$(s, M^2) = (-\frac{7}{4}, \frac{3}{5})$	ε^0	G_1; G_2	`AMFlow` values rotated into the canonical basis of [96]	57; 48
14	$(1,1,2)$, $s = -4$	ε^0	$I^{(0)}_{\text{kite}} = -0.66865601\ldots$, eq. (94)		
14	$(1,1,2)$, $s = -\frac{5}{2}, -3, -15$	ε^0		`AMFlow`	125
14	$(1,1,2)$, $s = 16$ $(s + i0)$	all orders, 40 nonzero components		`AMFlow`	64
14	$(1,1,3)$, $s = -\frac{5}{3}, -\frac{10}{3}$	all orders, 14 masters		`AMFlow`	128
15	$x = -2$	ε^0		`AMFlow`	134
15	$x = -3$	ε^0		`AMFlow`	110
15	$x = -1$	ε^0	$T(-1) = 0.60984239\ldots$	two-dimensional quadrature of eq. (97)	284
15	$x = 12$ $(x + i0)$	all orders, 14 components		`AMFlow`	57
16	masses^2 $(1,2,3,5)$, $x = -2$	ε^0		`AMFlow`	118
16	masses^2 $(1,2,3,5)$, $x = -1$	ε^0	$T(-1) = 0.13489705\ldots$	two-dimensional quadrature of eq. (97)	≥ 110
16	masses^2 $(1,3,2,7)$, $x = -2$	ε^0	$T(-2) = 0.10288957\ldots$	`AMFlow`	≥ 86
16	masses^2 $(1, \frac{5}{2}, \frac{1}{2}, 3)$, $x = -2$	ε^0	$T(-2) = 0.27115618\ldots$	`AMFlow`	51 (sixty working digits)
17	$x = -2$	ε^1		`AMFlow`	134
17	$x = -1$	ε^1	$f_{4,1}(-1) = -0.67751873\ldots$	one-dimensional transport integral from $x = -2$, $\int_{-2}^{-1} R_4\, dx' = 0.0072214198\ldots$	119
20	$(s,t) = (-\frac{1}{4}, -\frac{1}{3})$, $M = \frac{7}{25}$, $m_t^2 = 1$	ε^0; ε^1	$R_a = 0.55129454\ldots$; $R_a = 0.90052626\ldots$ (no factor $e^{\varepsilon\gamma_E}$)	`AMFlow`, all 22 masters, ε^{-2} to ε^4	109
20	$(s,t) = (-\frac{1}{5}, -\frac{1}{2})$, $(-\frac{1}{10}, -\frac{1}{2})$, $(-\frac{1}{20}, -\frac{5}{4})$, $(-\frac{9}{40}, -\frac{5}{4})$, $(-\frac{3}{20}, -\frac{5}{6})$	fourteen masters		`AMFlow`	≥ 47
27	$(s,t,m^2) = (-\frac{7}{3}, -\frac{11}{10}, 1)$	ε^{-2}; ε^{-1}; ε^0	I_{box} of eq. (130)	`AMFlow`	52; 53; 46
27	$(s,t,m^2) = (-\frac{3}{2}, -\frac{9}{5}, 1)$	ε^{-2}; ε^{-1}; ε^0	eq. (204)	`AMFlow`	52; 52; 45

Table 4: Reference values, elliptic entries (continued).

No.	point	order	value	compared with	digits
27	$(s,t,m^2) = (-\frac{5}{4}, -\frac{12}{5}, 1)$	ε^{-2}; ε^{-1}; ε^0	eq. (205)	`AMFlow`	52; 52; 45
27	sunrise insertion, $w = -\frac{7}{3}$, -4			`AMFlow`	71; 69
28	$(s,t,m^2) = (-1, -\frac{1}{3}, 1)$	ε^0	$I = 0.52495777\ldots$	`AMFlow`	59
28	$(s,t,m^2) = (-\frac{1}{2}, -1, 1)$	ε^0	$I = 0.55006901\ldots$	`AMFlow`	59
29	$(s,t,m^2) = (-1, -\frac{1}{3}, 1)$	ε^0	I_{KP}; I_{K_1}	`AMFlow`	68; 68
29	$(s,t,m^2) = (-\frac{1}{2}, -1, 1)$	ε^0	$I_{\mathrm{KP}} = 0.12675212\ldots$; $I_{K_1} = -0.23637432\ldots$	`AMFlow`	50; 50
33	$(s,t,m^2) = (-1, -\frac{1}{3}, 1)$	fixed $\varepsilon = 2^{-7}$	I_{VP} of eq. (206)	`AMFlow`	58
33	$(s,t,m^2) = (-1, -\frac{1}{3}, 1)$	fixed $\varepsilon = 2^{-6}$, 2^{-8}, …, 2^{-13}		`AMFlow`	56–59
33	$(s,t,m^2) = (-1, -\frac{1}{3}, 1)$	ε^{-2}; ε^{-1}	$c_{-2} = -0.04540615882\ldots$; $c_{-1} = -0.01534480\ldots$	pole coefficients extracted from the `AMFlow` values	45; 39
33	$(s,t,m^2) = (-1, -\frac{1}{3}, 1)$	ε^0	$c_0 = -0.14660534\ldots$	extrapolation to $\varepsilon \to 0$ of the fixed-ε dispersive values	39
33	$(s,t,m^2) = (-1, -\frac{1}{3}, 1)$	ε^1	$c_1 = 0.0397158224\ldots$		
33	$(-\frac{1}{2}, -1, 1)$, $(-\frac{3}{2}, -\frac{1}{4}, 1)$, $(-\frac{3}{4}, -\frac{1}{2}, 1)$, $(-\frac{1}{4}, -\frac{1}{2}, 1)$	fixed $\varepsilon = 2^{-6}$, …, 2^{-13}		`AMFlow`	≥ 37
35	line $(x,z) = (\frac{17}{2}, \frac{5}{3})$, $y = \frac{1}{2}$, $\frac{3}{5}$	ε^{-3} to ε^1, all 79 functions		`AMFlow`	≥ 37 (forty working digits)

The values of I_{box} (No. 27) at its second and third points in Table 4, where our dispersive representation eq. (127) and `AMFlow` agree to the accuracy given there, are

$$(-\tfrac{3}{2}, -\tfrac{9}{5}, 1): \quad \varepsilon^{-2}: \ -0.75475405\ldots, \quad \varepsilon^{-1}: \ -0.91371298\ldots, \quad \varepsilon^{0}: \ -0.13338047\ldots \tag{204}$$

$$(-\tfrac{5}{4}, -\tfrac{12}{5}, 1): \quad \varepsilon^{-2}: \ -0.76608418\ldots, \quad \varepsilon^{-1}: \ -0.96830417\ldots, \quad \varepsilon^{0}: \ -0.05036791\ldots \tag{205}$$

in the measure of eq. (1) without the factor $e^{L\gamma_E\varepsilon}$. All three points lie below the cuts at $s = 4m^2$ and $t = 16m^2$ and the values are real. For No. 33 the fixed-ε value listed in Table 4 is

$$I_{\mathrm{VP}}\big|_{\varepsilon=2^{-7}}(-1, -\tfrac{1}{3}, 1) = -746.044958090305972213392154049203741988 4\ldots . \tag{206}$$

Table 5: The finite part $J[1,1,1]^{(0)}(t)$ of the sunrise integral of section 5.1, eq. (67) in $d = 2$ with no factor $e^{2\gamma_E \varepsilon}$, from the coordinate-space representation $J[1,1,1]^{(0)}(t) = -4\int_0^\infty r\, J_0(\sqrt{-t}\, r)\, K_0(m_1 r) K_0(m_2 r) K_0(m_3 r)\, dr$ evaluated in ball arithmetic. Each value is enclosed to at least 103 digits and truncated here to forty figures. The fourth column indicates whether the point was used to determine coefficients of the closed form (fit) or only for comparison. The last column repeats from Table 4 the agreement of the closed form with `AMFlow` at the comparison points.

(m_1^2, m_2^2, m_3^2)	t	$J[1,1,1]^{(0)}(t)$	role	digits
$(1,1,1)$	-3	$-2.058976697925491872418279969148844904995\ldots$	comparison	140
$(1,1,1)$	-9	$-1.697946461195426121941926194883505305703\ldots$	comparison	159
$(1,1,2)$	$-\frac{1}{2}$	$-1.798157570767659926681502888104678862374\ldots$	fit	
$(1,1,2)$	-1	$-1.766120078874611770098817442459191586722\ldots$	fit	
$(1,1,2)$	-2	$-1.706678728845436215329563616943060744682\ldots$	fit	
$(1,1,2)$	-5	$-1.557651229351457426731311771769945612570\ldots$	fit	
$(1,1,2)$	-3	$-1.652616990806520655424150564273537185703\ldots$	comparison	159
$(1,1,2)$	-7	$-1.476584679023782856973196584499586861445\ldots$	comparison	159
$(1,2,3)$	$-\frac{1}{3}$	$-1.243506262771417933387193245599882919058\ldots$	fit	
$(1,2,3)$	-1	$-1.222999405866538014484513662682718992185\ldots$	fit	
$(1,2,3)$	-3	$-1.166861129923008182967470991079174908746\ldots$	comparison	159
$(1,2,3)$	-5	$-1.117499381893597773066147567586307132147\ldots$	fit	
$(1,2,3)$	-7	$-1.073624319028161941046716411279482557507\ldots$	fit	
$(1,2,3)$	-9	$-1.034270487719838397538544632285308095890\ldots$	comparison	159
$(1,1,4)$	$-\frac{1}{2}$	$-1.367358498588526055258498706505854763966\ldots$	fit	
$(1,1,4)$	-1	$-1.349147168117671049175430282381298431701\ldots$	fit	
$(1,1,4)$	$-\frac{5}{2}$	$-1.298417041347428472465588808239440386531\ldots$	comparison	159
$(1,1,4)$	-3	$-1.282679360193139967170265801918034297182\ldots$	comparison	289
$(1,1,4)$	-7	$-1.173612885903721499321535413304259348989\ldots$	comparison	160
$(1,1,4)$	-9	$-1.128038676179431861924871184562074727194\ldots$	comparison	159
$(1,1,4)$	-11	$-1.087064137816296680859645059334558943383\ldots$	comparison	159
$(1,1,3)$	-3	$-1.431084999013572201927873528803922517955\ldots$	comparison	160
$(1,1,3)$	-6	$-1.326823625357249315293622645103073273364\ldots$	comparison	159

Table 6: Reference values and comparisons for the K3 and Calabi–Yau entries of section 6, in the order of Table 1; columns as in Table 3. For Nos. 31 and 32 no auxiliary-mass-flow computation applies to a connection coefficient, and the comparisons are between independent determinations of the same number. The Bessel-moment quadrature of No. 34 evaluates $I_{11111}|_{\varepsilon^0} = -16\int_0^\infty x\, J_0(x\sqrt{-p^2})\, K_0(x)^5\, dx$. For No. 21, $u = -s - t$ and $m^2 = 1$ throughout, and the points marked "on the curve" satisfy $1/s + 1/t = -3/8$.

No.	point	order	value	compared with	digits
19	$t = -3$	ε^0	$m_1 = 8.0002891\ldots$, eq. (169), with $\varpi_0(-3) = 0.85621843\ldots$	`AMFlow`	119
19	18 points, $t = -\frac{7}{2}$, -3 and $t = \frac{1}{8}$, $\frac{1}{4}$, …, $\frac{7}{2}$	ε^0		`AMFlow`	≥ 110
19	same 18 points	ε^1		`AMFlow`	≥ 109
19	$t = 18$ $(t + i0)$; the same at $t = 25$, 40, 100, 200	ε^0	$m_1 = 16.0134447\ldots + 6.20325251\ldots\, i$ at $t = 18$	`AMFlow`	≥ 99
19	$t = 5$, 8, 12, $\frac{31}{2}$ $(t + i0)$	ε^0	real values	`AMFlow`	≥ 99
19	$t = -8$	ε^0 to ε^5	Bessel moment eq. (163) expanded in ε	`AMFlow`	≥ 41
34	$p^2 = -2$; $p^2 = -7$	ε^0	m_1	`AMFlow`	67; 67

Table 6: Reference values, K3 and Calabi–Yau entries (continued).

No.	point	order	value	compared with	digits
34	$p^2=-2;\ p^2=-7$	ε^{-4} to ε^0, five masters	worst of the 21 nonzero Laurent coefficients	`AMFlow`	67; 67
34	$p^2=-2;\ p^2=-7$	ε^0	m_1	Bessel-moment quadrature	116; 116
31	masses^2 $(1,1,1,9)$, threshold branch at $p^2=0$	period	$c_{3/2}=-\sqrt{3}/(36\pi)$, eq. (207)	ball-arithmetic transport; independent transport	195; 195
31	same	period	$c_{3/2}$	coefficient from the maximal-cut operator of the family	47
31	MUM point $z=-1/p^2=0$	ε^0	$a_0=19.2329104\ldots$, $a_1=0$, $a_2=-13.1833474\ldots$, $a_3=-38.5332202\ldots$, eq. (187)	`AMFlow` value of J_{31}, second working precision	31
32	masses^2 $(1,1,1,1,16)$, threshold branches at $p^2=0$	period	$c_{5/4}$, $c_{7/4}$, closed forms in [107]	ball-arithmetic transport; two independent transports	197; 71
32	same	period	$c_{5/4}$; $c_{7/4}$	coefficients from the maximal-cut operator of the family	45; 45
32	MUM point $z=0$	ε^0	$a_0=53.3249506\ldots$, $a_1=96.1645522\ldots$, $a_2=0$, $a_3=-66.5421293\ldots$, $a_4=-3210.34993\ldots$, $a_5=-1818.61697\ldots$, eq. (188)	`AMFlow` value of J_{32}, second working precision	31
21	$(s,t)=(-25,-25)$, $u=50$	ε^0	m_{17}, m_{34}, m_{35}	`AMFlow`	36
21	$(s,t)=(-11,-2)$, $u=13$	ε^0	same	`AMFlow`	34
21	$(s,t)=(-14,-3)$, $u=17$	ε^0	same	`AMFlow`	33
21	$(s,t)=(-23,-10)$, $u=33$	ε^0	same	`AMFlow`	38
21	$(s,t)=(-25,-11)$, $u=36$	ε^0	same	`AMFlow`	38
21	$(s,t)=(-19,-18)$, $u=37$	ε^0	same	`AMFlow`	46
21	$(s,t)=(-8,-4)$, on the curve	ε^0	m_{18}	`AMFlow`	72
21	$(s,t)=(-8,-4)$, on the curve	ε^{-1}	m_{18}: $2\zeta_3=2.4041138\ldots$ exactly	`AMFlow`	82
21	$(s,t)=(-7,-\frac{56}{13})$, on the curve	ε^0	$m_{18}^{(0)}=-10.41519682\ldots$ in the normalization of eq. (189)	`AMFlow`	72

The threshold coefficient of No. 31 to forty figures is

$$c_{3/2}=-\frac{\sqrt{3}}{36\pi}=-0.0153146915394942235975368471753602622610 3\ldots\,, \tag{207}$$

on the branch $\arg p^2 = -\pi$ of section 6.3.

B Word lists of the central-mass double box

In this appendix we list the weight-three and weight-four coefficients of the central-mass double box of section 4.6 (No. 7 of Table 1). For the massless planar double box (No. 2) all coefficients through order ε^0 are given in the main text, eq. (21). We set $m^2 = 1$ and use the pure function $g(\varepsilon) = \sum_w g^{(w)}\varepsilon^w$ with $g^{(0)} = 1$, whose coefficients at weights one and two are eqs. (47) and (48). We write the coefficients at weights three and four in the variables

$$x = -t, \qquad y = -s, \qquad \ell = \log(-s), \qquad \sigma = \frac{s}{1-s}, \tag{208}$$

as combinations of the polylogarithms $G(\vec{a};x)$ of eq. (4) with letters $a_i \in \{0,-1,s,\sigma\}$ and $G(\vec{b};y)$ with letters $b_i \in \{0,1,-1\}$. The four letters in x are the zeros of the alphabet letters t, $1-t$, $s+t$ and $s+t-st$ of eq. (45), and the three letters in y are the zeros of s, $s+1$ and $1-s$. Every word ends in a nonzero letter, and powers of logarithms are kept as separate factors. In the result these factors are powers $\ell^k/k!$ of $\log(-s)$ alone, and t enters only through the words $G(\vec{a};x)$. The weight-three coefficient has 39 terms,

$$\begin{aligned}
g^{(3)} = {} & 14\,G(0,0,1;y) - 6\,G(0,1,1;y) + 8\,G(0,-1,-1;y) - 6\,G(1,0,1;y) \\
& - 8\,G(1,0,-1;y) - 10\,\ell\,G(0,1;y) + 6\,\ell\,G(1,1;y) + 6\,\tfrac{\ell^2}{2!}\,G(1;y) \\
& - 8\,\tfrac{\ell^3}{3!} - 8\,G(-1;x)\,G(0,1;y) + 8\,G(-1;x)\,G(0,-1;y) + 8\,\ell\,G(-1;x)\,G(1;y) \\
& - 16\,\tfrac{\ell^2}{2!}\,G(-1;x) + 8\,G(s;x)\,G(0,1;y) + 4\,G(s;x)\,G(0,-1;y) \\
& - 8\,\ell\,G(s;x)\,G(1;y) - 8\,G(\sigma;x)\,G(0,-1;y) + 8\,G(\sigma;x)\,G(-1,-1;y) \\
& + 16\,\ell\,G(0,-1;x) - 12\,G(0,\sigma;x)\,G(-1;y) - 32\,\ell\,G(-1,-1;x) \\
& + 8\,G(-1,\sigma;x)\,G(-1;y) + 8\,\ell\,G(s,-1;x) - 4\,G(s,\sigma;x)\,G(-1;y) \\
& + 8\,G(\sigma,\sigma;x)\,G(-1;y) - 8\,G(0,0,-1;x) + 40\,G(0,-1,-1;x) - 12\,G(0,\sigma,-1;x) \\
& + 40\,G(-1,0,-1;x) - 64\,G(-1,-1,-1;x) + 8\,G(-1,\sigma,-1;x) - 4\,G(s,\sigma,-1;x) \\
& - 16\,G(\sigma,0,-1;x) + 8\,G(\sigma,-1,-1;x) + 8\,G(\sigma,\sigma,-1;x) - 2\,\zeta_2\,G(1;y) + 2\,\zeta_2\,\ell \\
& + 4\,\zeta_2\,G(-1;x) - \tfrac{14}{3}\,\zeta_3
\end{aligned} \tag{209}$$

with coefficients in $\mathbb{Q}[\zeta_2,\zeta_3]$. The weight-four coefficient is the sum

$$g^{(4)}(s,t) = g_t^{(4)}(s,t) + g_y^{(4)}(s) \tag{210}$$

of a part $g_t^{(4)}$ with 123 terms, each of which contains a word in x, and a remainder $g_y^{(4)}$ that depends on s alone. The first part is

$$\begin{aligned}
g_t^{(4)} = {} & -56\,G(-1;x)\,G(0,0,1;y) + 24\,G(-1;x)\,G(0,1,1;y) - 32\,G(-1;x)\,G(0,-1,-1;y) \\
& + 24\,G(-1;x)\,G(1,0,1;y) + 32\,G(-1;x)\,G(1,0,-1;y) + 40\,\ell\,G(-1;x)\,G(0,1;y) \\
& - 24\,\ell\,G(-1;x)\,G(1,1;y) - 24\,\tfrac{\ell^2}{2!}\,G(-1;x)\,G(1;y) + 32\,\tfrac{\ell^3}{3!}\,G(-1;x) \\
& + 36\,G(s;x)\,G(0,0,1;y) + 12\,G(s;x)\,G(0,0,-1;y) - 24\,G(s;x)\,G(0,1,1;y) \\
& - 16\,G(s;x)\,G(0,-1,-1;y) - 24\,G(s;x)\,G(1,0,1;y) - 24\,G(s;x)\,G(1,0,-1;y) \\
& - 28\,\ell\,G(s;x)\,G(0,1;y) + 24\,\ell\,G(s;x)\,G(1,1;y) + 20\,\tfrac{\ell^2}{2!}\,G(s;x)\,G(1;y)
\end{aligned}$$

$$
\begin{aligned}
&- 12\,G(\sigma;x)\,G(0,0,-1;y) + 32\,G(\sigma;x)\,G(0,-1,-1;y) + 12\,G(\sigma;x)\,G(-1,0,-1;y)\\
&- 32\,G(\sigma;x)\,G(-1,-1,-1;y) - 16\,G(0,-1;x)\,G(0,1;y) + 12\,G(0,-1;x)\,G(0,-1;y)\\
&+ 16\,\ell\,G(0,-1;x)\,G(1;y) - 28\,\tfrac{\ell^2}{2!}\,G(0,-1;x) + 16\,G(0,s;x)\,G(0,1;y)\\
&+ 40\,G(0,s;x)\,G(0,-1;y) - 16\,\ell\,G(0,s;x)\,G(1;y) - 48\,G(0,\sigma;x)\,G(0,-1;y)\\
&+ 48\,G(0,\sigma;x)\,G(-1,-1;y) + 32\,G(-1,-1;x)\,G(0,1;y) - 32\,G(-1,-1;x)\,G(0,-1;y)\\
&- 32\,\ell\,G(-1,-1;x)\,G(1;y) + 64\,\tfrac{\ell^2}{2!}\,G(-1,-1;x) - 32\,G(-1,s;x)\,G(0,1;y)\\
&- 16\,G(-1,s;x)\,G(0,-1;y) + 32\,\ell\,G(-1,s;x)\,G(1;y) + 32\,G(-1,\sigma;x)\,G(0,-1;y)\\
&- 32\,G(-1,\sigma;x)\,G(-1,-1;y) - 8\,G(s,-1;x)\,G(0,1;y) + 12\,G(s,-1;x)\,G(0,-1;y)\\
&+ 8\,\ell\,G(s,-1;x)\,G(1;y) - 20\,\tfrac{\ell^2}{2!}\,G(s,-1;x) + 8\,G(s,s;x)\,G(0,1;y)\\
&+ 4\,G(s,s;x)\,G(0,-1;y) - 8\,\ell\,G(s,s;x)\,G(1;y) - 16\,G(s,\sigma;x)\,G(0,-1;y)\\
&+ 16\,G(s,\sigma;x)\,G(-1,-1;y) - 20\,G(\sigma,s;x)\,G(0,-1;y) + 32\,G(\sigma,\sigma;x)\,G(0,-1;y)\\
&- 32\,G(\sigma,\sigma;x)\,G(-1,-1;y) + 20\,\ell\,G(0,0,-1;x) - 20\,G(0,0,\sigma;x)\,G(-1;y)\\
&- 64\,\ell\,G(0,-1,-1;x) + 12\,G(0,-1,\sigma;x)\,G(-1;y) + 16\,\ell\,G(0,s,-1;x)\\
&- 40\,G(0,s,\sigma;x)\,G(-1;y) + 48\,G(0,\sigma,\sigma;x)\,G(-1;y) - 64\,\ell\,G(-1,0,-1;x)\\
&+ 48\,G(-1,0,\sigma;x)\,G(-1;y) + 128\,\ell\,G(-1,-1,-1;x) - 32\,G(-1,-1,\sigma;x)\,G(-1;y)\\
&- 32\,\ell\,G(-1,s,-1;x) + 16\,G(-1,s,\sigma;x)\,G(-1;y) - 32\,G(-1,\sigma,\sigma;x)\,G(-1;y)\\
&+ 20\,\ell\,G(s,0,-1;x) - 24\,G(s,0,\sigma;x)\,G(-1;y) - 32\,\ell\,G(s,-1,-1;x)\\
&+ 12\,G(s,-1,\sigma;x)\,G(-1;y) + 8\,\ell\,G(s,s,-1;x) - 4\,G(s,s,\sigma;x)\,G(-1;y)\\
&+ 16\,G(s,\sigma,\sigma;x)\,G(-1;y) + 12\,G(\sigma,0,\sigma;x)\,G(-1;y) + 20\,G(\sigma,s,\sigma;x)\,G(-1;y)\\
&- 32\,G(\sigma,\sigma,\sigma;x)\,G(-1;y) + 32\,G(0,0,-1,-1;x) - 20\,G(0,0,\sigma,-1;x)\\
&+ 100\,G(0,-1,0,-1;x) - 160\,G(0,-1,-1,-1;x) + 12\,G(0,-1,\sigma,-1;x)\\
&+ 64\,G(0,s,0,-1;x) - 40\,G(0,s,\sigma,-1;x) - 96\,G(0,\sigma,0,-1;x)\\
&+ 48\,G(0,\sigma,-1,-1;x) + 48\,G(0,\sigma,\sigma,-1;x) + 32\,G(-1,0,0,-1;x)\\
&- 160\,G(-1,0,-1,-1;x) + 48\,G(-1,0,\sigma,-1;x) - 160\,G(-1,-1,0,-1;x)\\
&+ 256\,G(-1,-1,-1,-1;x) - 32\,G(-1,-1,\sigma,-1;x) + 16\,G(-1,s,\sigma,-1;x)\\
&+ 64\,G(-1,\sigma,0,-1;x) - 32\,G(-1,\sigma,-1,-1;x) - 32\,G(-1,\sigma,\sigma,-1;x)\\
&+ 20\,G(s,0,0,-1;x) - 24\,G(s,0,\sigma,-1;x) + 8\,G(s,-1,0,-1;x)\\
&+ 12\,G(s,-1,\sigma,-1;x) - 4\,G(s,s,\sigma,-1;x) - 32\,G(s,\sigma,0,-1;x)\\
&+ 16\,G(s,\sigma,-1,-1;x) + 16\,G(s,\sigma,\sigma,-1;x) - 36\,G(\sigma,0,0,-1;x)\\
&+ 64\,G(\sigma,0,-1,-1;x) + 12\,G(\sigma,0,\sigma,-1;x) + 12\,G(\sigma,-1,0,-1;x)\\
&- 32\,G(\sigma,-1,-1,-1;x) - 40\,G(\sigma,s,0,-1;x) + 20\,G(\sigma,s,\sigma,-1;x)\\
&+ 64\,G(\sigma,\sigma,0,-1;x) - 32\,G(\sigma,\sigma,-1,-1;x) - 32\,G(\sigma,\sigma,\sigma,-1;x)\\
&+ 8\,\zeta_2\,G(-1;x)\,G(1;y) - 8\,\zeta_2\,\ell\,G(-1;x) - 12\,\zeta_2\,G(s;x)\,G(1;y)\\
&- 6\,\zeta_2\,G(\sigma;x)\,G(-1;y) + 6\,\zeta_2\,G(0,-1;x) - 16\,\zeta_2\,G(-1,-1;x) + 12\,\zeta_2\,G(s,-1;x)\\
&- 6\,\zeta_2\,G(\sigma,-1;x) + \tfrac{56}{3}\,\zeta_3\,G(-1;x)
\end{aligned}
\tag{211}
$$

and the remainder, with 29 terms, is

$$
\begin{aligned}
g_y^{(4)} = {}& 38\,G(0,0,0,1;y) - 34\,G(0,0,1,1;y) - 28\,G(0,1,0,1;y) - 8\,G(0,1,0,-1;y)\\
&+ 18\,G(0,1,1,1;y) + 12\,G(0,-1,0,-1;y) - 32\,G(0,-1,-1,-1;y)
\end{aligned}
$$

$$
\begin{aligned}
&- 22\,G(1,0,0,1;y) - 12\,G(1,0,0,-1;y) + 18\,G(1,0,1,1;y) \\
&+ 32\,G(1,0,-1,-1;y) + 18\,G(1,1,0,1;y) + 8\,G(1,1,0,-1;y) \\
&- 30\,\ell\,G(0,0,1;y) + 22\,\ell\,G(0,1,1;y) + 16\,\ell\,G(1,0,1;y) \\
&- 18\,\ell\,G(1,1,1;y) + 22\,\tfrac{\ell^2}{2!}\,G(0,1;y) - 10\,\tfrac{\ell^2}{2!}\,G(1,1;y) \\
&- 14\,\tfrac{\ell^3}{3!}\,G(1;y) + 16\,\tfrac{\ell^4}{4!} - 12\,\zeta_2\,G(0,1;y) - 6\,\zeta_2\,G(0,-1;y) \\
&+ 14\,\zeta_2\,G(1,1;y) + 4\,\zeta_2\,\ell\,G(1;y) - 4\,\zeta_2\,\tfrac{\ell^2}{2!} - 4\,\zeta_3\,G(1;y) \\
&+ \tfrac{28}{3}\,\zeta_3\,\ell - \tfrac{21}{4}\,\zeta_4\,.
\end{aligned}
\tag{212}
$$

For $s,t<0$ the words in x are real, and so are the words in y when $-s<1$. When $-s>1$ we continue the words that contain the letter 1 past their branch point at $y=1$, above or below the real y axis, and for either choice the resulting imaginary parts cancel in $g^{(3)}$ and in $g^{(4)}$. At $s=-1$, where the letter $s+1$ vanishes, the words that begin with the letter 1 diverge while $g^{(3)}$ and $g^{(4)}$ remain finite and are obtained as limits. On that slice $\sigma=-\frac{1}{2}$, and both reduce to polylogarithms in x with letters $\{0,-1,-\frac{1}{2}\}$ and constant coefficients. The three lists, with exact rational coefficients, are also supplied as a data file [106] (Appendix G).

C Data for the elliptic entries

In this appendix we collect supplementary data for the ice-cream cone integrals, Nos. 15–17 of Table 1, and for the $gg\to Z\gamma$ masters, No. 20.

C.1 The cone alphabet for generic masses

We keep the squared masses $\mu_i\equiv m_i^2$ of eq. (95) symbolic, with $\mu_1=1$, on the slice $p_{12}^2=p_{34}^2=x$, $p_{56}^2=-1$. The family then has nineteen master integrals, the 132 nonzero entries of its connection matrix in x are rational functions of (d,x,μ_2,μ_3,μ_4), and every denominator among them is a product of letters from an alphabet of nine. Three do not depend on the masses, $\{x,\ 2x{+}1,\ 4x{+}1\}$. Two are the threshold quartics of the scoop sunrise $[1,0,1,1]$ and of the sunrise $[0,1,1,1]$,

$$
\begin{aligned}
Q_{\text{scoop}}(x;\mu_3,\mu_4) &= \prod_{\pm\pm}\,\big(x-(1\pm\sqrt{\mu_3}\pm\sqrt{\mu_4})^2\big), \\
Q_{14}(x;\mu_2,\mu_3,\mu_4) &= \prod_{\pm\pm}\,\big(x-(\sqrt{\mu_2}\pm\sqrt{\mu_3}\pm\sqrt{\mu_4})^2\big).
\end{aligned}
\tag{213}
$$

The sixth is the bubble locus $L_{\text{bub}}(x;\mu_2,\mu_3,\mu_4)$, a quartic in x with polynomial coefficients in the masses. Its equal-mass limit

$$
L_{\text{bub}}\big|_{\mu_i=1} = (x-1)^2\,(x^2-10x+5)
\tag{214}
$$

is the letter $x^2-10x+5$ of No. 15, denoted L_{bub} there, times a square whose zero coincides with the sunrise threshold $x=1$. The seventh is the quadratic

$$
L_r(x;\mu_2) = x^2-(\mu_2^2-\mu_2+2)\,x+\mu_2\,,
\tag{215}
$$

which depends on the bubble mass μ_2 alone and degenerates to $(x-1)^2$ at equal masses. Hence the zeros of L_r are singularities of the generic-mass cone with no equal-mass counterpart. The last two letters, $d-1$ and $d+4x$, occur only in the d-dependent denominators.

We have checked the completeness of this alphabet in exact arithmetic at 336 rational mass points, chosen on the mass axes, on a mass diagonal and at generic tuples. At every point each x-denominator of the 132 entries divides the product of the nine letters and therefore has no factor outside the alphabet. We supply the 132 entries of the connection and the mass-dependent coefficients of $L_{\rm bub}$ as a data file with the evaluation code of Nos. 15–17 (Appendix G) [106].

C.2 Resonant boundary constants of the generic-mass cone

For No. 16 the boundary values of the nineteen masters at $x=-1$ follow from their expansions about $u=1/x=0$, as for No. 15. Four subsector masters with numerators have a resonant pair of indicial exponents at $u=0$. They are $[1,0,1,1,-1,0,0]$ and $[1,-2,1,1]$ in the sector of the scoop sunrise and $[0,1,1,1,-1,0,0]$ and $[-2,1,1,1]$ in the sector of the (m_2,m_3,m_4) sunrise, numbered 7, 8, 13 and 14 among the nineteen masters. The resonance occurs at order u^1 for masters 7 and 13 and at order u^0 for masters 8 and 14, and the recursion leaves one coefficient free in each. We write $y^{(j)}_{(n,0)}$ for the coefficient of u^n without a logarithm in the expansion of master j. In this notation the four free coefficients at $(\mu_1,\mu_2,\mu_3,\mu_4)=(1,2,3,5)$ are, with $g\equiv\gamma_E$,

$$\begin{aligned}
y^{(8)}_{(0,0)} &= 6g^2+4g+6g\ln 15+3\zeta_2+\tfrac{5}{2}\ln^2 15-\ln^2 3-\ln^2 5+4\ln 15+2,\\
y^{(14)}_{(0,0)} &= 12g^2+4g+12g\ln 15+6\zeta_2+4\ln^2 15-\ln^2 3-\ln^2 5+4\ln 15+2,\\
y^{(7)}_{(1,0)} &= 2\ln 3\,\ln 5, \qquad y^{(13)}_{(1,0)} = 2\ln 2\,\ln 3+\ln 2\,\ln 5+2\ln 3\,\ln 5,
\end{aligned} \tag{216}$$

all in the ring $\mathbb{Q}[\gamma_E,\ln 2,\ln 3,\ln 5,\zeta_2]$.

C.3 Ice-cream cones away from the slice

Away from the slice $p_{12}^2=p_{34}^2$ the equal-mass family has nine master integrals (seven on the slice), because the two sunrise subgraphs, which coincide on the slice, become distinct and the second one contributes two masters. With `Kira` [81] we obtain the connection matrices A_x and A_y in $(x,y)=(p_{12}^2,p_{34}^2)$ at $p_{56}^2=-1$, $m^2=1$, as rational 9×9 matrices in (d,x,y). They satisfy the integrability condition $dA=A\wedge A$ identically, and at fixed $p_{12}^2=-3$ or $p_{12}^2=-2$ the matrix A_y is the connection in p_{34}^2 that we use in lines 4–9 of Table 7.

Table 7 lists the checks. In each line we take the nine masters from `AMFlow` [95] at the first point, integrate the connection to the second point, and compare there with an independent `AMFlow` evaluation. At fixed $p_{12}^2=-2$ the real path meets the singular point $p_{34}^2=-(2+\sqrt{3})$ of the letter $(p_{34}^2+2)^2-3$, and we integrate along rectangles in the complex p_{34}^2 plane below and above the axis, with the same result on both sides. The path of line 3 to $(-15/4,-5/2)$ crosses the diagonal $p_{12}^2=p_{34}^2$, where the connection is singular, on a detour in the complex plane.

The diagonal $p_{12}^2=p_{34}^2$ is an apparent singularity of the nine-master system, with integer local exponents and no logarithms. We obtain the values on the slice as the mean of the continued solution over a circle of radius $1/16$ about the diagonal point. Six of the nine masters coincide on the diagonal with elements of the seven-master slice basis, and in lines 8 and 9 we compare their values with the on-slice values from `AMFlow` and from the slice connection. For reference, at $(p_{12}^2,p_{34}^2,p_{56}^2,m^2)=(-2,-3,-1,1)$ the order-ε^0 coefficient of the top integral $[1,1,1,1]$ computed with `AMFlow` is $0.541202970\ldots$.

Table 7: Checks of the equal-mass ice-cream cone connection away from the slice $p_{12}^2 = p_{34}^2$, at $p_{56}^2 = -1$ and $m^2 = 1$; points are (p_{12}^2, p_{34}^2). On each line we integrate the stated connection from `AMFlow` values of the nine masters at the first point to the second point. The last column gives the smallest number of digits, over all masters and the orders in ε shown, to which the result agrees with an independent `AMFlow` evaluation at the second point (lines 1–7) or with the on-slice values (lines 8–9, six masters); on line 3 the comparison value has lower precision.

	connection	from	to	orders	digits
1	(A_x, A_y)	$(-3, -4)$	$(-3, -15/4)$	$\varepsilon^{-2}, \ldots, \varepsilon^{1}$	64
2	(A_x, A_y)	$(-3, -4)$	$(-5/2, -15/4)$	$\varepsilon^{-2}, \ldots, \varepsilon^{1}$	64
3	(A_x, A_y)	$(-3, -4)$	$(-15/4, -5/2)$	$\varepsilon^{-2}, \ldots, \varepsilon^{1}$	48
4	A_y on $p_{12}^2 = -2$	$(-2, -3)$	$(-2, -4)$	$\varepsilon^{-2}, \ldots, \varepsilon^{0}$	57
5	A_y on $p_{12}^2 = -3$	$(-3, -4)$	$(-3, -5)$	$\varepsilon^{-2}, \ldots, \varepsilon^{0}$	57
6	A_y on $p_{12}^2 = -2$	$(-2, -3)$	$(-2, -4)$	ε^{1}	47
7	A_y on $p_{12}^2 = -3$	$(-3, -4)$	$(-3, -5)$	ε^{1}	47
8	A_y on $p_{12}^2 = -3$	$(-3, -4)$	$(-3, -3)$	$\varepsilon^{-2}, \ldots, \varepsilon^{1}$	47
9	A_y on $p_{12}^2 = -2$	$(-2, -3)$	$(-2, -2)$	$\varepsilon^{-2}, \ldots, \varepsilon^{1}$	48

C.4 The $gg \to Z\gamma$ masters at fixed s

Reducing the sector-125 family at fixed $s = -1/4$, with $M = 7/25$ and $m_t^2 = 1$, we obtain the fourteen master integrals of Table 8, normalized as in eq. (1). Only entries 8, 11 and 13 carry the numerator $D_2 = (k_1 - p_1)^2$. They are the three t-dependent masters M_8, M_{11} and R_b of eq. (122), where R_b enters as $g_{32} = e^{2\gamma_E \varepsilon} R_b$, and entry 12 is R_a. The matrix A_t defined by $\partial_t I = A_t\, I$ on this basis has nonzero entries in rows 8, 11 and 13 alone. Row 8 reads

$$\partial_t M_8 = \frac{200\, M_8 - 100\, K_5 - 25\, K_6 - 100\, K_7}{200\, t - 53}\,, \tag{217}$$

where K_5, K_6 and K_7 are entries 5–7 of the table. The general solution of this equation is the expression for M_8 in eq. (122). The diagonal entries of rows 11 and 13 are $\partial_t \log L_1$ and $\partial_t \log D_{2q}$, and the entry $(13, 12)$, the coupling of R_a into R_b, is the lower-left entry of eq. (119) at $s = -1/4$. We supply the remaining 23 entries of rows 11 and 13, rational functions of (ε, t), with the evaluation code of No. 20 (Appendix G) [106].

D Nonplanar W-pair data on the line

For the nonplanar W-pair family, No. 35 of Table 1 (section 5.9), this appendix describes the diagonal blocks of eq. (152) by sector, the alphabets, the local data of sector 481, the boundary constants together with the integer-relation searches, and $A(d, y)$ on the second line, $(x, z) = (17/2, 7/4)$. Unless the second line is specified, every statement refers to the line of eq. (151).

D.1 Block content and alphabets

Table 9 lists the 36 diagonal blocks of $A(d, y)$ by class. Twenty-one of the 79 functions have identically vanishing derivative in eq. (152) and are constant on the line.

We generated candidate letters in (x, y, z) from the Landau singularities of the graph and its contractions [74, 97] and from the Symanzik polynomials [63, 64], in both cases face by face over the Newton polytopes. However, these face-by-face scans missed four of the 36 letters, among them the

Table 8: The fourteen master integrals $I_{\nu_1\cdots\nu_7}$ of the $gg \to Z\gamma$ sector-125 family at fixed $s = -1/4$, with $M = 7/25$, $m_t^2 = 1$ and the propagators $D_1, \ldots, D_7$ of eq. (114). Sectors are labeled by the binary code of the positive indices; negative indices denote numerators. The last column gives the symbol used for the entry in eq. (122), where R_a and R_b enter through g_{31} and g_{32}. Only entries 8, 11 and 13, which contain the numerator $D_2 = (k_1 - p_1)^2$, depend on t.

entry	sector	$(\nu_1, \nu_2, \nu_3, \nu_4, \nu_5, \nu_6, \nu_7)$	in eq. (122)
0	40	$(0, 0, 0, 1, 0, 1, 0)$	
1	44	$(0, 0, 1, 1, 0, 1, 0)$	
2	44	$(-1, 0, 1, 1, 0, 1, 0)$	
3	49	$(1, 0, 0, 0, 1, 1, 0)$	
4	49	$(1, 0, 0, -1, 1, 1, 0)$	
5	56	$(0, 0, 0, 1, 1, 1, 0)$	K_5
6	60	$(0, 0, 1, 1, 1, 1, 0)$	K_6
7	60	$(-1, 0, 1, 1, 1, 1, 0)$	K_7
8	60	$(0, -1, 1, 1, 1, 1, 0)$	M_8
9	108	$(0, 0, 1, 1, 0, 1, 1)$	
10	121	$(1, 0, 0, 1, 1, 1, 1)$	
11	121	$(1, -1, 0, 1, 1, 1, 1)$	M_{11}
12	125	$(1, 0, 1, 1, 1, 1, 1)$	R_a
13	125	$(1, -2, 1, 1, 1, 1, 1)$	R_b

pseudo-threshold $x + y - z + 1$, and we identified those four as loci on which the Euler characteristic of the hypersurface complement drops [63]. On a line of constant x and z the 11 letters independent of y drop out of eq. (152). No integrability condition in (x, y, z) can therefore be tested on such lines. The 15 line letters arise from the (x, y, z) alphabet by restriction, and both alphabets are in the data files described below.

D.2 Local data of sector 481

The family of curves E_{z_5} of eq. (154) has seven singular fibers over the z_5 line, of Kodaira types $2\,I_1 + 5\,I_2$. The point $(y, z) = (0, 1)$ used as the boundary point in Ref. [75] is not a degeneration point of E_{z_5}, which degenerates instead as $z \to 0$. Because the ε^0 block factorizes completely into the first-order operators of eq. (156), its six solutions are d'Alembertian, two rational in y and four iterated integrals of algebraic functions. We find the same factorization along the ray $(s, t, m_W^2) = \lambda\,(-17/2, -1/3, -5/3)\,m_t^2$, which meets the line at $y_0 = 1/3$ for $\lambda = 1$, and along the ray $\lambda\,(67/8, -25/9, 13/60)\,m_t^2$. On the line and on the first ray the full ε-dependent block is regular singular at every singular point, and at generic fixed d we bring it to Fuchsian form by an exact rational gauge transformation. The exponent $-3/2$ at the zeros of Q_1 and Q_2 of eq. (157) recurs along the first ray at the zeros of

$$46225\lambda^2 + 35190\lambda + 5049 \qquad \text{and} \qquad 1600\lambda^2 - 18360\lambda + 5049. \tag{218}$$

As the homogeneous basis for the variation of parameters we use the two rational solutions, two Lefschetz-thimble integrals of the maximal cut (154), and two further solutions fixed by numerical initial conditions at y_0.

class	blocks	sectors and functions	letters and local behavior
ε-factorized, rational d log letters, eq. (153)	29	all sectors other than the seven below; 52 functions, among them the 40 MPLs (34 coupled through their sources, 12 of these in one tower, six decoupled) and the four functions of the top sector 487 in the basis with $F_C[1,1,1,-1,-1,1,1,1,1]$	the 15 line letters, 13 rational in y and the pair $r_\pm$; for sector 487 the letters $18y^2+93y+50$ and $18y^2+93y+203$ (on the second line $16y^2+80y+49$ and $16y^2+80y+185$), regular at $y=\infty$
algebraic letters, no rational rotation to eq. (153)	6	417 (three functions), 421 and 453 (f_{33}–f_{35} and f_{48}–f_{50}), 449, 482, 483; fifteen functions in the five sectors other than 483	two quadratic polynomials in y with complex roots (sectors 417, 421, 449, 453, 482); for sector 483 the letters $3y-5$, $6y+41$, $18y^2+93y+67$ and $18y^2+93y+305$; blocks of 417, 449 not Moser-reducible by a rational transformation, those of 421, 453, 482, 483 obstructed in the ε^0 part
elliptic maximal cut, eq. (154)	1	$481=[1,0,0,0,0,1,1,1,1]$, six functions f_{54}–f_{59}	ε^0 block factorized as in eq. (156); local exponents in $\mathbb{Z}+\mathbb{Z}\varepsilon$ except $-3/2$ at the zeros of Q_1 and Q_2 of eq. (157)

Table 9: The 36 diagonal blocks of the exact differential equation (152) for the 79 basis functions $f_1,\ldots,f_{79}$ of the nonplanar W-pair family (No. 35) on the line (151), by class. The third column names the sectors, whose labels are defined below eq. (149), and some of the functions f_i they contain, with indices referring to the basis of the data files. The 27 functions of the last two classes, and every function whose source terms involve them, lie outside the MPLs. Sectors 483 and 487 contain sector 481 as a subsector, which enters their blocks only through the source terms.

D.3 Boundary constants

Table 10 lists the boundary constants by class. The basis is normalized such that the square of the one-loop tadpole with the top-quark mass equals $\Gamma(\varepsilon-1)^2$. The 36 functions that are complex on the line are given on the branch $u\to u+i0$, as determined from the u-channel functions f_{19} and f_{20}. Of the 40 constants of the last class, 23 have imaginary parts, of relative size between 7×10^{-7} and order one. The other seventeen are real to working precision. For the constants of f_{42} and f_{69} we also have Mellin–Barnes representations, which we did not use to fix their values.

For the 40 constants without closed form we searched for integer relations of the form of eq. (6) at $\varepsilon=1/1013$, where they are known to 128–141 digits, treating real and imaginary parts separately, and found none. For the 16 constants whose leading Laurent coefficient is neither rational nor logarithmic, the candidate set has twelve elements, the family's Γ-function vacuum products and algebraic letter constants. We exclude relations over this full set with coefficients below 10^4, and the remaining precision margin of 12–25 digits is too small to test larger coefficients. Within the subsets of six algebraic and of five Γ-function constants we exclude coefficients below 10^6. For all 40 constants we exclude relations with coefficients below 10^4 to the eleven closed-form constants and below 10^6 within three eight-element sets assembled by block, with the same precision margin. The first set consists of the square roots of the algebraic letters' radicands and of the constants 67 and 305 of the sector-483 letters. The second set contains these two roots and the five vacuum products. For the polylogarithmic functions, the third set contains the vacuum products, the massless double bubble and the massive–massless bubble at the same ε.

number	how the constant is fixed	remarks
23	$y \to 0$ limit of the planar GPL expression of Ref. [75], taken from their ancillary files and continued to the line	the function is among the 53 shared with the planar branches
11	closed form in the Γ-function and hypergeometric values of the vacuum integrals of the family	
5	convergent integral representation	
40	value of the function at $y_0 = 1/3$ from the auxiliary-mass transport of eq. (161), stored at the 24 values $\varepsilon = 1/q$ with q prime from 1013 to 10037; no closed form known	includes all functions of sectors 417, 421, 449, 453, 481, 482 and 483; leading Laurent coefficient rational for 22, logarithmic for 2 (f_{75}, f_{78}), neither for 16

Table 10: The 79 boundary constants of the nonplanar W-pair family (No. 35) on the line (151), by the way they are fixed. The residue matrix of eq. (152) at $y = 0$ is semisimple with no resonance, so that every function has a finite $y \to 0$ limit. The first three classes give that limit directly, and the fourth gives the value at the reference point y_0, to which the limit is related by integrating eq. (152) along the line.

D.4 The second line and the data files

On the second line, $(x, z) = (17/2, 7/4)$, we obtained $A(d, y)$ by rational reconstruction from 89 of 91 reductions and found the same 79 functions and 1240 nonzero entries. Twenty of these entries, all in the equations of $f_{75}, \ldots, f_{78}$, require on either line a second fit, in which we set each denominator to the least common multiple of those already found for the same function. At $d = 7/3$, outside the 27 values of d used in the reconstruction, all 1240 entries agree as exact rational numbers with the reductions at the two points left out of the fit, $y = 296/101$ and $y = 306/103$. The 29 blocks that admit the form of eq. (153) are the same on both lines, as are the six sectors whose blocks do not. For the 28 blocks other than that of the top sector, the ε-factorized forms on the two lines are related by constant rotations once the 36 letters are restricted to each line. In 23 of these cases the residue matrices $M_{B,i}$ are identical. At one point off both lines, $(x, y, z) = (8, 1/3, 3/2)$, we compared these 28 blocks of the exact reduction with the residue matrices of the first line, continuing each rotation T_B off the line letter by letter. The 15 blocks whose T_B is a product of letters agree exactly, 12 of them with T_B unchanged, whereas the rotations of the other 13 blocks do not continue off the line in this way.

The data files of this entry (Appendix G) [106] contain $A(d, y)$ on both lines in exact form, together with the rotations T_B and residue matrices $M_{B,i}$ of the 29 ε-factorized blocks and the two alphabets. They include the symbolic expressions of the functions on the first line at orders ε^{-3} to ε^1, their values at y_0 for the 24 fixed values of ε, and the $y \to 0$ limits taken from the ancillary files of Ref. [75]. Moreover, they contain the auxiliary-mass systems $B(\varepsilon, \eta)$ of eq. (161) with their Γ-function boundary tables, from which the 40 constants fixed at y_0 can be recomputed at any precision. The expressions for the six functions of sectors 421 and 453 are much larger than the rest and are not included. These six functions are evaluated by integrating eq. (152) along the line from the stored values at y_0.

E Five-point alphabet and symbol-space bound

This appendix supplements section 4.8 with the generic-mass sub-alphabet, its symbol-space counts and the layered forms of the hexa-box.

E.1 The sub-alphabet of the generic-mass families

We take the candidate letters of each family from the principal A-determinant of its Lee–Pomeransky polynomial $\mathcal{G} = \mathcal{U} + \mathcal{F}$ [94, 97, 63]. Every irreducible kinematic factor of the discriminant of $\mathcal{G}$ restricted to a face of its Newton polytope is a candidate letter. On the faces of codimension four and higher we find 22 distinct letters for the hexa-box of Figure 9(a) and 25 for the double-pentagon (b). A partial scan at codimension three raises these counts to 27 and 32, and the top-sector faces are beyond our computation. Restricting to the seven physical invariants $s_{12}, s_{23}, s_{34}, s_{45}, s_{15}$ and $M_{3,4} = p_{3,4}^2$, we retain a multiplicatively independent set of twenty letters common to the two families, nineteen of them parity-even,

$$\begin{aligned}\{\, & s_{12},\ s_{23},\ s_{34},\ s_{45},\ s_{15},\quad M_3,\ M_4,\quad s_{34}-(\sqrt{M_3}+\sqrt{M_4})^2,\quad s_{34}-(\sqrt{M_3}-\sqrt{M_4})^2,\\ & s_{45}-M_4,\quad s_{23}-M_3,\quad s_{34}-s_{12},\quad s_{34}-s_{15},\quad M_4+s_{12}-s_{34}-s_{45},\\ & M_3+s_{15}-s_{34}-s_{23},\quad M_3+M_4+s_{12}-s_{34}-s_{45},\quad M_3+M_4+s_{15}-s_{34}-s_{23},\\ & s_{23}+s_{34}+s_{45}-M_3-M_4,\quad s_{12}+s_{15}-s_{34}\,\},\end{aligned} \tag{219}$$

and one parity-odd letter built from Δ_5 of eq. (61). The pair $s_{34}-(\sqrt{M_3}\pm\sqrt{M_4})^2$, with product r_{34}^2, corresponds to the two-mass threshold, and the last eight letters vanish on singular hypersurfaces of the differential equations of the 219- and 190-master systems. The only residual symmetry of the kinematics is the reflection

$$\sigma: \quad s_{12} \leftrightarrow s_{15}, \quad s_{23} \leftrightarrow s_{45}, \quad s_{34} \text{ fixed}, \quad M_3 \leftrightarrow M_4, \tag{220}$$

which maps the alphabet to itself and splits each symbol space by σ-parity.

E.2 Symbol-space dimensions

We count integrable symbols of weight $w \le 4$ in the twenty-letter sub-alphabet subject to four conditions, as in the pentagon-function bootstrap [43, 50].

1. The first entry is one of the 9 thresholds: the five s_{ij}, $s_{34}-(\sqrt{M_3}\pm\sqrt{M_4})^2$, $s_{45}-M_4$ and $s_{23}-M_3$.
2. The last entry is one of 15 letters: the first-entry set, the two masses and the channel letters shifted by a threshold.
3. Letters with branch cuts in overlapping channels never occupy adjacent entries, at any depth [111, 39]. Cluster adjacency [53] forbids no further pair here. These two rules allow 83 of the 361 ordered pairs of parity-even letters.
4. Integrability [71, 54] is imposed on every pair of adjacent entries by exact linear algebra modulo the primes $2^{31}-1$ and 1000003 at 6–12 rational kinematic points, with ranks independent of the prime and the points.

These conditions reduce the $19^4 = 130321$ words of weight four in the parity-even letters to 120 and give

$$K = [\,9,\ 28,\ 62,\ 120\,] \quad \text{for } w = 1,2,3,4, \tag{221}$$

channel of the first entry	s_{12}	s_{15}	s_{23}	s_{45}	s_{34}
weight 3	1	1	4	4	10
weight 4	1	1	5	5	15

Table 11: Dimension of the space of integrable symbols of weight three and four with first entry in a given two-particle channel, within the sub-alphabet (219) and subject to conditions 1–4 of Appendix E. This is the space available to a master integral of the generic-mass hexa-box or double-pentagon family whose leading discontinuity lies in that channel. Columns related by the reflection σ of eq. (220) are equal; s_{34} is the two-mass threshold channel.

split by σ as $(\text{even}, \text{odd}) = (6,3), (18,10), (36,26), (69,51)$. Since the alphabet (219) is incomplete, the K_w bound the symbol spaces of the two families from below, and a more permissive last-entry set could only raise them.

A master whose leading discontinuity is in one channel has its weight-three and weight-four symbols in smaller spaces, whose dimensions are given in Table 11. In particular, the s_{34} subspace is σ-even, and its dimensions at weights one to four are the triangular numbers $3, 6, 10, 15$. Products of zeta values with functions of lower weight, such as $\zeta_2 \log$ or $\zeta_2 \operatorname{Li}_2$, are fixed by the lower components of the coproduct, and the only constant beyond the symbol at each weight is

$$w = 2 : \ \zeta_2 = \tfrac{\pi^2}{6}, \qquad w = 3 : \ \zeta_3, \qquad w = 4 : \ \zeta_4 = \tfrac{\pi^4}{90}, \tag{222}$$

all σ-even. The weight-w coefficient of a master of either family is then

$$F^{(w)} \ = \sum_{i_1,\ldots,i_w} c_{\,i_1\cdots i_w} \left[\, a_{i_1} \otimes \cdots \otimes a_{i_w} \,\right] \ + \ (\text{terms in the tower of } \zeta_2,\ \zeta_3,\ \zeta_4), \tag{223}$$

where the a_i are the 20 letters, the sum may be restricted to a basis of the space counted in (221) or in Table 11, and the c are rational. We have not determined the c or the accompanying rational multiples of the constants (222) for any master; a few numerical values of each master would fix them.

E.3 Layered forms and boundary constants of the hexa-box

On segment I of eq. (60) the connection of the 98 masters of No. 24, $A = \sum_m \varepsilon^m A^{(m)}(t)$, has 8160 nonzero kernels $A^{(m)}_{ij}(t)$, all rational functions of t over $\mathbb{Q}$. Nine of them, in the row of the third top-sector master, are expansion coefficients of entries of $A(t,\varepsilon)$ with ε-dependent denominators, and their degree in t grows with m. We solve eq. (63) block by block and order by order. For a diagonal block b, with $M(t)$ a fundamental matrix of $M' = A^{(0)}_{bb} M$, the order-k solution in that block is

$$y_k(t) = M(t)\Big[\, C_k + \int_0^t M^{-1}(t')\, S_k(t')\, dt' \,\Big], \tag{224}$$

where S_k collects the $m \geq 1$ and lower-sector terms of eq. (63) and C_k is a vector of boundary constants. In the top block, M contains $\sqrt{Q_4}$ of eq. (62). We expand the ε^{-3} coefficients fully in the class (64) and keep the ε^{-2} to ε^0 coefficients in the nested form (224) with exact kernels. We take the contour of eq. (224) from $t = 0$ to $t = 1$ above five points,

$$t^* \in \{0.12625\ldots,\ 0.34589\ldots,\ 0.36598\ldots,\ \tfrac{2}{5},\ \tfrac{1}{2}\}, \tag{225}$$

at which some kernels have poles. These poles are apparent singularities, since the masters have no monodromy around them and a contour below all five gives the same values.

The layered top-sector expressions contain 447 boundary constants C. We define them by the auxiliary-mass method of Ref. [95], implemented independently of `AMFlow`. With an auxiliary mass η in the propagators the masters reduce at large η to vacuum integrals given by Γ functions, and at the boundary point of segment I we transport them in η to $\eta = 0$. Regularity of the solution at the points (225) gives residue conditions of rank 39 on the C that fix ten of them independently of the auxiliary-mass computation. Finally, the exact kernels and the decimal strings of the constants are supplied as data files with the evaluation code of No. 24 (Appendix G) [106], which includes the transport in η that regenerates the constants.

F Crossed light-by-light box data

In this appendix we collect supporting material for the crossed light-by-light box, No. 21 of Table 1 (section 6.4). It comprises the two-variable connection in the forty-one-element basis, the depth of the differential system in the raw frame, the kernels of the word form, and the boundary constants of the kernel components. We write $f_0, \dots, f_{40}$ for the basis, with $f_0, \dots, f_{38}$ the thirty-nine masters ($m_0, \dots, m_{38}$ in section 6.4), and A^s, A^t for the 41×41 connection matrices in s and t at $m^2 = 1$. The two additional elements f_{39}, f_{40} reduce to the masters by relations independent of d and m^2,

$$f_{39} \;=\; -\,f_{18}\,, \qquad f_{40} \;=\; f_{20} - f_{19} + 2\,f_{18} - \tfrac{t}{2}\,f_{17} + f_{16}\,, \tag{226}$$

whose one kinematic coefficient comes from $p_2 \cdot p_3 = t/2$.

F.1 The connection in two variables

We reconstruct every entry of A^s and A^t as a rational function of (s, t) from reductions over finite fields at rational kinematic points [81, 89]. Each entry is a rational prefactor plus a sum of such prefactors times reduction coefficients $c(d, s, t)$, whose denominators are products of the polynomial letters of the family, of their images under $s \leftrightarrow t$, and of $T_2 = t^2 + d\,t + 2(d-3)$. We give the dependence on d by tabulating these rational functions of (s, t) at thirty-four values of d. Of the 2045 nonzero entries, 1989 are determined exactly and 16 modulo two primes, and 40 are undetermined.

The pair (A^s, A^t) is not flat on the (s, t) plane, since $\partial_t A^s - \partial_s A^t + [A^s, A^t]$ is nonzero on a fixed set of entries at every rational point we tested. This failure of flatness, which we call the defect, is caused by an off-shell term involving p_4^2 in the derivative operators used to construct the pair. The term is absent from the equations of the eleven subsector elements whose sectors cannot depend on p_4^2, and it can be isolated by Euler's relation for integrals homogeneous in (s, t, m^2). With α_j the scaling dimension of f_j and A^{m^2} the connection in m^2 at $m^2 = 1$, we define the matrix C by

$$s\,A^s + t\,A^t + A^{m^2} - \mathrm{diag}(\alpha) \;=\; u\,C\,, \tag{227}$$

and C would vanish for a pair free of the defect.

Along a leaf of the foliation $1/s + 1/t = \text{const}$ one has $\mathrm{d}t/\mathrm{d}s = -t^2/s^2$, and the connection along the leaf,

$$V \;=\; A^s - \frac{t^2}{s^2}\,A^t\,, \tag{228}$$

is free of the defect. We integrate V along the curve $1/s + 1/t = -3/8$ to obtain the word form of $m_{18}^{(0)}$ (section 6.4).

Off the curve we determine C from eq. (227) at seven points, on both sides of the threshold $u = 16$, with A^{m^2} derived anew at each point. On the eleven equations free of the defect, C vanishes identically. On the six other subsector equations the 28 nonzero entries of C are rational functions with denominators of the same form as those of A^s and A^t. We determine them from five of the seven points, and they reproduce C at the other two exactly. Once corrected for the off-shell term, the pair is flat on all of $f_0, \ldots, f_{16}$ in exact rational arithmetic at the seven points and at two values of d. By contrast, the uncorrected pair is not flat on four of the eleven defect-free equations, whose curvature the correction changes only through the commutator $[A^s, A^t]$. In the top-sector block the same construction with thirty-seven points determines 790 of the 828 entries of C at each value of d. All forty undetermined entries of (A^s, A^t) lie in this block, and for this reason we give no evaluation of $m_{18}^{(0)}$ as a function of (s, t) away from the curve and the points listed in section 6.4.

F.2 Depth of the system in the raw frame

The statement in section 6.4 on the depth of the system in the raw frame follows from a finite computation on (A^s, A^t). Since the dependence on (s, t) is complete at each tabulated value of d, the connection at a single value of d suffices for this computation, and we use $d = 101$. The data file of No. 21 (Appendix G) [106] gives, at $d = 101$, the map from the 2045 entries to their prefactors and reduction coefficients, the denominator polynomials, and the 4255 reduction coefficients that are known exactly, as rational functions of (s, t).

From the tabulated connection we determine which couplings $f_j \to f_k$ are nonzero at order ε^0 and contract the strongly connected components of the resulting directed graph, which gives an acyclic graph of depth four. Its top component consists of the twenty-four elements $f_{17}, \ldots, f_{40}$, coupled irreducibly at order ε^0 through a block of size 23×23, and in the raw frame the solution requires the fundamental matrix of that block [41, 93]. Finally, the data file yields the exact value of every determined entry at any rational (s, t). When we integrate along the curve, we use the two-variable connection only through such values.

F.3 Kernels of the word form

On the curve $1/s + 1/t = -3/8$ the finite part $m_{18}^{(0)}$ is a combination with exact coefficients of words in thirteen kernels, the word form of section 6.4. In the data file of No. 21 we list these kernels as one-forms on the curve, the words with their coefficients, and the boundary constants. The general solution of the top block has a branch point on the curve, but the physical combination $m_{18}^{(0)}$ is single valued there, since the coefficients c_q of the branched words vanish: the transported values give $|c_q| \leq 7.2 \times 10^{-146}$.

The kernels that the banana block contributes are modular. An exact change of basis, rational in ε and of determinant $-1/(6(d-1))$, takes $\{f_{13}, f_{14}, f_{15}\}$ to the basis of Ref. [101], in which the connection of the equal-mass banana is ε-factorized [76] with kernels that are modular forms for $\Gamma_1(6)$. In the rotated basis the block contributes six kernels (the pullbacks of these forms along $u = -s - t$) and no further kernels of Eichler-integral type.

The smallest subsystem that contains the banana block and is closed under the differential equation is $\{f_{13}, \ldots, f_{16}\}$. In particular, $f_0, \ldots, f_{12}$ do not couple to the block. In that subsystem exactly one further kernel appears at order ε^0. It is a quadrature of weight one over the same periods as the six modular kernels, namely the periods of the symmetric square of the sunrise curve [24, 101], with parity opposite to theirs. Such quadratures are classes in H^1 of the symmetric-square local system, which bounds their number at order ε^0 by thirty.

F.4 Boundary constants of the kernel components

The word form of $m_{18}^{(0)}$ contains the constants $c_7, \ldots, c_{10}$. We obtain their numerical values from the transport and identify them in $\{1, \pi^2, \zeta_3\}$ by integer-relation fits [18], which gives eq. (202). We call f_j in the gauge of the word form the j-th kernel component and write R_j for its boundary constant at $(s,t) \to (0,0)$. Ten of these constants lie in the $\mathbb{Q}$-span of $\{1, \pi^2, \zeta_3\}$,

$$\begin{gathered} R_{13} = \tfrac{1}{12}(275 + 23\pi^2 - 24\zeta_3)\,, \qquad R_{14} = \tfrac{1}{288}(36143 + 2588\pi^2 - 2880\zeta_3)\,, \\ R_{15} = \tfrac{1}{576}(37457 + 3236\pi^2 - 4032\zeta_3)\,, \qquad R_{16} = 60 + \pi^2 - \tfrac{58}{3}\zeta_3\,, \\ R_{18} = -30 - \tfrac{\pi^2}{2} + \tfrac{29}{3}\zeta_3\,, \qquad R_{21} = \tfrac{1}{48}(2001 + 48\pi^2 - 460\zeta_3)\,, \qquad R_{22} = -\tfrac{1}{64}(413 + 43\pi^2 + 16\zeta_3)\,, \\ R_{23} = \tfrac{1}{96}(139 + 37\pi^2 + 144\zeta_3)\,, \qquad R_{30} = 2\,R_{23}\,, \qquad R_{39} = -R_{18}\,. \end{gathered} \tag{229}$$

The residuals of these ten relations, between 10^{-269} and 10^{-304}, lie roughly 250 to 300 digits below the precision at which the fits were made. Moreover, R_{13} and R_{14} coincide with boundary values at the base point of the transport that were fixed independently of these fits.

We have found no closed form for the boundary constants R_j of the components coupled to the banana block, $j = 17, 34, 35, 37, 38$, and they enter the word form as numerical constants determined by the transport. For $j = 34$, 35 and 37 an integer relation of height at most 12 expresses R_j as one further constant of its component plus an element of the zeta ring. The constants that then remain satisfy no integer relation at 300 digits with zeta values through weight eight, with the boundary constants of the banana at its point of maximal unipotent monodromy, or with the periods of the K3 fiber.

G Evaluation codes and data files

For each of the thirty integrals we provide a standalone code that evaluates the result of its entry to a requested working precision. Table 12 lists the codes. The codes, with their data files, are on the pages of their integrals at the BootLoops site [106], all of which are linked from the page of this paper, `https://bootloops.ai/amplitudes.html`.

Several entries share a page. In particular, Nos. 2, 4 and 6 are on the polylogarithmic-suite page, Nos. 9–12 on the sunrise page, and Nos. 13, 14 and 23 on the kite page. Nos. 15–17 are on the ice-cream-cone page, where one code covers the three entries through a configuration option, and Nos. 27, 28, 29 and 33 are on the light-by-light page. Nos. 8, 18, 19, 31 and 32 are evaluated by the general codes of their graphs, which Table 12 names in parentheses.

No code performs an integral reduction or an auxiliary-mass-flow computation at run time. The `AMFlow` values stored with some codes serve only to repeat the comparisons of their entries, except that the codes of No. 24 and of sector 127 (No. 20) start each solution segment from stored `AMFlow` values. Some expressions are too long to print in full, and we distribute them together with the corresponding codes. They include the word lists of Nos. 7, 17 and 21, the iterated integrals of No. 23, the layered forms and boundary constants of No. 24, the boundary constants of No. 20, the dispersion kernel and subtraction terms of No. 27, and the connection matrices and boundary data of Nos. 14, 34 and 35.

Table 12: Evaluation codes for the thirty integrals, in the order of Table 1. *Code* is the file name on the integral's page of the BootLoops site [106], with the option that selects the entry or the mode when one code has several. *Computes* is the object returned at the working precision requested on the command line. *Imports* lists the Python packages used beyond the standard library. The last column gives what the code reads at run time other than the printed formulas, stated limits on its precision, and further modes. Comparison values stored with a code, `AMFlow` [95] values or values of the cited closed forms, enter no computed number unless the last column says otherwise.

No.	Code	Computes	Imports	Data read at run time; limits; modes
Polylogarithmic integrals (section 4)				
6	`sudakov-evaluate.py`	eq. (11), order by order in ε	`mpmath`	
2	`massless-dbox-evaluate.py`	the closed form in $x = t/s$ through ε^0; an independent polylogarithm implementation and a Mellin–Barnes quadrature for comparison	`mpmath`	`AMFlow` comparison values in a data file
4	`c5-ladder-evaluate.py`; `c5-ladder-xy-evaluate.py`	the one-variable block $f_3(x)$; the two-variable function $\Phi^{(3)}(X, Y)$, with its two comparison points	`mpmath`	
5	`pentagon-evaluate.py`	eq. (34) through ε^0 at Euclidean v_i	`mpmath`	
1	`outer-dbox-evaluate.py`	$g_{10}(u, v)$ of eq. (41) at Euclidean (u, v)	`mpmath`	
7	`c3-dbox-evaluate.py`	the coefficients $g^{(0)}, \ldots, g^{(4)}$ of eq. (44) for the scalar top-sector master in (s, t)	`mpmath`	exact word lists (Appendix B) as a data file
23	`kite-threshold-evaluate.py`; `-masses 1,4,9,3,0` for the second mass assignment	the 22 master integrals at masses^2 $(1, 4, 9, 2, 0)$, $t < 0$, by series solution of the differential equation from the boundary values at $t = 0$	`mpmath`	exact connection matrix as a data file; boundary values generated at run time; `-check` repeats the `AMFlow` comparison
24	`hexabox-evaluate.py`	the layered forms of the top sector and its subsectors along the path segments of the entry, the top-sector recursion rederived at each run	`mpmath`, `sympy`, `python-flint`	starts from stored `AMFlow` boundary values at the base points of the segments, to 50 and 70 significant digits, which limit its precision at the orders above ε^{-4}; the 447 boundary constants and the layered expressions as data files (Appendix E)
Elliptic integrals (section 5)				
8	`sunrise-evaluate.py` (code of the equal-mass sunrise graph)	the equal-mass sunrise at order ε^0, eq. (71), at Euclidean t	`mpmath`	
9	`sunrise-row09-evaluate.py`	eq. (72) at Euclidean $t < 0$ and, by continuation, at $t > 0$	`mpmath`	shared eMPL module `sunrise_empl.py` (Nos. 9–12)
10	`sunrise-row10-evaluate.py`	the $(1, 2, 3)$ sunrise at order ε^0, Euclidean t	`mpmath`	
11	`sunrise-row11-evaluate.py`	the $(1, 1, 4)$ sunrise at order ε^0, Euclidean t	`mpmath`	
12	`sunrise-row12-evaluate.py`	the order-ε^1 terms $E^{(1)}$ of eq. (74) for the three mass sets, together with $E^{(0)}$	`mpmath`	the 101 rational coefficients of the polynomial in eq. (74) from a data file
13	`kite-equal-evaluate.py`	eq. (78) at any Euclidean $t < 1$, $t \neq 0$	`mpmath`	no data file: periods, nome, $\overline{E}$ q-series and harmonic polylogarithms built from their definitions
18	`ggH-evaluate.py` (code of the $gg \to H$ graphs)	G_1, G_2 of eq. (80) at Euclidean $s < 0$, $0 < M^2 < 4$	`mpmath`	

continued

Table 12: Evaluation codes (continued).

No.	Code	Computes	Imports	Data read at run time; limits; modes
14	`kite-evaluate.py`; `-masses 1,1,3` for the second mass assignment	the top integral and its subsectors at $(m_1^2, m_3^2, m_5^2) = (1, 1, 2)$, Euclidean $s < 0$, by series solution from the vacuum boundary values	`mpmath`, `python-flint`	exact connection matrix $A(d, s)$ as a data file; `-boundary-recompute` rederives the boundary values from the classical constants through `kite-boundary.py`
15	`icc-evaluate.py`, equal-mass configuration	the equal-mass cone on the slice at order ε^0 for $x < -\frac{1}{4}$: series solution for $x < -\frac{1}{2}$, continuation around $x = -\frac{1}{2}$, and the integral of eq. (97) for $-\frac{1}{2} < x < -\frac{1}{4}$	`mpmath`, `sympy`	boundary values at $x = -1$ derived at run time from the cusp conditions; `sympy` only in the generic-mass configuration
16	`icc-evaluate.py -config generic`; `icc-genmass-evaluate.py`	the cone at masses^2 $(1, 2, 3, 5)$ on the slice; the same derivation at any rational masses, with the $(1, 3, 2, 7)$ comparison point included	`mpmath`, `sympy`	of the 46 boundary values, 21 from closed forms and written integrals and 25 recomputed at run time (`-boundary-recompute` sets the depth)
17	`icc-evaluate.py`, order-ε^1 mode; `icc-offslice-evaluate.py`	the order-ε^1 terms on the slice; checks of the two-variable connection off the slice on the lines $p_{12}^2 = -2$ and -3	`mpmath`, `sympy`	all boundary values, including $f_{4,1}(-1)$, derived at run time; the 88-word list as a data file
20	`zgamma-evaluate.py`; `zgamma-s127-evaluate.py`	the sector-125 pair as functions of s on the line $t = -1/3$ at $M = 7/25$; for sector 127, the solution of the t-equation between pairs of reference points	`mpmath`	boundary constants from their closed forms where these exist and otherwise as stored values, all of which `-boundary-recompute` rederives at a requested precision; the sector-127 code starts each segment from `AMFlow` values at a reference point
27	`lbl3e-master-evaluate.py`; `lbl3e-evaluate.py`; `lbl3e-box-evaluate.py`	the sunrise insertion S_{111}, the sector-15 master, at orders ε^0 through ε^2; the period ψ_1/π and the constant $B^{(0)}$ alone; the box I_{box} at orders ε^{-2} through ε^0 from eq. (127) at the three Euclidean points of the entry	`mpmath`	the density, subtracted kernel and triangle integrals of eq. (127) as data files
28	`lbl3se-evaluate.py`, with `lbl3se-w5-seed.py`	the $\nu = 0$ member I by the dispersion relation of the entry at Euclidean (s, t, m^2)	`mpmath`	exact connection read by the parser module `kite_de_exact_parse.py`
29	`lbl3kp-evaluate.py`	the two QED members I_{KP} and I_{K_1} by the same dispersion relation	`mpmath`	same parser module
33	`lbl3vp-evaluate.py`; `lbl3vp-eps0-evaluate.py`; `lbl3vp-points-evaluate.py`	the vacuum-polarization insertion at fixed ε at the reference point; its Laurent coefficients c_{-2}, c_{-1}, c_0 there; the fixed-ε values at the four further (s, t) points of the entry	`mpmath`, `sympy`	exact rational differential-equation data, parsed with `sympy`; initial values at $w' = 5$ from Feynman-parameter representations

continued

Table 12: Evaluation codes (continued).

No.	Code	Computes	Imports	Data read at run time; limits; modes
35	`eval_row35.py`	the Laurent coefficients ε^{-3} through ε^{1} of the 79 functions at a point y of the line eq. (151), by Taylor steps of eq. (152) from $y = 1/3$	`mpmath`, `python-flint`	starts from stored values of the 79 functions at 24 values of ε at $y = 1/3$, which limits the accuracy to 40 digits; `-boundary-recompute` regenerates them from eq. (161) when the archive `row35_chain.tar.gz` is present; the closed-form files of sectors 421 and 453 are not on the page because of their size, and the six functions they cover are evaluated by the Taylor steps; $A(d, y)$ and the boundary constants as data files (Appendix D)
K3 and Calabi–Yau integrals (section 6)				
19	`banana-evaluate.py` (code of the three-loop banana graph)	the top master m_1 at order ε^0 on the disk $\lvert t\rvert < 4$, Euclidean and below threshold	`mpmath`	
34	`banana-4loop-evaluate.py`	the top master at order ε^0 from the Frobenius solution at the MUM point and the boundary vector of the entry	`mpmath`	exact connection matrix $C(z, \varepsilon)$, boundary vector and comparison values written into the file; `-check` repeats the comparisons
31	`threshold-banana-evaluate.py` (code of the $(1, 1, 1, 9)$ banana graph)	the $(1, 1, 1, 9)$ three-loop banana, covering the coefficient $c_{3/2}$	`mpmath`, `sympy`	
32	`cy3-banana-evaluate.py` (code of the $(1, 1, 1, 1, 16)$ banana graph)	the $(1, 1, 1, 1, 16)$ four-loop banana, covering the coefficients $c_{5/4}$, $c_{7/4}$	`mpmath`	
21	`lbl3x-evaluate.py` (`-m18-eps0`); `row21-offcurve-evaluate.py`	the on-curve values of m_{18} at order ε^0 and the closed-form pieces of the entry (the K3 component of the banana master m_{13} and the four boundary constants); checks of the two-variable connection at the entry's comparison points off the curve	`mpmath`, `python-flint`, `gmpy2`	boundary values rederived at each run, stored reference values used only as checks; `-derive-constants` rederives the four constants; `-theorem-check` runs the finite-depth computation of Appendix F on its own data set; the kernels and word list as a data file

References

[1] Ajjath A H, Ekta Chaubey, and Hua-Sheng Shao. Two-loop massive qcd and qed helicity amplitudes for light-by-light scattering. 2023. arXiv:2312.16966.

[2] S. Abreu, F. Febres Cordero, H. Ita, B. Page, and V. Sotnikov. Leading-color two-loop qcd corrections for three-jet production at hadron colliders. 2021. arXiv:2102.13609, JHEP **07** (2021) 095; see also arXiv:1809.06240.

[3] Samuel Abreu, Dmitry Chicherin, Vasily Sotnikov, and Simone Zoia. Two-loop five-point two-mass planar integrals and double lagrangian insertions in a wilson loop. 2024. arXiv:2408.05201.

[4] Samuel Abreu, Harald Ita, Ben Page, and Wladimir Tschernow. Two-loop hexa-box integrals for non-planar five-point one-mass processes. *JHEP*, 03:182, 2022.

[5] Luise Adams, Christian Bogner, Armin Schweitzer, and Stefan Weinzierl. The kite integral to all orders in terms of elliptic polylogarithms. 2016. arXiv:1607.01571, MITP/16-069.

[6] Luise Adams, Christian Bogner, and Stefan Weinzierl. The two-loop sunrise graph with arbitrary masses. 2013. arXiv:1302.7004, J. Math. Phys. **54** (2013) 052303.

[7] Luise Adams, Christian Bogner, and Stefan Weinzierl. The two-loop sunrise graph in two space-time dimensions with arbitrary masses in terms of elliptic dilogarithms. 2014. arXiv:1405.5640, J. Math. Phys. **55** (2014) 102301.

[8] Luise Adams, Christian Bogner, and Stefan Weinzierl. The two-loop sunrise integral around four space-time dimensions and generalisations of the clausen and glaisher functions towards the elliptic case. 2015. arXiv:1504.03255.

[9] Luise Adams, Christian Bogner, and Stefan Weinzierl. The iterated structure of the all-order result for the two-loop sunrise integral. 2016. arXiv:1512.05630, J. Math. Phys. **57** (2016) 032304.

[10] Luise Adams and Stefan Weinzierl. Feynman integrals and iterated integrals of modular forms. 2017. arXiv:1704.08895.

[11] Luise Adams and Stefan Weinzierl. The ε-form of the differential equations for Feynman integrals in the elliptic case. 2018. arXiv:1802.05020, Phys. Lett. B **781** (2018) 270–278.

[12] Taushif Ahmed, Amlan Chakraborty, Ekta Chaubey, and Mandeep Kaur. Two-loop helicity amplitudes for diphoton production with massive quark loop. 2025. arXiv:2502.03282, JHEP **12** (2025) 106.

[13] Taushif Ahmed, Ekta Chaubey, Mandeep Kaur, and Sara Maggio. Two-loop non-planar four-point topology with massive internal loop. 2024. arXiv:2402.07311, JHEP **05** (2024) 064, doi 10.1007/JHEP05(2024)064.

[14] Gert Almkvist, Christian van Enckevort, Duco van Straten, and Wadim Zudilin. Tables of Calabi–Yau equations. 2005. arXiv:math/0507430.

[15] Tommaso Armadillo, Roberto Bonciani, Simone Devoto, Narayan Rana, and Alessandro Vicini. Evaluation of Feynman integrals with arbitrary complex masses via series expansions. *Comput. Phys. Commun.*, 282:108545, 2023. arXiv:2205.03345.

[16] David H. Bailey, Jonathan M. Borwein, David Broadhurst, and M. L. Glasser. Elliptic integral evaluations of Bessel moments and applications. *J. Phys. A*, 41(20):205203, 2008. arXiv:0801.0891.

[17] Piotr Bargiela, Amlan Chakraborty, Giulio Gambuti, and Melih A. Ozcelik. Light-by-light scattering at three loops in massless qcd and qed: amplitudes and cross sections. 2026. arXiv:2603.22423.

[18] Oscar Barrera, Aurélien Dersy, Rabia Husain, Matthew D. Schwartz, and Xiaoyuan Zhang. Analytic regression of Feynman integrals from high-precision numerical sampling. 2025. arXiv:2507.17815, JHEP **01** (2026) 014.

[19] Benjamin Basso and Lance J. Dixon. Gluing ladder Feynman diagrams into fishnets. 2017. arXiv:1705.03545, Phys. Rev. Lett. **119** (2017) 071601.

[20] S. Bauberger, F. A. Berends, M. Böhm, and M. Buza. Analytical and numerical methods for massive two-loop self-energy diagrams. 1995. arXiv:hep-ph/9409388, Nucl. Phys. B **434** (1995) 383–407.

[21] Konstantin Baune, Johannes Broedel, Egor Im, Artyom Lisitsyn, and Federico Zerbini. Schottky–Kronecker forms and hyperelliptic polylogarithms. 2024. arXiv:2406.10051, J. Phys. A **57** (2024) 445202.

[22] Matteo Becchetti, Federico Coro, Christoph Nega, Lorenzo Tancredi, and Fabian J. Wagner. Analytic two-loop amplitudes for $q\bar{q} \to \gamma\gamma$ and $gg \to \gamma\gamma$ mediated by a heavy-quark loop. 2025. arXiv:2502.00118, JHEP **06** (2025) 033, doi 10.1007/JHEP06(2025)033; ancillary files Zenodo 10.5281/zenodo.14733100.

[23] Zvi Bern, Lance J. Dixon, and David A. Kosower. Dimensionally regulated pentagon integrals. *Nucl. Phys. B*, 412:751–816, 1994.

[24] Spencer Bloch, Matt Kerr, and Pierre Vanhove. A Feynman integral via higher normal functions. *Compos. Math.*, 151(12):2329–2375, 2015. arXiv:1406.2664.

[25] Spencer Bloch and Pierre Vanhove. The elliptic dilogarithm for the sunset graph. 2015. arXiv:1309.5865, J. Number Theory **148** (2015) 328–364.

[26] Christian Bogner, Stefan Müller-Stach, and Stefan Weinzierl. The unequal mass sunrise integral expressed through iterated integrals on $\overline{\Updownarrow}_{1,3}$. *arXiv:1907.01251*, 2019.

[27] Kilian Bönisch, Claude Duhr, Fabian Fischbach, Albrecht Klemm, and Christoph Nega. Feynman integrals in dimensional regularization and extensions of Calabi–Yau motives. 2021. arXiv:2108.05310, JHEP **09** (2022) 156.

[28] Kilian Bönisch, Fabian Fischbach, Albrecht Klemm, Christoph Nega, and Reza Safari. Analytic structure of all loop banana integrals. 2020. arXiv:2008.10574, JHEP **05** (2021) 066.

[29] D. J. Broadhurst. Massive 3-loop Feynman diagrams reducible to SC^* primitives of algebras of the sixth root of unity. *Eur. Phys. J. C*, 8:311–333, 1999.

[30] D. J. Broadhurst, J. Fleischer, and O. V. Tarasov. Two-loop two-point functions with masses: asymptotic expansions and Taylor series, in any dimension. 1993. arXiv:hep-ph/9304303, Z. Phys. C **60** (1993) 287–302.

[31] David Broadhurst. Feynman integrals, L-series and Kloosterman moments. *Commun. Num. Theor. Phys.*, 10:527–569, 2016. arXiv:1604.03057.

[32] David J. Broadhurst and Andrei I. Davydychev. Exponential suppression with four legs and an infinity of loops. *Nucl. Phys. B Proc. Suppl.*, 205-206:326–330, 2010.

[33] Johannes Broedel, Claude Duhr, Falko Dulat, Brenda Penante, and Lorenzo Tancredi. Elliptic symbol calculus: from elliptic polylogarithms to iterated integrals of Eisenstein series. 2018. arXiv:1803.10256, JHEP **08** (2018) 014.

[34] Johannes Broedel, Claude Duhr, Falko Dulat, Brenda Penante, and Lorenzo Tancredi. Elliptic Feynman integrals and pure functions. 2019. arXiv:1809.10698, JHEP **01** (2019) 023.

[35] Johannes Broedel, Claude Duhr, Falko Dulat, Brenda Penante, and Lorenzo Tancredi. Elliptic polylogarithms and Feynman parameter integrals. 2019. arXiv:1902.09971, JHEP **05** (2019) 120.

[36] Johannes Broedel, Claude Duhr, Falko Dulat, and Lorenzo Tancredi. Elliptic polylogarithms and iterated integrals on elliptic curves. part i: general formalism. 2017. arXiv:1712.07089, JHEP **05** (2018) 093; see also 1712.07095 (part II: sunrise).

[37] Johannes Broedel, Claude Duhr, and Nils Matthes. Meromorphic modular forms and the three-loop equal-mass banana integral. 2021. arXiv:2109.15251, JHEP **02** (2022) 184.

[38] Francis Brown and Andrey Levin. Multiple elliptic polylogarithms. 2011. arXiv:1110.6917.

[39] Simon Caron-Huot, Lance J. Dixon, Falko Dulat, Matt von Hippel, Andrew J. McLeod, and Georgios Papathanasiou. The Cosmic Galois Group and extended Steinmann relations for planar $\mathcal{N} = 4$ SYM amplitudes. 2019. arXiv:1906.07116, JHEP **09** (2019) 061.

[40] Simon Caron-Huot and Johannes M. Henn. Iterative structure of finite loop integrals. 2014. arXiv:1404.2922, JHEP **06** (2014) 114.

[41] Kuo-Tsai Chen. Iterated path integrals. *Bull. Amer. Math. Soc.*, 83(5):831–879, 1977.

[42] Vsevolod Chestnov, Giulio Crisanti, and Mathieu Giroux. Landau's leviathans. 2026. arXiv:2606.29612.

[43] Dmitry Chicherin, Johannes Henn, and Vladimir Mitev. Bootstrapping pentagon functions. *JHEP*, 05:164, 2018.

[44] Federico Coro, Christoph Nega, Lorenzo Tancredi, and Fabian J. Wagner. Analytic two-loop amplitudes for di-jet and γ+jet production mediated by a heavy-quark loop. 2026. arXiv:2509.15315, JHEP **01** (2026) 090, doi 10.1007/JHEP01(2026)090; ancillary files Zenodo 10.5281/zenodo.17141555.

[45] M. Correia, M. Giroux, and S. Mizera. SOFIA: Singularities of Feynman integrals automatized. 2025. arXiv:2503.16601.

[46] A. I. Davydychev. Some exact results for N-point massive Feynman integrals. *J. Math. Phys.*, 32:1052–1060, 1991.

[47] Leonardo de la Cruz and Pierre Vanhove. Algorithm for differential equations for Feynman integrals in general dimensions. 2024. arXiv:2401.09908.

[48] Vittorio Del Duca, Claude Duhr, E. W. Nigel Glover, and Vladimir A. Smirnov. The one-loop pentagon to higher orders in epsilon. *JHEP*, 01:042, 2010.

[49] S. E. Derkachov, A. P. Isaev, and L. A. Shumilov. Ladder and zig-zag Feynman diagrams, operator formalism and conformal triangles. 2023. arXiv:2302.11238, JHEP **06** (2023) 059.

[50] Lance J. Dixon, James M. Drummond, and Johannes M. Henn. Bootstrapping the three-loop hexagon. 2011. arXiv:1108.4461, JHEP **11** (2011) 023.

[51] Charles F. Doran, Andrew Harder, Eric Pichon-Pharabod, and Pierre Vanhove. Motivic geometry of two-loop Feynman integrals. *Quart. J. Math.*, 75(3):901–967, 2024.

[52] James Drummond, Claude Duhr, Burkhard Eden, Paul Heslop, Jeffrey Pennington, and Vladimir A. Smirnov. Leading singularities and off-shell conformal integrals. *JHEP*, 08:133, 2013.

[53] James Drummond, Jack Foster, and Ömer Gürdoğan. Cluster adjacency properties of scattering amplitudes in $\mathcal{N} = 4$ supersymmetric Yang–Mills theory. 2018. arXiv:1710.10953, Phys. Rev. Lett. **120** (2018) 161601.

[54] Claude Duhr. Mathematical aspects of scattering amplitudes. 2015. arXiv:1411.7538, TASI 2014 lectures, in: Journeys Through the Precision Frontier (WSP, 2015) 419–476.

[55] Claude Duhr, Albrecht Klemm, Florian Loebbert, Christoph Nega, and Franziska Porkert. Yangian-invariant fishnet integrals in two dimensions as volumes of Calabi-Yau varieties. 2022. arXiv:2209.05291; 2310.08625.

[56] Claude Duhr, Albrecht Klemm, Christoph Nega, and Lorenzo Tancredi. The ice cone family and iterated integrals for Calabi–Yau varieties. 2022. arXiv:2212.09550, JHEP **02** (2023) 228.

[57] Claude Duhr and Sara Maggio. Feynman integrals, elliptic integrals and two-parameter K3 surfaces. 2025. arXiv:2502.15326.

[58] Claude Duhr and Sara Maggio. Three-loop banana integrals with three equal masses. 2025. arXiv:2511.19245.

[59] Claude Duhr, Sara Maggio, Christoph Nega, Benjamin Sauer, Lorenzo Tancredi, and Fabian J. Wagner. Aspects of canonical differential equations for Calabi–Yau geometries and beyond. 2025. arXiv:2503.20655, JHEP **06** (2025) 128.

[60] Claude Duhr, Sara Maggio, Franziska Porkert, Cathrin Semper, and Sven F. Stawinski. Three-loop banana integrals with four unequal masses. 2025. arXiv:2507.23061, JHEP **12** (2025) 034.

[61] Claude Duhr, Franziska Porkert, and Sven F. Stawinski. Canonical differential equations beyond genus one. 2024. arXiv:2412.02300, JHEP **02** (2025) 014.

[62] Martin Eichler. Eine Verallgemeinerung der Abelschen Integrale. 1957. Math. Z. **67** (1957) 267–298.

[63] Claudia Fevola, Sebastian Mizera, and Simon Telen. Landau singularities revisited: Computational algebraic geometry for Feynman integrals. 2023. arXiv:2311.14669, Phys. Rev. Lett. **132** (2024) 101601; see also the companion arXiv:2311.16219.

[64] Claudia Fevola, Sebastian Mizera, and Simon Telen. Principal Landau determinants. 2023. arXiv:2311.16219, Comput. Phys. Commun. **303** (2024) 109278; see also 2311.14669.

[65] Hjalte Frellesvig. On epsilon factorized differential equations for elliptic Feynman integrals. 2021. arXiv:2110.07968.

[66] T. Gehrmann, T. Huber, and D. Maitre. Two-loop quark and gluon form-factors in dimensional regularisation. 2005. arXiv:hep-ph/0507061, Phys. Lett. B **622** (2005) 295–302.

[67] Thomas Gehrmann, Johannes M. Henn, and Nigel A. Lo Presti. Analytic form of the two-loop planar five-gluon all-plus-helicity amplitude in qcd. *Phys. Rev. Lett.*, 116:062001, 2016.

[68] Thomas Gehrmann, Lorenzo Tancredi, and Erich Weihs. Two-loop qcd helicity amplitudes for $g\,g \to z\,g$ and $g\,g \to z\,\gamma$. 2013. arXiv:1302.2630.

[69] Mathieu Giroux, Andrzej Pokraka, Franziska Porkert, and Yoann Sohnle. The soaring kite: a tale of two punctured tori. 2024. arXiv:2401.14307, JHEP **05** (2024) 239.

[70] Alexander B. Goncharov. Multiple polylogarithms and mixed Tate motives. 2001. arXiv:math/0103059.

[71] Alexander B. Goncharov, Marcus Spradlin, C. Vergu, and Anastasia Volovich. Classical polylogarithms for amplitudes and Wilson loops. 2010. arXiv:1006.5703, Phys. Rev. Lett. **105** (2010) 151605.

[72] Richard J. Gonsalves. Dimensionally regularized two-loop on-shell quark form-factor. *Phys. Rev. D*, 28:1542, 1983.

[73] Holmfridur S. Hannesdottir, Andrew J. McLeod, Matthew D. Schwartz, and Cristian Vergu. Constraints on sequential discontinuities from the geometry of on-shell spaces. *JHEP*, 07:236, 2023.

[74] Holmfridur S. Hannesdottir, Andrew J. McLeod, Matthew D. Schwartz, and Cristian Vergu. Applications of the Landau bootstrap. 2024. arXiv:2410.02424, Phys. Rev. D **111** (2025) 085003.

[75] Wen-Jie He, Ren-You Zhang, Liang Han, Yi Jiang, Zhe Li, Xiao-Feng Wang, Shu-Xiang Li, Pan-Feng Li, and Qing-hai Wang. Two-loop planar master integrals for nnlo qcd corrections to w-pair production in quark-antiquark annihilation. *JHEP*, 12:136, 2024. arXiv:2409.08879.

[76] Johannes M. Henn. Multiloop integrals in dimensional regularization made simple. 2013. arXiv:1304.1806, Phys. Rev. Lett. **110** (2013) 251601.

[77] Johannes M. Henn. Lectures on differential equations for Feynman integrals. *J. Phys. A*, 48:153001, 2015.

[78] Martijn Hidding. DiffExp, a Mathematica package for computing Feynman integrals in terms of one-dimensional series expansions. *Comput. Phys. Commun.*, 269:108125, 2021. arXiv:2006.05510.

[79] Ina Hönemann, Kirsten Tempest, and Stefan Weinzierl. Electron self-energy in qed at two loops revisited. 2018. arXiv:1811.09308, Phys. Rev. D **98** (2018) 113008; erratum Phys. Rev. D **110** (2024) 059901.

[80] Adam Kardos, Costas G. Papadopoulos, Alexander V. Smirnov, Nikolaos Syrrakos, and Christopher Wever. Two-loop non-planar hexa-box integrals with one massive leg. *JHEP*, 05:033, 2022.

[81] Jonas Klappert, Fabian Lange, Philipp Maierhöfer, and Johann Usovitsch. Integral reduction with Kira 2.0 and finite-field methods. 2021. arXiv:2008.06494, Comput. Phys. Commun. **266** (2021) 108024.

[82] Albrecht Klemm, Christoph Nega, and Reza Safari. The l-loop banana amplitude from GKZ systems and relative Calabi–Yau periods. 2019. arXiv:1912.06201, JHEP **04** (2020) 088.

[83] Albrecht Klemm, Christoph Nega, Benjamin Sauer, and Jan Plefka. Calabi-Yau periods for black hole scattering in classical general relativity. *Phys. Rev. D*, 109(12):124046, 2024.

[84] Bernd A. Kniehl and Oleg V. Tarasov. Analytic result for the one-loop scalar pentagon integral with massless propagators. *Nucl. Phys. B*, 833:298–319, 2010.

[85] A.V. Kotikov and S. Teber. Multi-loop techniques for massless Feynman diagram calculations. 2018. arXiv:1805.05109, Phys. Part. Nucl. **50** (2019) 1–41; see also A. G. Grozin, "Lectures on multiloop calculations," Int. J. Mod. Phys. A **19** (2004) 473–520, hep-ph/0307297.

[86] Mikhail G. Kozlov and Roman N. Lee. One-loop pentagon integral in d dimensions from differential equations in ϵ-form. *JHEP*, 02:021, 2016.

[87] G. Kramer and B. Lampe. Integrals for two loop calculations in massless qcd. *J. Math. Phys.*, 28:945, 1987.

[88] Pierre Lairez and Pierre Vanhove. Algorithms for minimal Picard–Fuchs operators of Feynman integrals. *Lett. Math. Phys.*, 113(2):37, 2023.

[89] S. Laporta. High-precision calculation of multiloop Feynman integrals by difference equations. 2000. arXiv:hep-ph/0102033, Int. J. Mod. Phys. A **15** (2000) 5087–5159.

[90] S. Laporta. High-precision calculation of the 4-loop contribution to the electron $g-2$ in QED. 2017. arXiv:1704.06996; see also 1805.00227.

[91] S. Laporta and E. Remiddi. The analytical value of the electron $(g-2)$ at order α^3 in QED. 1996. arXiv:hep-ph/9602417, Phys. Lett. B **379** (1996) 283–291.

[92] S. Laporta and E. Remiddi. Analytic treatment of the two-loop equal-mass sunrise graph. 2005. arXiv:hep-ph/0406160, Nucl. Phys. B **704** (2005) 349–386.

[93] Roman N. Lee. Reducing differential equations for multiloop master integrals. *JHEP*, 04:108, 2015. arXiv:1411.0911.

[94] Roman N. Lee and Andrei A. Pomeransky. Critical points and number of master integrals. 2013. arXiv:1308.6676, JHEP **11** (2013) 165.

[95] Xiao Liu and Yan-Qing Ma. AMFlow: a Mathematica package for Feynman integrals computation via auxiliary mass flow. 2022. arXiv:2201.11669; package amflow; amflow-cpp github.com/chang18/amflow-cpp.

[96] Robin Marzucca, Andrew J. McLeod, and Christoph Nega. Two-loop master integrals for mixed QCD-EW corrections to $gg \to h$ through $\mathcal{O}(\epsilon^2)$. 2025. arXiv:2501.14435, Phys. Rev. D **112** (2025) 113007, doi 10.1103/d62t-55k2.

[97] Sebastian Mizera and Simon Telen. Landau discriminants. 2021. arXiv:2109.08036, JHEP **08** (2022) 200.

[98] G. Passarino and M. J. G. Veltman. One-loop corrections for e^+e^- annihilation into $\mu^+\mu^-$ in the Weinberg model. 1979. Nucl. Phys. B **160** (1979) 151–207.

[99] Sebastian Pögel, Xing Wang, and Stefan Weinzierl. Bananas of equal mass: any loop, any order in the dimensional regularisation parameter. 2022. arXiv:2212.08908, JHEP **04** (2023) 117.

[100] Sebastian Pögel, Xing Wang, and Stefan Weinzierl. Taming Calabi–Yau Feynman integrals: the four-loop equal-mass banana integral. 2022. arXiv:2211.04292, Phys. Rev. Lett. **130** (2023) 101601.

[101] Sebastian Pögel, Xing Wang, and Stefan Weinzierl. The three-loop equal-mass banana integral in ε-factorised form with meromorphic modular forms. 2022. arXiv:2207.12893, JHEP **09** (2022) 062.

[102] Ettore Remiddi and Lorenzo Tancredi. Differential equations and dispersion relations for Feynman amplitudes. the two-loop massive sunrise and the kite integral. 2016. arXiv:1602.01481, Nucl. Phys. B **907** (2016) 400–444.

[103] A. Sabry. Fourth order spectral functions for the electron propagator. 1962. Nucl. Phys. **33** (1962) 401–430.

[104] Niklas Schwanemann and Stefan Weinzierl. Electroweak double-box integrals for Møller scattering. *SciPost Phys.*, 18:172, 2025.

[105] Matthew D. Schwartz. Automated computation of Feynman integrals with BootLoops. companion methods paper, https://bootloops.ai/FeynmanBootstrap.pdf, 2026.

[106] Matthew D. Schwartz. The BootLoops toolkit. https://bootloops.ai/tools/, 2026.

[107] Matthew D. Schwartz. Bootstrapping elliptic and Calabi–Yau Feynman integrals. companion geometry paper, https://bootloops.ai/FeynmanGeometry.pdf, 2026.

[108] Atle Selberg and Sarvadaman Chowla. On Epstein's zeta-function. *J. Reine Angew. Math.*, 227:86–110, 1967.

[109] V. A. Smirnov. Analytical result for dimensionally regularized massless on-shell double box. 1999. arXiv:hep-ph/9905323, Phys. Lett. B **460** (1999) 397–404.

[110] Vladimir A. Smirnov. *Analytic Tools for Feynman Integrals*, volume 250 of *Springer Tracts in Modern Physics*. Springer, 2012.

[111] Othmar Steinmann. Über den Zusammenhang zwischen den Wightmanfunktionen und den retardierten Kommutatoren. *Helv. Phys. Acta*, 33:257–303, 1960.

[112] Gerard 't Hooft and M. J. G. Veltman. Regularization and renormalization of gauge fields. 1972. Nucl. Phys. B **44** (1972) 189–213.

[113] J. B. Tausk. Non-planar massless two-loop Feynman diagrams with four on-shell legs. 1999. arXiv:hep-ph/9909506, Phys. Lett. B **469** (1999) 225.

[114] N. I. Ussyukina and A. I. Davydychev. An approach to the evaluation of three- and four-point ladder diagrams; exact results for three- and four-point ladder diagrams with an arbitrary number of rungs. 1993. Phys. Lett. B **298** (1993) 363–370 and Phys. Lett. B **305** (1993) 136–143 (the $\Phi^{(L)}$ ladder function).

[115] Andreas von Manteuffel and Lorenzo Tancredi. A non-planar two-loop three-point function beyond multiple polylogarithms. 2017. arXiv:1701.05905, JHEP **06** (2017) 127, doi 10.1007/JHEP06(2017)127.

[116] Moritz Walden and Stefan Weinzierl. Numerical evaluation of iterated integrals related to elliptic Feynman integrals. 2020. arXiv:2010.05271; see also 2602.09956.

[117] Stefan Weinzierl. *Feynman Integrals: A Comprehensive Treatment for Students and Researchers*. UNITEXT for Physics. Springer, 2022. arXiv:2201.03593, Springer (2022), DOI 10.1007/978-3-030-99558-4.

[118] Li Lin Yang and Yiyang Zhang. From dlog to dE: Canonical elliptic integrands and modular symbol letters with pure eMPLs. 2025. arXiv:2512.19370.